

Errata

- p. 5 After equation 1.14, the following paragraph is to be inserted:
Equations 1.13 and 1.14 are known as the Condon approximation.
- p. 22 The first paragraph is to be replaced with the following:
The greater part of the work was performed on zinc phthalocyanine (ZnPc) (Strem Chemicals, purity 98 per cent), although zinc octaethylporphyrin (ZnOep) (Strem Chemicals, 97 per cent), zinc tetrabenzoporphyrin (ZnTbp) (synthesised by C.L. Dunford [95]), zinc 1,4,8,11,15,18,22,25-octabutoxyphthalocyanine (ZnObuPc) (Aldrich) and lutecium bisphthalocyanine (LuPc₂) (synthesised by T.C. VanCott [96]) have also been investigated. These molecules are all depicted in figure 2.1.
- p. 23 The first paragraph is to be replaced with the following:
Most of these substances were doped into polymer films. In addition, some work with samples doped into glasses was done. The polymers most commonly used were polymethylmethacrylate (PMMA) (obtained from Aldrich, medium molecular weight) and polyvinylbutyral (PVB) (Mowital supplied by Hoechst). (See figure 2.2.) These polymers may have some impurities present in them. The levels of impurities was not able to be obtained.
- p. 92 The first paragraph is to be replaced with the following:
For this calculation, rather than an explicit CF splitting, magnetic moment, Ham factor and field strength, a value for the shift of E_1 and E_2 was put directly into the calculation. To account for the distribution of CF splittings, this shift was given a distribution. The root mean square value for the shift was 1.5 GHz (as observed in the high resolution Zeeman experiments). The distribution was a Gaussian with the width related to the root mean square value (as in equation 4.3). A read-out function (a Gaussian) 1 cm^{-1} wide was used. An advanced stage in burning is simulated (as is the case in the experiments undertaken here). PW contributions are not included in these calculations.

Applications of Laser Selective Spectroscopy

A thesis submitted for the degree of Doctor of Philosophy of
The Australian National University

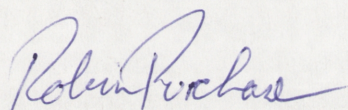
by

Robin Lavinia Purchase

March 1999

Declaration

The work in this thesis is my own other than where due reference is given in the text. The holographically detected Stark-broadened spectral holes were measured at the laboratory of Prof. Urs Wild in Zürich at the Swiss Federal Institute of Technology with the assistance of Dr Bernd Plagermann. The Stark-broadened spectral holes monitored in transmission were measured in the laboratory of Dr Neil Manson at the Research School of Physical Sciences and Engineering at the Australian National University with the assistance of Dr Matthew Sellars. He designed and constructed the laser intensity stabilisation system used in these experiments. No part of the research described in this thesis has been submitted for any other degree.

A handwritten signature in blue ink, appearing to read 'Robin Purchase', written in a cursive style.

Robin Purchase

Acknowledgments

The work in this thesis could not have been completed without the support of many people.

First of all, I wish to thank my supervisor, Dr Elmars Krausz, for his wisdom and guidance as a teacher. His support, enthusiasm and willingness to help are greatly appreciated.

I also wish to thank Dr Hans Riesen for his help and encouragement. His willingness to share his great knowledge on both experimental and theoretical matters is greatly appreciated.

Many thanks are due also to Dr Bryce Williamson of the University of Canterbury. He was always patient and helpful in our e-mail discussions

A large debt of gratitude is due to Mr Keith Jackman for his technical craftsmanship. Many experiments would not have happened without his technical expertise and on-the-spot brilliant ideas.

I wish to acknowledge the generosity of Prof. Urs Wild of the ETH in Zürich for allowing me to work in his laboratory for four and a half months in 1997. Not only did I learn a great deal while working there, but I also enjoyed the friendship of his research group. Within this group, I would particularly like to thank Dr Bernd Plagemann who looked after me while I was there. He was very patient in teaching me how to 'drive' the equipment in the laboratory.

I would like to thank Dr Neil Manson of The Research School of Physical Sciences and Engineering, ANU for allowing me to work in his laboratory for some months in 1998. Within his group I am especially grateful to Dr Matthew Sellars for all his patience, tutelage, and help while I was performing experiments there.

My parents have been a great source of love and support throughout the time of my study. I would particularly like to thank them for the careful reading of a thesis they did not fully understand.

I gratefully acknowledge the ANU for the provision of a scholarship for the period over which I worked towards completing my PhD.

Abstract

Laser selective spectroscopy, in particular spectral hole-burning, is used to gain information about porphyrin derivatives (zinc phthalocyanine, zinc octaethylporphyrin, zinc tetrabenzoporphyrin, zinc octabutoxyphthalocyanine and lutecium bisphthalocyanine) in polymer matrices. The work here concentrates on the Q band which is a ligand-centred $\pi - \pi^*$ transition.

Excited state vibrational frequencies have been obtained for zinc phthalocyanine, zinc tetrabenzoporphyrin and lutecium bisphthalocyanine by hole-burning into vibrational sidelines.

Fluorescence line narrowing is reported for zinc phthalocyanine and zinc octaethylporphyrin. Little narrowing is observed in these spectra. This lack of narrowing is rationalised in terms of rapid hole-burning at the excitation wavelength.

An extrapolated hole width of 600 ± 50 MHz is measured for zinc phthalocyanine.

A Debye–Waller factor of 0.63 is measured in zinc phthalocyanine by hole-burning on a long time scale.

Magneto-optic measurements on spectral holes in zinc phthalocyanine, zinc octaethylporphyrin and zinc tetrabenzoporphyrin are reported. The Zeeman shifts and broadenings observed are anomalously small. This is interpreted as being a result of the combined action of local crystal fields and Jahn–Teller effects.

Higher resolution Zeeman experiments are reported for zinc phthalocyanine. Zeeman shifts of 1.5 ± 0.25 GHz are observed in a 5 T field. The shift and broadening of the hole shape in the magnetic field is analysed in terms of a distribution of crystal fields with a root mean square value of 110 cm^{-1} and a Ham factor of 0.52.

Hole magnetic circular dichroism spectra are reported for features resulting from burning in both the Q band origin and vibrational sideline regions. The results provide information about the distribution of environmentally induced crystal-field splittings of the (nominally degenerate) excited state. Modelling of hole absorption and MCD provides insights into the changes which occur in these systems upon the application of a magnetic field.

The influence of an externally applied electric field on spectral holes burnt into zinc phthalocyanine and zinc tetrabenzoporphyrin is investigated. The changes in hole shape, as a function of electric field, are monitored holographically and in transmission. A linear Stark effect is observed. The transmission data are collected in two experimental geometries: the polarisation direction of the laser perpendicular to the applied field, and the polarisation direction of the laser parallel to the applied field. The broadening in the electric field is analysed as having contributions from in-plane distortions of the chromophore that remove its nominal four-fold symmetry and thus the degeneracy of the Q band. Other contributions, perhaps associated with axial ligation of the chromophore, remove the plane of symmetry and contribute differently to the broadened profile.

Table of Contents

	Page
List of Figures	ix
List of Tables	xv
Frequently Used Abbreviations and Acronyms	xvi
List of Symbols	xvii
1. Introduction	1
1.1 The chromophores	1
1.2 Vibronic transitions	3
1.3 Laser selective spectroscopy	7
1.3.1 Fluorescence line narrowing	10
1.3.2 Spectral hole-burning	11
1.4 The Zeeman effect and magnetic circular dichroism	17
1.5 The Stark effect	20
2. Experimental Methods and Techniques	22
2.1 Sample Preparation	22
2.2 Measurement techniques	25
2.2.1 Low resolution experiments	25
2.2.2 High resolution hole-burning experiments	29
2.3 Calculations	39

3. Broadband Spectroscopy, Fluorescence Line Narrowing and Spectral Hole-burning	41
3.1 Broadband Spectroscopy	41
3.1.1 Absorption	41
3.1.2 Emission	41
3.1.3 Aggregation of zinc phthalocyanine	44
3.2 Spectral hole-burning in vibrational sidebands	46
3.3 Fluorescence line narrowing experiments in zinc phthalocyanine and zinc octaethylporphyrin	52
3.4 Fluorescence line narrowing in zinc octaethylporphyrin: some further experiments	56
3.5 The development of a spectral hole shape with burn time	58
3.6 Hole width extrapolation to zero fluence	59
3.7 Hole-burning to long time	62
3.8 Hole-burning in zinc 1,4,8,11,15,18,22,25-octabutoxyphthalocyanine	63
4. Magneto-optic Measurements of Spectral Holes	65
4.1 Zeeman experiments on spectral holes	65
4.1.1 Spectral hole-burning in a system with a degenerate excited state	65
4.1.2 Low resolution Zeeman experiments on spectral holes in zinc phthalocyanine and zinc octaethylporphyrin	67
4.1.3 High resolution Zeeman experiments on zinc phthalocyanine	70
4.2 Magnetic circular dichroism experiments on spectral holes	79
4.3 Simulations of magnetic circular dichroism of spectral holes	90
4.4 Magnetic circular dichroism measurements of sidehole spectra	93

5. Stark Spectroscopy and Spectral Hole-burning	95
5.1 Modelling of spectral hole shapes in an applied electric field	95
5.2 Holographic read-out of Stark broadened spectral holes in zinc phthalocyanine and zinc tetrabenzoporphyrin	98
5.3 Polarisation dependence of Stark broadenings of spectral holes in zinc phthalocyanine	108
5.4 Wavelength dependence of Stark broadenings in spectral holes	117
6. Concluding Remarks	125
6.1 The aim of the project and the systems studied	125
6.2 The experiments	125
6.3 Summary of the results obtained	126
6.4 Further remarks about the results	128
6.5 Possible future experiments	129
References	130
Appendix: Publications and Presentations	135

List of Figures

	Page
1.1 Examples of porphyrin-type compounds.	2
1.2 Potential energy curves for a ground state, A, and an excited state, J.	6
1.3 Inhomogeneous broadening.	8
1.4 A schematic representation of a zero-phonon line (ZPL) and a phonon wing (PW).	9
1.5 A schematic representation of a fluorescence line narrowing (FLN) experiment.	10
1.6 Transient hole-burning.	11
1.7 Photochemical hole-burning.	12
1.8 The two level system (TLS) model.	13
1.9 The changes in a spectrum upon photophysical hole-burning.	14
1.10 The shape of a spectral hole.	16
1.11 MCD is generally described by three terms.	18
1.12 Pseudo \mathcal{A} -terms have a similar shape to \mathcal{A} -terms, but are in fact two overlapping \mathcal{B} -terms arising from nominally degenerate states which have been split.	19
2.1 Chromophores studied in this thesis.	22
2.2 The two polymers most frequently used as host matrices for the experiments.	23
2.3 A schematic diagram of the apparatus used to measure broadband absorption and MCD.	26
2.4 A schematic diagram of the apparatus used to obtain FLN spectra.	28
2.5 A schematic representation of the apparatus used to obtain the transmission read-out of spectral holes.	30
2.6 The interference of light reflected off two parallel surfaces.	32
2.7 A schematic diagram of a step-index multimode fibre.	33
2.8 A representation of the sequence of steps involved in burning a hole and then reading it out in several fields.	34

2.9	The experimental geometry used for Stark experiments performed in transmission.	35
2.10	The experimental geometry used for Zeeman experiments performed in transmission.	35
2.11	Holographic read-out.	36
2.12	A schematic representation of the apparatus used to measure holographically detected spectral holes.	37
2.13	The experimental geometry used for the holographically detected Stark broadened spectral holes.	39
3.1	Absorption spectra of the Q bands of samples studied in this thesis.	42
3.2	Broadband absorption (solid line) and emission (dashed line) of ZnPc/PMMA.	43
3.3	Broadband absorption (solid line) and emission (dashed line) of ZnOep/PMMA.	43
3.4	A broadband absorption spectrum of ZnPc/PMMA showing the aggregate absorption band and a hole spectrum where the hole was burnt into the red edge of the Q band with a sidehole in the aggregate band.	45
3.5	The sidehole spectrum of ZnPc/PMMA where the hole was burnt into Q(1,0) at 632.8 nm.	47
3.6	Correlation and non-correlation of two energy levels having an inhomogeneous distribution.	48
3.7	The sidehole spectrum of ZnPc/PVB where the hole was burnt into the blue edge of Q(0,0) at 665.7 nm.	49
3.8	The sidehole spectrum of ZnTbp/PVB where the hole was burnt into the blue edge of Q(0,0) at 620.3 nm.	49
3.9	The sidehole spectrum of LuPc ₂ /PMMA where the hole was burnt into the blue edge of Q(0,0) at 647.1 nm.	50
3.10	Selective emission from ZnPc/PMMA excited at a number of places in the Q band.	53
3.11	Selective emission from ZnOep/PMMA excited at a number of places in the Q band.	54
3.12	Emission from ZnOep in a 1:1 mixture of ethyl iodide/bromobutane excited at 543 nm (solid line) compared to the emission excited at 530.9 nm in ZnOep/PMMA (dashed line).	57
3.13	Phosphorescence from ZnOep/THF excited at 543 nm.	58

3.14	The development of a spectral hole with time.	59
3.15	Hole width as a function of burn power.	61
3.16	Absorption before (solid line and circles) and after (dashed line and squares) burning for a long time.	63
3.17	Broadband absorption of ZnObuPc/PMMA showing the appearance of the new absorption after exposure to light.	64
4.1	When a spectral hole is burnt into a band which consists of a distribution of two CF-split levels, E_1 and E_2 , then chromophores selected by hole-burning will comprise transitions to both the excited state levels.	65
4.2	Electronic sideholes from burning into a system with a CF-split excited state.	66
4.3	The contributions from E_1 and E_2 have different lifetimes.	67
4.4	Absorption spectra of a 676.4 nm hole in ZnPc/PMMA in 0 and 5 T.	68
4.5	Absorption spectra of a 568.2 nm hole in ZnOep/PVB in 0 and 5 T.	68
4.6	Changes in hole shape as a function of magnetic field in ZnPc/PMMA.	71
4.7	Changes in hole shape as a function of magnetic field in ZnPc/PMMA.	71
4.8	Shift of hole maximum as a function of applied magnetic field for a hole in ZnPc/PMMA burnt at 669.1 nm.	72
4.9	A spectral hole burnt into ZnPc/PMMA at 670.1 nm in a 5 T field parallel to the polarisation direction of the burning and reading light.	74
4.10	A spectral hole burnt into ZnPc/PMMA at 669.1 nm in a 5 T field perpendicular to the polarisation direction of the burning and reading light.	74
4.11	Spectral holes burnt into ZnPc/PMMA at 669.1 nm in magnetic fields of 0 – 5 T perpendicular to the polarisation direction of the burning and reading light.	76
4.12	The wavelength dependence of the shift of the hole maximum in a 5 T field, where the field is perpendicular to the polarisation direction of the burning and reading light.	78

- 4.13 Hole absorption (lower) and hole MCD (upper) for a hole burnt into ZnPc/PMMA at 676.4 nm. 79
- 4.14 Hole absorption (lower) and hole MCD (upper) for a hole burnt into ZnOep/PVB at 568.2 nm. 80
- 4.15 An absorption spectrum of the Q band of ZnPc/PVB showing the positions of the holes burnt for the wavelength dependence of the hole MCD experiment. 82
- 4.16 An absorption spectrum of the Q band of ZnTbp/PVB showing the positions of the holes burnt for the wavelength dependence of the hole MCD experiment. 83
- 4.17 Hole absorption (lower) and hole MCD (upper) for the spectral hole burnt at 676.4 nm in ZnPc/PVB. 84
- 4.18 Hole absorption (lower) and hole MCD (upper) for the spectral hole burnt at 670.8 nm in ZnPc/PVB. 84
- 4.19 Hole absorption (lower) and hole MCD (upper) for the spectral hole burnt at 666.1 nm in ZnPc/PVB. 85
- 4.20 Hole absorption (lower) and hole MCD (upper) for the spectral hole burnt at 629.3 nm in ZnTbp/PVB. 86
- 4.21 Hole absorption (lower) and hole MCD (upper) for the spectral hole burnt at 624.2 nm in ZnTbp/PVB. 86
- 4.22 Hole absorption (lower) and hole MCD (upper) for the spectral hole burnt at 620.3 nm in ZnTbp/PVB. 87
- 4.23 A simulation of a hole absorption (lower) and hole MCD (upper). 91
- 4.24 Absorption (lower) and MCD (upper) of a spectral hole and the accompanying sideholes as a result of burning at 632.8 nm. 93
- 5.1 Characteristic changes in hole shape in an applied electric field for a random (induced) change in dipole ($\Delta\mu_{\text{ind}}$) and a fixed (molecular) dipole ($\Delta\mu_{\text{mol}}$) parallel to the electric field. 96
- 5.2 Absorption of the Q band of ZnPc/PVB showing the positions of spectral holes burnt for the holographically detected Stark experiment. 98
- 5.3 Absorption of the Q band of ZnTbp/PVB showing the positions of spectral holes burnt for the holographically detected Stark experiment. 99

- 5.4 Changes in hole shape in ZnPc/PVB, monitored holographically, as a function of electric field. 100
- 5.5 Changes in hole shape in ZnTbp/PVB, monitored holographically, as a function of electric field. 100
- 5.6 Change in hole width as a function of field strength for holes burnt in ZnPc/PVB. 101
- 5.7 Change in hole width as a function of field strength for holes burnt in ZnTbp/PVB. 101
- 5.8 Change in width in ZnPc/PVB as a function of field strength for permanent and induced components as obtained from fitting to the model. 105
- 5.9 Change in width in ZnTbp/PVB as a function of field strength for permanent and induced components as obtained from fitting to the model. 105
- 5.10 When ZnPc has an axial ligand, the Zn adopts an out-of-plane position. 106
- 5.11 The sum of the contributions from $\Delta\mu_{\text{ind}}$ and $\Delta\mu_{\text{mol}}$ may be such that the resulting hole shape has a characteristic 'rectangular' appearance. 107
- 5.12 A holographically detected spectral hole burnt into ZnPc/PVB at 673.5 nm in an applied electric field of 36.6 kV/cm. 108
- 5.13 Changes in hole shape as a function of electric field for holes burnt into ZnPc/PMMA and read out in transmission. 109
- 5.14 Changes in hole width as a function of electric field for ZnPc/PMMA showing the two different experimental geometries - perpendicular (boxes and dashed line) and parallel (crosses and solid line). 110
- 5.15 Changes in hole shape as a function of electric field for holes burnt into ZnPc/PMMA without solvent and read out in transmission. 112
- 5.16 Changes in hole width as a function of electric field for ZnPc/PMMA without solvent showing the two different experimental geometries - perpendicular (boxes and dashed line) and parallel (crosses and solid line). 113

- 5.17 The presence of solvent may explain the reduction in the crystal field as the solvent forms a 'loose cage' around the chromophore. 115
- 5.18 Dispersion interactions. 118
- 5.19 A chromophore in a matrix field. 119
- 5.20 Wavelength dependence of the total dipole moment calculated for ZnPc/PVB from the holographically read-out holes. 120
- 5.21 Wavelength dependence of the total dipole moment calculated for ZnTbp/PVB from the holographically read-out holes. 120
- 5.22 Wavelength dependence of the dipole moment calculated for the ZnPc/PMMA sample with solvent using the parallel experimental geometry. 121
- 5.23 Wavelength dependence of the dipole moment calculated for the ZnPc/PMMA sample with solvent using the perpendicular experimental geometry. 121
- 5.24 Wavelength dependence of the dipole moment calculated for the ZnPc/PMMA sample without solvent using the parallel experimental geometry. 122
- 5.25 Wavelength dependence of the dipole moment calculated for the ZnPc/PMMA sample without solvent using the perpendicular experimental geometry. 122

List of Tables

	Page
3.1 Excited state vibrational frequencies yielded by hole-burning in vibrational sidebands.	51
5.1 $\Delta\mu_{\text{eff}}$ calculated from the change in hole width with electric field for ZnPc/PVB and ZnTbp/PVB for holographically read-out spectral holes.	102
5.2 $\Delta\mu_{\text{ind}}$ and $\Delta\mu_{\text{mol}}$ calculated from modelling the change in hole width with electric field for ZnPc/PVB and ZnTbp/PVB for holographically read-out spectral holes.	104
5.3 $\Delta\mu_{\text{eff}}$ calculated from the change in hole width with electric field for ZnPc/PMMA for the two experimental geometries.	110
5.4 $\Delta\mu_{\text{eff}}$ calculated from the change in hole width with electric field for ZnPc/PMMA without solvent for the two experimental geometries.	113
5.5 The wavenumber resulting from a linear extrapolation of the wavelength dependent Stark data to $\Delta\mu_{\text{eff}} = 0$.	123

Frequently Used Abbreviations and Acronyms

The following abbreviations and acronyms appear in two or more chapters

CF	crystal field
DWF	Debye–Waller factor
FLN	fluorescence line narrowing
HT	Herzberg–Teller
JT	Jahn–Teller
lcp	left circularly polarised
LuPc ₂	lutecium bisphthalocyanine
MCD	magnetic circular dichroism
MMA	methylmethacrylate
PMMA	polymethylmethacrylate
PVB	polyvinylbutyral
PW	phonon wing
rcp	right circularly polarised
THF	tetrahydrofuran
ZnObuPc	zinc 1,4,8,11,15,18,22,25-octabutoxyphthalocyanine
ZnOep	zinc octaethylporphyrin
ZnPc	zinc phthalocyanine
ZnPc/PMMA	denotes a guest–host combination - in this case ZnPc doped into PMMA
ZnTbp	zinc tetrabenzoporphyrin
ZPL	zero-phonon line

List of Symbols

The following symbols appear in more than one chapter

B	applied magnetic field
D	transition dipole
$\Delta\mu'_{\text{ind}}$	root-mean-square value of a matrix-induced dipole moment
$\Delta\mu_{\text{eff}}$	effective change in dipole moment between the ground and excited states
$\Delta\mu_{\text{ind}}$	matrix-induced change in dipole moment between the ground and excited states
$\Delta\mu_{\text{mol}}$	permanent (molecular) change in dipole moment between the ground and excited states
$\Delta v'_0$	root mean square crystal-field splitting
Δv_0	crystal-field splitting
Δv_B	frequency shift in a magnetic field
Δv_E	frequency shift in an electric field
ϵ	dielectric constant of a given substance
E_{app}	applied electric field
E_{pol}	polarisation direction of light
f	f , when a Lorentz field correction has been made
f	tensor to describe the transformation of an applied electric field to the field experienced by a chromophore
h	Planck's constant
μ_B	excited state static magnetic moment
θ_{mol}	angle between $\Delta\mu_{\text{mol}}$ and D

1. Introduction

The aim of the work presented in this thesis is to obtain information about systems in condensed phases using some of the techniques of laser selective spectroscopy. The techniques of laser selective spectroscopy (in particular hole-burning and photon echo) are often used to determine homogeneous linewidths and probe processes such as dephasing and spectral diffusion. These techniques show a potential for a range of other applications [1-4]. Hole-burning, in particular, may be used to gain detailed information about samples in amorphous environments. The thesis focusses on this technique.

1.1 The chromophores

The chromophores chosen for this study are all metallo-porphyrin derivatives. Porphyrins, and their close relatives the phthalocyanines, are a class of compounds with a wide variety of interesting properties [5, 6].

Porphyrins and phthalocyanines are planar molecules with an extensive array of π conjugation. Examples of these types of systems are shown in figure 1.1. It is the π -electron delocalisation with which many of the properties of these molecules are associated.

Firstly, porphyrins and phthalocyanines are strongly coloured. This characteristic, combined with their chemical stability, makes them ideal for use as dyes. Secondly, their electrochemical properties are widely investigated for applications such as photovoltaic cells. Thirdly, many biological systems (chlorophyll and haems, for example) are based upon porphyrins. Porphyrins and their derivatives make ideal models for these biologically important systems.

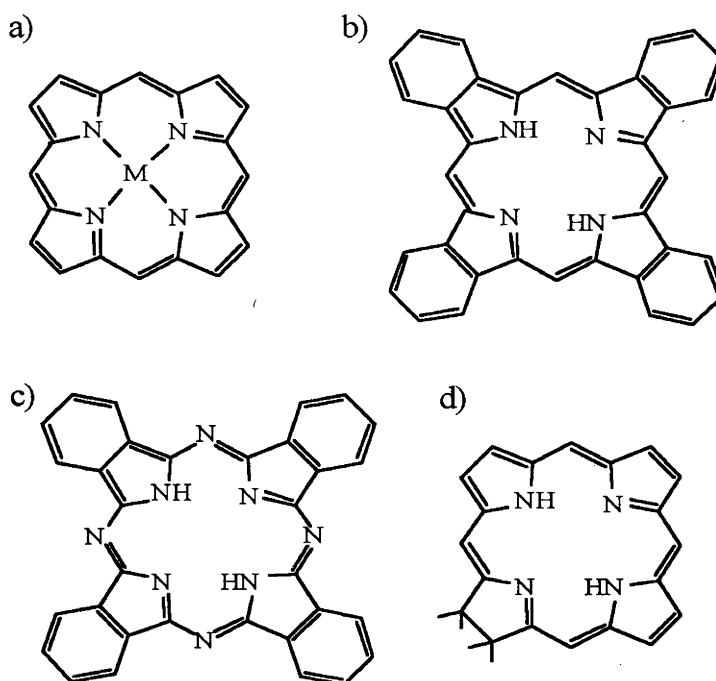


Figure 1.1: Examples of porphyrin-type compounds. a) Metallo-porphyrin. b) Free-base tetrabenzoporphyrin. c) Free-base phthalocyanine. d) chlorin.

The metallo-porphyrins and phthalocyanines absorb strongly in the visible region (hence their strong colours). The two lowest energy electronic transitions are conventionally labelled the Q and B bands [7]. These transitions are associated with the π electron system in the porphyrins/phthalocyanine ring. It is the Q band on which the work here concentrates. It is a $\pi - \pi^*$ transition. The greater part of the work performed for this thesis was done on symmetrically substituted porphyrins and phthalocyanines. These chromophores are considered to nominally possess D_{4h} symmetry[8-10]. The symmetries of the states involved in the Q transition are therefore ${}^1A_{1g}$ and 1E_u for the ground and excited states respectively. The degeneracy of the excited state, the lifting of this degeneracy, and the effect this has on the spectroscopy of the systems under consideration are matters of importance in this thesis, particularly with reference to the magneto-optical work.

More information on the electronic structures of porphyrins may be found in reference [7].

1.2 Vibronic transitions

The solving of the Schrödinger equation (equation 1.1) presents theoreticians with a formidable problem.

$$\mathcal{H}(q,Q)\Psi_k(q,Q)=E_k\Psi_k(q,Q) \quad (1.1)$$

Without simplification, the Schrödinger equation describes all the particles (electrons and nuclei in this case) simultaneously. Even from a classical perspective, this equation is insoluble for more than three particles.

Equation 1.1 has a Hamiltonian

$$\mathcal{H}(q,Q)=T(q,Q)+V(q,Q) \quad (1.2)$$

which consists of a kinetic energy part

$$T(q,Q)=T_n(Q)+T_e(q) \quad (1.3)$$

and a potential energy part

$$V(q,Q)=V_{nn}(Q)+V_{ee}(q)+V_{en}(q,Q) \quad (1.4)$$

In order to render the Schrödinger equation more tractable, a number of approximations are made.

The Born–Oppenheimer (BO) approximation arises from the very different masses (and therefore relative speeds) of the nuclei and electrons. Thus, under this approximation, the vibrational and electronic parts are separable. For each shift in nuclear position, the electrons adjust instantaneously.

Therefore, \mathcal{H} may be split into electronic and nuclear components:

$$\mathcal{H}(q,Q)=T_n(Q)+T_e(q)+V(q,Q) \quad (1.5)$$

From this, the electronic components are separated

$$\mathcal{H}_E(q, Q) = T_e(q) + V(q, Q) \quad (1.6)$$

Note, however, that $V(q, Q)$ contains a nuclear–nuclear repulsion contribution and therefore \mathcal{H}_E depends parametrically on Q . Using this electronic Hamiltonian, an electronic Schrödinger equation may be given:

$$\mathcal{H}_E(q, Q)\phi_k(q, Q) = W_k(Q)\phi_k(q, Q) \quad (1.7)$$

This is an electronic Schrödinger equation at a given fixed nuclear co-ordinate.

As a result of the separation of the Hamiltonian, wave functions are multiplicative and potential and kinetic energies are additive. Thus, within this approximation, the solutions to equation 1.1 may be written:

$$\Psi_k(q, Q) = \phi_k(q, Q)\chi_{ki}(Q) \quad (1.8)$$

and

$$E_k = T_{nk}(Q) + W_k(Q) \quad (1.9)$$

The term 'adiabatic' is applied to systems which comply with the BO approximation. This is because the changes in nuclear co-ordinate are so slow relative to the electronic motions. Therefore they are decoupled.

A further approximation that may be made is to confine the description of the electronic Hamiltonian to terms which are only dependent on the equilibrium nuclear co-ordinate. Such an approximation is known as the crude adiabatic approximation:

$$\mathcal{H}_E(q, Q_0)\phi_k(q, Q_0) = W_k(Q_0)\phi_k(q, Q_0) \quad (1.10)$$

Another related approximation that is commonly made is the Franck–Condon (FC) approximation. Within this approximation, the electronic transition moment is independent of nuclear co-ordinate.

Consider a transition between two eigenstates, $|A\rangle$ and $|J\rangle$. There is some dipole moment operator which may be split into electronic and nuclear parts:

$$\mathbf{m}(\mathbf{q}, \mathbf{Q}) = \mathbf{m}(\mathbf{q}) + \mathbf{m}(\mathbf{Q}) \quad (1.11)$$

A transition can then be described

$$\langle \Psi_A(\mathbf{q}, \mathbf{Q}) | \mathbf{m}(\mathbf{q}, \mathbf{Q}) | \Psi_J(\mathbf{q}, \mathbf{Q}) \rangle \quad (1.12)$$

Using equation 1.8:

$$\begin{aligned} & \langle \phi_A(\mathbf{q}, \mathbf{Q}) \chi_A(\mathbf{Q}) | \mathbf{m}(\mathbf{q}) + \mathbf{m}(\mathbf{Q}) | \phi_J(\mathbf{q}, \mathbf{Q}) \chi_J(\mathbf{Q}) \rangle \\ & \approx \langle \phi_A(\mathbf{q}, \mathbf{Q}) | \mathbf{m}(\mathbf{q}) | \phi_J(\mathbf{q}, \mathbf{Q}) \rangle \langle \chi_A(\mathbf{Q}) | \chi_J(\mathbf{Q}) \rangle + \\ & \quad \langle \chi_A(\mathbf{Q}) | \mathbf{m}(\mathbf{Q}) | \chi_J(\mathbf{Q}) \rangle \langle \phi_A(\mathbf{q}, \mathbf{Q}) | \phi_J(\mathbf{q}, \mathbf{Q}) \rangle \end{aligned} \quad (1.13)$$

The second term of equation 1.13 is equal to zero as a result of the ground and excited electronic states being orthogonal. This leads to:

$$\langle \phi_A(\mathbf{q}, \mathbf{Q}_0) | \mathbf{m}(\mathbf{q}) | \phi_J(\mathbf{q}, \mathbf{Q}_0) \rangle \langle \chi_A(\mathbf{Q}) | \chi_J(\mathbf{Q}) \rangle \quad (1.14)$$

The term $\langle \chi_A(\mathbf{Q}) | \chi_J(\mathbf{Q}) \rangle$ is known as the FC overlap integral.

In a semi-classical description of this approximation, there is little change in nuclear co-ordinate on the timescale of an electronic transition. Thus, in a figure such as 1.2, the most probable electronic transitions are represented by a vertical line.

If $\langle \phi_A(\mathbf{q}, \mathbf{Q}) | \mathbf{m}(\mathbf{q}) | \phi_J(\mathbf{q}, \mathbf{Q}) \rangle$ is non-zero, then the transition is said to be an allowed electronic transition. The intensity of a vibrational sideline is dictated by the Huang–Rhys parameter (S). The Huang–Rhys parameter is related to the relative displacement (D) of the ground and excited state potentials. When the BO and FC approximations hold, the intensity pattern of vibrational structure is given by the S values.

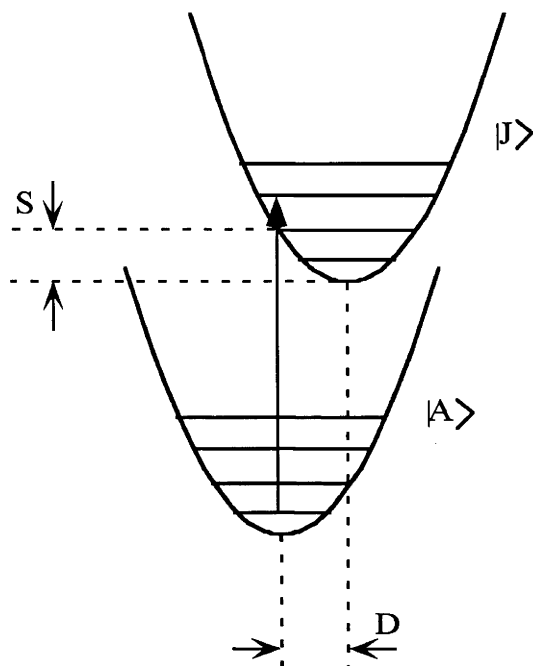


Figure 1.2: Potential energy curves for a ground state, A, and an excited state, J. Vertical arrows show various Franck–Condon allowed transitions. D is the displacement of the two surfaces, which is related to S, the Huang–Rhys parameter.

From a group theoretical point of view, a transition is allowed when the direct product of the transition dipole moment operator and the ground and excited state wavefunctions contain the totally symmetric irreducible representation of the point group of the system under consideration. While the BO and FC approximations hold, vibrational progressions in totally symmetric modes prevail. In systems where the FC approximation is not valid, transitions whose direct product contain the totally symmetric irreducible representation (but whose vibrational modes are not totally symmetric themselves) start to dominate.

Equation 1.12 may also be expanded in a Taylor series about Q_0 , the first term of which is the FC approximation (equation 1.14). When equation 1.14 is zero, then the transition is said to be electronically or FC forbidden. In this case, if the higher terms in the Taylor expression are non-zero, then the FC approximation clearly fails and the transition is

said to be vibrationally induced. The inducing mode (or modes) are the non-totally symmetric vibrations referred to in the previous paragraph. This dependence of the electronic motion upon nuclear co-ordinate is referred to as Herzberg–Teller (HT) coupling. In this scenario, the adiabatic description holds, but the crude adiabatic approximation is no longer valid.

If electronic potentials are degenerate, then the BO approximation ceases to be valid. The system can no longer be said to be adiabatic and ϕ_k is a strong function of nuclear co-ordinate. This failure of the BO approximation is called the Jahn–Teller (JT) effect. A similar, but not so large, effect occurs when electronic levels are close (say, within a few vibrational quanta). This situation is called the pseudo JT effect. In the JT effect, a loss of electronic degeneracy occurs along the co-ordinate of a non-totally symmetric vibration.

The preceding discussion follows that of Piepho and Schatz [11]. The reader is directed to this reference and to Herzberg [12] for further information.

1.3 Laser selective spectroscopy

In any condensed phase, there is a distribution of local environments. This leads to a distribution of transition energies and the resulting optical feature is said to be inhomogeneously broadened (see figure 1.3). The bandwidth of a laser may be far narrower than that of an inhomogeneously broadened band. The use of a laser enables the selection of a subset of chromophores from an inhomogeneously broadened transition. Detailed information about a chromophore and its environment may be obtained through the use of such selective techniques.

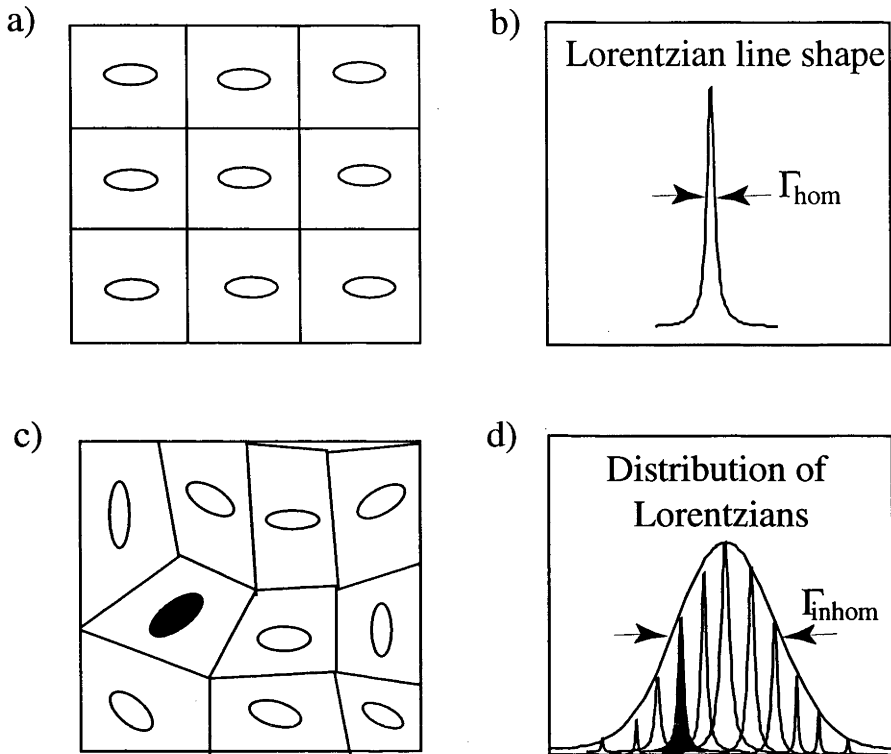


Figure 1.3: Inhomogeneous broadening. A perfect crystal, a), gives rise to a Lorentzian line shape with width Γ_{hom} , b). Disordered systems, c), lead to a distribution of Lorentzian lineshapes with width Γ_{inhom} , d).

There are two main contributions to the homogeneous linewidth of an optical transition: the lifetime of the excited state, and the pure dephasing time. The homogeneous linewidth may be expressed as follows:

$$\Gamma_{\text{hom}} = \frac{1}{\pi} \left(\frac{1}{2T_1} + \frac{1}{T_2^*} \right) \quad (1.15)$$

where T_1 is the lifetime of the excited state and T_2^* is the pure dephasing time. T_2^* is strongly temperature dependent, leading to a rapid increase in the transition linewidth with increase in temperature. At lowest temperatures, however, the linewidth of allowed transitions is dominated by the lifetime of the excited state. Laser selective experiments are therefore performed at liquid helium temperatures. At these temperatures the ratio of Γ_{hom} to Γ_{inhom} is minimised; therefore the selectivity is maximised.

Optical lineshapes in the solid state have a characteristic contour. Not only is there a Lorentzian shape from the electronic transition, but also a sideband (usually best described as a Gaussian) which is as a result of coupling between the electronic transition and lattice vibrations (phonons) of the host. These two components are referred to as the zero-phonon line (ZPL) and the phonon wing (PW) respectively (see figure 1.4). Their relative areas are given by the Debye–Waller factor (DWF), α .

$$\alpha = \frac{A_{\text{ZPL}}}{A_{\text{ZPL}} + A_{\text{PW}}} \quad (1.16)$$

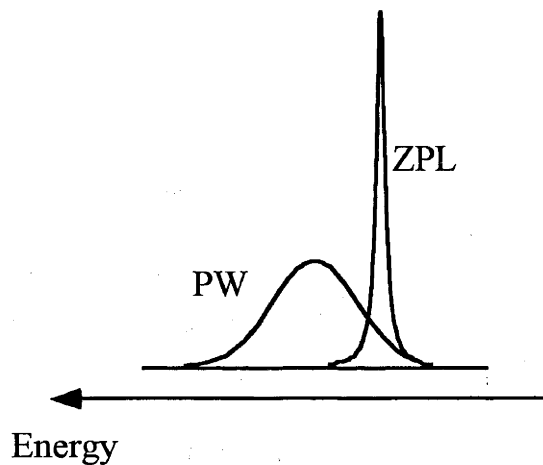


Figure 1.4: A schematic representation of a zero-phonon line (ZPL) and a phonon wing (PW).

Laser selective techniques include fluorescence line narrowing, excitation line narrowing, spectral hole-burning and photon echo. This work concentrates on two laser selective techniques: spectral hole-burning and fluorescence line narrowing. Most experiments have been conducted using the former technique, although the latter has been used in some experiments.

1.3.1 Fluorescence line narrowing

Fluorescence line narrowing (FLN) is a technique that involves the observation of narrowed fluorescence from selectively excited chromophores. The basic principle is depicted in figure 1.5.

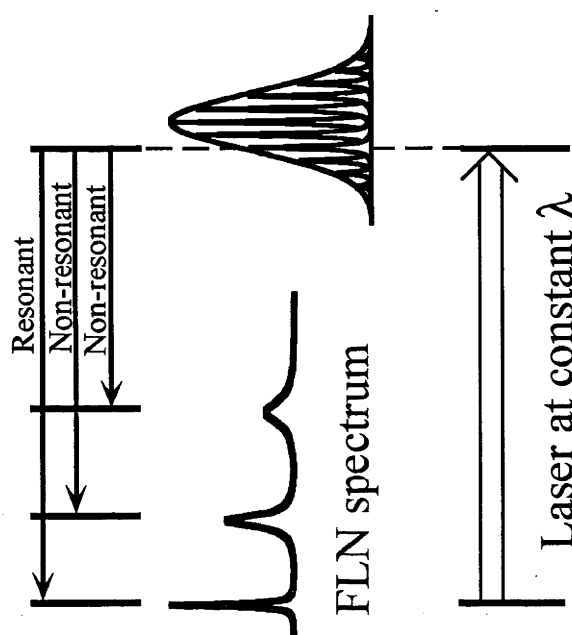


Figure 1.5: A schematic representation of a fluorescence line narrowing (FLN) experiment. FLN may be measured either resonantly or non-resonantly.

Fluorescence may be detected either resonantly or non-resonantly. In the former case precautions have to be taken to prevent the detection of the exciting laser light.

Because of the selectivity of the excitation, detailed spectra of the subset of chromophores whose transition energy coincides with the laser energy may be obtained. Narrowed emission experiments have the potential to provide detailed information about vibrational frequencies and vibronic interactions. Also, selective excitation can be used to 'see' into an inhomogeneously broadened band and to probe changes which occur across the band and observe details which may be masked by the inhomogeneous broadening.

1.3.2 Spectral hole-burning

Spectral hole-burning involves selectively depleting the ground state population of transitions whose energy coincides with that of the laser. This leads to a 'hole' in the spectrum where the chromophores had previously been absorbing, and a 'photoproduct' where the new absorption occurs. This depopulation may fall into one of three categories: transient hole-burning, photochemical hole-burning and photophysical hole-burning.

Transient hole-burning occurs as a result of the chromophore relaxing via some metastable state. This situation is depicted in figure 1.6. This metastable trapping state may either be the excited state of the transition under consideration, some long-lived excited state such as a triplet state, or a hyperfine level of the ground state [4].

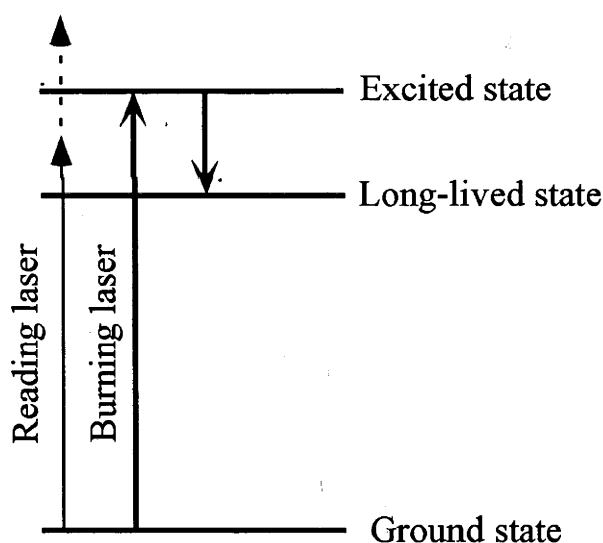


Figure 1.6: Transient hole-burning. The ground state is depleted by chromophores being trapped in a long-lived state. This metastable trapping state may either be the excited state of the transition under consideration, some long-lived excited state such as a triplet state, or a hyperfine level of the ground state. The reading laser is then scanned over the region of interest.

Photochemical and photophysical changes produce what are known as persistent spectral holes. Measurements are normally made on a timescale of seconds to minutes (although changes on the scale of hours to days have been measured [13]).

As the name suggests, photochemical hole-burning involves the selected chromophores undergoing a chemical change of some description. Photoionisations and tautomerisms are common examples. The changes which the chromophores undergo are relatively large; therefore photochemical hole-burning is often characterised by relatively large energy differences between the hole and the photoproduct (see figure 1.7).

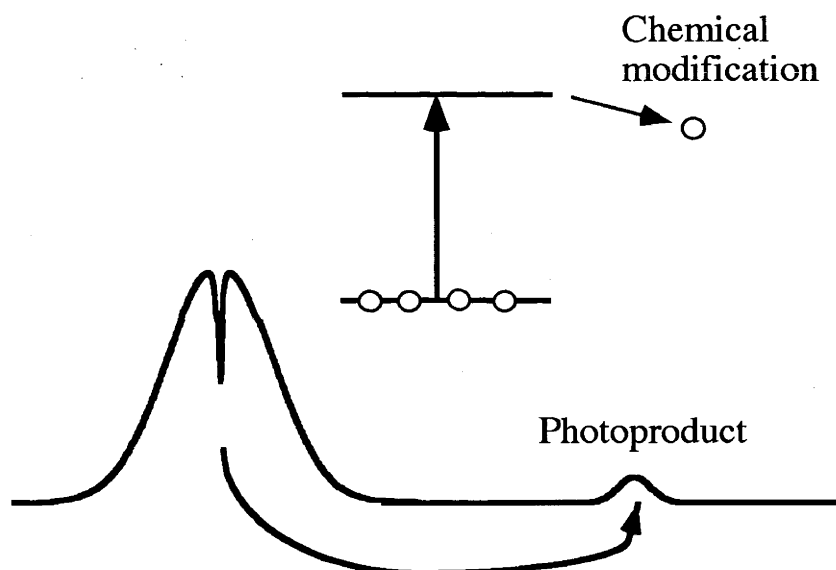


Figure 1.7: Photochemical hole-burning. Selective depletion occurs by chemical modification. This process is often characterised by large transition energy differences between the hole and the photoproduct.

Photophysical hole-burning may be understood in terms of a 'rearrangement' of the chromophore in its environment. This process is normally described in terms of a two level system (or TLS) model [1, 2, 4] (see figure 1.8).

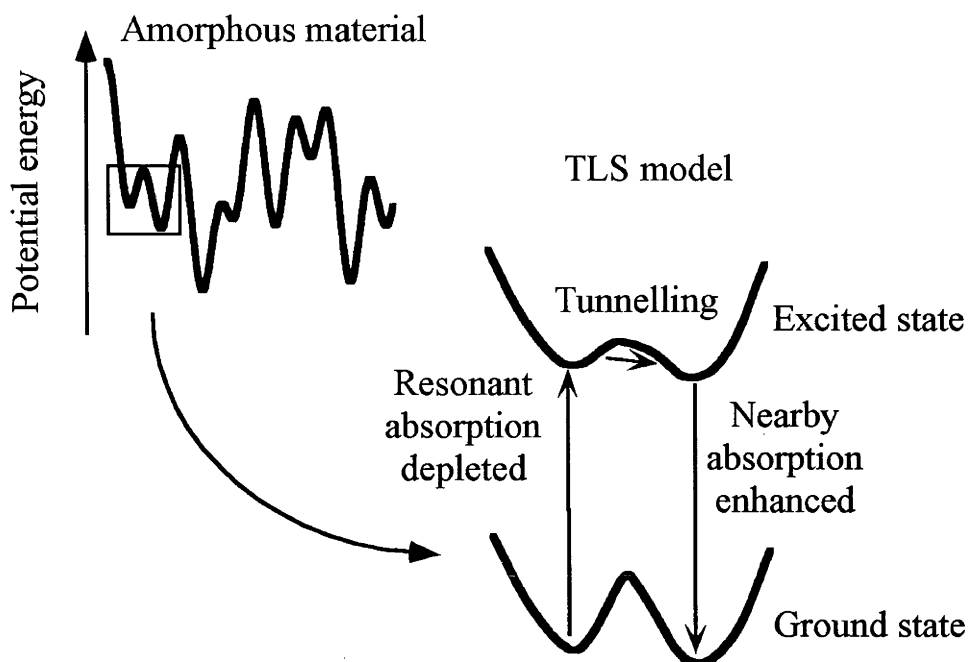


Figure 1.8: The two level system (TLS) model. Amorphous environments may be described in terms of two neighbouring potentials. Photophysical hole-burning occurs by means of tunnelling in the excited state.

In an amorphous environment, there is a distribution of potential wells. Taking two adjacent wells for the model, a chromophore is excited from the ground state to the excited state. In the excited state, the probability of tunnelling between wells may be greater. Thus, the resonant absorption is depleted, and nearby absorption is enhanced. This is only a small change that the chromophore is undergoing; therefore the difference in transition energy between the hole and the photoproduct tends to be small (see figure 1.9). This small energy difference is often characteristic of photophysical hole-burning.

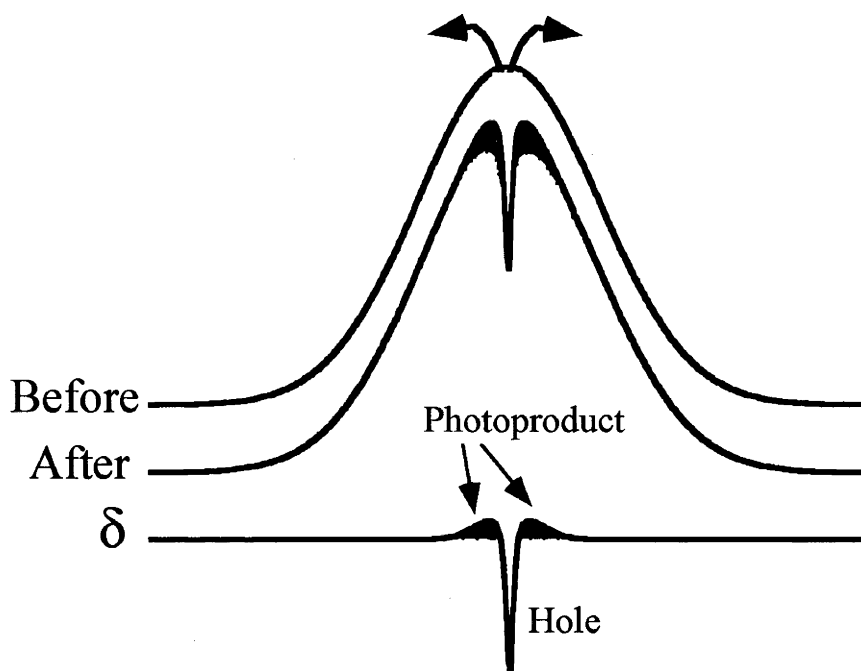


Figure 1.9: The changes in a spectrum upon photophysical hole-burning. Photophysical hole-burning involves small changes and is often characterised by a small difference in transition energy between a spectral hole and the accompanying photoproduct. δ denotes the difference between the absorption after burning less the absorption before burning.

The measure of how readily a system undergoes spectral hole-burning is quantified by the hole-burning quantum efficiency. The hole-burning quantum efficiency may be viewed as the probability of a photoinduced change per chromophore per photon absorbed [14]. For persistent spectral holes, hole-burning quantum efficiencies may range from as high as ~ 0.1 for efficient chemical hole-burning systems, through to $\sim 10^{-6}$ for photophysical hole-burning [15]. As an example, chlorin, which undergoes spectral hole-burning with a mechanism involving the tautomerism of the two inner protons, is reported as having a hole-burning quantum efficiency of $(3 \pm 0.5) \times 10^{-4}$ [15].

In most systems, the hole-burning process may be reversed. Because some of the barriers between TLS potentials are small (relative to kT), holes begin to fill spontaneously. A slight rise in temperature (say, a few tens of K) is often enough to eradicate a spectral hole. Systems which display spectral hole-burning at temperatures higher than the order of tens of K are rare, as processes such as dephasing and spectral diffusion (a concept introduced later) lead to hole widths being so broad that they are no longer observable. Systems in which measurable spectral holes may be burnt at high temperatures (say, at room temperature) are greatly sought after for technological applications such as data storage and processing [16-18].

The development of the shape of a spectral hole with increased burning time may be modelled [19]. Initially, a linear increase in the depth of the ZPL with burn time is observed. At the energy of the laser there are also PWs of chromophores whose ZPL is to the red of the burn energy. At longer burn times a wing appears on the low energy side of the zero-phonon hole, which occurs as a result of the depletion of chromophores whose PW coincides with the energy of the laser (see figure 1.10). Direct observation of the depletion of the PW is not readily made, as the PW is broad relative to the ZPL and the removal of a large area of PW will only result in a relatively small change in absorption at a given wavelength.

As the hole-burning process progresses, a point will be reached where all the chromophores having ZPLs at the laser energy have been bleached. The hole is then said to be saturated. Any further depletion happens by means of chromophores whose PWs absorb at the energy of the laser. From this point on, the PW of the hole grows preferentially to the ZPL.

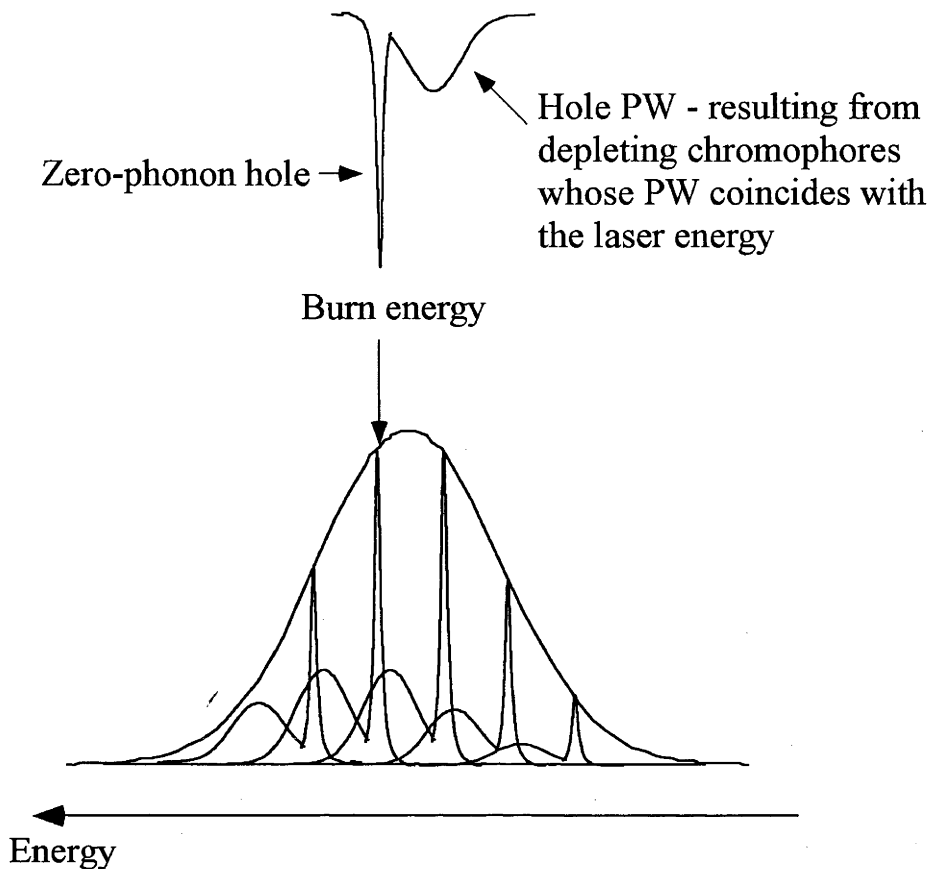


Figure 1.10: The shape of a spectral hole. A hole has a zero-phonon line (ZPL) resulting from the depletion of chromophores whose ZPLs are resonant with the laser, and a phonon wing (PW) from the depletion of chromophores whose PW is resonant with the laser.

When a spectral hole is burnt, chromophores whose transition dipoles are at a small angle to the polarisation direction of the exciting light will be preferentially selected. Therefore, hole-burning may be used to select not only chromophores with a particular transition energy, but also those of a small range of orientations. This is especially useful in experiments involving the application of an external field, as the orientation of the chromophore relative to the direction of the applied field can be controlled by the use of this technique.

A spectral hole may be used as a 'frequency marker' for a change that occurs upon the application of an externally applied field. The work in this thesis is concerned with magnetic and electric fields in particular. The relatively small changes in broadband lineshapes arising from the

application of an external field may be difficult to observe and/or interpret. Changes may become easier to observe and interpret on the narrower spectral hole.

The preceding discussion is only a brief introduction to the concepts pertinent to this work. Further information may be found in references [1-4, 20].

1.4 The Zeeman effect and magnetic circular dichroism

The Zeeman effect refers to the interaction of a state with an externally applied magnetic field. Shifts in transition energies as a function of applied field give information about excited state angular momenta and transition mechanisms.

In an applied magnetic field, a degenerate level may split. In the case of the Q transition in symmetric metallo-porphyrins and phthalocyanines, the excited (1E_u) state is nominally degenerate. The degeneracy of this state is often lifted by crystal fields within the matrix. Under these circumstances, a Zeeman shift of the split levels may still be observed, but the magnitude of this shift is reduced. The magnitude of this reduced Zeeman, $\Delta\nu_B$, shift may be modelled by solving the secular equation for an appropriate electronic Hamiltonian [21].

$$\Delta\nu_B = \pm \frac{\Delta\nu_0}{2} \left\{ \left[1 + \left(\frac{2\mu_B \cdot \mathbf{B}}{\Delta\nu_0} \right)^2 \right]^{1/2} - 1 \right\} \quad (1.17)$$

where $\Delta\nu_0$ is the crystal-field (CF) splitting, μ_B is the molecular static magnetic moment of the unsplit excited state and \mathbf{B} is the magnetic field.

Magnetic circular dichroism (MCD) is a manifestation of the Faraday effect. For an MCD experiment, as in a circular dichroism experiment, the absorption of left circularly polarised light minus the absorption of right circularly polarised light is measured. Unlike circular dichroism MCD arises as a result of Zeeman interactions rather than the inherent chirality of the system under consideration.

MCD is generally described by three terms: \mathcal{A} -terms, \mathcal{B} -terms and \mathcal{C} -terms [11] (see figure 1.11).

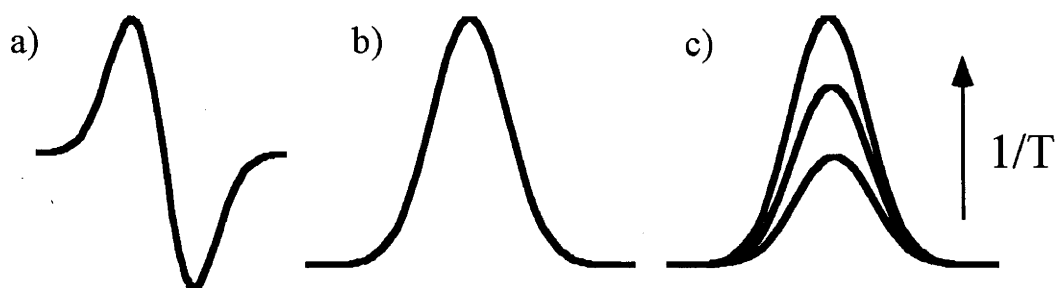


Figure 1.11: MCD is generally described by three terms. a) \mathcal{A} -terms which have a derivative shape. b) \mathcal{B} -terms which are single signed. c) \mathcal{C} -terms which are also single signed, but have a $1/T$ temperature dependence.

\mathcal{A} -terms arise as a result of excited state degeneracy. In the presence of the magnetic field the degenerate level splits. This leads to a characteristic derivative shape.

\mathcal{B} -terms are what make MCD a ubiquitous phenomenon. \mathcal{B} -terms are single signed and are caused by field-induced mixing of states.

\mathcal{C} -terms are also single signed. They are distinguishable from \mathcal{B} -terms because the magnitude of a \mathcal{C} -term is inversely proportional to temperature. This characteristic temperature dependence is caused by ground state degeneracy. Upon the application of a magnetic field, the degenerate level splits. A Boltzmann population distribution is found in the magnetic-field-split ground state levels.

The Q band of a symmetric metallo-porphyrin derivative displays an \mathcal{A} -term for the MCD. When the chromophore is placed into an amorphous environment, the degeneracy of the excited state is split by crystal fields within the host. The MCD signal of the Q band still retains its derivative appearance, but, because the degeneracy is no longer present, this signal is in fact two overlapping, oppositely signed \mathcal{B} -terms. This type of signal is known as a pseudo \mathcal{A} -term (see figure 1.12). Such a signal occurs in systems where the lifting of the degeneracy is less than the linewidth of the transition.

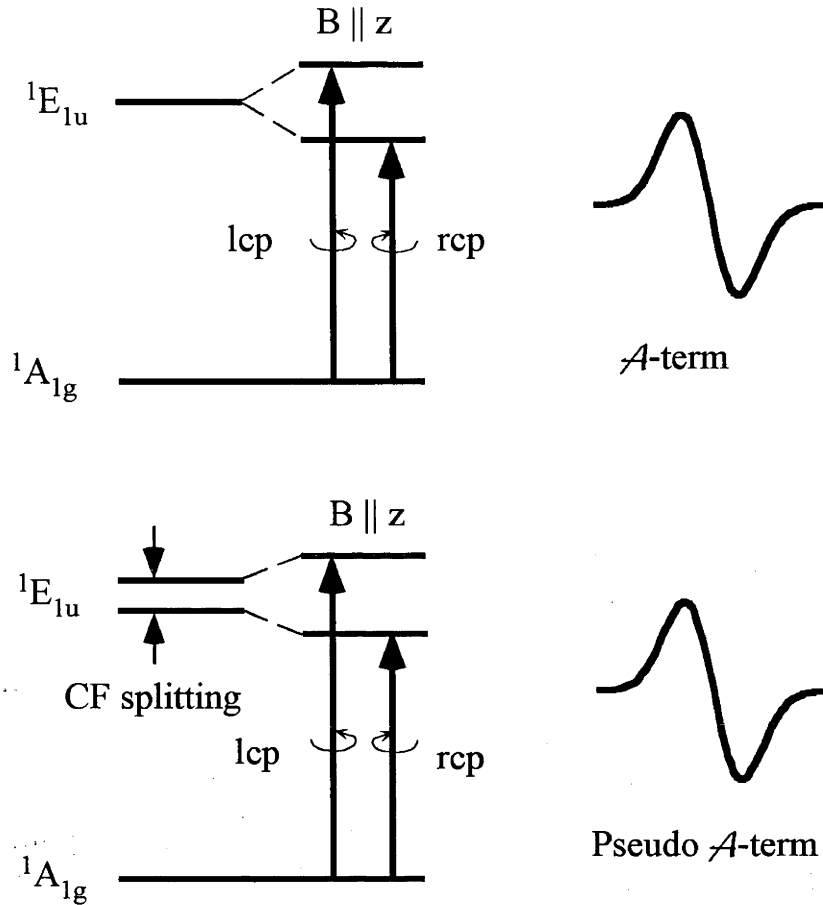


Figure 1.12: Pseudo \mathcal{A} -terms have a similar shape to \mathcal{A} -terms, but are in fact two overlapping \mathcal{B} -terms arising from nominally degenerate states which have been split.

MCD band shapes are commonly analysed using a technique known as the method of moments [11]. The n th moment is given by:

$$\int f(\omega)(\omega - \omega_0)^n d\omega \quad (1.18)$$

where $f(\omega)$ describes the band shape of some observable as a function of energy, ω . ω_0 is some energy about which the moments are taken. Usually, ω_0 is some average energy. The integration in equation 1.18 is taken between the ends of the band. These points must be chosen such that $f(\omega)=0$. Thus, moments may only be calculated for discrete bands. Moment analysis is not appropriate for the MCD of spectral holes.

The advantage of measuring the MCD of spectral holes is that changes across the band may be measured, and information about the distribution of parameters may be obtained.

1.5 The Stark effect

If the assumption is made that a guest species is described as a point dipole [22], then, upon application of an external electric field, \mathbf{E}_{app} , the transition under consideration will undergo a frequency shift $\Delta\nu_{\text{E}}$:

$$\Delta\nu_{\text{E}} = \frac{1}{h} \left(\Delta\boldsymbol{\mu}_{\text{eff}} \mathbf{f} \mathbf{E}_{\text{app}} + \frac{1}{2} \mathbf{f} \mathbf{E}_{\text{app}} \Delta\boldsymbol{\alpha} \mathbf{f} \mathbf{E}_{\text{app}} \right) \quad (1.19)$$

where: $\Delta\boldsymbol{\mu}_{\text{eff}}$ is the difference in dipole moments between the ground and excited states; $\Delta\boldsymbol{\alpha}$ is the difference in polarisability tensors between the two states; and \mathbf{f} is a tensor which transforms the applied field into the local field experienced by the host. When \mathbf{f} is effectively isotropic, a Lorentz field correction can be applied [23].

$$\mathbf{f} = \frac{\epsilon + 2}{3} \quad (1.20)$$

where ϵ is the dielectric constant for the host.

The Stark effect observed in the experiments reported here is linear in the electric field; therefore the second portion of equation (1.19) may be neglected, leading to:

$$\Delta\nu_{\text{E}} = \frac{\mathbf{f}}{h} \Delta\boldsymbol{\mu}_{\text{eff}} \mathbf{E}_{\text{app}} \quad (1.21)$$

In a solid state environment, a dipole may be induced in a chromophore as a result of host–guest interactions. $\Delta\boldsymbol{\mu}_{\text{eff}}$ may therefore be broken into two components. The first of these, $\Delta\boldsymbol{\mu}_{\text{mol}}$, is associated with a dipole intrinsic to the species. $\Delta\boldsymbol{\mu}_{\text{mol}}$ often has a well-defined magnitude and is fixed at some angle, θ_{mol} , to the transition dipole, \mathbf{D} . The other component, $\Delta\boldsymbol{\mu}_{\text{ind}}$, is a change in dipole moment induced by the environment experienced by the species. $\Delta\boldsymbol{\mu}_{\text{ind}}$ more likely has a

distribution of magnitudes and angles. The variation of the magnitude of $\Delta\mu_{\text{ind}}$ may be described by [24]:

$$G(|\Delta\mu_{\text{ind}}|) = \frac{2 \times |\Delta\mu_{\text{ind}}|}{(\Delta\mu'_{\text{ind}})^2} \text{Exp} \left[- \left(\frac{|\Delta\mu_{\text{ind}}|}{\Delta\mu'_{\text{ind}}} \right)^2 \right] \quad (1.22)$$

$\Delta\mu'_{\text{ind}}$ is the root mean square value of the matrix-induced dipole moment. If \mathbf{E}_{app} is parallel to $\Delta\mu_{\text{ind}}$, then a hole burnt at zero field develops a shape with a double maximum upon the application of a strong field. If \mathbf{E}_{app} is perpendicular to $\Delta\mu_{\text{mol}}$, then the hole shape will broaden without splitting. For reasons associated with their distributed values, induced dipole moment changes are likely to lead to a broadening rather than an apparent splitting. (These changes in hole shape in an applied electric field are discussed in greater detail in chapter 5.) Hole-burning experiments using polarised light allow the orientation of \mathbf{E}_{app} to $\Delta\mu_{\text{mol}}$ to be influenced experimentally.

Upon the application of an electric field, the different dipole moments, molecular and induced, and their various angular dependencies, result in distinctive hole shapes. With careful modelling and analysis, these components may be separated. Hole-burning Stark spectroscopy enables the detection of changes in the symmetry of a molecule and its environment.

2. Experimental Methods and Techniques

2.1 Sample preparation

The greater part of the work was performed on zinc phthalocyanine (ZnPc), although zinc octaethylporphyrin (ZnOep), zinc tetrabenzoporphyrin (ZnTbp), zinc 1,4,8,11,15,18,22,25-octabutoxyphthalocyanine (ZnObuPc) and lutecium bisphthalocyanine (LuPc₂) have also been investigated. These molecules are all depicted in figure 2.1.

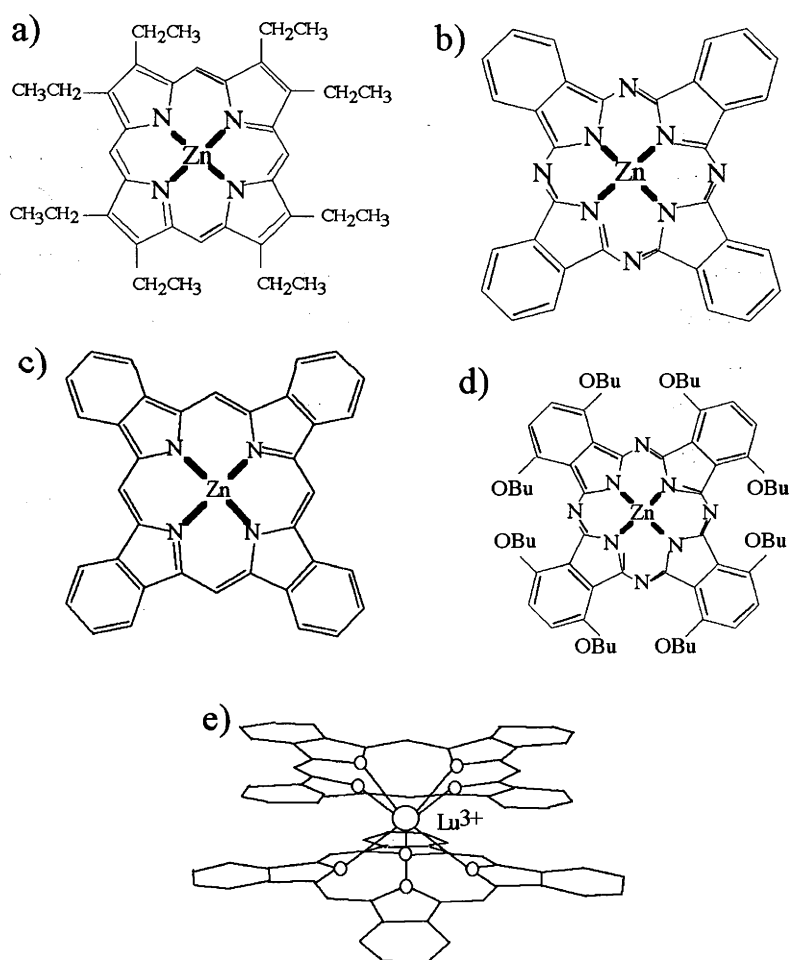


Figure 2.1: Chromophores studied in this thesis. a) Zinc octaethylporphyrin (ZnOep). b) Zinc phthalocyanine (ZnPc). c) Zinc tetrabenzoporphyrin (ZnTbp). d) Zinc 1,4,8,11,18,22,25-octabutoxyphthalocyanine (ZnObuPc). e) Lutecium bisphthalocyanine (LuPc₂).

Most of these substances were doped into polymer films. In addition, some work with samples doped into glasses was done. The polymers most commonly used were polymethylmethacrylate (PMMA) and polyvinylbutyral (PVB). (See figure 2.2.)

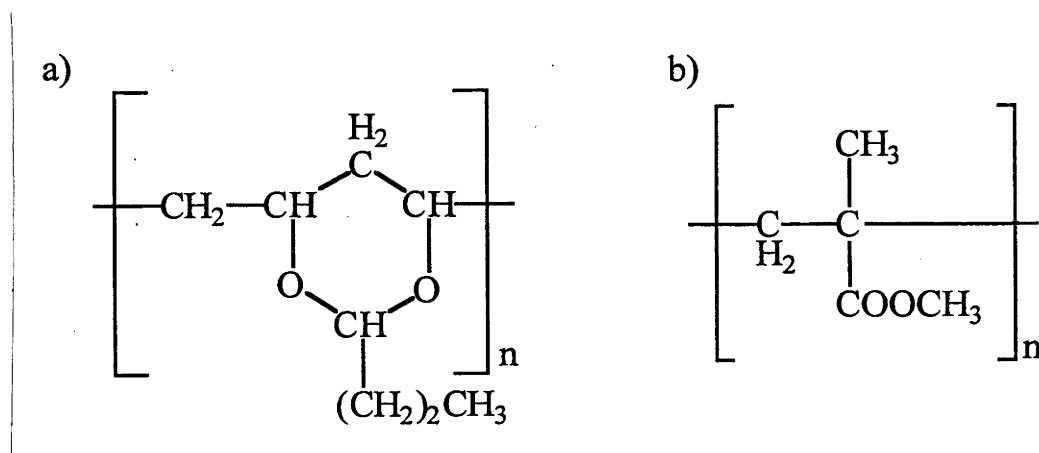


Figure 2.2: The two polymers most frequently used as host matrices for the experiments. a) Polyvinylbutyral. b) Polymethylmethacrylate.

Polymer films were made by one of two techniques. The most frequently used of these techniques was that of mixing a solution of the host substance in a solvent (usually tetrahydrofuran (THF)) with a solution of the polymer in the same solvent. The resulting mixture was left to dry. The films produced this way were of the order of 0.1 – 1 mm in thickness.

The other film preparation technique was used when samples with no solvent present in them were required. The only host-guest combination for which this style of experiment was performed was ZnPc in PMMA. These samples were prepared as described below [25]:

Commercially available methylmethacrylate (MMA) (obtained from Aldrich) contains an inhibitor (hydroquinone monomethyl ether) to prevent polymerisation. The MMA was treated as follows:

- a) The inhibitor was removed by distillation.
- b) ZnPc was dissolved in the purified MMA (the degree of dissolution was only slight).
- c) 2,2'-azobisisobutyronitrile (AIBN) was added to the solution as an initiator for polymerisation. The ratio AIBN/MMA was ~ 1 mg:3 ml.
- d) This mixture was then heated in stages of 1 – 2 days: from ~ 40°C to ~ 50°C and finally to ~ 80°C.

There were a number of points in this process where care was required. Of primary concern was ensuring that the resulting plastic was of high optical quality. The presence of bubbles rendered the sample optically useless, thus the slow heating process was necessary. Likewise, the vessel in which the polymerisation was performed needed to be firmly sealed and care taken not to exceed the ratio of AIBN to MMA, as lack of attention to these procedures lead to the appearance of bubbles in the sample. Careful sealing of the container also prevented the volatile MMA evaporating before polymerisation.

Once a solid sample had been obtained it was removed from its container and heated at ~ 80°C for a further 1 – 2 days. After it had been polymerised in a closed vessel, the sample became strained and consequently was strongly birefringent. The second heating served to anneal the sample and remove the birefringence.

Samples were prepared for holographic Stark experiments by the doped polymer film being sandwiched between two transparent electrodes. The electrodes consisted of a pair of glass plates coated with a conducting film of indium tin oxide. The electrode-sample 'sandwich' was put in a press in an oven overnight and heated to $\sim 80^{\circ}\text{C}$. This procedure ensured good contact between the sample and the electrode - the heat causing the sample to melt slightly and adhere to the electrodes.

2.2 Measurement techniques

The work conducted here falls roughly into two types of experimental techniques: 'low resolution' experiments and 'high resolution' experiments. The low resolution experiments consisted of broadband absorption and MCD measurements, FLN, and hole-burning experiments where the hole was read out with a monochromator. High resolution experiments were performed by burning a hole with a single-frequency laser and then scanning the wavelength of the same laser across the feature.

2.2.1 Low resolution experiments

Broadband absorption and MCD spectra and the lower resolution spectral holes were obtained using the same experimental set-up. This apparatus is shown in figure 2.3.

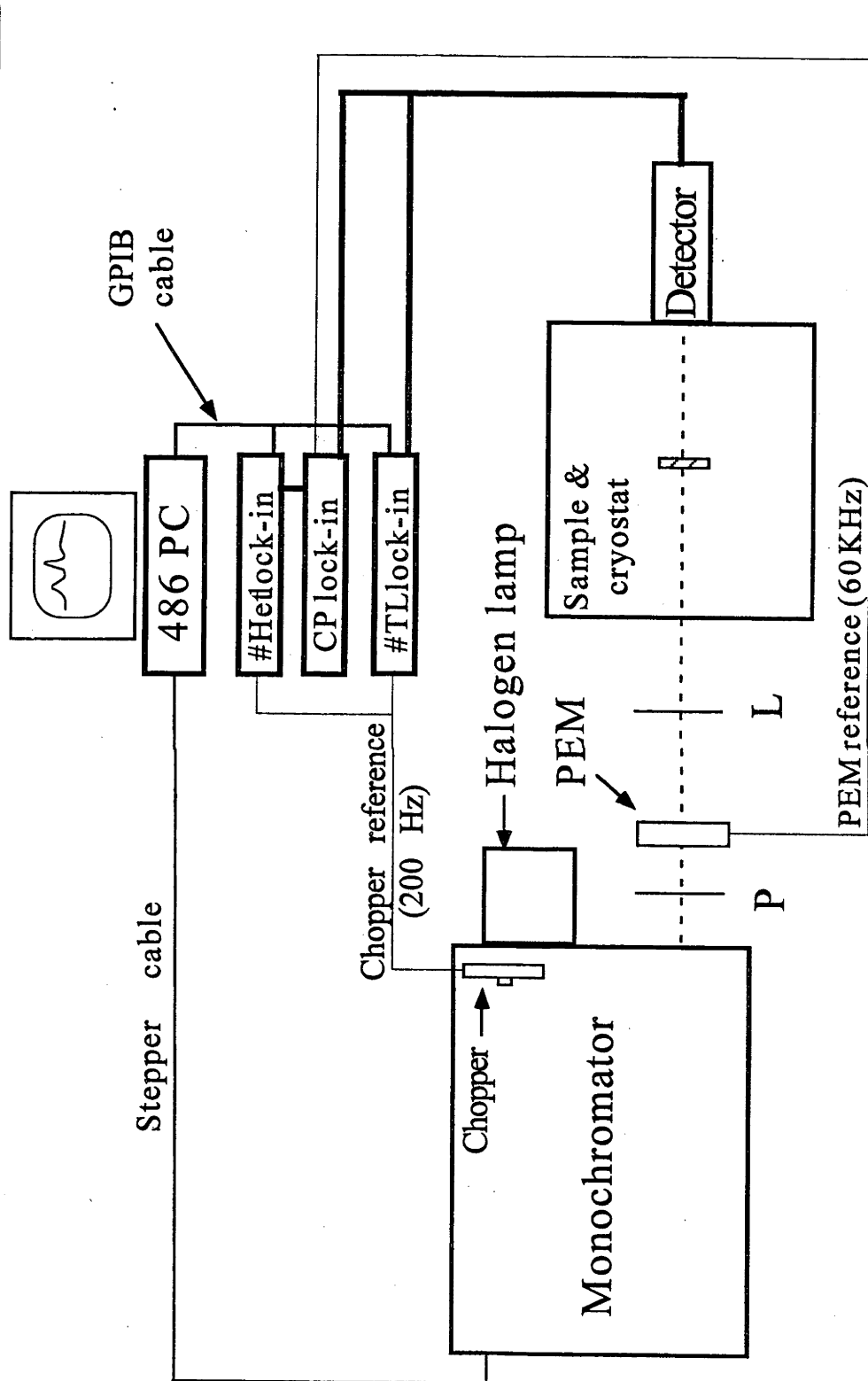


Figure 2.3: A schematic diagram of the apparatus used to measure broadband absorption and MCD. PEM = photoelastic modulator, P = polariser, L = lens.

This apparatus enables the simultaneous measurement of absorption and MCD [26]. A heterodyning technique was used to eliminate artifacts and therefore ensure a reliable baseline for the MCD. The interrogating beam was chopped with a mechanical chopper and left and right circularly polarised (lcp and rcp) light were produced by the use of a polariser and a photoelastic modulator. The signal from the detector was sent to two lock-in amplifiers - one referenced to the chopper (the TL lock-in, giving the intensity signal - I) and the other referenced to the photoelastic modulator (the CP lock-in, giving the lcp intensity minus the rcp intensity - ΔI). The output from the CP lock-in was sent to the heterodyning lock-in which was referenced to the chopper. This step rejected any artefacts from the MCD.

The equipment was driven and the data collected by computer code written in Quick Basic.

Absorption and MCD spectra were generated on the computer. The relative absorption was calculated by taking the intensity in the absence of the sample divided by the intensity in the presence of the sample - the former having been previously measured. Then the ratio $\Delta I/I$ was calculated. In the limit where $\Delta I/I \ll 0.1$ this ratio is proportional to the MCD. The MCD was calibrated according to the proportionality constant.

The data acquisition code was such that the full dynamic range of the lock-in amplifiers could be used and the changes in scale were joined seamlessly.

Detection was generally made with a Thorn EMI S20 photomultiplier tube. Broadband measurements were performed with 1200 grooves/mm gratings blazed at 500 nm. The reading out of spectral holes was done with 2400 grooves/mm gratings blazed at 240 nm. The latter arrangement made a resolution of $\sim 1 \text{ cm}^{-1}$ possible.

When the absorption/MCD apparatus was used, samples were placed in an Oxford Instruments SM4 cryostat. Samples were immersed in super-fluid helium (1.8 K). The cryostat has a split-pair superconducting magnet which allows fields of up to 6 T to be applied either parallel or perpendicular to the propagation direction of the light.

The FLN spectra were obtained on the apparatus shown in figure 2.4.

The photon-counting technique used in this apparatus (designed for Raman experiments) made possible the detection of very small signals. The detector used was a cooled C31034a GaAs photomultiplier.

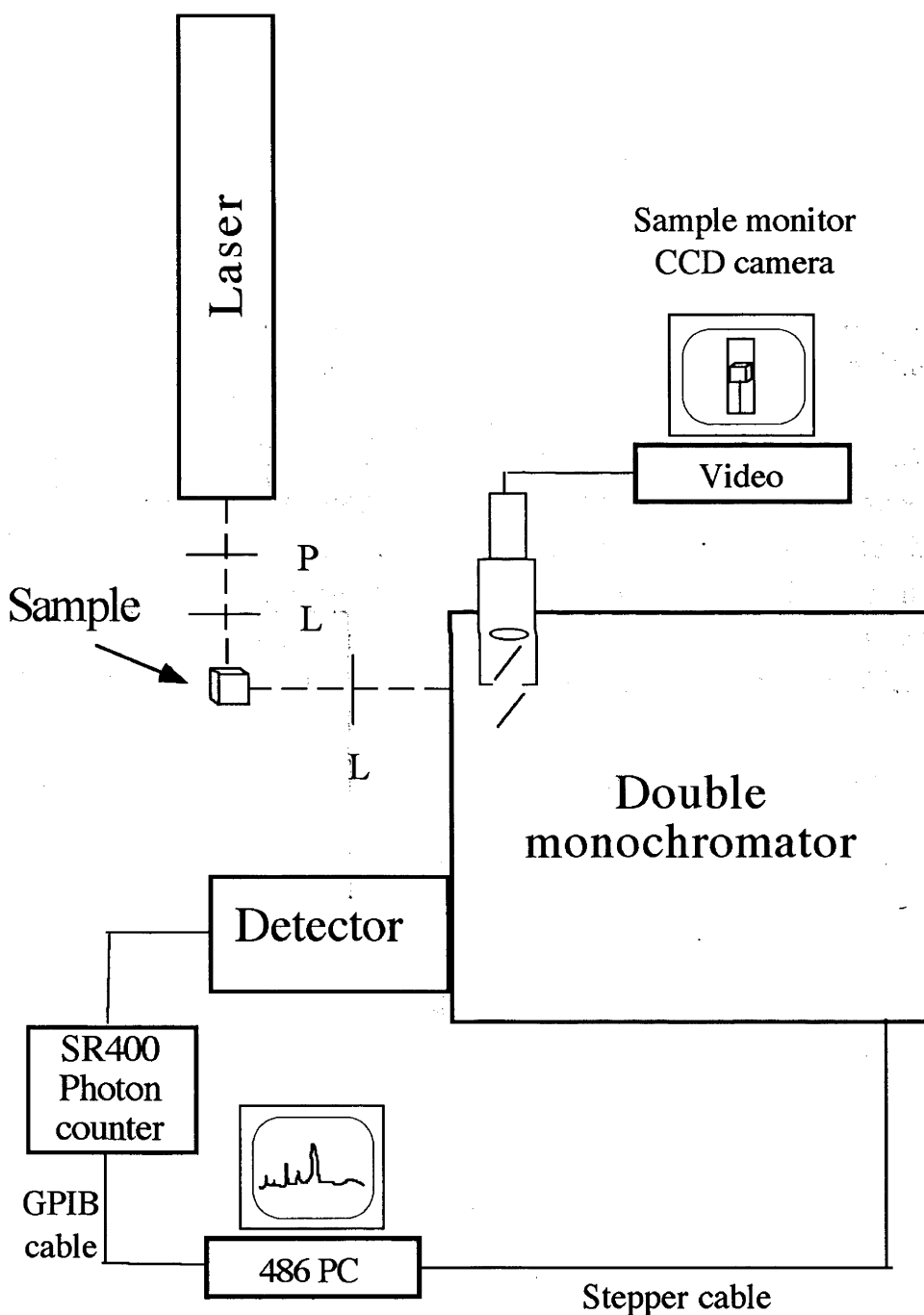


Figure 2.4: A schematic diagram of the apparatus used to obtain FLN spectra. P = polariser, L = lens.

Sample cooling was achieved through the use of a flow tube [27]. This is a double-walled quartz tube. The outer section is evacuated. The inner section contains the sample and liquid helium boil-off is passed over it. Temperatures of ≥ 5 K are achievable through the use of this technique.

The lasers used for these experiments were a Spectra-Physics 164 Kr⁺ laser, a Spectra-Physics 156 HeNe laser (632.8 nm) and a Spectra-Physics 375 dye laser. There were also a number of experiments performed with a Melles Griot green HeNe laser (543 nm) and a Schwartz Electro-Optics Titan CWBB Ti:sapphire ring laser.

For the hole-burning experiments, the entire area of the sample was evenly illuminated with a laser power density of 0.1 – 10 mW/cm². Burn powers and times varied a little with the sample and the position in the absorption band where the hole was being burnt. Burn times were of the order of a few minutes through to half an hour.

When Zeeman and MCD experiments were performed on the spectral holes, fields of 0 – 5 T were used. A ‘hole MCD’ is obtained by measuring the MCD before the hole is burnt, measuring the MCD after the hole is burnt, and then subtracting the former from the latter.

2.2.2 High resolution hole-burning experiments

High resolution experiments were performed using a single-frequency scanning dye laser with DCM as the dye. Commonly, the steps involved in such an experiment are to burn the hole with a laser power and burn time appropriate to the quantum efficiency of the sample, then decrease the power of the laser (to prevent more burning occurring whilst the hole is being read) and scan the laser wavelength across the hole.

Such experiments are usually conducted in either transmission or emission. Transmission experiments were performed here using a Coherent CR-699 dye laser. The experimental set-up is depicted in figure 2.5.

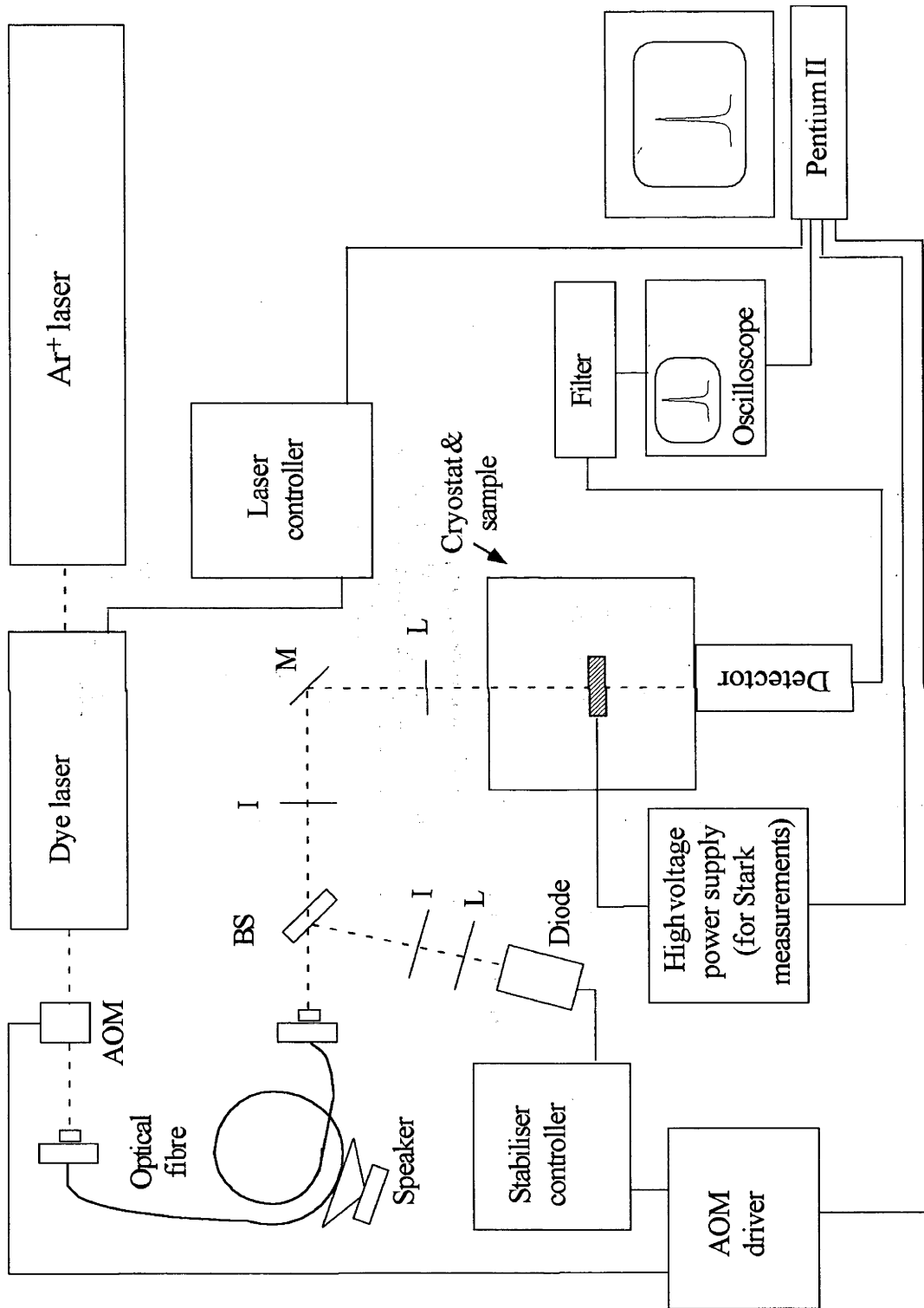


Figure 2.5: A schematic representation of the apparatus used to obtain the transmission read-out of spectral holes. BS = beam splitter, I = iris, L = lens, M = mirror.

Experiments were performed as described above with one slight modification: there was no difference in burn and read powers. Laser powers of $\sim 250 - 500 \text{ nW/cm}^2$ and burn times of 10 s – 3 minutes were used. For the read process, the laser was scanned 30 GHz in 3 s. Because of the very low burn powers and the difference between the burn and read times, no change in laser power was deemed necessary.

The acousto-optic modulator (AOM) in figure 2.5 not only served the purpose of switching the laser on and off for burning and reading, but also played a part in stabilising the intensity of the laser.

The holes burnt in these experiments were only a few per cent of the total absorption. In order to measure such a small change, the intensity stability of the read beam was crucial. Accordingly, a stabiliser was built which consisted of an AOM, a photodiode and feedback circuit.

The optical fibre and the speaker shown in figure 2.5 were there to prevent interference from parallel surfaces in the apparatus (eg cryostat windows and the faces of the sample) which act as an etalon.

This interference is a result of light reflecting off parallel surfaces (see figure 2.6). An analagous process may occur in transmission. This type of effect may be observed in the 'rainbow' patterns seen on an oily road, or on the surface of a bubble. In such examples, there is a thin film (the oil coating, or the wall of the bubble) whose thickness is of a similar magnitude to the wavelength of light. This results in the selective constructive or destructive interference of the light according to its wavelength. As the distance between the parallel surfaces is increased, this interference process occurs, but white light is not coherent over these lengths and so, on average, the effect may not be observed. Laser light, however, has a far greater coherence length ($\sim 300 \text{ m}$ in this case). This results in an appreciable sinusoidal modulation of the transmitted light as the wavelength is scanned. Such a background 'wave' is undesirable when small changes in transmitted intensity need to be measured. If the coherence length of the light is shortened, then, on average, this process is 'washed out'.

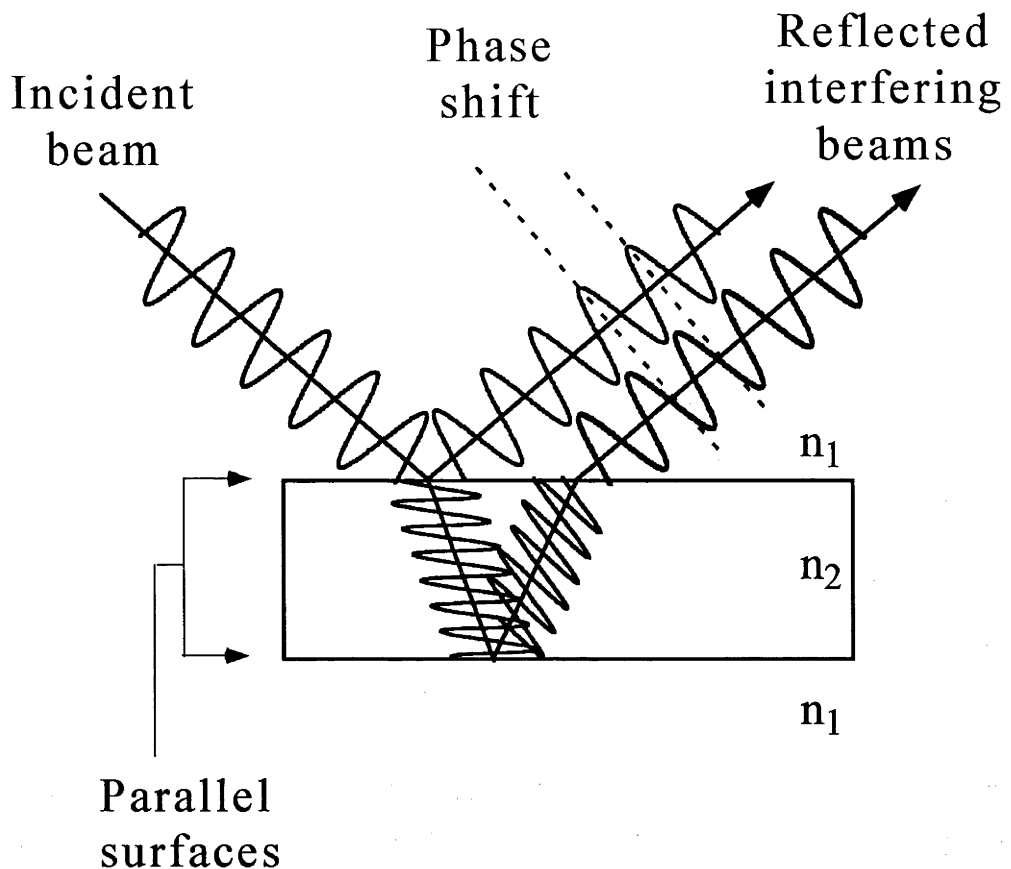


Figure 2.6: The interference of light reflected off two parallel surfaces. The refractive index is denoted by n_i . (After reference [28].)

The method used to shorten the coherence length of the light in this experiment was to pass it down a multimode fibre. The transverse mode of the laser output excites hundreds of modes within the fibre. Each of these modes has (in general) a slightly different optical path length (see figure 2.7). Light emerging from a given mode is not (in general) in phase with light from another mode. By means of this method, the interference effects are averaged out.

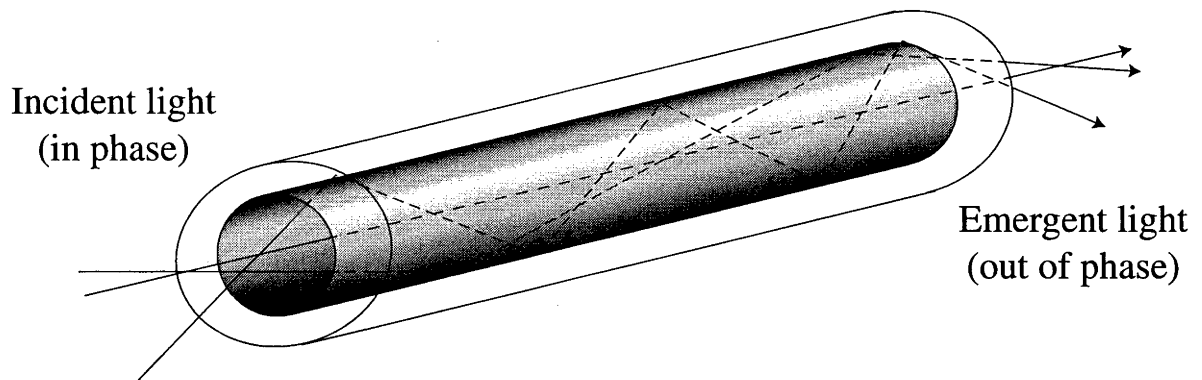


Figure 2.7: A schematic diagram of a step-index multimode fibre. Each of the modes has a different path length associated with it. Therefore the relative phase of the light is destroyed. (After reference [28].)

As a result of the introduction of the fibre, another problem arises. If the output of the fibre is projected onto a screen, then a speckle pattern may be observed. When an average is taken across the area of the beam (as is the case when the light intensity is measured with a detector) there are no variations in intensity as a result of interference. When the fine structure of the beam area is considered, however, then interference effects may be observed. The speckle pattern occurs as a result of the emergent light from the various fibre modes interfering with each other. This speckle pattern changes with time as a result of pointing instabilities in the dye laser. Because of the different optical components that the beam to the diode used in the intensity stabiliser, and the beam to the detector passed through, the two detectors were not seeing the same beam profile (for example, the beam may have been slightly clipped in either case). Spatial instabilities were seen as intensity instabilities by either or both of the detectors. These intensity variations prevented the measurement of the small spectral holes. This problem was alleviated by averaging out the speckle pattern.

The speckle pattern may be 'washed out' by shaking the fibre at a frequency higher than the characteristic frequency of the measurement. Shaking the fibre (by taping it to the speaker) changes the optical path lengths of the modes in the fibre. The variations in the speckle pattern then happen at higher frequencies (\sim kHz in this case) than the measurement, and this effect is averaged out.

The holes read out using this apparatus were then used for Stark and Zeeman experiments. Both these experiments involved burning a hole and then reading out the hole multiple times with different fields. The method used in both the Zeeman and the Stark experiments is basically the same, and is illustrated in figure 2.8. The field strengths used for the Stark experiments were 0 – 28 kV/cm. For the Zeeman experiments, fields of 0 to 5 T were used. The main difference between these two experiments is the amount of time required to turn on the field: for the Stark experiments 1 s was allowed for the field to be turned on, but in the case of the Zeeman experiments approximately 8 minutes were required for the field to come up to 5 T.

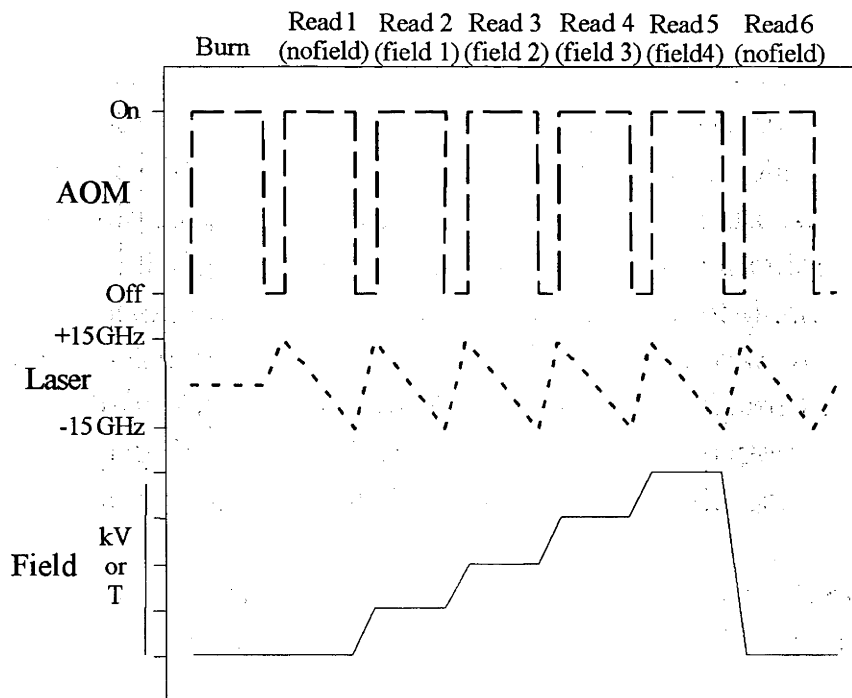


Figure 2.8: A representation of the sequence of steps involved in burning a hole and then reading it out in several fields.

Computer code written in Visual Basic was used to drive the apparatus and collect the data.

The geometry of the Stark and Zeeman experiments is depicted in figures 2.9 and 2.10. The advantage of using such a set-up in either case is that the angle of the electric field of the laser relative to the direction of the

applied field may be altered simply by rotating the polarisation direction of the laser.

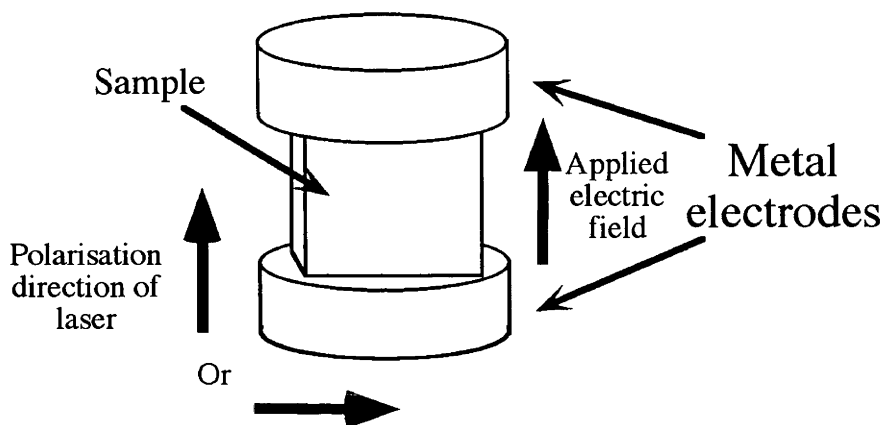


Figure 2.9: The experimental geometry used for Stark experiments performed in transmission.

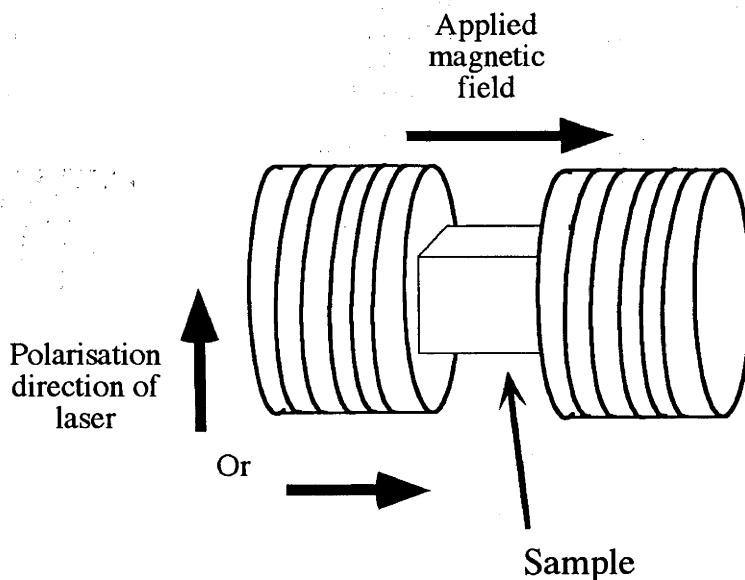


Figure 2.10: The experimental geometry used for Zeeman experiments performed in transmission.

A very elegant means of reading out a spectral hole is to use a technique known as holographic read-out. Details of holographic detection are given in reference [29]. Holographic read-out was used for the first series of Stark experiments using a Coherent CR-899 dye laser. This

procedure involved illuminating the sample with two overlapping beams during the burning process to burn a spatial grating into the sample. One beam was used for reading. This beam is scattered off the grating. Both the transmitted beam and the scattered beam were measured (see figure 2.11).

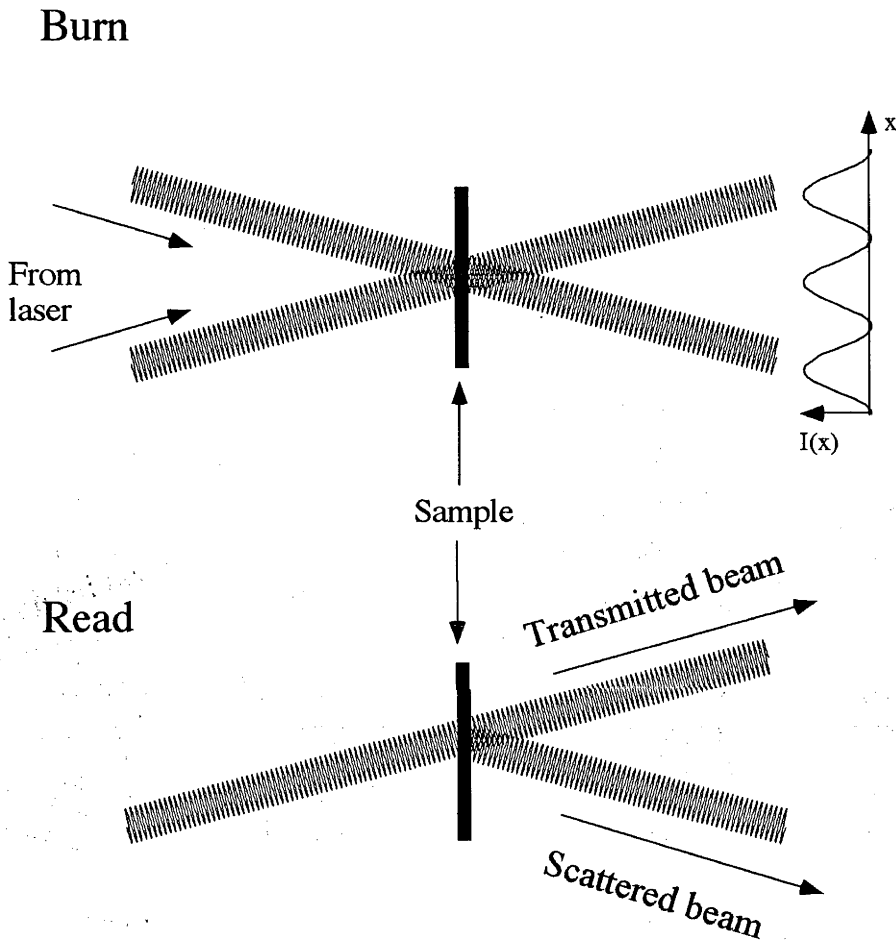


Figure 2.11: Holographic read-out. The burn is performed with two lasers to form a spatial grating upon the sample. One beam is used for reading. This beam is scattered off the grating and both the scattered and transmitted beams may be measured.

The experimental set-up is shown in figure 2.12. Holographic detection is an effective way of measuring shallow holes. It is a background-free detection technique. Even when the depth of a hole has been diminished through the application of an electric field, holographic read-out enables the hole to be readily detected.

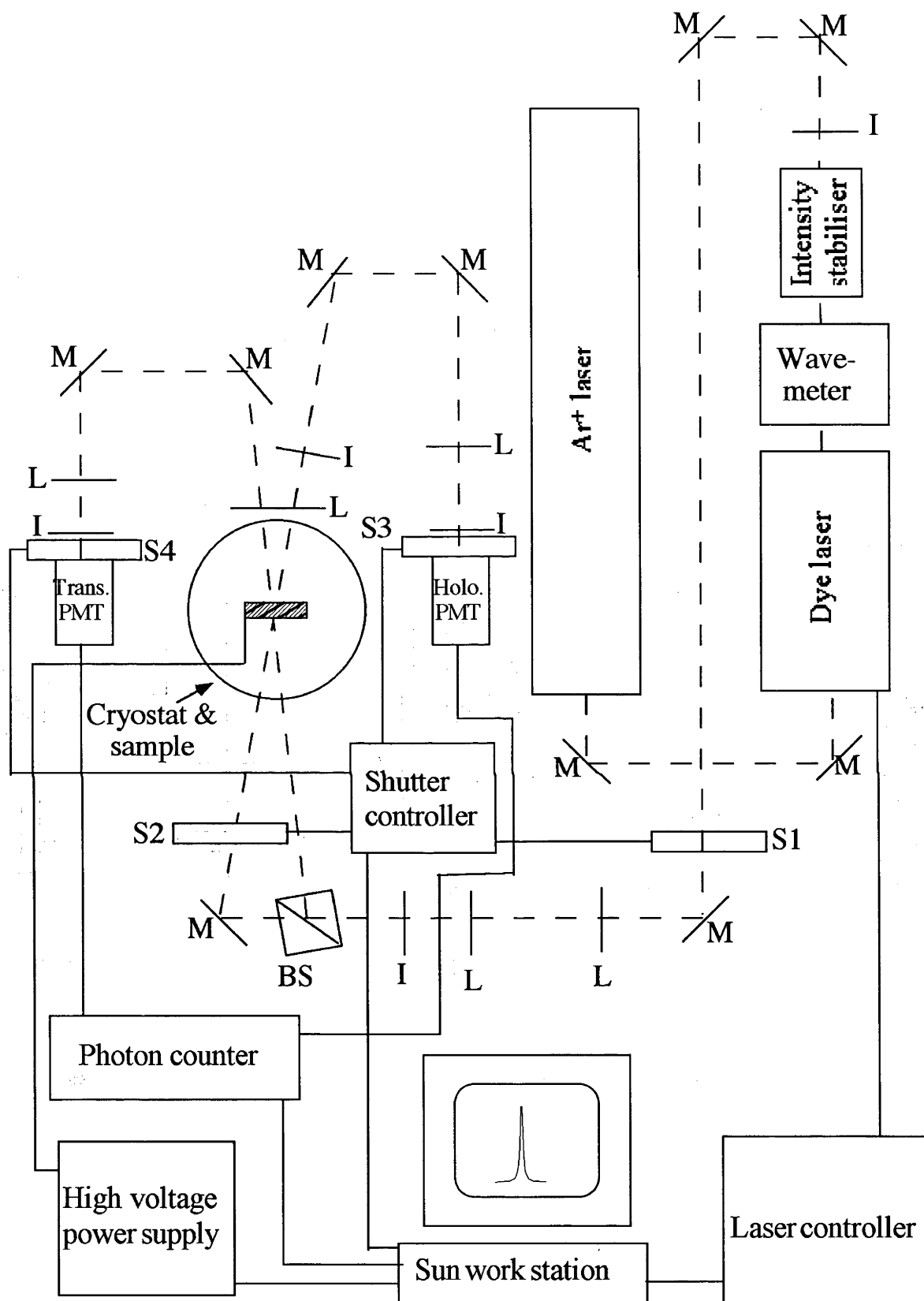


Figure 2.12: A schematic representation of the apparatus used to measure holographically detected spectral holes. M = mirror, L = lens, I = iris, BS = beam splitter, S = shutter.

The signal quality from holographically detected spectral holes is generally excellent. Because it is a background-free detection technique, variations in intensity arising from interference effects do not degrade the signal appreciably. Also, laser intensity stabilisation is not as critical in the holographic experiments. It is a means of measuring spectral holes which clearly has many advantages. The main disadvantages to this method are the limitations it places on the sample - samples must have a short optical path length ($\sim 100 \mu\text{m}$) and be of a very high optical quality; also, performing experiments in different geometries (ie with the electric field applied at different angles to the polarisation direction of the light) is more difficult.

The experiments using holographic read-out proceeded in a similar manner to the transmission experiments. Holes were burnt for 60 s using powers of $\sim 100 \mu\text{W}/\text{cm}^2$. The power was reduced by a factor of ~ 10 and the laser was scanned 30 GHz over the hole. Holes were read out a further 10 times with 10 different electric field strengths up to 46 kV/cm.

For the burn, shutters one and two were open and shutters three and four were closed. For the read, shutters one, three and four were open and shutter two was closed. Both the scattered and the transmitted beams were measured with Hamamatsu R 928 photomultiplier tubes.

In the holographic set-up, there were a number of points which required care:

- a) The quality of the beam was crucial. To obtain a good holographic signal, the sample needed to be as evenly illuminated as possible over the largest area achievable. Accordingly, the lenses and irises before the cryostat serve to spatially filter and expand the beam.
- b) The overlap of the two beams on the sample for the burning process was very important. This aspect of the alignment required great attention.
- c) The measurements were very sensitive to stray light. The lenses and irises after the cryostat acted as a spatial filter to reject stray light.

Holographic detection requires a flat, thin sample of high optical quality. Accordingly, samples were prepared as previously described and the experimental geometry used was the one shown in figure 2.13.

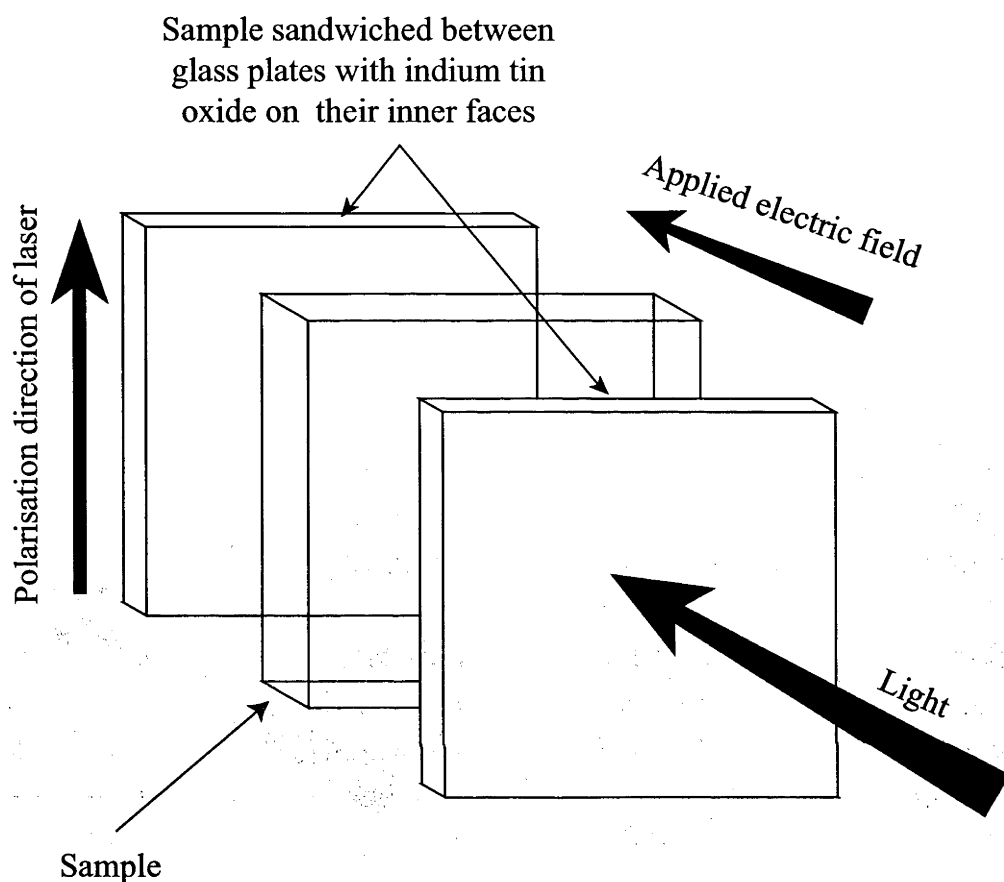


Figure 2.13: The experimental geometry used for the holographically detected Stark broadened spectral holes.

2.3 Calculations

The modelling of hole shapes was performed using *Mathematica 2.2.2* running on a Power Macintosh 7200/75. *Mathematica* is divided into two parts: the kernel, which performs the calculation; and the front end which is where the interaction with the user occurs [30]. It is the front end where the input is typed and the output appears. Initially, calculations were performed using the local kernel on the Power Macintosh, but the calculations were of a size that the computation time was too long to be practical. To solve this problem, an external kernel was used (use of the

local front end was maintained, however). These calculations were performed interactively on The Australian National University Supercomputer Facility's Silicon Graphics Power Challenge. This reduced the calculation time to a scale of seconds to minutes.

Mathematica was chosen to do these calculations for the following reasons:

- a) The input syntax is easy to learn.
- b) *Mathematica* performs both analytical and numerical computations.
- c) Graphical output is easily achieved. Comparisons with data are therefore easily made.

3. Broadband Spectroscopy, Fluorescence Line Narrowing and Spectral Hole-burning

3.1 Broadband spectroscopy

3.1.1 Absorption

The broadband absorption spectra of the Q bands of the chromophores studied for this thesis all have similar shapes. These are shown in figure 3.1. The bands observed in these spectra are commonly labelled Q(0,0), Q(1,0) and Q(2,0) [6, 9, 31, 32]. As an example, this labelling is shown on ZnTbp in figure 3.1. Q(0,0) consists predominantly of origin transitions, with some contributions from low frequency vibrational modes. Q(1,0) and Q(2,0) arise from unresolved overlapping vibrational sidelines.

3.1.2 Emission

If laser excitation is performed into the B band, relaxation occurs via vibrational levels which bridge the energy gap between the B and the Q states. Emission from the Q state may then be observed. Generally, emission is not observed from the B state. An exception to this is ZnTbp. ZnTbp is reported to emit from the B band [33]. No attempt was made to record this emission here.

The Q and the B states are uncorrelated (correlation is discussed later in this chapter). Therefore, emission which has been excited in the B band, but observed in the Q band, is broad and unstructured.

Broadband emission, obtained by exciting into the B band, was recorded for ZnPc/PMMA and ZnOep/PMMA using the UV lines of the Kr⁺ laser (350.7 and 356.4 nm). The results are shown in figures 3.2 and 3.3.

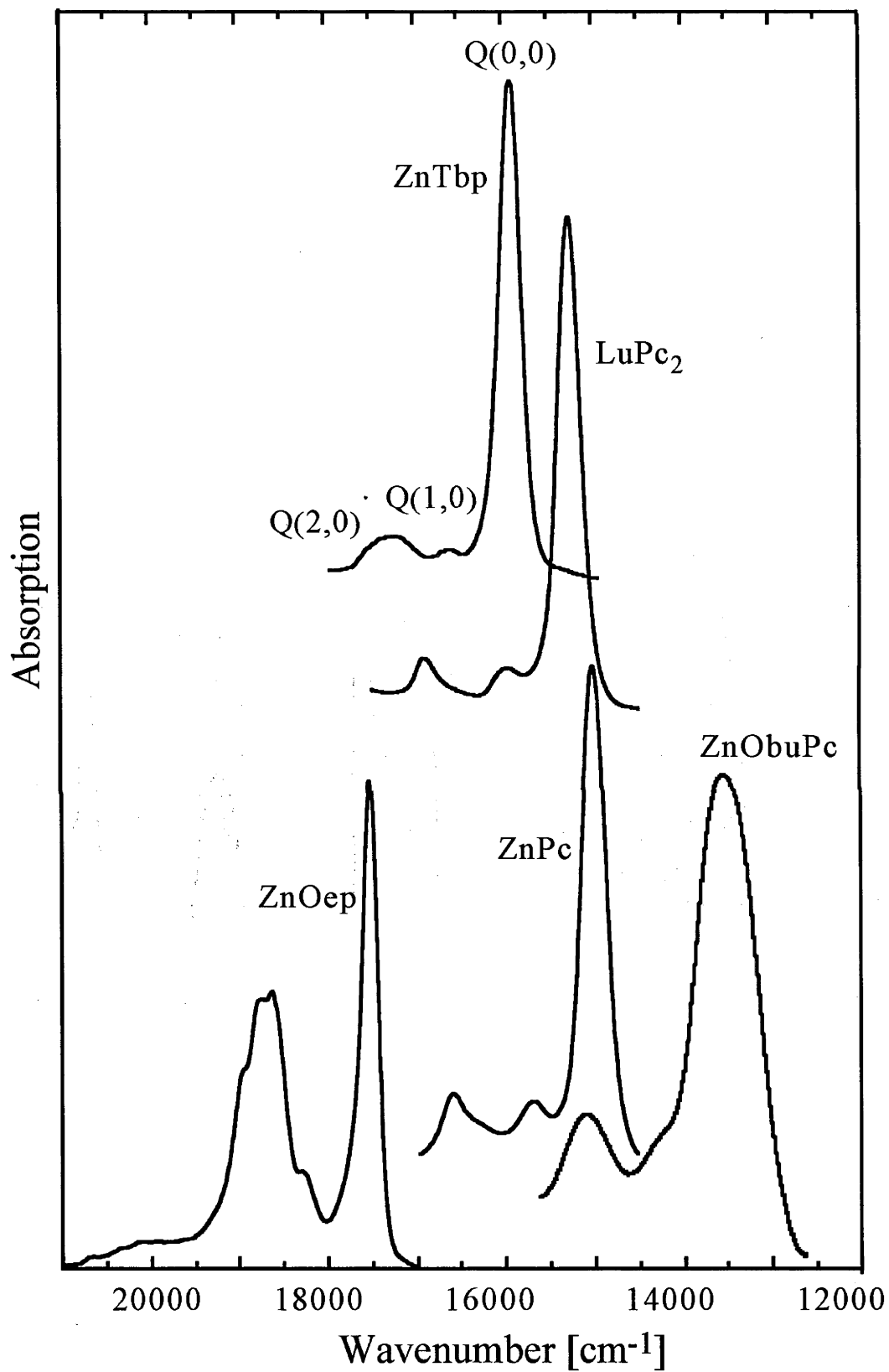


Figure 3.1: Absorption spectra of the Q bands of samples studied in this thesis.

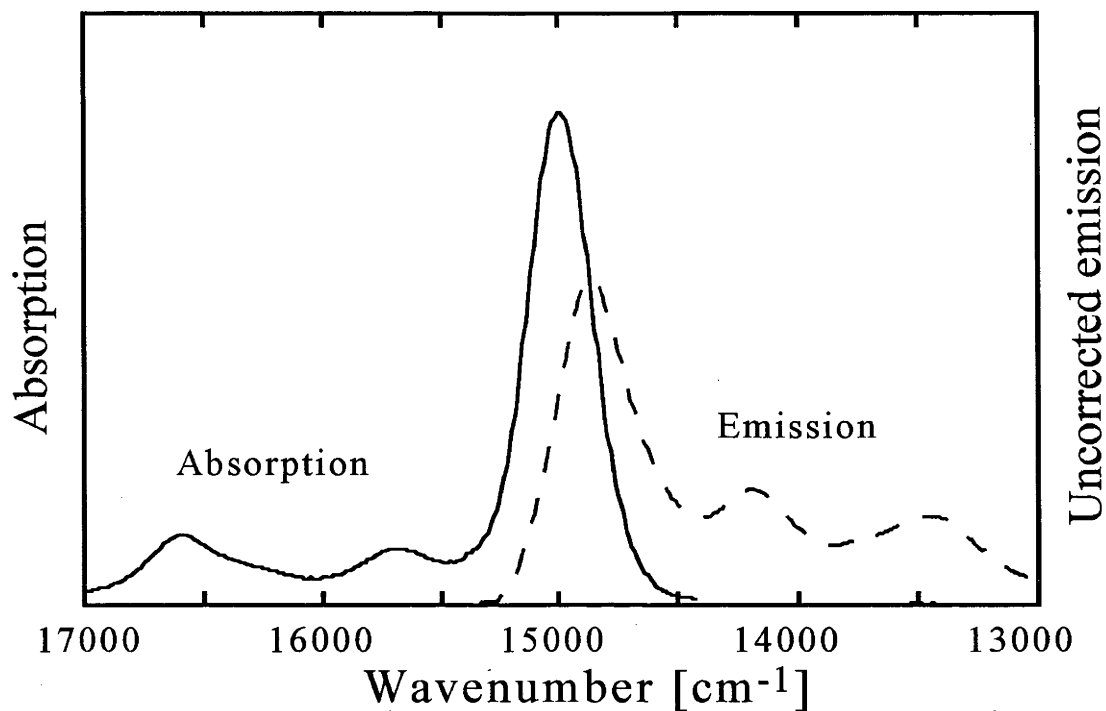


Figure 3.2: Broadband absorption (solid line) and emission (dashed line) of ZnPc/PMMA. The two curves are normalised to the same area.

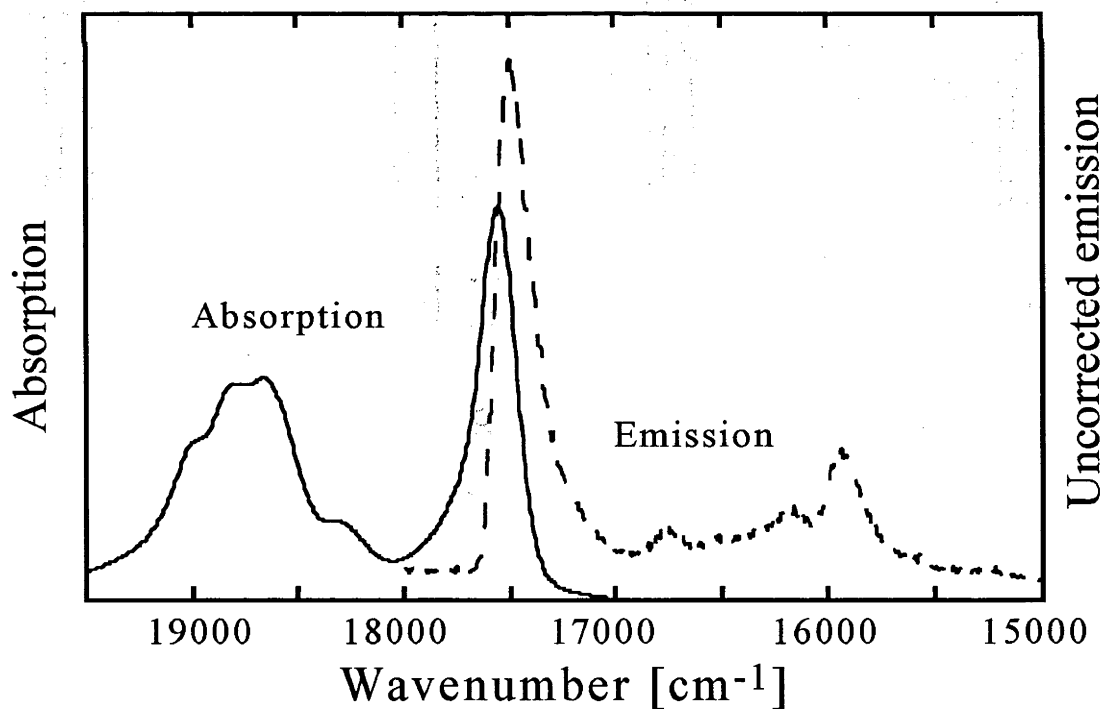


Figure 3.3: Broadband absorption (solid line) and emission (dashed line) of ZnOep/PMMA. The two curves are normalised to the same area.

In the spectra in figures 3.2 and 3.3, the vibrational sidebands of the ZnPc absorption and emission have approximately the same shape. For ZnOep, this is not the case. The emission spectra are not corrected for detector response. The detector response decreases towards the red. If a correction were made, then the intensities observed at the red end of the emission spectra would be increased. This correction may make the emitted vibrational sidebands of ZnPc look more like those in absorption (notice how Q(2,0) is a little more intense than Q(1,0) in absorption, but not in emission). In the case of ZnOep, however, the shapes of the vibrational sidebands are quite different in absorption and emission. The correction may make the intensities of the vibrational sidebands in absorption and emission more alike, but the reflection symmetry will remain absent. This lack of reflection symmetry is attributed to HT coupling in ZnOep [10]. Additionally, in more concentrated samples, emission from aggregated species (see section 3.1.3) may also remove reflection symmetry in absorption and emission.

3.1.3 Aggregation of zinc phthalocyanine

When ZnPc is doped into its host at higher concentrations, another peak appears to the red of the origin band. This peak is attributed to aggregates of ZnPc [34-36].

When a hole is burnt in the red edge of the origin band a sidehole appears in the aggregate band (see figure 3.4). This suggests that, at the energy of the laser, not only monomeric, but also aggregated species absorb. The area of the sidehole is less than the area of the hole at the burn energy. The relative areas of the holes suggest that the absorption at the laser energy is predominantly monomeric.

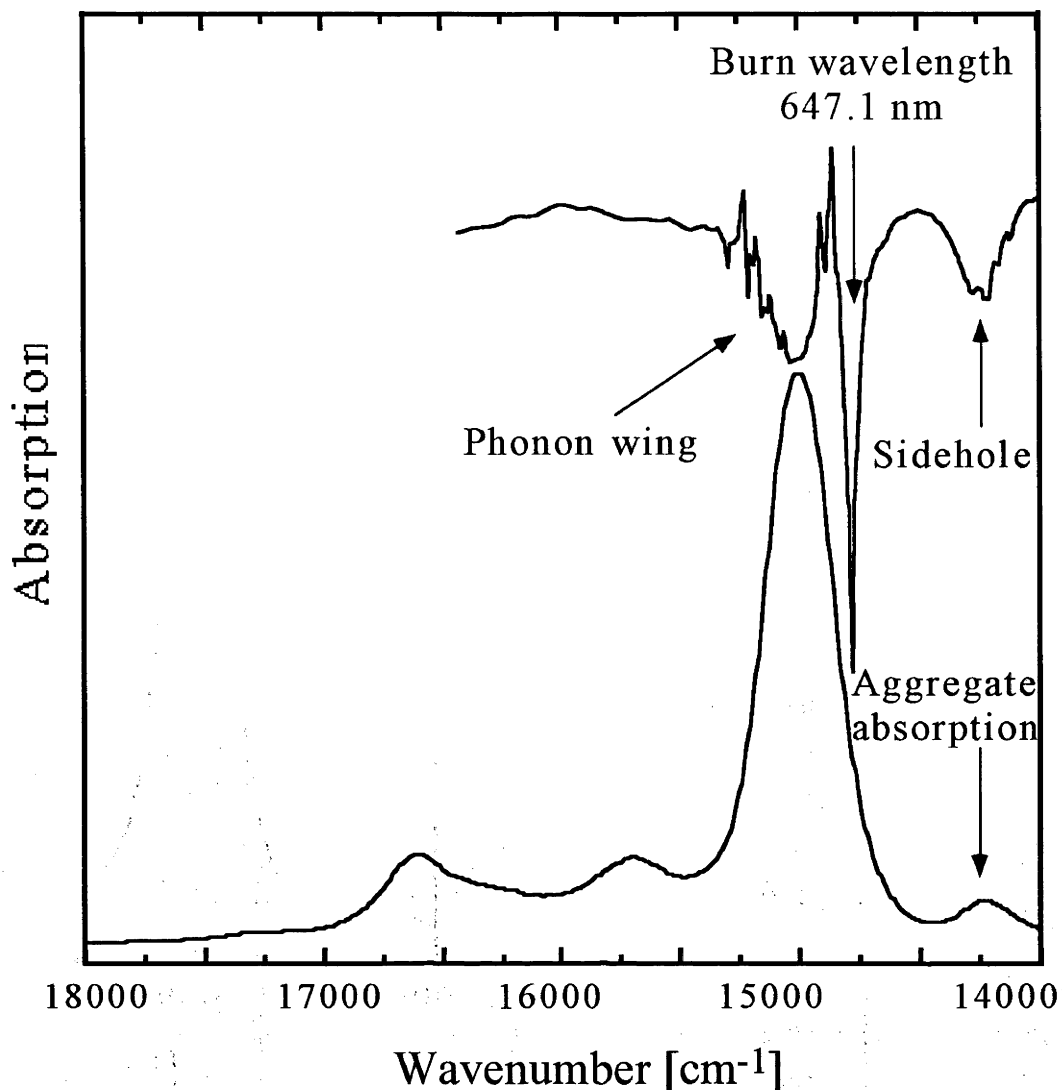


Figure 3.4: A broadband absorption spectrum of ZnPc/PMMA showing the aggregate absorption band and a hole spectrum where the hole was burnt into the red edge of the Q band with a sidehole in the aggregate band.

It has been proposed by Dunford et al. [32] that the hole-burning mechanism in copper phthalocyanine in argon matrices is as a result of photo-induced electron transfer between close-lying chromophores.

When the polymer films are made, the chromophore is predissolved before being added to a polymer solution. If the chromophores are not predissolved, the aggregate band always appears in the absorption spectrum. This observation suggests that predissolution makes the formation of aggregates less likely.

In polymer films where the chromophore is predissolved, the aggregate absorption band begins to appear at concentrations between 10^{-2} to 10^{-3} mol/l. It is advisable to keep the concentration of the chromophores well below this value (say, below 10^{-4} mol/l) to prevent chromophore–chromophore energy and electron transfer complicating the results in any way [37].

3.2 Spectral hole-burning in vibrational sidebands

The overlapping and convoluted nature of the inhomogeneously broadened bands observed in the broadband spectra is illustrated in the following experiment.

A spectral hole was burnt in the Q(1,0) band of ZnPc/PMMA using a HeNe laser (632.8 nm). As well as the hole at the burn energy, strong sideholes appear in the origin band (see figure 3.5).

As stated previously, the vibrational sidebands, Q(1,0) and Q(2,0), consist of many overlapping vibrational sidelines. When a hole is burnt into a vibrational sideband, many vibrational sidelines are excited. When a chromophore is depleted by means of hole-burning, its entire absorption spectrum is removed. Hence, the origin bands which are associated with the vibrational sidelines are also depleted and sideholes appear in Q(0,0). The difference in energy between the wavelength of the burn and the sidehole corresponds to the energy of the vibration involved [31, 38-41].

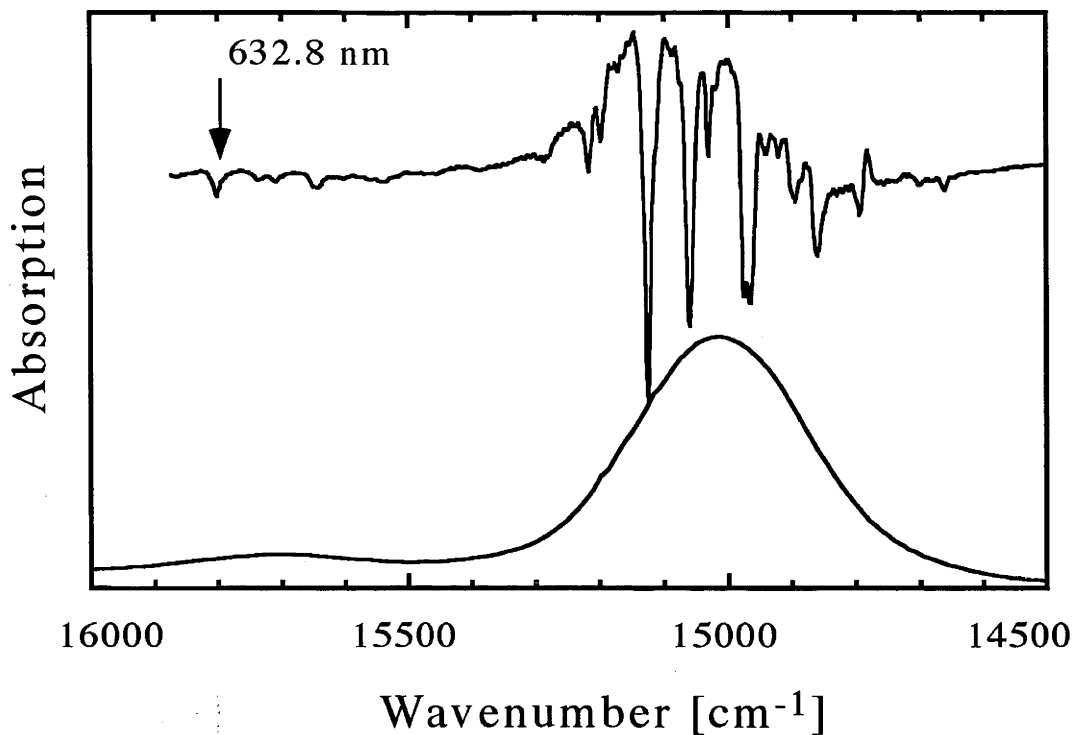


Figure 3.5: The sidehole spectrum of ZnPc/PMMA where the hole was burnt into Q(1,0) at 632.8 nm. The broadband absorption spectrum is also shown.

The concept of correlation may be introduced at this point. Correlation refers to the distribution of the relative energy differences between transitions. If, for example, a chromophore is selected by its vibrational sideline in a hole-burning experiment, then the corresponding origin will also be depleted. If all the chromophores selected by the energy of their vibrational sideline have the same relative energy gap to the origin band, then a sharp sidehole will result. If there is a distribution of the energy between the origin and the vibrational sideline, then a broad, shallow sidehole will result. Where there is little distribution, the system is considered to be well correlated, but when the distribution is great then the system is said to be poorly correlated (see figure 3.6).

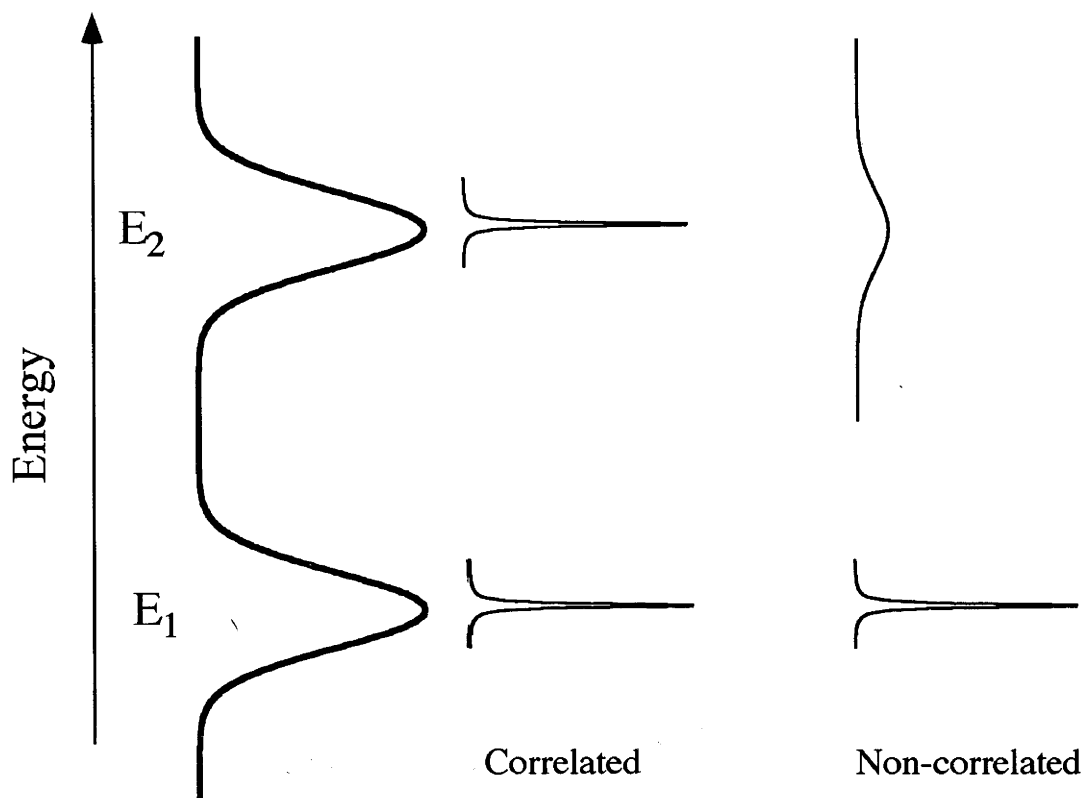


Figure 3.6: Correlation and non-correlation of two energy levels having an inhomogeneous distribution.

A similar sidehole experiment can be performed by burning on the blue edge of the origin band. Within the inhomogeneously broadened profile of the origin band are contributions from low frequency vibrations. The contributions from these vibrations are greatest on the blue side of the origin band. (This is because, in absorption, the vibrations observed are those associated with the excited state and are built upon the high energy side of the origin transition.) Therefore, if a hole is burnt on the blue edge of the origin band, sideholes appear to the red in the origin band. Once again, the difference in energy between the burn wavelength and the sidehole corresponds to the frequency of the vibration involved.

Such an experiment was performed in ZnPc/PVB, ZnTbp/PVB and LuPc₂/PMMA. The results are displayed in figures 3.7–3.9.

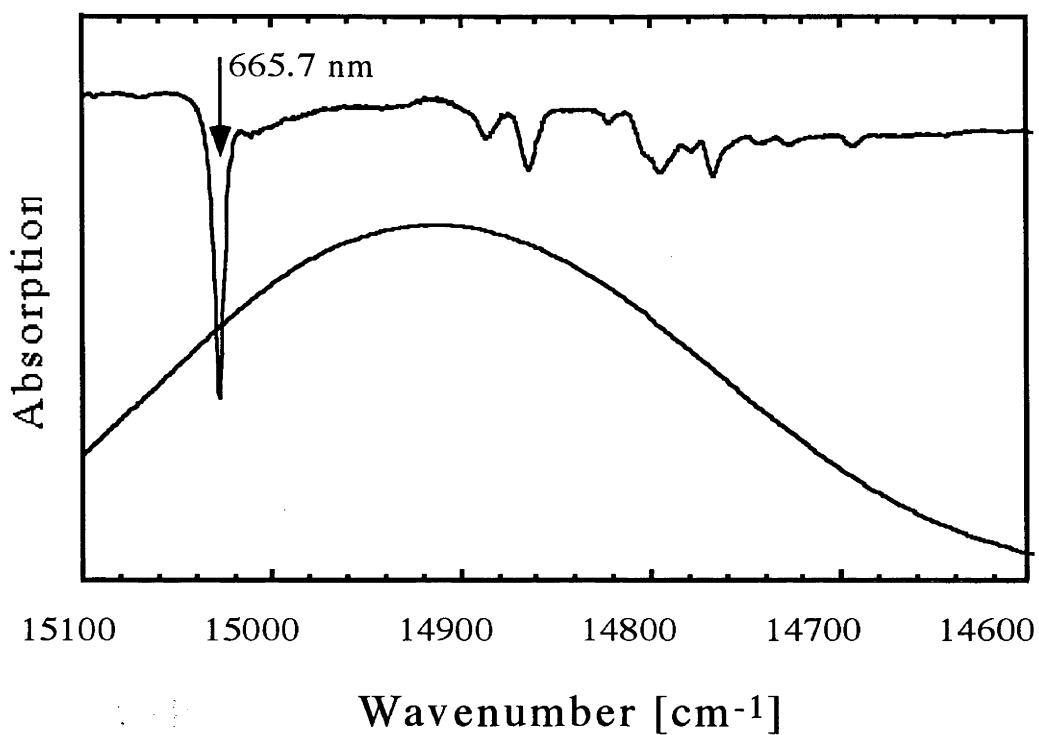


Figure 3.7: The sidehole spectrum of ZnPc/PVB where the hole was burnt into the blue edge of Q(0,0) at 665.7 nm. The broadband absorption spectrum is also shown.

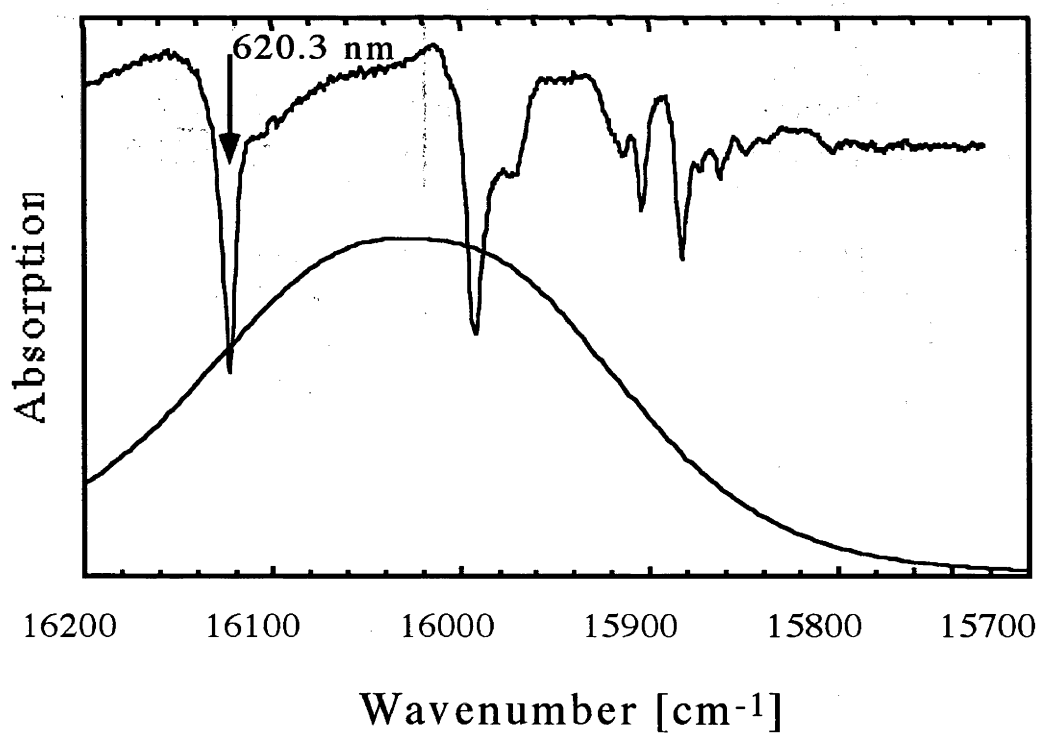


Figure 3.8: The sidehole spectrum of ZnTbp/PVB where the hole was burnt into the blue edge of Q(0,0) at 620.3 nm. The broadband absorption spectrum is also shown.

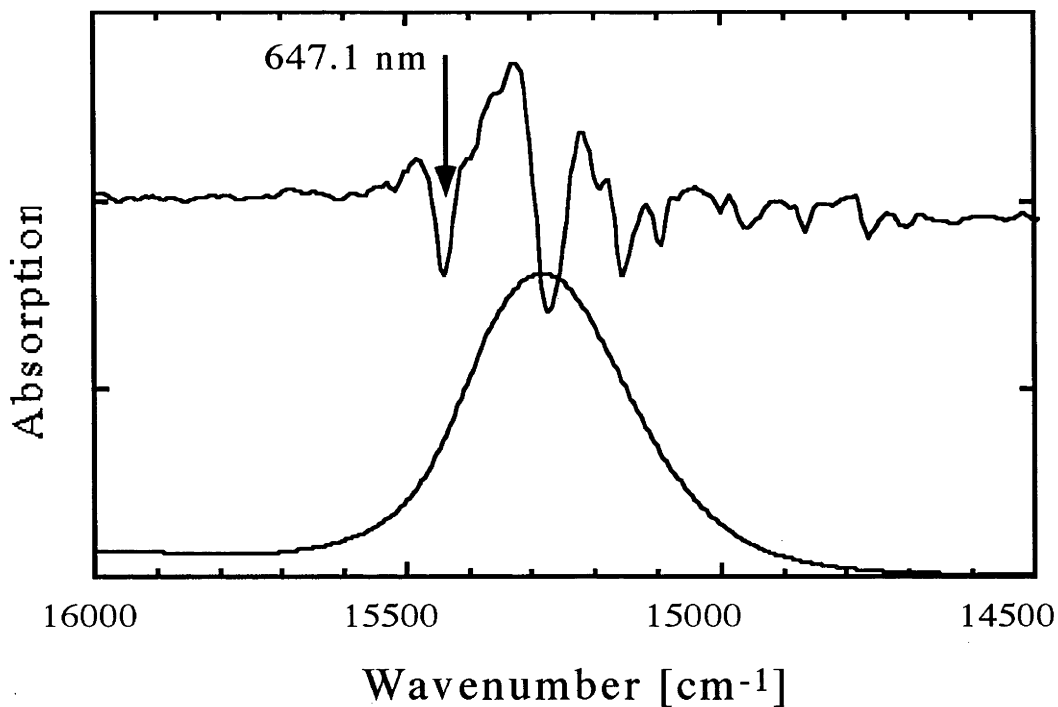


Figure 3.9: The sidehole spectrum of LuPc₂/PMMA where the hole was burnt into the blue edge of Q(0,0) at 647.1 nm. The broadband absorption spectrum is also shown.

This type of hole-burning experiment may be used as a means to obtain excited state vibrational frequencies [40]. Such a technique is useful for samples which have little vibrational structure visible in their absorption spectra.

Vibrational frequencies obtained from the experiments described above are given in table 3.1. These frequencies agree favourably with those obtained from a detailed fitting of both absorption and MCD line shapes [9] and from measurements in Shpol'skii matrices [6, 42] for this class of chromophore.

ZnPc		ZnTbp	LuPc ₂
Vibrational sideband burn	Burn in blue side of origin	Burn in blue side of origin	Burn in blue side of origin
64			
92			
150	142	132	
	162	151	169
201	206	210	
	232	219	
	250	240	
258	261	249	251
	285	260	289
		275	
		286	
	300	320	
	335	347	347
			444
513			485
585			579
604			
676			679
741			740
772			
826			
836			
860			
880			
905			
939			
1007			

Table 3.1: Excited state vibrational frequencies yielded by hole-burning in vibrational sidebands.

The holes at the burn energy are broad (FWHM ~ 10 cm⁻¹) with Lorentzian profiles. Sideholes have similar or slightly larger widths (a factor of two or three). The loss of correlation relative to the inhomogeneous broadening of the origin band is not great, therefore sideholes may be clearly observed [41]. The broad shapes of the holes may be attributed to fast relaxation (\sim ps) of the vibrationally excited states.

3.3 Fluorescence line narrowing experiments in zinc phthalocyanine and zinc octaethylporphyrin

An experiment which is complementary to hole-burning in a vibrational sideband is non-resonant FLN excited in the vibrational sideband. Such an experiment was performed on ZnPc/PMMA and ZnOep/PMMA. The results are displayed in figures 3.10 and 3.11.

Ideally, such an experiment should yield distinct peaks for the origin and vibrational sidelines of the subset of chromophores excited. As may be seen in figures 3.10 and 3.11, the spectra obtained from excitation in a vibrational sideband do not show well-defined structure in either ZnPc or ZnOep.

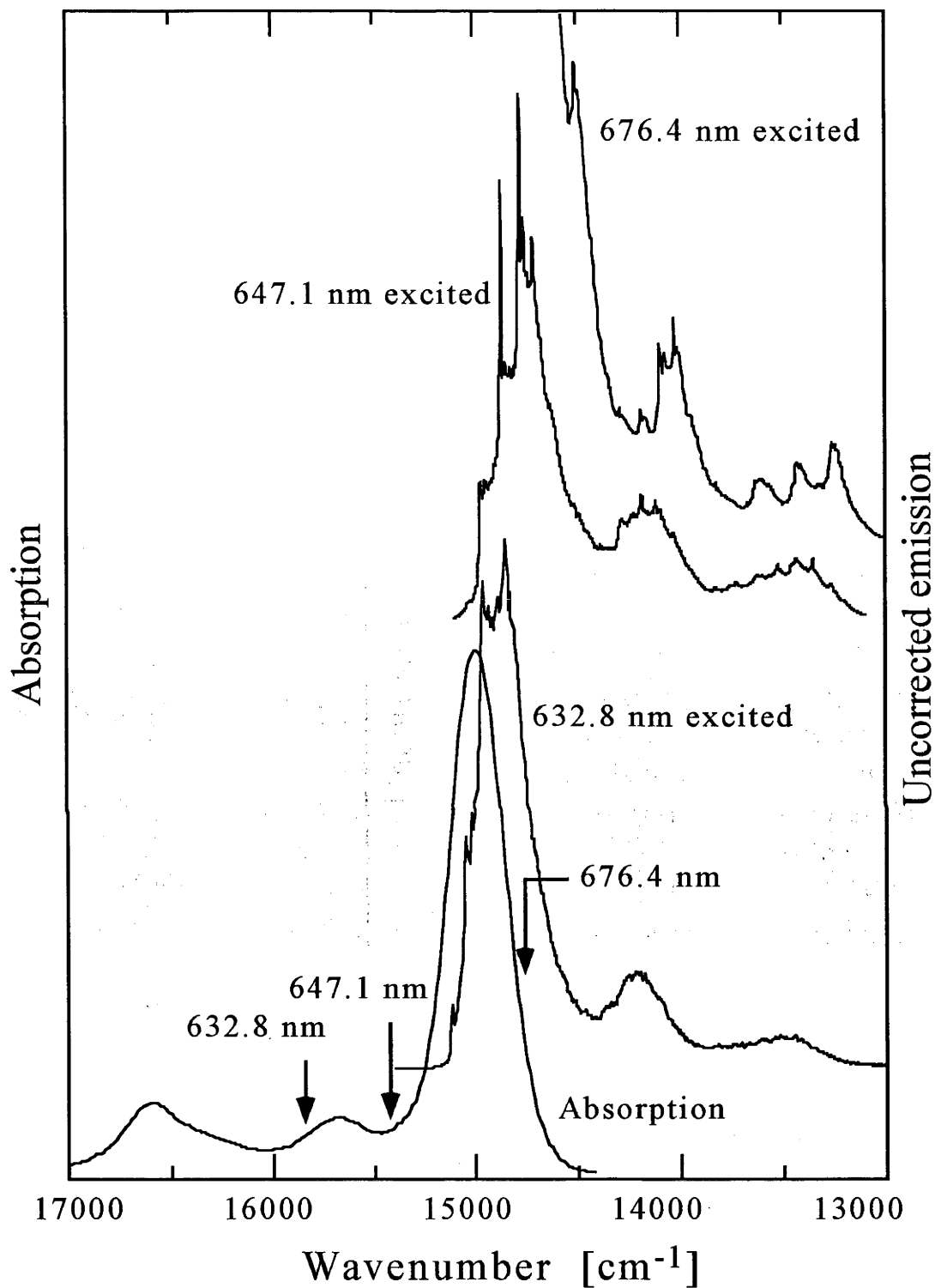


Figure 3.10: Selective emission from ZnPc/PMMA excited at a number of places in the Q band.

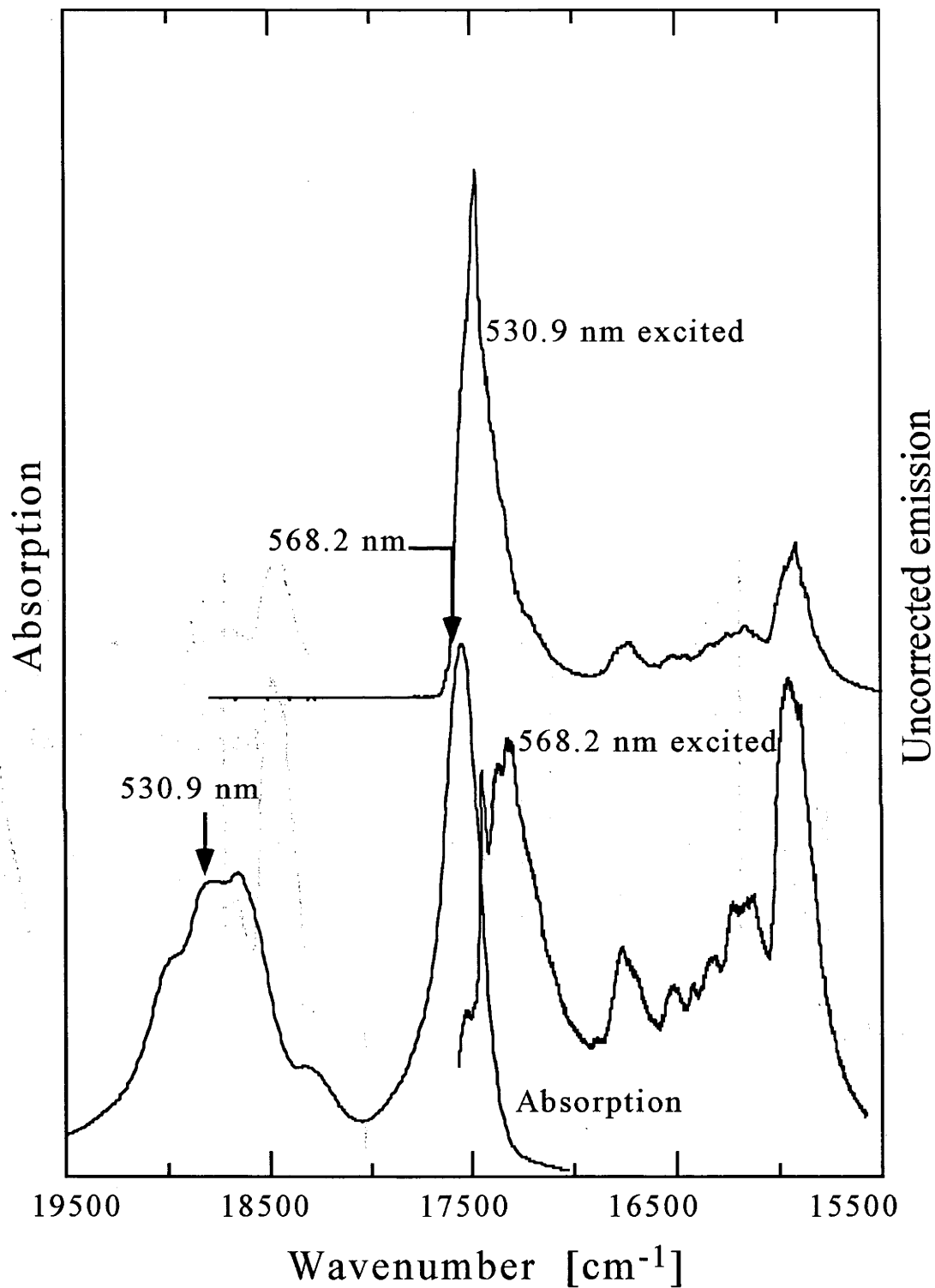


Figure 3.11: Selective emission from ZnOep/PMMA excited at two places in the Q band.

The conditions under which the experiments were performed were varied to try and improve the narrowing. The parameters altered were:

- a) The host in which the chromophore was doped. A range of polymers were tried (polystyrene, polyethylene, PMMA, PVB) and an alcoholic glass (n-butylalcohol - after reference [43]).
- b) The amount of solvent present in polymer samples. Newly prepared 'wet' samples through to carefully heated and evacuated 'dry' samples were tried [44].
- c) The laser power used (~ 1 to 100 mW/cm^2).

The spectra resulting from these variations have a similar appearance to the spectra in figures 3.10 and 3.11.

A possible reason for the poor narrowing in the fluorescence spectra was that the exciting laser was causing spectral hole-burning at the excitation frequency.

As explained in chapter 1, because of the different widths of the ZPL and the PW, at a given wavelength, the reduction in absorption as a result of spectral hole-burning is primarily from ZPL depletion. PW depletion at a given wavelength is a more gradual process. Therefore, if hole-burning is occurring at the excitation wavelength, the narrow ZPLs are going to be rapidly removed, and broader features such as PWs will remain. These broad features will possess correspondingly broad emission.

To test this hypothesis, emission was monitored at a fixed wavelength. If hole-burning was occurring then a decrease in emission should be seen, corresponding to the selective depletion of the chromophores at the excitation wavelength. This test was performed with the same variety of parameters as for the FLN spectra. Laser powers were lowered to the lowest practical point that fluorescence could be measured. A reduction in emission was observed in some cases, but this reduction was neither large nor reproducible. Often an increase in emission was observed.

A possible explanation of the observations made above is that rapid hole-burning is occurring at the excitation wavelength. At the laser powers

required to measure fluorescence from these samples, hole-burning happens so fast that the depletion is not readily measured. The increase in emission may be caused by hole filling which happens as a result of heating of the sample by the laser.

From the data displayed in figures 3.10 and 3.11, it can be seen that the structure of the emission has a strong dependence on excitation wavelength. Fluorescence excited on the blue side of the origin band resulted in the highest degree of structure, while excitation on the red side of the band was broader. Following from the previous discussion, it may be the case that there is a variation of hole-burning efficiencies across the band. This postulation is corroborated by the observation of variation in hole-burning efficiencies across the inhomogeneously broadened band in wavelength dependent hole-burning studies performed for this thesis.

3.4 Fluorescence line narrowing in zinc octaethylporphyrin: some further experiments

In ZnOep, intersystem crossing from the first excited singlet state to the triplet manifold is a relatively efficient process [45]. Emission (phosphorescence) from the triplet state may be observed. To enhance the phosphorescence, ZnOep was dissolved in a 1:1 mixture of ethyl iodide/bromobutane. This mixture enhances the phosphorescence by means of the external heavy atom effect. The presence of heavy atoms increases the spin-orbit coupling. Greater spin-orbit coupling results in an increase of the efficiency of the intersystem crossing and the (nominally forbidden) relaxation from the triplet to the ground state [46].

Excitation was performed with a green HeNe laser at 543 nm. The temperature was ~ 5 K.

The resulting spectrum was not highly structured (see figure 3.12), but the phosphorescence is clearly enhanced.

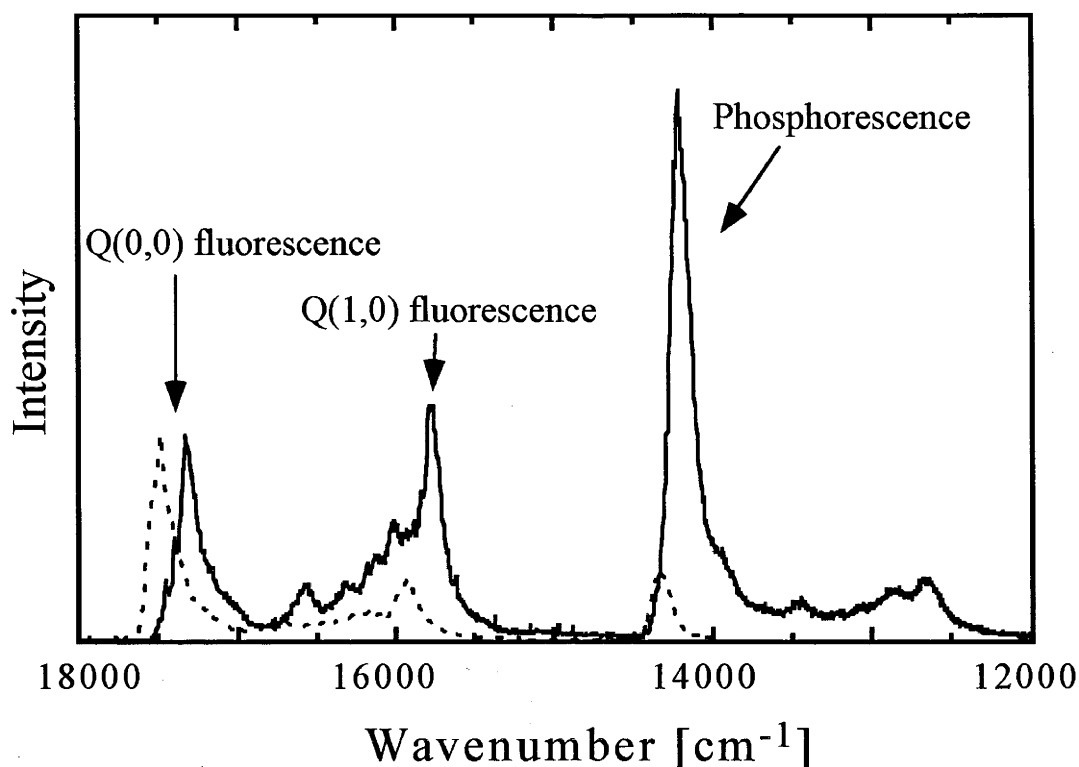


Figure 3.12: Emission from ZnOep in a 1:1 mixture of ethyl iodide/bromobutane excited at 543 nm (solid line) compared to emission excited at 530.9 nm in ZnOep/PMMA (dashed line). The enhancement of the phosphorescence can clearly be seen.

Starukhin et al. [47, 48] measured the FLN of cyclopentane porphyrin dimers in THF/toluene 3:1 at 4.2 K. The spectra they obtained were highly structured. Following the lack of narrowing in the ZnOep and ZnPc emission spectra in polymer films, this mixture was tried with ZnOep.

This mixture does not glass; instead it forms microcrystals. Pure toluene and pure THF were also attempted and they are also microcrystalline. The spectra obtained in these environments display some structure, probably as a result of the microcrystalline nature of the environment.

An experiment was performed where the sample was excited at 543 nm (this corresponds to the red side of the vibrational sideband in absorption). A single strong line in the phosphorescence resulted (see figure 3.13). The appearance of a single line in the phosphorescence suggests a very high degree of correlation in the system. When the sample was warmed to ~ 50 K, the phosphorescence disappeared.

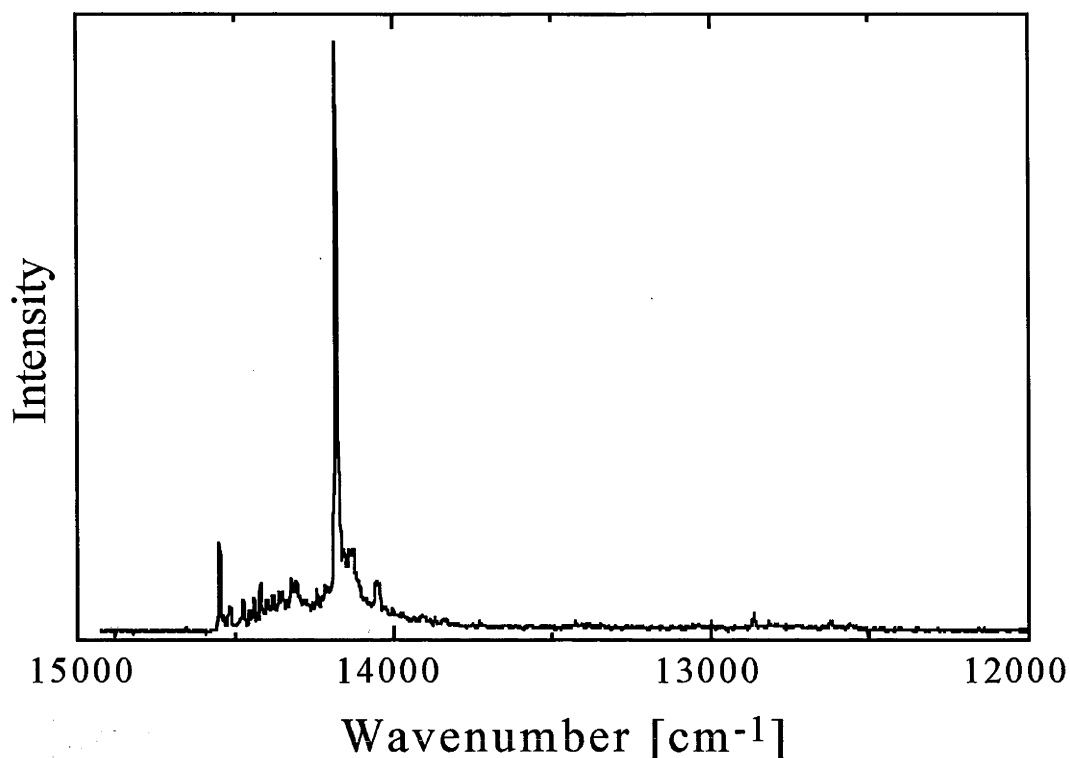


Figure 3.13: Phosphorescence from ZnOep/THF excited at 543 nm.

3.5 The development of a spectral hole shape with burn time

A brief discussion of the change in hole shape with burn time was given in chapter 1. These changes have been measured in ZnPc/PMMA. The results are shown in figure 3.14. It can be seen from this figure that, as described in chapter 1, initially the ZPL grows. As the hole develops, a PW appears. Shortly after the appearance of the PW the ZPL stops deepening and the PW grows preferentially. At this point, the hole is saturated (ie there are no more chromophores with ZPLs at the energy of the laser). The appearance of the wing indicates that chromophores whose PW absorb at the energy of the laser are now being depleted.

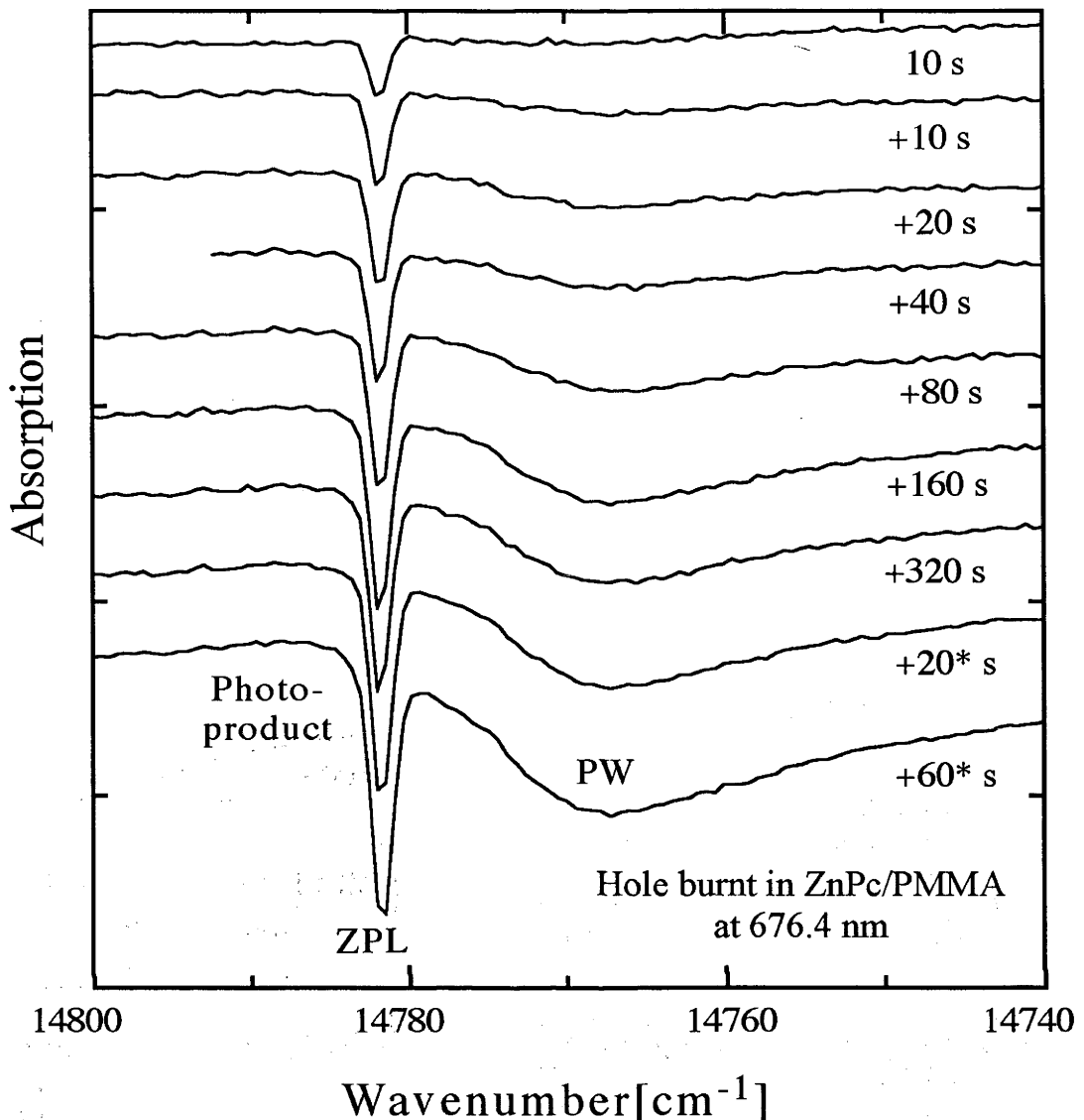


Figure 3.14: The development of a spectral hole with burn time. This hole was burnt into ZnPc/PMMA at 676.4 nm. The initial hole was burnt for 10 s using 2 mW/cm^2 . Additional burn times are marked on the figure. The final two holes (marked with asterisks) were burnt with 10 mW/cm^2 .

3.6 Hole width extrapolation to zero fluence

A commonly performed experiment in spectral hole-burning spectroscopy is to burn holes at a range of fluences (fluence = laser power \times illumination time / beam area), measure the hole width as a function of fluence, and then extrapolate to zero fluence [4]. The hole width given by the extrapolated value may come to reflect the homogeneous linewidth.

There are a number of factors which give a spectral hole its width. These may be expressed [4]:

$$\Gamma_{\text{hole}} = 2\Gamma_{\text{hom}} + 2\Gamma_{\text{laser}} + \Gamma_{\text{SD}} \quad (3.1)$$

Γ_{hom} is the homogeneous linewidth, an expression for which was given in section 1.3. This is restated here:

$$\Gamma_{\text{hom}} = \frac{1}{\pi} \left(\frac{1}{2T_1} + \frac{1}{T_2^*} \right) \quad (3.2)$$

T_1 is the homogeneous lifetime of the excited state and T_2^* is the pure dephasing time. T_2^* results from the dephasing of the ground and excited state wavefunctions through electron-phonon coupling. T_2^* is strongly temperature dependent.

Γ_{laser} is the contribution from the width of the laser. If $\Gamma_{\text{laser}} \ll \Gamma_{\text{hom}}$ then its effect is negligible.

The factors of two in equation 3.1 arise because measuring a spectral hole is a two-step process: the hole is burnt and then read [4].

The last factor in equation 3.1 is known as spectral diffusion [49-51]. Amorphous hosts at low temperatures are far from equilibrium [13]. The relaxation processes of the host occur over a wide range of time scales (from \sim ns to days). These changes in the environment cause shifts of transition energies of the chromophores embedded in the host. As a result of the shifts of transition energies, the width of a spectral hole will broaden with time. Spectral diffusion is also temperature dependent.

Caution is therefore required in the interpretation of the extrapolation of hole widths to zero fluence. The timescale on which these experiments are performed is important. Processes such as optical dephasing and spectral diffusion mean that the width of a hole changes with time and with temperature. Thus, to understand fully the processes which give a spectral hole its width, hole widths should be measured as a function both of delay time between burning and reading, and of temperature. Generally, the shorter the delay time between burning and reading and

the lower the temperature, the more closely the extrapolated value will come to represent the homogeneous linewidth.

An extrapolation to zero fluence was performed on ZnPc/PVB. To alter the fluence, the beam area and the burn time (60 s) were kept constant and the laser power was changed. The temperature was 1.8 K and the delay time between burning and reading was of the order of 30 s. The data are displayed in figure 3.15. An extrapolated value of 600 ± 50 MHz resulted.

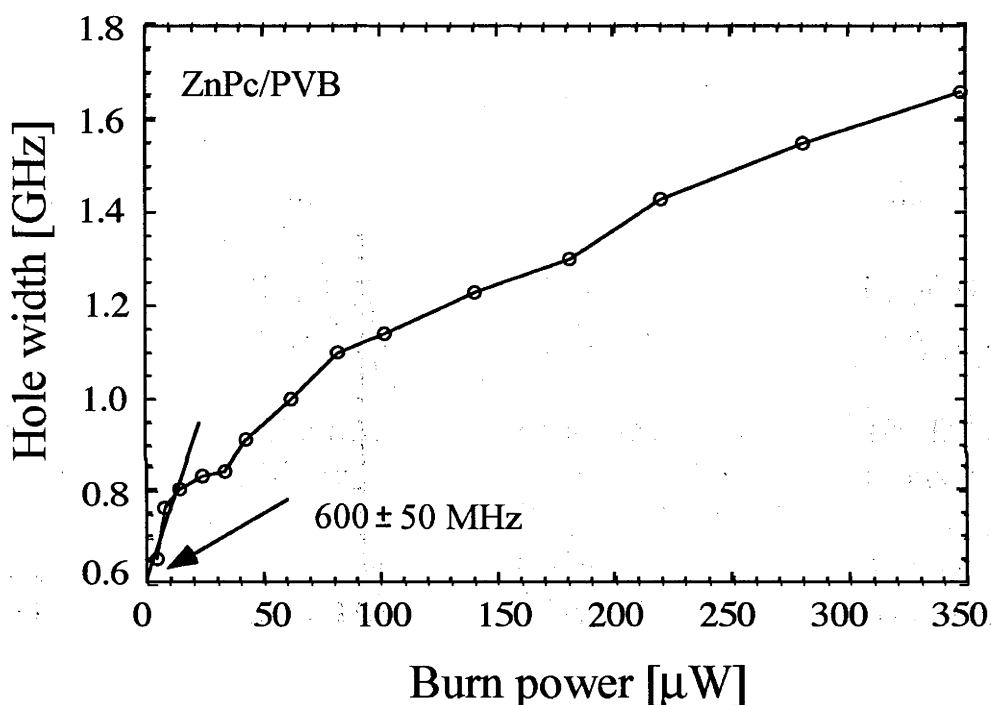


Figure 3.15: Hole width as a function of burn power. Using a linear extrapolation, a hole width of 600 ± 50 MHz at zero fluence is calculated.

The excited state lifetime of the Q transition of ZnPc has been estimated as 10 ns [52]. The lowest excited state lifetimes of a number of Zn porphyrins have been measured as 2 – 4 ns in a number of solvents [45]. The lifetime limited linewidth is therefore going to be of the order of tens of MHz. The extrapolated hole width is clearly far removed from this value.

There appear to be additional processes such as dephasing and spectral diffusion giving the observed holes their width [49-51]. Without further information on the changes that occur at this temperature and in this timescale, the extrapolated hole width given above is of limited usefulness.

3.7 Hole-burning to long time

An inhomogeneously broadened band has both ZPLs and PWs contributing to its shape. As outlined in chapter 1, at a fixed frequency, the rates at which these two components are diminished are very different. These different rates arise from their different widths.

If the change in absorption is monitored with burn time, then the point at which this change in rate occurs may be noted. The absorption remaining at this point may be attributed to PWs. If the absorption after this burn to long time is compared to the absorption before burning, then a DWF may be calculated [53, 54].

The experiment described above was performed on ZnPc/PVB. The long time burn was performed in a number of places across the band. The area of the absorption before compared to the area after burning was used to calculate the DWF. The results are displayed in figure 3.16. A DWF of 0.63 was calculated.

It can be seen from figure 3.16 that the contribution from PWs is greater on the high energy side of the origin band. This is because, as previously discussed, the phonons behave in a fashion analogous to molecular vibrations, and in absorption are built upon the high energy side of the ZPL. Therefore the greatest contribution from the PWs will be on the blue side of the inhomogeneously broadened band. In addition, Flatscher and Friedrich [55] observed a wavelength dependence of the DWF of anthracene in 2-methyl-THF. They observed a decrease in DWF with an increase in ZPL energy.

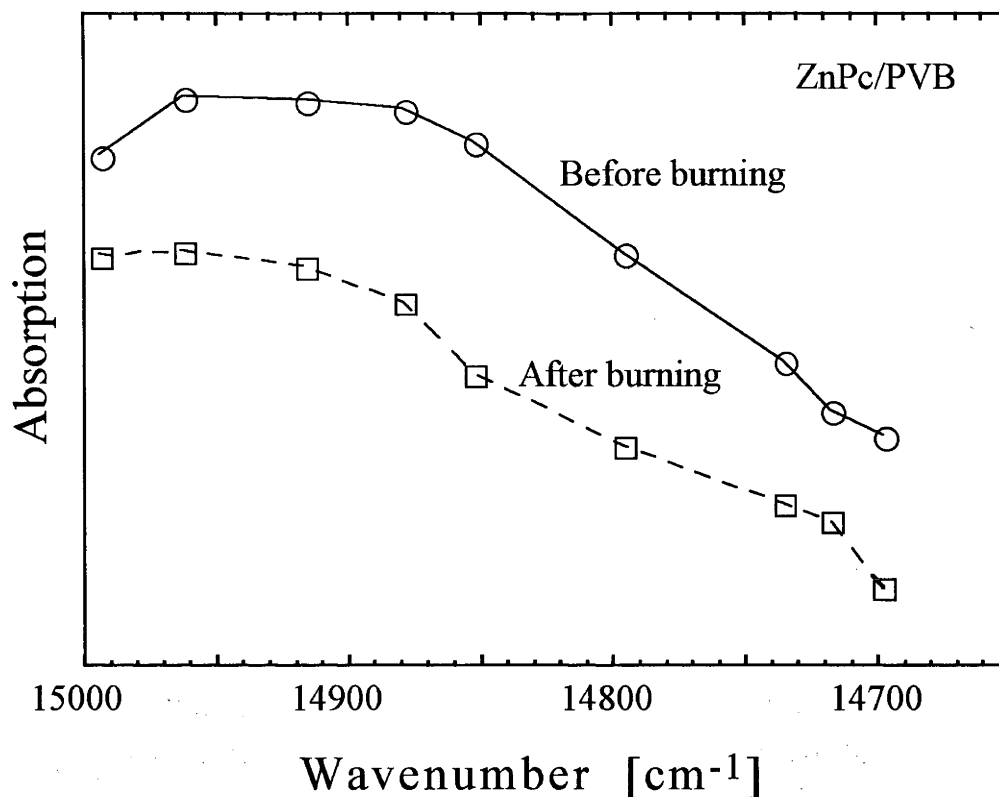


Figure 3.16: Absorption before (solid line and circles) and after (dashed line and squares) burning for a long time.

3.8 Hole-burning in zinc 1,4,8,11,15,18,22,25-octabutoxyphthalocyanine

Preliminary hole-burning experiments were performed upon ZnObuPc. This compound is useful because its absorption coincides with the wavelength range of the Ti:sapphire laser. During the course of these experiments, it was found that, in solution, upon exposure to light, a new absorption appeared to the red of the Q band (see figure 3.17). This new absorption was tentatively assigned to the ZnObuPc \cdot^+ radical cation. (Aggregation is unlikely to be the cause of this new absorption as it grew with increased exposure to light - aggregates would be more likely to do the reverse.) The appearance of an absorption band to the red of the Q band is consistent with the absorption of Pc \cdot^+ . Also a new band appeared between the Q and the B bands (this may be observed in measurements further to the blue not shown here). This is also characteristic of Pc \cdot^+ absorption [5, 56-58].

Some derivatives of phthalocyanines are known to be readily ionised. There is interest in such systems for various electrochemical applications [5, 56]. Upon further exposure to light, all absorption disappeared. The chromophore may have been further ionised or decomposed. The new absorption created in the process also shows efficient hole-burning (see figure 3.17).

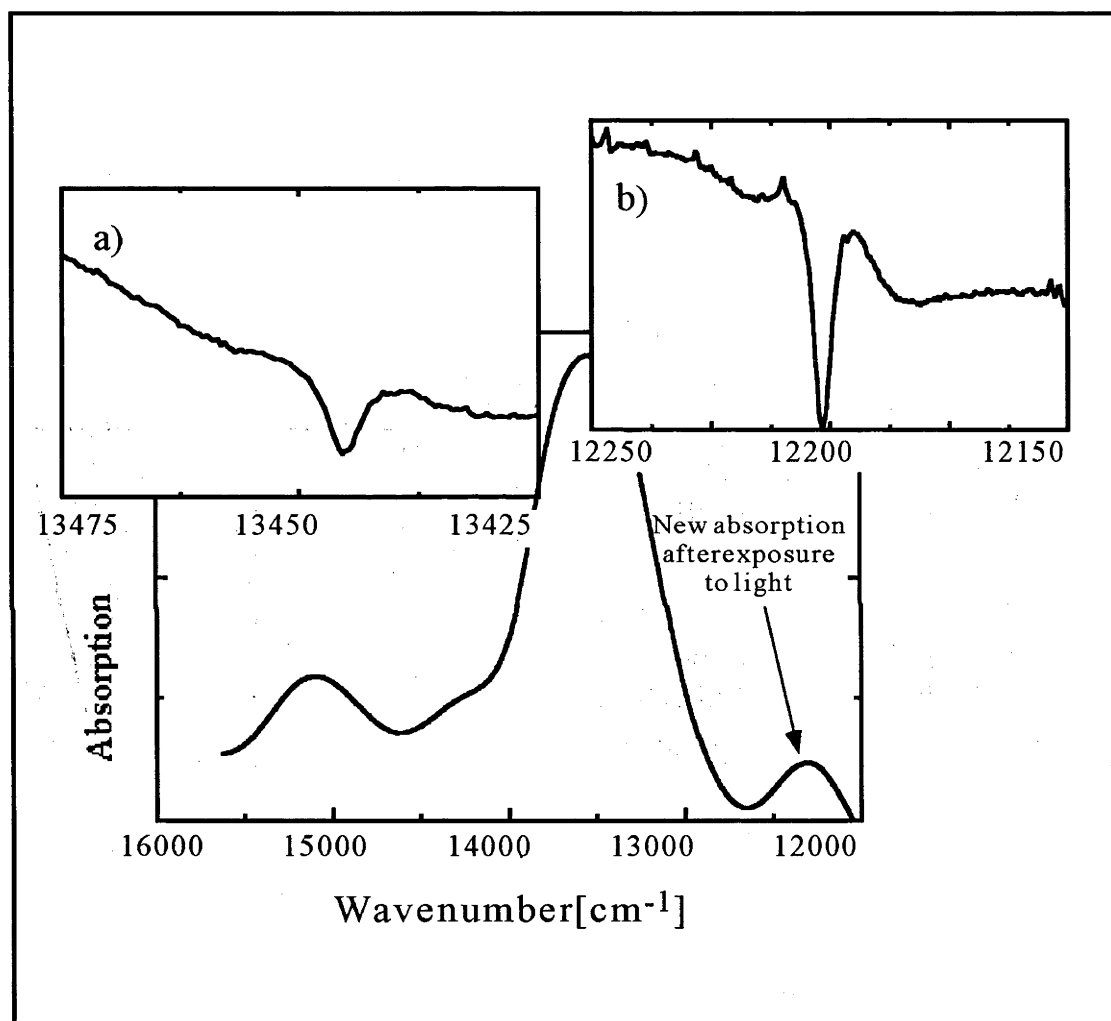


Figure 3.17: Broadband absorption of ZnObuPc/PMMA showing the appearance of the new absorption after exposure to light. Inserts a) and b) show spectral holes burnt into the Q band and the new absorption band respectively.

4. Magneto-optic Measurements of Spectral Holes

4.1 Zeeman experiments on spectral holes

4.1.1 Spectral hole-burning in a system with a degenerate excited state

Within an inhomogeneously broadened band, there is some distribution of transition energies. When the transition has a doubly degenerate excited state which has been split by crystal fields within the host - such as the case in the chromophores studied here - then the inhomogeneously broadened band will consist of overlapping contributions from the two CF-split levels (see figure 4.1). In the system studied here, these two contributions are uncorrelated. When selection is performed at a given wavelength, the subset of chromophores selected will comprise of transitions to both CF-split levels.

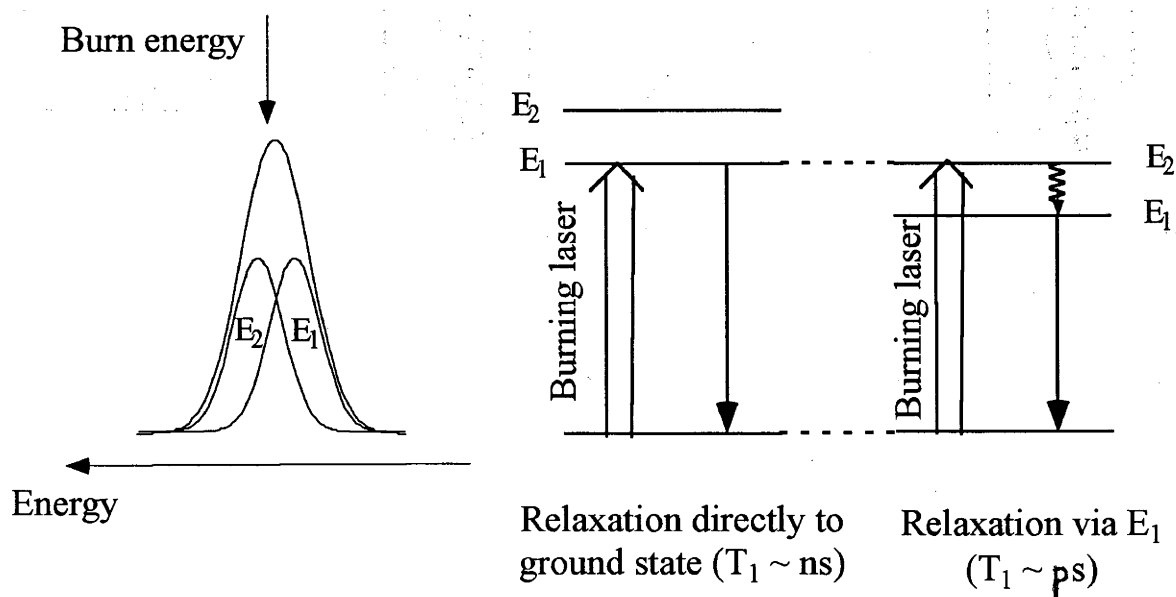


Figure 4.1: When a spectral hole is burnt into a band which consists of a distribution of two CF-split levels, E_1 and E_2 , then chromophores selected by hole-burning will comprise transitions to both the excited state levels. These two contributions will have two different lifetimes associated with them.

For the purpose of discussion here, the lower CF level is called E_1 and the upper one E_2 , as labelled in figure 4.1.

If the system was well correlated, three holes would be expected upon burning: a hole at the energy of the laser; an E_1 sidehole which occurs as a result of the depletion of E_2 at the laser energy; and an E_2 sidehole as a result of the depletion of E_1 at the energy of the laser. In the systems studied here, however, correlation is poor. There is a broad distribution of CF splittings (this is discussed later in this chapter). As a result, no sideholes are observed (see figure 4.2). In general, the electronic energy levels of chromophores in crystalline host tend to be well correlated, whilst in amorphous hosts correlation tends to be poor [3].

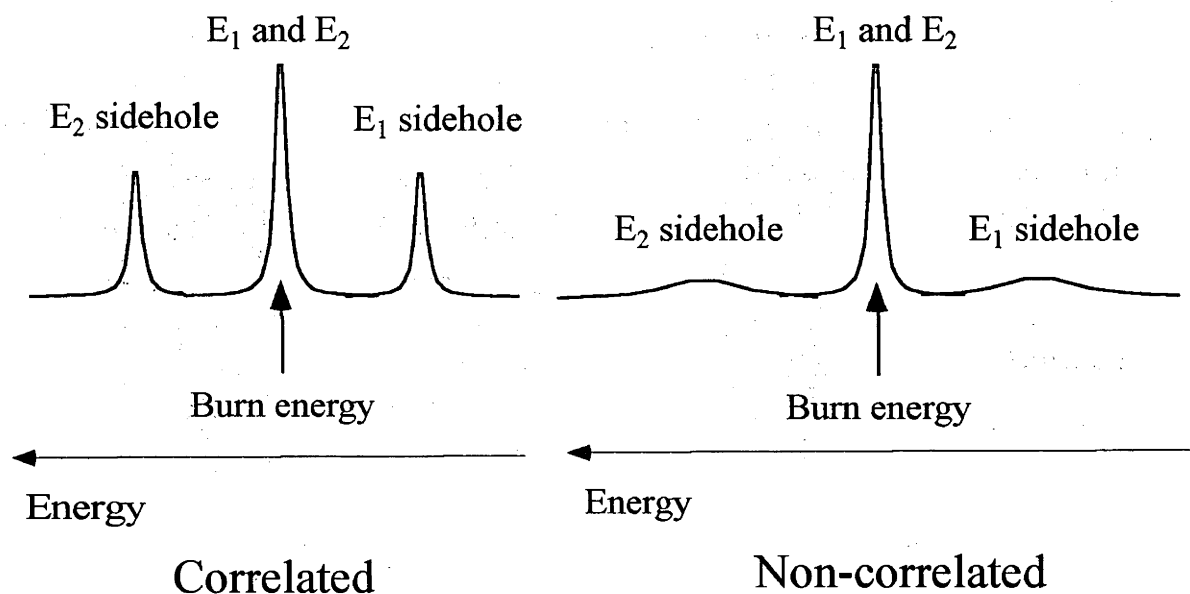


Figure 4.2: Electronic sideholes from burning into a system with a CF-split excited state. If the system is correlated, then sideholes are readily observed. If it is not correlated, then sideholes are more difficult to measure.

The contributions from E_1 and E_2 will have different linewidths (see figure 4.1). E_1 relaxes directly to the ground state with a lifetime of \sim ns [45, 52] while E_2 relaxes to E_1 with a far shorter lifetime (\sim ps [59]). The hole shape thus consists of a broader shallower component belonging to E_2 , and a narrower deeper component belonging to E_1 (see figure 4.3).

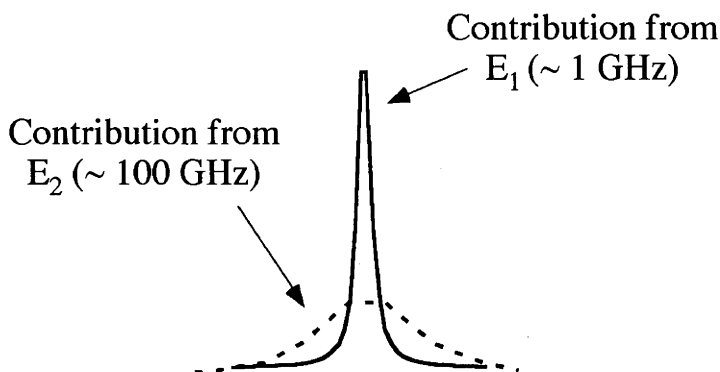


Figure 4.3: The contributions from E_1 and E_2 have different lifetimes. Therefore they contribute differently to the hole profile.

If the spectral hole shape shown in figure 4.3 is read out with a resolution appropriate for the widths of the features, then the deep narrow E_1 component dominates the observed shape. The resolution available with the lamp and monochromator used in some of the experiments here is not sufficient to read out the top of the hole. The hole shape which is observed is convoluted with the read-out function. The true depth of the hole is not observed. Nevertheless, the top of the hole shape is associated predominantly with the narrower E_1 component.

As outlined in chapter 1, the CF-split levels of the excited state can shift further apart upon the application of a magnetic field. Because the E_1 component is more prominent, any shifts the E_1 level undergoes in a magnetic field will be more readily observed than the shifts of the E_2 level. As a result, a shift of the hole maximum may be expected as well as a broadening of the hole in a magnetic field.

4.1.2 Low resolution Zeeman experiments on spectral holes in zinc phthalocyanine and zinc octaethylporphyrin

Zeeman experiments were performed on spectral holes in ZnPc and ZnOep and the results are displayed in figures 4.4 and 4.5. Holes were burnt using the 676.4 nm line of a Kr^+ laser for ZnPc and the 568.2 nm line for ZnOep. Holes were read out in transmission using a monochromator. From figures 4.4 and 4.5 it can be seen that, at this resolution ($\sim 1 \text{ cm}^{-1}$), the Zeeman shifts are not clearly measurable.

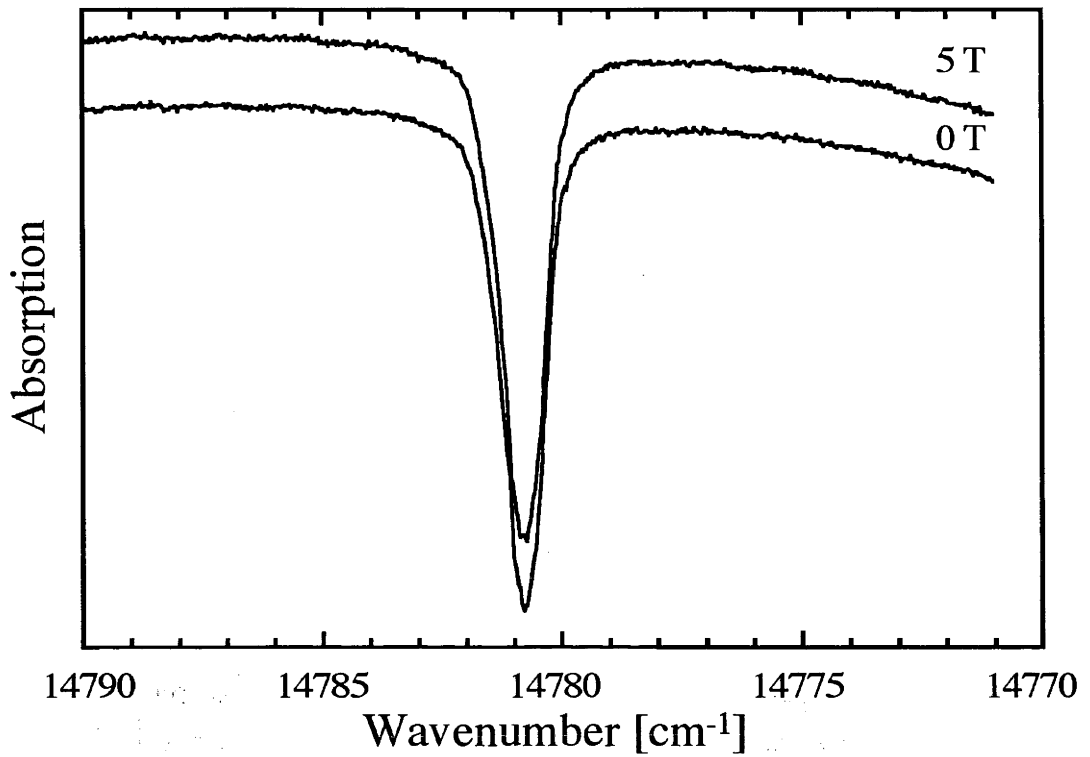


Figure 4.4: Absorption spectra of a 676.4 nm hole in ZnPc/PMMA in 0 and 5 T.

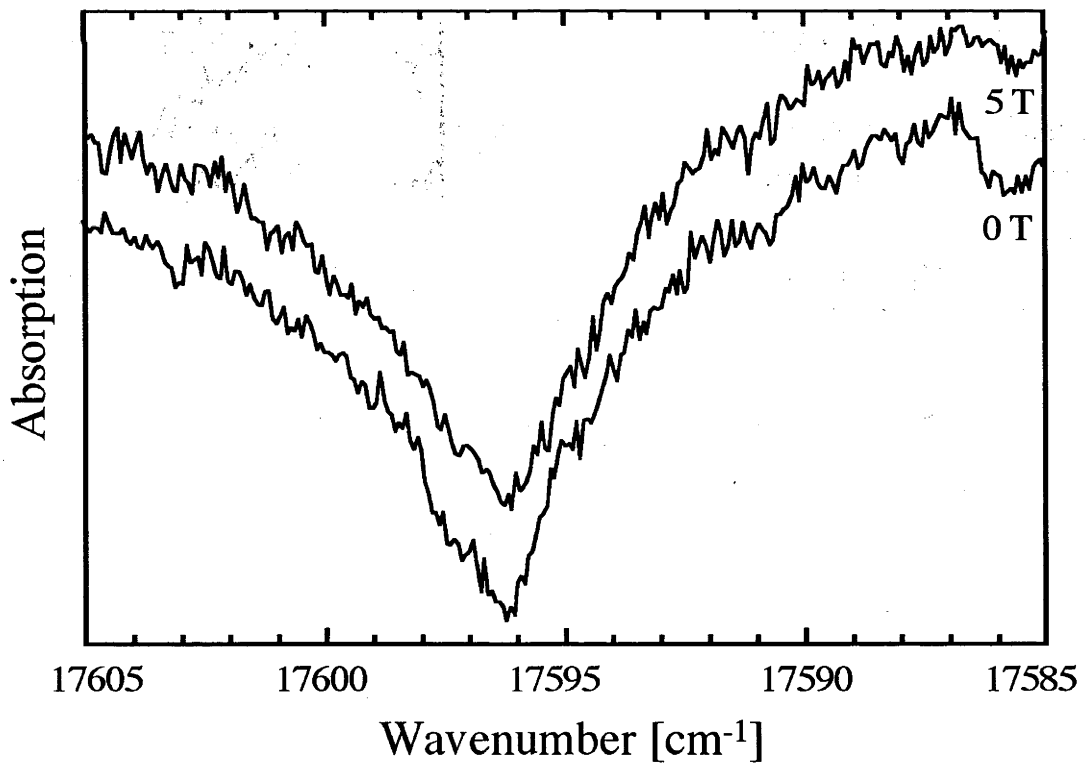


Figure 4.5: Absorption spectra of a 568.2 nm hole in ZnOep/PVB in 0 and 5 T.

In Ar matrices, chromophores may be identified as occupying distinct sites in the matrix [9, 10, 60]. More structured spectra may result from such an environment. From such spectra CF splittings of $\sim 30 \text{ cm}^{-1}$ for ZnOep and $\sim 50 \text{ cm}^{-1}$ for ZnPc have been identified [9, 10]. The absorption bands of ZnPc and ZnOep in polymer films are ~ 330 and $\sim 210 \text{ cm}^{-1}$ wide respectively. CF splittings similar to (or larger than) those measured in Ar could easily be masked by the inhomogeneous broadening.

Equation 1.17 (restated and renumbered here for convenience) may be used as a means to model the magnitude of the Zeeman shift.

$$\Delta v_B = \pm \frac{\Delta v_0}{2} \left\{ \left[1 + \left(\frac{2\mu_B \cdot \mathbf{B}}{\Delta v_0} \right)^2 \right]^{1/2} - 1 \right\} \quad (4.1)$$

Using a value of $1.4 \text{ cm}^{-1}/\text{T}$ for μ_B [21] and the above CF splittings, equation 4.1 yields Zeeman shifts of 1.55 cm^{-1} for ZnOep and 0.96 cm^{-1} for ZnPc in the case where μ_B and \mathbf{B} are parallel. This is far greater than the observed shifts.

For the purposes of this experiment, deep saturated holes were burnt to obtain an adequate signal-to-noise ratio. When saturated holes are burnt, orientational selectivity is reduced. (As the hole-burning process progresses, chromophores of orientations other than those with their transition dipoles at a small angle to the polarisation direction of the laser are depleted.) The chromophores are therefore assumed to be randomly oriented. This random orientation causes a reduction of the observed Zeeman shifts by a factor approaching $4/15$ [61]. With this reduction, the experimental shift ($< 0.2 \text{ cm}^{-1}$) remains lower than predicted. However, the Q excited states of both ZnPc and ZnOep are known to involve substantial JT interactions, which quench the excited state magnetic moments. The extent of the quenching is determined by the Ham factor, which has been reported to be 0.67 for ZnOep and 0.63 for ZnPc [8, 10]. These added contributions lead to calculated Zeeman shifts of 0.19 cm^{-1} for ZnOep and 0.10 cm^{-1} for ZnPc. These values are within the range of the experimental observations. The mean CF splittings in polymer films

may be greater than in Ar. These increased CF splittings would reduce the Zeeman shifts further.

An experiment with higher resolution is required to render the Zeeman shifts observable. Such an experiment was done in the case of ZnPc using a single-frequency scanning dye laser. This experiment is discussed in the next section.

4.1.3 High resolution Zeeman experiments on zinc phthalocyanine

These experiments were performed in transmission as described in chapter 2. When holes are burnt with a single-frequency laser, for reasons outlined at the beginning of this chapter, the contribution from the broader upper CF-split level may be neglected. Also, the holes burnt in this experiment were only a few per cent of the absorption at the burning wavelength. Therefore, orientational selectivity may be used advantageously. Accordingly, holes were burnt in experimental geometries where the polarisation direction of the burning and reading laser was parallel or perpendicular to the applied field. The results are displayed in figures 4.6 and 4.7.

The excited state magnetic moment of the Q transition in ZnPc is perpendicular to the molecular plane. Therefore it may be expected that the perpendicular experimental geometry is going to show the greatest Zeeman shift (as the transition dipole is in the molecular plane). The magnetic-field-induced shift or broadening observed with the parallel geometry is going to be greatly reduced in comparison to the perpendicular geometry, as the chromophores selected in this experiment will not be appropriately oriented to interact strongly with the magnetic field. Any changes which are observed with the increase in magnetic field are as a result of angular variation (as a result of the slight distribution associated with the photoselection). The above phenomena may indeed be observed in figures 4.6 and 4.7.

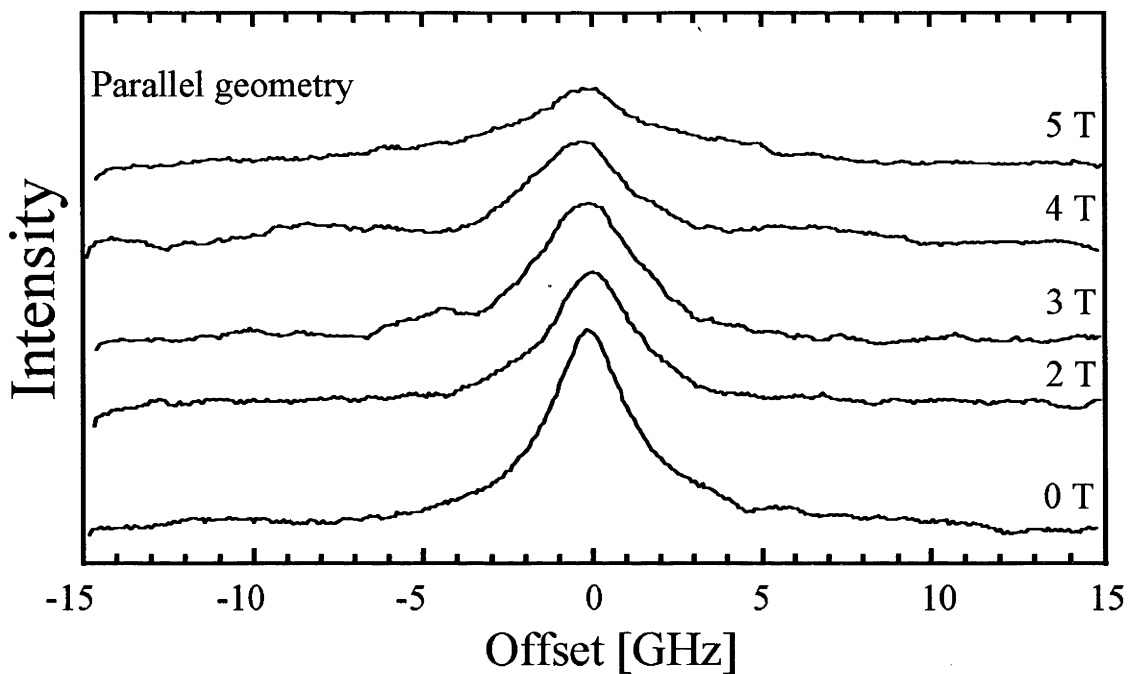


Figure 4.6: Changes in hole shape as a function of magnetic field in ZnPc/PMMA. The hole was burnt at 670.1 nm and the magnetic field was parallel to the polarisation direction of the burning and reading light.

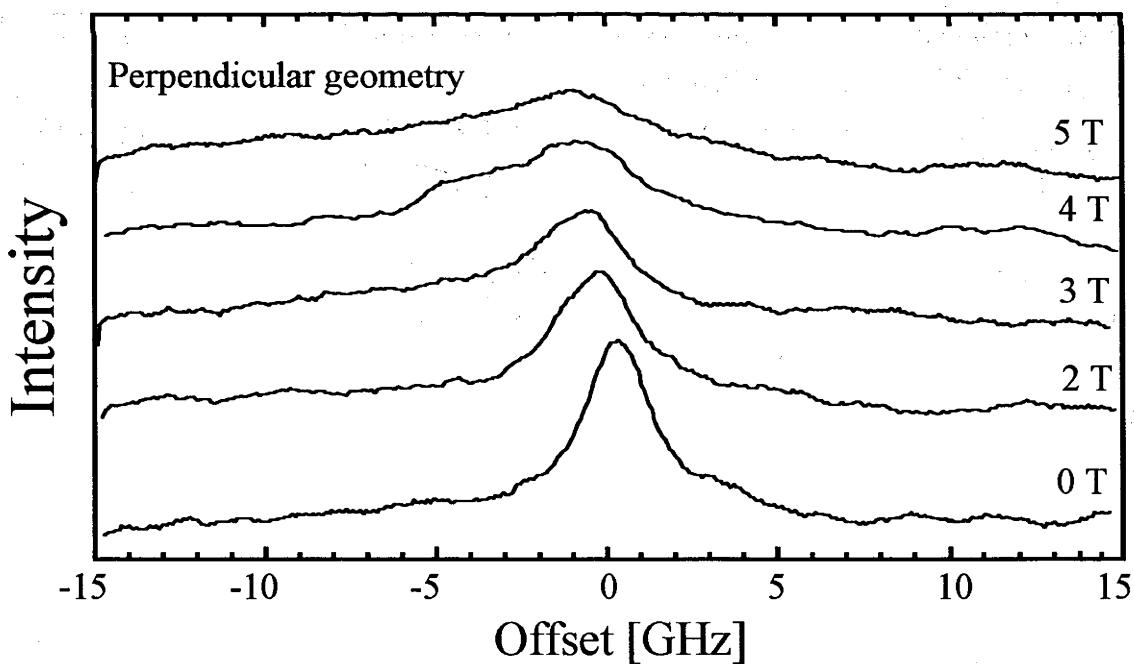


Figure 4.7: Changes in hole shape as a function of magnetic field in ZnPc/PMMA. The hole was burnt at 669.1 nm and the magnetic field was perpendicular to the polarisation direction of the burning and reading light.

A plot of the shift of the hole maximum with magnetic field for the perpendicular geometry is given in figure 4.8. The shift is linear with field strength.

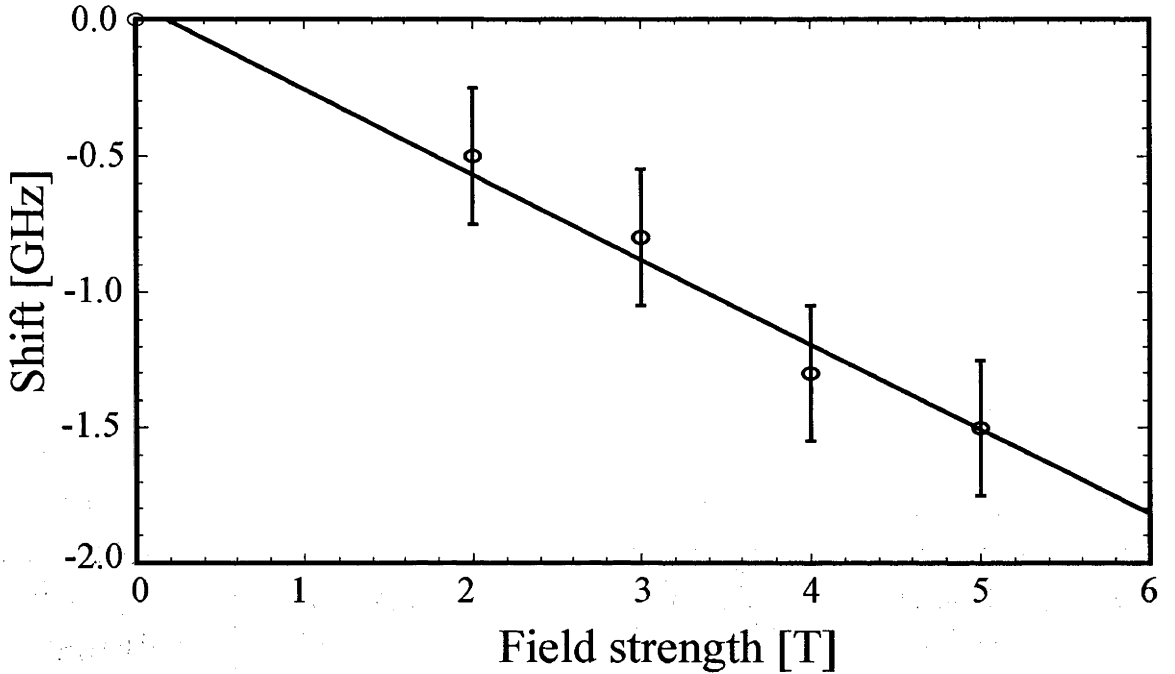


Figure 4.8: Shift of hole maximum as a function of applied magnetic field for a hole in ZnPc/PMMA burnt at 669.1 nm. The magnetic field was perpendicular to the polarisation direction of the burning and reading light.

The change in hole shape with magnetic field may be modelled following references [21, 62]. This model describes the orientational selectivity of the hole-burning process and a Zeeman shift given by equation 4.1. A Ham factor of 0.63 is also included [8]. The hole shape in the presence of the field is described by:

$$\frac{\frac{\Gamma}{2}f(\theta)}{(\nu - \Delta\nu_B)^2 + \left(\frac{\Gamma}{2}\right)^2} \quad (4.2)$$

where Γ is the zero field hole width, θ is the angle between \mathbf{B} and $\boldsymbol{\mu}_B$, $\Delta\nu_B$ is given by equation 4.1 and ν is the frequency variable. The function $f(\theta)$ describes the orientational selectivity of the burning and reading processes (see reference [62]). This is described in terms of θ as the orientation of the selected chromophores defines the orientation of $\boldsymbol{\mu}_B$ relative to \mathbf{B} . $f(\theta)$ changes according to the geometry of the experiment.

To model the data, a range of θ values were included to describe the distribution of chromophore angles. $f(\theta)$ in equation 4.2 then acts as a weighting function.

The authors of reference [21] noted that in an amorphous host there is likely to be some distribution of CF splittings. This distribution may be characterised by some mean value. These authors made the simplification of describing the CF splittings using a fixed mean value rather than including an expression for the distribution of the CF splittings. Initially, such a simplification was made here. A fixed CF value leads to a fixed value for $\Delta\nu_B$, whilst a distribution leads to a distribution of $\Delta\nu_B$ values.

This model described the data from the parallel experiment adequately (figure 4.9), but failed to reproduce the hole shapes in the presence of the field for the perpendicular experimental geometry (figure 4.10). This suggests that the changes with magnetic field strength in the parallel geometry may be predominantly caused by a distribution of molecular orientations. In the case of the perpendicular experimental geometry, however, the changes in shape may be dominated by a distribution of CF values.

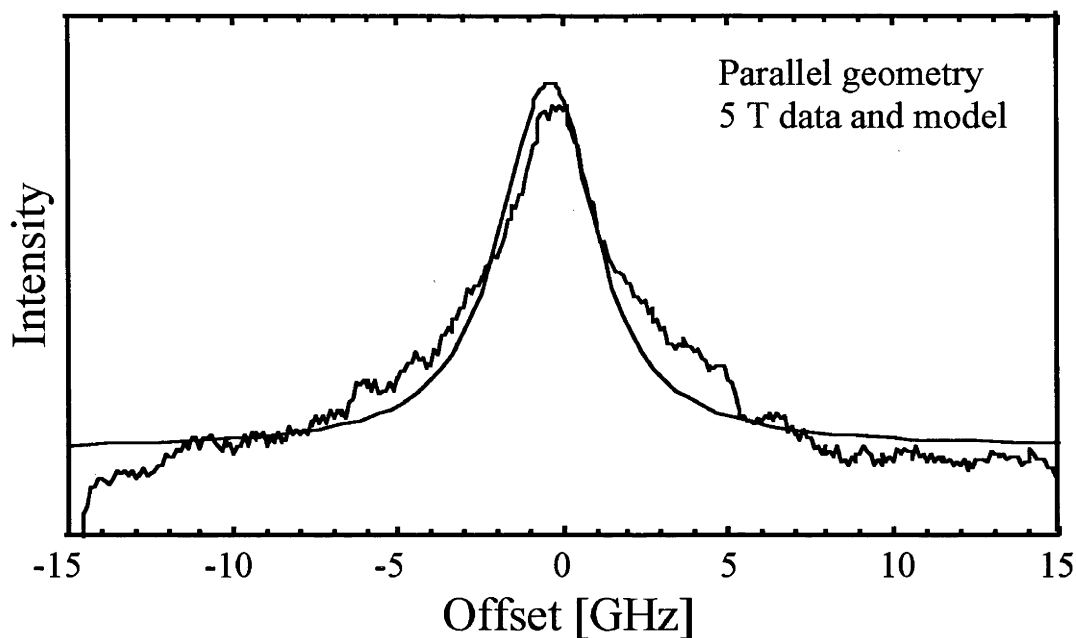


Figure 4.9: A spectral hole burnt into ZnPc/PMMA at 670.1 nm in a 5 T field parallel to the polarisation direction of the burning and reading light. This is accompanied by a model describing the changes in the field of a spectral hole shape where there is some distribution of the orientation of the chromophores.

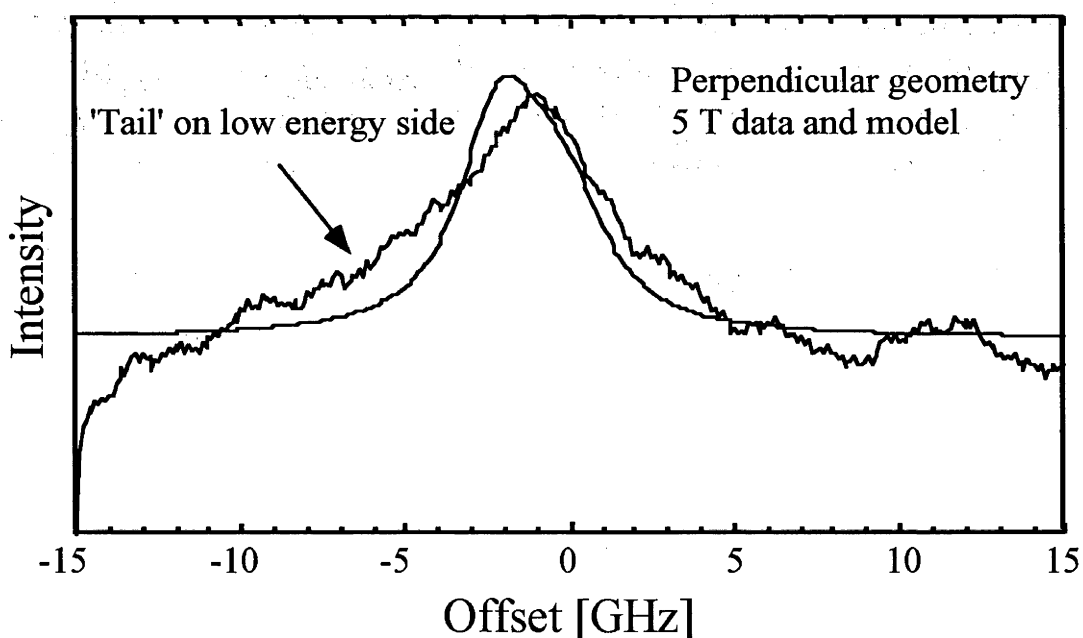


Figure 4.10: A spectral hole burnt into ZnPc/PMMA at 669.1 nm in a 5 T field perpendicular to the polarisation direction of the burning and reading light. This is accompanied by a model describing the changes in the field of a spectral hole shape where there is some distribution of the orientation of the chromophores.

The most notable feature of the inadequacy of the model is its failure to reproduce the 'tail' on the data from the perpendicular experimental geometry. Such a tail would be consistent with a distribution of CF values.

Accordingly, a Gaussian expression for the distribution of CF splittings was expressly included. This Gaussian was characterised by a root mean square value and had a width related to the root mean square value.

$$\frac{2 \times \Delta v_0}{\Delta v'_0} \text{Exp} \left[- \left(\frac{\Delta v_0}{\Delta v'_0} \right)^2 \right] \quad (4.3)$$

$\Delta v'_0$ is the root mean square CF value. Δv_0 values of 0 to $2\Delta v'_0$ were included in the model.

In the experiment performed by Ulitsky et al. [21], a hole was burnt into the Q band of ZnPc/PVB using the 676.4 nm line of a Kr⁺ laser. The zero-field hole was $\sim 2 \text{ cm}^{-1}$ wide. To see a Zeeman effect on a hole of this width a 30 T field was used. In their experiment a Zeeman shift is observed, but perhaps some of the smaller effects, such as the effect of the distribution of the CF splittings, are concealed within the width of the feature. Such an explanation rationalises why a distribution of CF splittings is required for the work here, but not in reference [21].

This modified model accounted for the shape of the data satisfactorily, but the changes in hole shape with magnetic field could only be modelled by varying $\Delta v'_0$ with the magnetic field. The origin of this problem may be understood if equation 4.1 is rewritten with the Ham factor expressly included:

$$\Delta v_B = \pm \frac{\Delta v_0}{2} \left\{ \left[1 + \left(\frac{2\gamma \mu_B \cdot \mathbf{B}}{\Delta v_0} \right)^2 \right]^{1/2} - 1 \right\} \quad (4.4)$$

It can be seen from equation 4.4 that the Ham factor, γ , and the CF splitting, Δv_0 , play two different roles in altering the magnitude of the Zeeman shift. Exploration of these differences established that if γ is

changed the problem observed above may be reduced. If γ is reduced to 0.52, then the model follows the changes in hole shape with field quite well (figure 4.11). A root mean square CF splitting of 110 cm^{-1} is required under these circumstances. (The shoulder on the low energy side of the 4 T data is an experimental artefact.)

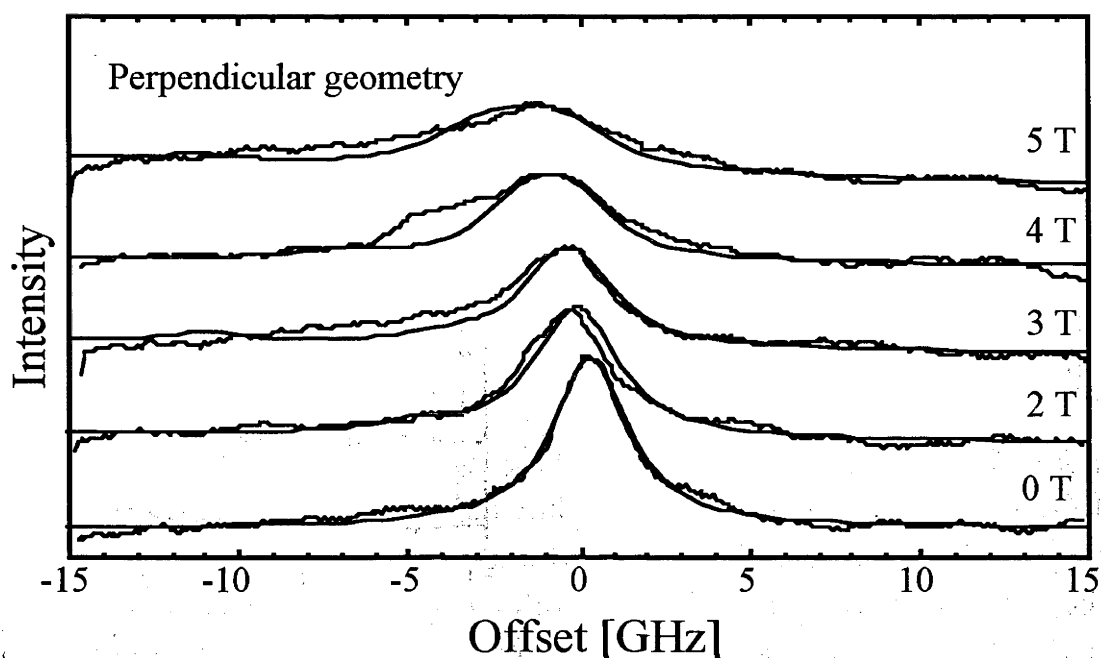


Figure 4.11: Spectral holes burnt into ZnPc/PMMA at 669.1 nm in magnetic fields of 0 – 5 T perpendicular to the polarisation direction of the burning and reading light. The data is accompanied by a model describing the changes in the field of a spectral hole shape where there is some distribution of the orientation of the chromophores and a distribution of CF splittings. The shoulder on the low energy side of the 4 T data is an experimental artefact.

Two Gaussians 160 cm^{-1} wide and 110 cm^{-1} apart fit the broadband absorption and MCD quite well, so a CF splitting of 110 cm^{-1} is not unreasonable.

The error on the fit of the modified model to the perpendicular geometry high resolution Zeeman data is approximately 10 per cent for the 2 T data through to 20 per cent for the 5 T data.

The fit of the model has a certain degree of invariance to the values for $\Delta v'_0$ and γ . Values $\pm 10 \text{ cm}^{-1}$ of the 110 cm^{-1} used for Δv_0 reproduce the data satisfactorily. Variations of the Ham factor of ± 0.03 also reproduce the data satisfactorily, but values outside this margin lead to the situation where one $\Delta v'_0$ value no longer models the data for all the field strengths.

Jansen et al. report the Ham factor as a molecular property of zinc porphyrin [63]. VanCott et al. [60] report a dependence of the Ham factor upon molecular site in ZnTbp/Ar. The fact that the Ham factor needed to be altered to accommodate the data in polymer matrices suggests that the observations here appear to support those of VanCott. If the Ham factor does vary with molecular site, then a more realistic model might also include a distribution of Ham factors.

A parameter which was explored in this work was the width of the distribution of CF splittings. In the distribution given in equation 4.2, the width is related to $\Delta v'_0$. A model which had a separate parameter for the width was investigated, but the goodness of fit to the data was found to be invariant to the width of the distribution to nearly ± 50 per cent of $\Delta v'_0$.

There are a number of difficulties associated with describing the behaviour of chromophores in amorphous hosts. In an amorphous environment, many parameters may have a distribution of values. A given parameter may then be represented by some characteristic mean value, or more fully described by a distribution. If a distribution is used, the question arises as to what type of function one uses to describe the distribution. In the case of the CF splittings here, a number of functions were attempted, all of which were based around the Gaussian form. The main limit on the accuracy of the values of the parameters obtained is the appropriateness of the model.

Another difficulty with modelling CF splittings and a JT effect is that these two processes interact with each other. The effects of these two processes are therefore difficult to separate. For the values given for the parameters from the modelling to be at all reliable, the same values must fit all the data. This is the case here. The best fit over all the magnetic field dependent data was obtained qualitatively.

From the results obtained, it can be seen that it is possible to acquire information upon CF splittings and JT activity from spectra which initially had no structure. These results demonstrate the potential of this technique. Similar information has been obtained for this class of chromophore in Ar and Shpol'skii matrices, but the structure of the spectra obtainable in these hosts was heavily relied upon [6, 8, 9, 60, 63]. In a polymer environment, it seems that the CF splittings are large and widely distributed and that the JT coupling is a little stronger in comparison to the data from Ar matrices.

The wavelength dependence of the Zeeman shift of ZnPc/PMMA was measured. The shift of the hole maximum in 5 T as a function of wavelength for the perpendicular experimental geometry is shown in figure 4.12. Little wavelength dependence is observable. Therefore it seems that the mean CF splitting is constant across the inhomogeneously broadened band. This result is in contrast to the observation in Ar matrices [9].

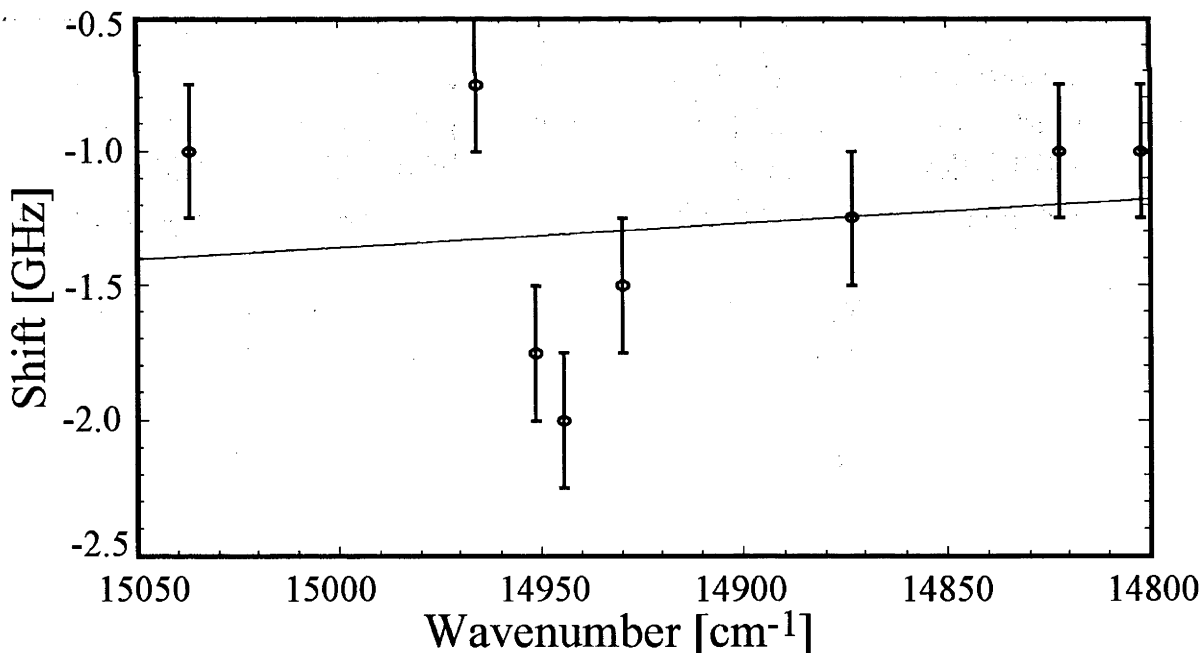


Figure 4.12: The wavelength dependence of the shift of the hole maximum in a 5 T field, where the field is perpendicular to the polarisation direction of the burning and reading light.

4.2 Magnetic circular dichroism experiments on spectral holes

The CF components of the Q band are immediately distinguishable by the opposite signs of their MCD. Thus MCD is a useful tool in helping determine which of the levels contribute to a given hole shape.

Consider the hole in ZnPc/PMMA, which was burnt at 676.4 nm using a Kr⁺ laser (figure 4.13). This burn wavelength is approximately halfway down the red edge of the Q band. Therefore the hole could be expected to be burnt predominantly in E₁. E₁ gives a negative MCD and thus the hole MCD must be positive. This is indeed observed for both the ZPL and the PW. The rise on the high energy side of the ZPL observable in the absorption may be assigned to the photoproduct. The photoproduct appears to have an oppositely signed MCD from that of the hole, as would be expected.

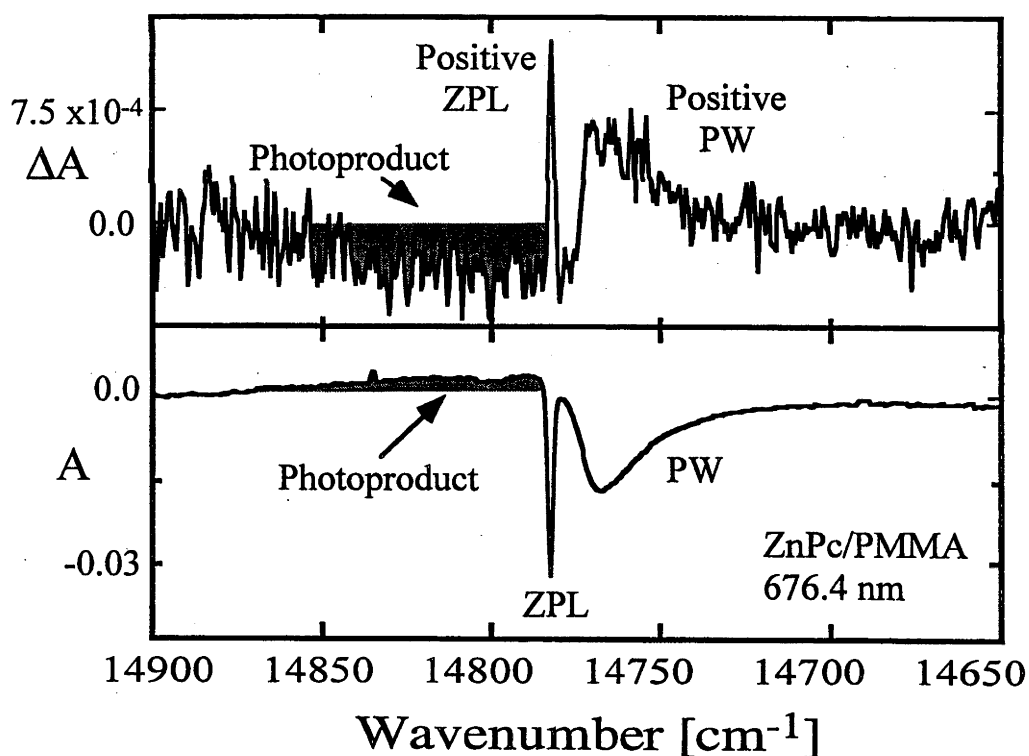


Figure 4.13: Hole absorption (lower) and hole MCD (upper) for a hole burnt into ZnPc/PMMA at 676.4 nm.

A hole MCD for ZnOep/PVB is shown in figure 4.14. The hole was burnt at 568.2 nm using a Kr⁺ laser. The burn wavelength is close to the top of the absorption. Both E₁ and E₂ may contribute. The hole MCD will thus have negative and positive MCD contributions. Only a negative contribution is immediately observable (arising from E₂). Notice that the centre of the hole MCD does not coincide with that of the hole absorption (see the insert of figure 4.14).

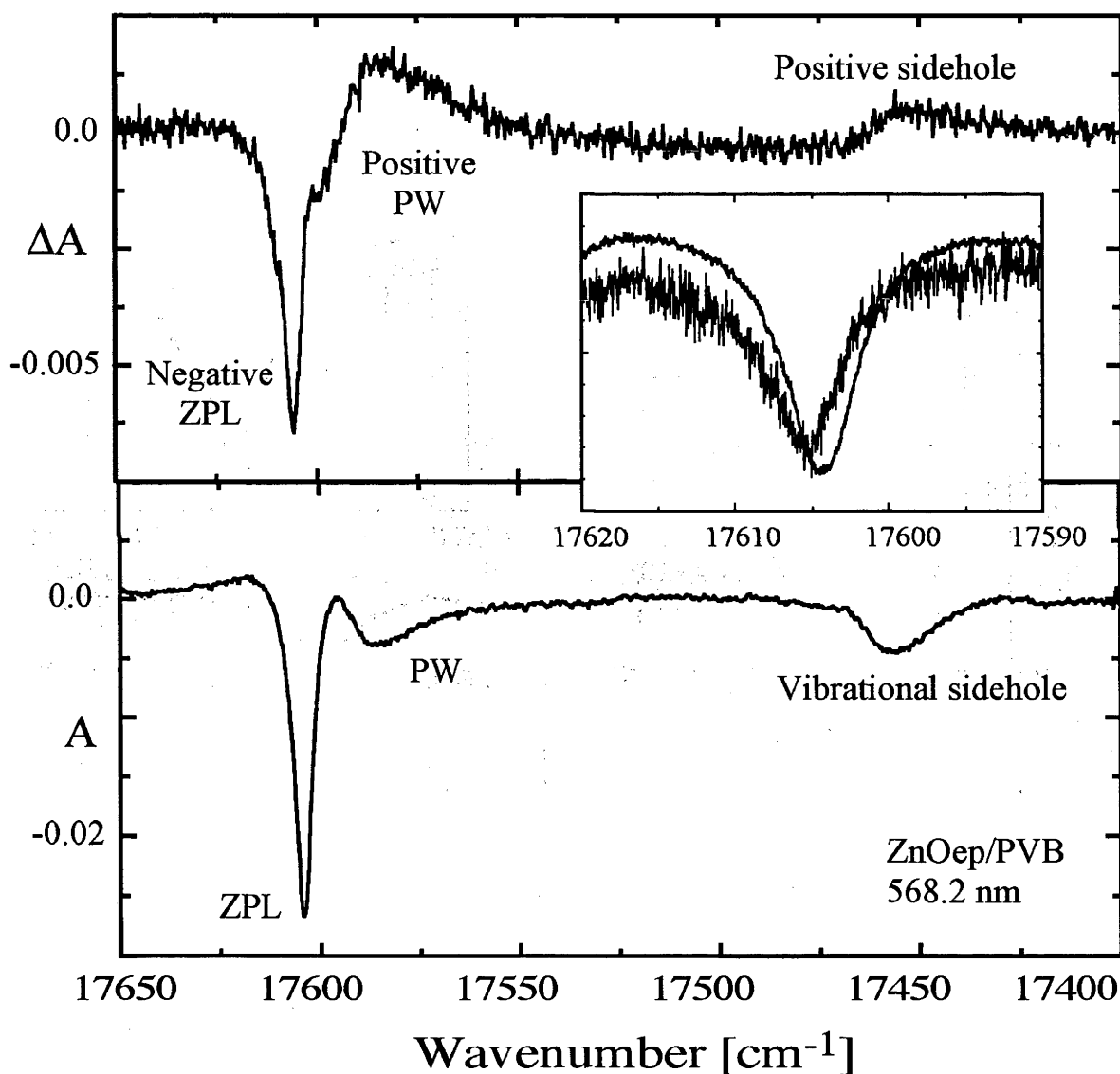


Figure 4.14: Hole absorption (lower) and hole MCD (upper) of a hole burnt into ZnOep/PVB at 568.2 nm. The insert shows a higher resolution scan of the ZPL.

Other interesting features of the hole MCD of ZnOep are the sidehole to the red of the burn energy and the sign of the phonon wing MCD. The sidehole is indicative of hole-burning into a vibrational sideline of a (lower-energy) origin. The separation between the hole at the burn wavelength and the sidehole gives a mode frequency of $\sim 145 \text{ cm}^{-1}$. This frequency corresponds to the JT active mode [10]. The sidehole is rather broad ($\sim 25 \text{ cm}^{-1}$). This width is likely to be attributable to interactions between the JT and CF effects [61] leading to relatively poor correlation of the JT frequency. The area of the sidehole is much smaller than the area of the hole at the burn energy. If the hole was burnt purely into a vibrational sideline, then the areas of the hole at the burn energy and the sidehole would scale according to the appropriate Huang–Rhys parameter. The relative areas observed suggest that the hole at the burn energy is dominated by burning in the electronic origins.

The PW shows an MCD signal of the opposite sign to that of the ZPL. This result is in marked contrast to the observations in ZnPc. The sign of the PW suggests that the phonons are associated mostly with E_1 . However, the corresponding ZPL of E_1 is not apparent from the hole MCD. There are some other possible interpretations of the sign of the MCD of the PW relative to that of the ZPL. It is possible for JT activity to reverse the sign in a single mode [11]; if phonons are not totally symmetric, then the sign of their MCD may be reversed. Also, if there is photoproduct absorbing in the region where the PW is, then a change of sign would be expected. In this last case the shape of the absorption would be affected. Another possible situation is that the lineshapes are such that the contribution of E_2 to the PW is not readily observed, for example if this contribution is very broad.

A question then arises: is the difference observed between ZnPc and ZnOep hole MCDs simply a result of their different positions in their respective inhomogeneously broadened bands, or is it related to the differences between the two chromophores and the way they interact with their environment?

In an attempt to answer this question, holes were burnt in three places across the inhomogeneously broadened band of ZnPc/PVB. The holes were burnt using a Spectra-Physics 375 dye laser with DCM as the dye. To form a comparison, this experiment was also performed on ZnTbp/PVB. This second sample was chosen as a matter of practicality as it also absorbs in the working region of DCM. ZnOep was not investigated as it does not absorb in the region of DCM. The positions of the holes in the Q bands of the two samples are shown in figures 4.15 and 4.16.

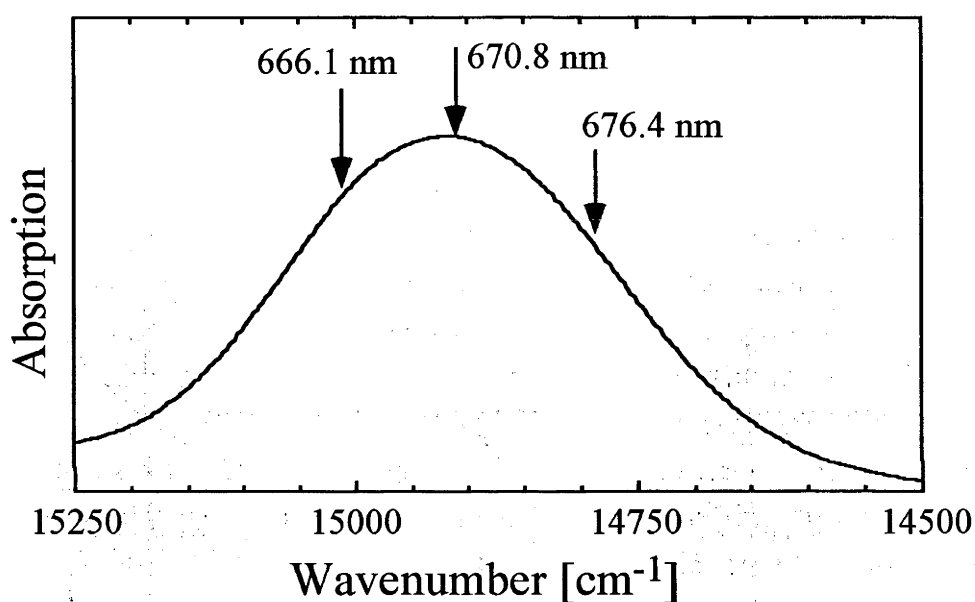


Figure 4.15: An absorption spectrum of the Q band of ZnPc/PVB showing the positions of the holes burnt for the wavelength dependence of the hole MCD experiment.

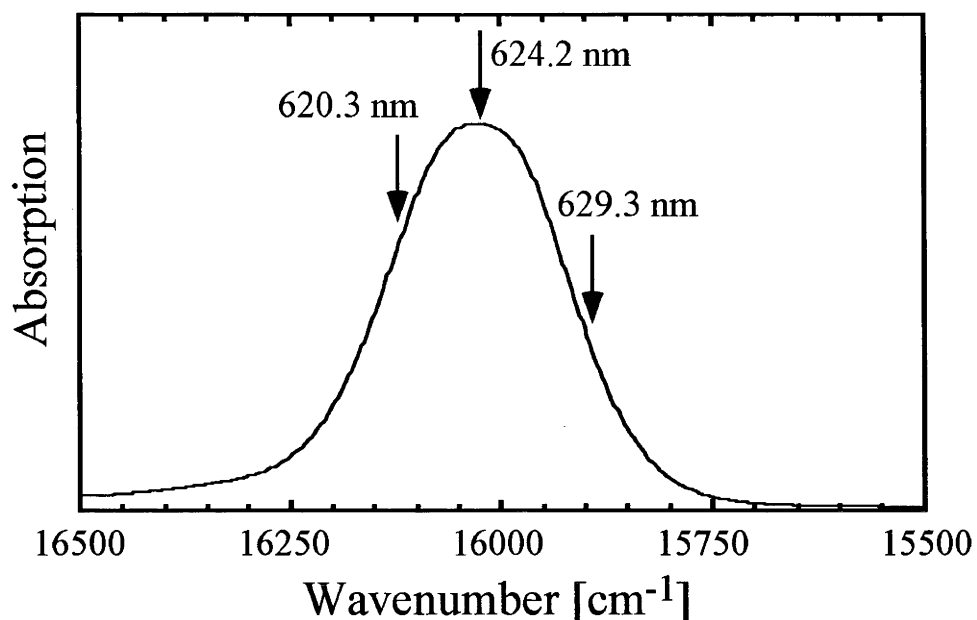


Figure 4.16: An absorption spectrum of the Q band of ZnTbp/PVB showing the positions of the holes burnt for the wavelength dependence of the hole MCD experiment.

First, consider the three hole MCD spectra for ZnPc/PVB. These are shown in figures 4.17 – 4.19. The hole burnt at 676.4 nm (figure 4.17) closely resembles the previous ZnPc/PMMA hole MCD burnt using a Kr⁺ laser (figure 4.13). There is a small contribution from E₂. This is evident from the broad negative baseline to the narrower feature, but the MCD indicates that the hole has been predominantly burnt into E₁. This is to be expected from a hole burnt at this position in the inhomogeneously broadened band.

Moving to the blue, the next hole was burnt at 670.8 nm (figure 4.18). This is close to the top of the absorption band. It can be seen clearly from the MCD of the ZPL that there is an increase in the contribution of E₂.

Moving further to the blue, the hole at 666.1 nm (figure 4.19) is dominated by the upper CF level. Unfortunately the signal-to-noise is poorer here as it is hard to burn holes of an appreciable depth on this side of the origin band. The MCD of the ZPL is shown in greater detail in the insert of figure 4.19.

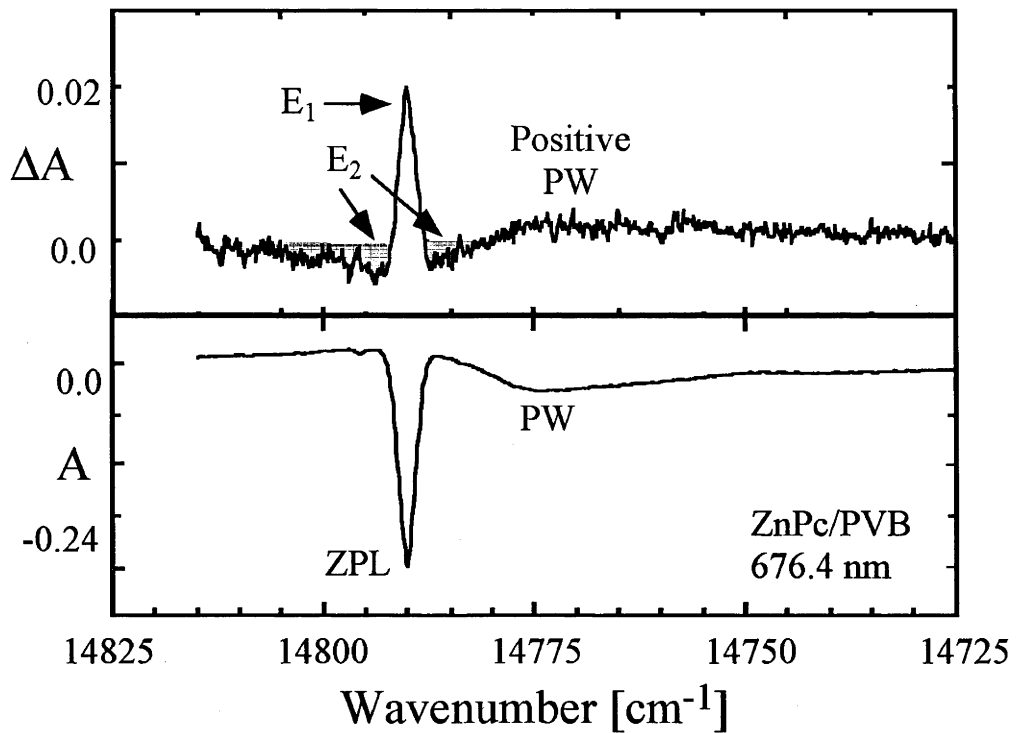


Figure 4.17: Hole absorption (lower) and hole MCD (upper) for the spectral hole burnt at 676.4 nm in ZnPc/PVB.

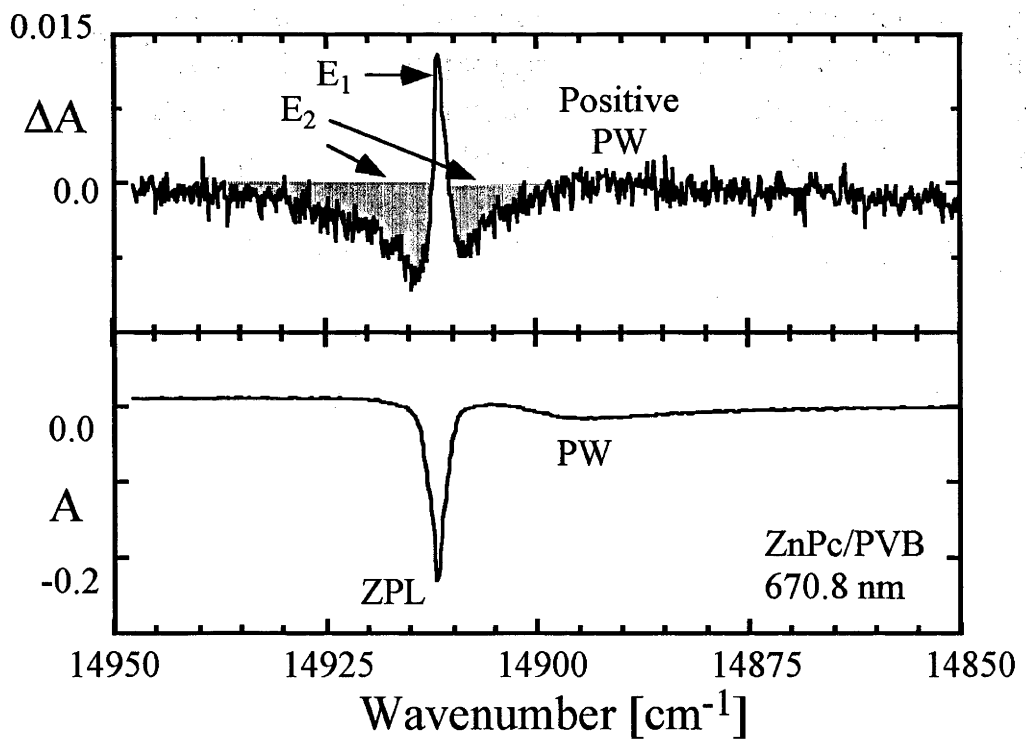


Figure 4.18: Hole absorption (lower) and hole MCD (upper) for the spectral hole burnt at 670.8 nm in ZnPc/PVB.

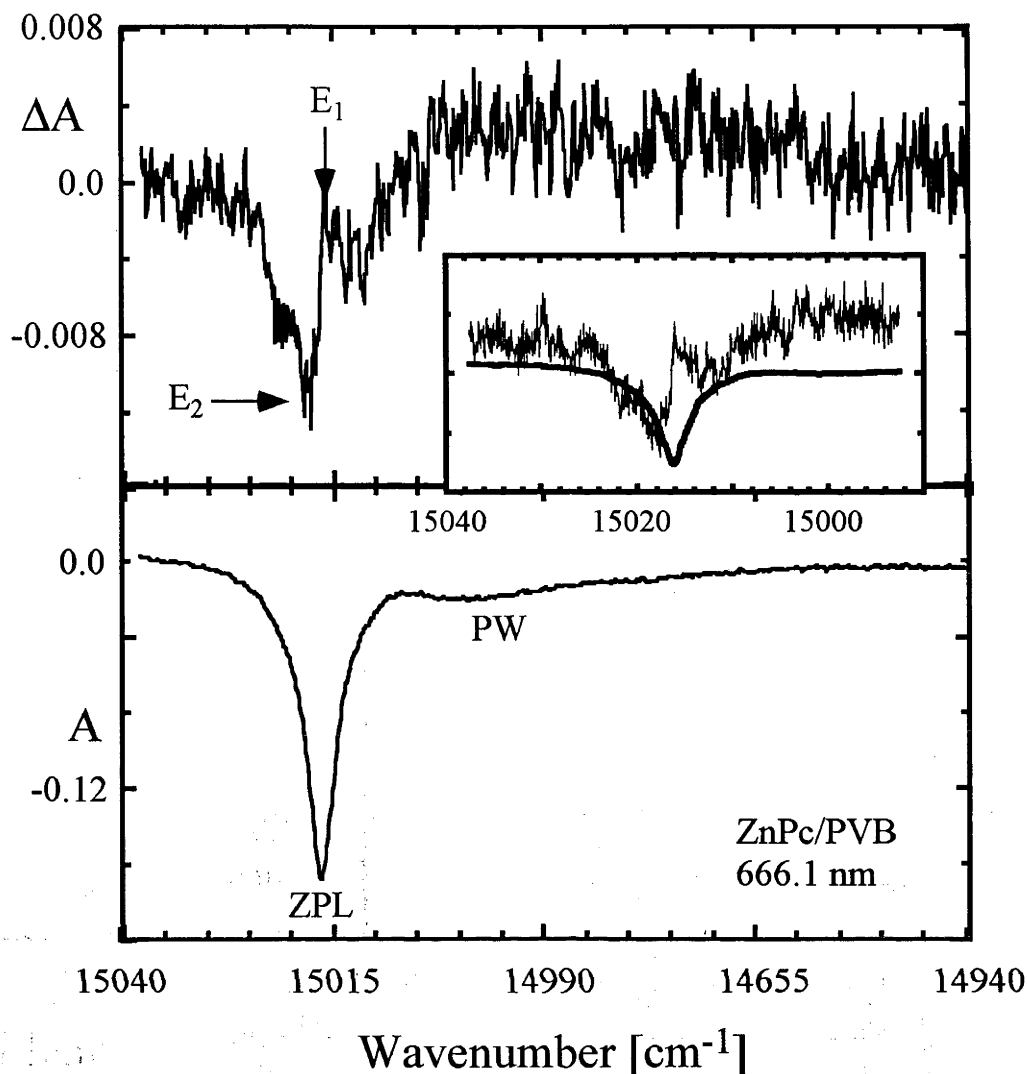


Figure 4.19: Hole absorption (lower) and hole MCD (upper) for the spectral hole burnt at 666.1 nm in ZnPc/PVB. The insert shows a higher resolution scan of the ZPL region.

Now consider the hole MCD spectra for ZnTbp/PVB (figures 4.20 – 4.22). Once again, the hole on the red edge has a predominantly narrow positive MCD (figure 4.20). Towards the middle of the band both CF-split levels are evident (figure 4.21). On the blue side (figure 4.22), the contribution from E₁ is not immediately observable. A spectrum with greater resolution is shown in the insert of figure 4.22: a narrower positive shape is still not evident in the MCD. This observation is in contrast to the observation in ZnPc.

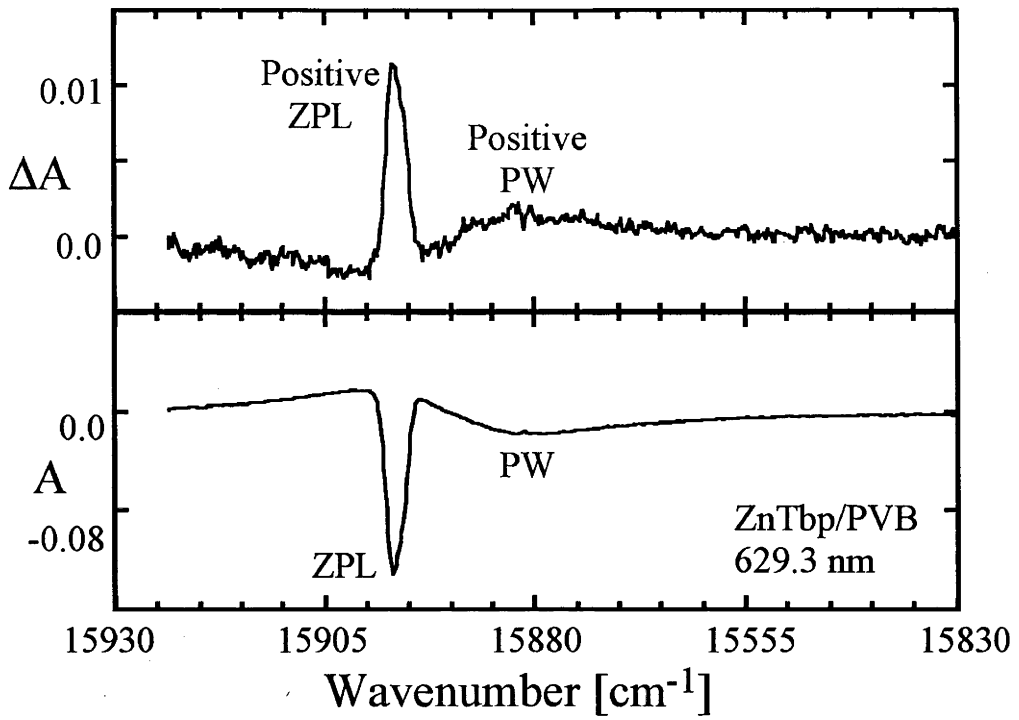


Figure 4.20: Hole absorption (lower) and hole MCD (upper) for the spectral hole burnt at 629.3 nm in ZnTbp/PVB.

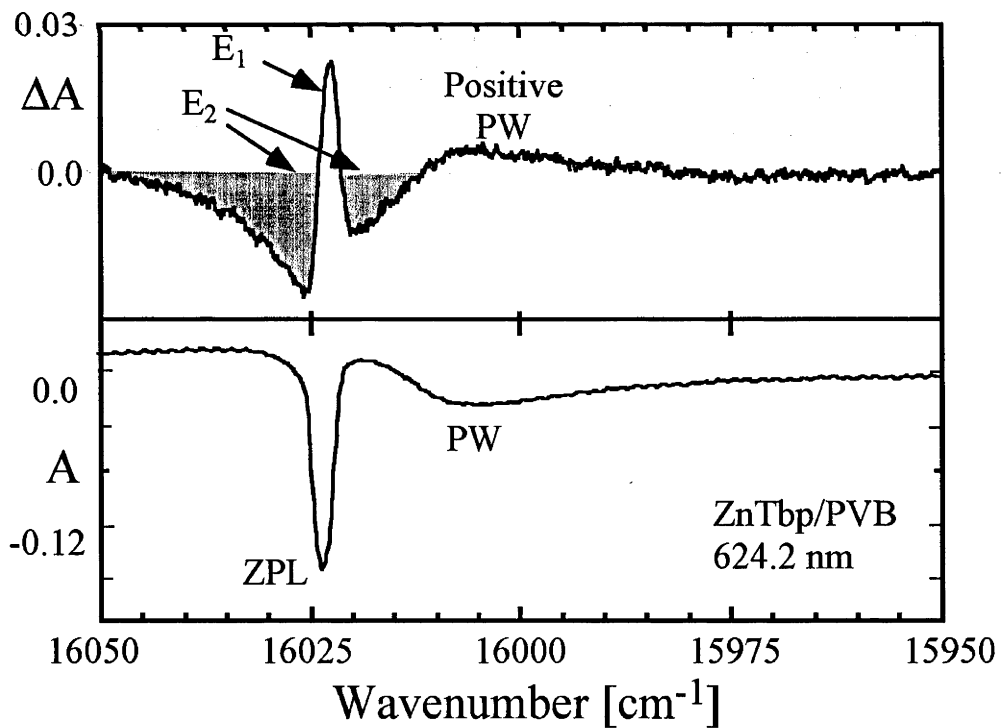


Figure 4.21: Hole absorption (lower) and hole MCD (upper) for the spectral hole burnt at 624.2 nm in ZnTbp/PVB.

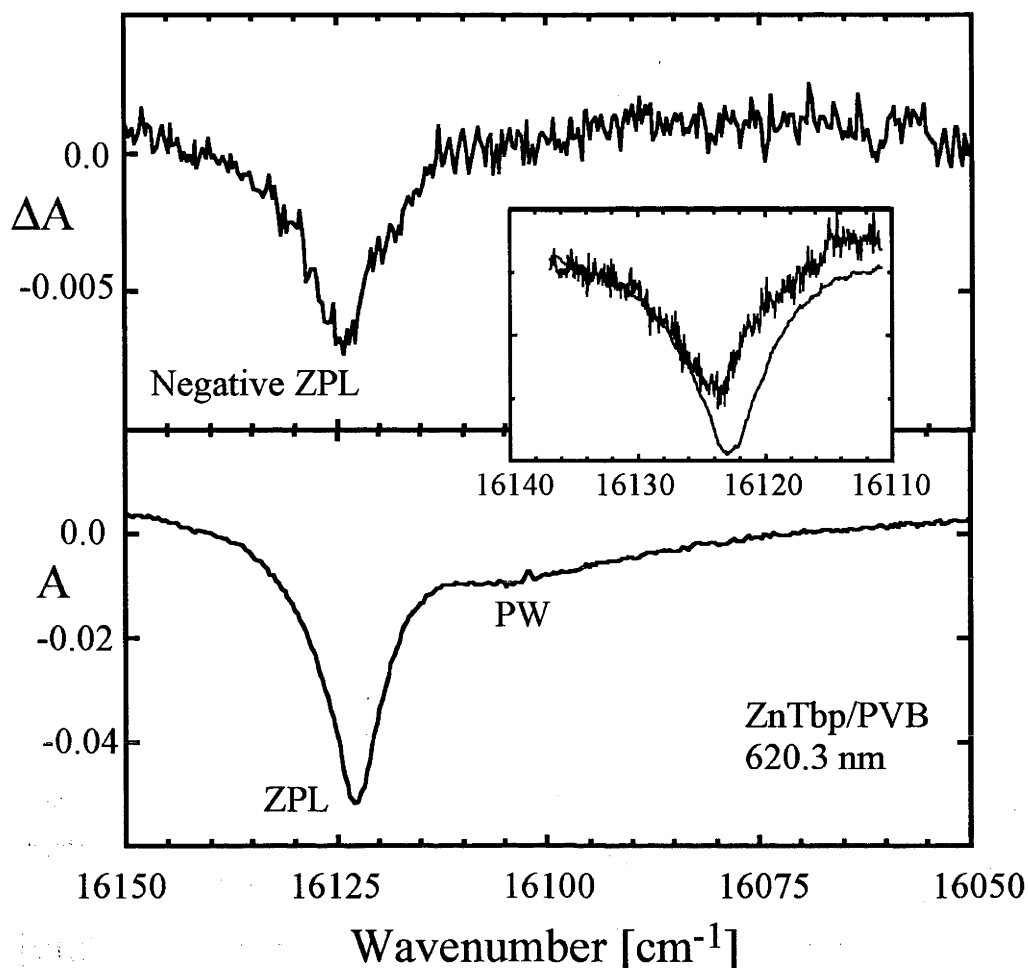


Figure 4.22: Hole absorption (lower) and hole MCD (upper) for the spectral hole burnt at 620.3 nm in ZnTbp/PVB. The insert shows a higher resolution scan of the ZPL region.

The hole MCD of figure 4.22 is similar to the ZnOep/PVB spectrum previously recorded (figure 4.14). It is not immediately apparent why the hole MCD shapes obtained on the blue side of the band in ZnOep and ZnTbp should be the shape that they are, and why they should differ from that observed in ZnPc. As in the case in ZnOep/PVB, the wavelength of the most negative point of the hole MCD does not coincide with the centre of the hole absorption (see the insert of figure 4.22).

It may be noted on the hole MCD shapes where contributions from both E_1 and E_2 are observed, the hole minimum is at the energy of the maximum of the E_2 contribution. This observation is consistent with the description of hole-burning in a system with two CF-split levels given

earlier. In this description, the top of the hole is dominated by contributions from E_1 (see figure 4.3).

An asymmetry may be observed in all the hole MCD spectra: the centre of the E_1 component and the centre of the E_2 component are not at the same energy. Such an asymmetry is not consistent with the description of the hole shape given earlier (see figure 4.3).

There may be a number of factors contributing to the asymmetrical appearance of the hole MCD spectra:

a) E_1 and E_2 undergo small shifts in the magnetic field. These shifts were measured as being ~ 1.5 GHz in ZnPc/PMMA in the high resolution Zeeman experiments described previously in this chapter. Such a small shift is not measurable using the lamp and monochromator used for these hole MCD experiments, but it may play a part in giving the hole MCD its shape.

b) On the low energy side of the ZPL, the PW will contribute to the shape of the hole. The PWs appear to have a positive MCD signal associated with them in all the hole MCD spectra, whilst the contribution from E_2 is negative. In the region where these two shapes overlap, an asymmetry may occur in the ZPL MCD as the PW MCD cancels the E_2 MCD.

c) There may be some distribution of photoproduct about the ZPL. The photoproduct will have an oppositely signed MCD from that of the hole. Where it contributes it will cancel the hole MCD signal (as it is of the opposite sign). If the contribution of the photoproduct is greater on one side of the ZPL than on the other, then the hole MCD will develop an asymmetry.

The origin of the contributions to the shape of the hole MCD might be better distinguished if measurements were made at a higher resolution.

High resolution MCD experiments on ZnPc/PMMA were attempted using a single-frequency scanning laser. However, these did not succeed. The frequency of the photoelastic modulator (57 kHz), used to generate the lcp and rcp light, operates in a frequency region where there is severe

intensity noise on the dye jet. This experiment would be better performed by modulating the circular polarisation at frequencies where there is less intensity noise on the dye jet, or perhaps by measuring lcp and rcp light separately in a static experiment.

The hole MCD from the blue side of the Q band observed in ZnTbP and ZnOep is clearly different from that observed in ZnPc. It may be seen in the ZnPc data that the contribution arising from E_1 is clearly visible, but in the ZnOep and ZnTbp data this is not the case. There may be a number of reasons for this observation including the following:

a) The holes were not burnt in the same relative positions in the inhomogeneously broadened band. Therefore the relative contributions of E_1 and E_2 are going to be different in each case. If the relative contribution of E_1 is less, then it will be less visible.

b) As a result of the asymmetry observable in the hole MCD shapes which was discussed earlier, the contribution from E_1 is going to be on a slope. When a small feature is on a slope it is more difficult to see. With the presence of noise, it may effectively disappear altogether.

The MCD of the PWs in the spectra shown in figures 4.17 – 4.22 all appear to be positive (although this is more convincing in some cases than it is in others). This observation may be interpreted as the phonons being associated mostly with E_1 . Alternatively, this observation may be as a result of the E_2 contribution to the PW being in some way difficult to measure (say, if it were very broad). There is no clear evidence for JT activity of the phonons. This matter cannot be fully clarified without spectra of higher resolution where the ratio of positive to negative contributions in the hole MCD may be more precisely determined.

In the wavelength dependent spectra discussed above, it can be seen that the relative position of the PW and ZPL change across the inhomogeneously broadened band. Moving from red to blue across the band, in both ZnPc and ZnTbp, the energy separation between the ZPL and the maximum of the PW decreases. This observation can be related to a variation in DWF across the inhomogeneously broadened band [55]. This observation is

therefore consistent with that made in chapter 3 with the hole-burning on a long time scale (section 3.7). A similar observation has been made by Flatscher and Friedrich [55] in anthracene in 2-methyl-THF. They noted a variation in phonon coupling (DWF) with transition energy. This variation in phonon coupling was manifested not only in a variation of the relative areas of the ZPL and the PW, but also in the energy difference between their maxima. They attributed this variation to a change in the dispersion and/or dipole-dipole interactions between the anthracene and its solvent which cause the inhomogeneous broadening. Because the interactions between the host and guest change, then the equilibrium positions of the lattice molecules change. Thus, a variation of the phonon coupling is observed.

4.3 Simulations of magnetic circular dichroism of spectral holes

Changes in shape of a spectral hole with increasing burn time may be simulated [19]. The calculation is readily generalised to a situation where there are two transitions with different linewidths in order to allow for the hole-burning processes in symmetric metallo-porphyrin derivatives. The simulations can be easily adapted to simulate hole MCDs in parallel, as well as to allow for the limited resolution of the read process.

Simulations show that a hole burnt into a transition with a narrow linewidth will deepen far more rapidly than a hole burnt into a transition with a broad linewidth. A hole which is burnt into a system with transitions with two different linewidths is characterised by a broad shallow component and a narrow deep component. When fully resolved, the narrow deep component dominates the spectrum. In absorption, it may be difficult to discriminate between the broad component and the wings of the narrow component. Critical evidence of the presence of two components is provided by MCD spectra, as the signs of the two components are opposite. If the hole detection has limited resolution, the narrow component becomes less evident and the broad component becomes more dominant.

As indicated previously, when a magnetic field is applied, E_1 and E_2 may shift apart. In the high resolution experiments this shift was measured to be ~ 1.5 GHz. Such a small shift will not be observable with the lamp and monochromator set-up used for the hole MCD measurements, but, as mentioned previously, this shift may have an effect on the hole MCD shape.

The effect of these small shifts of E_1 and E_2 in the magnetic field may be investigated by means of a simulation.

A calculation simulating the hole-burning process in two transitions, the limited resolution of the read process and the shift in the presence of the magnetic field has been undertaken. For the calculation, a burn wavelength slightly to the blue of the band maximum has been simulated. The ratio of E_1 to E_2 in the calculation is 1:1.5. The result of this calculation is displayed in figure 4.23.

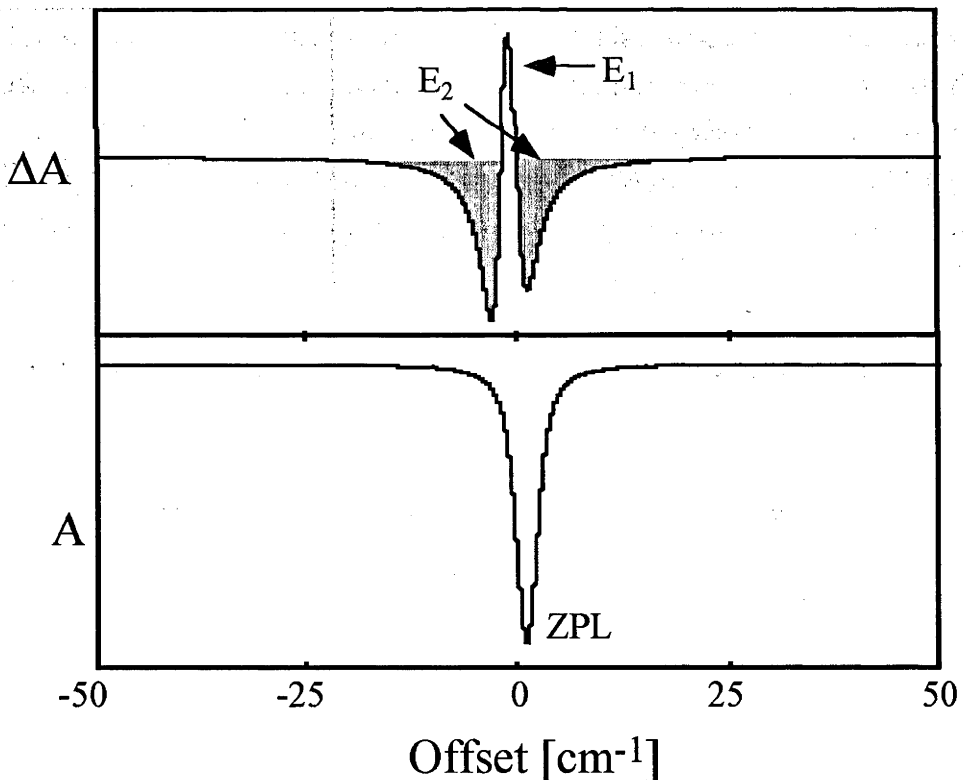


Figure 4.23: A simulation of a hole absorption (lower) and hole MCD (upper). An average shift of E_1 and E_2 in a magnetic field of 1.5 GHz and a burn energy slightly to the blue of the band maximum has been simulated.

A Gaussian distribution of Zeeman shifts was used for this calculation. The root mean square value of this distribution was 1.5 GHz (as observed in the high resolution Zeeman experiments). A read-out function (a Gaussian) 1 cm^{-1} wide was used. An advanced stage in burning is simulated (as is the case in the experiments undertaken here). PW contributions are not included in these calculations.

It may be observed in figure 4.23 that this small shift is sufficient to make the simulated hole MCD slightly asymmetric. The asymmetry is not as pronounced as it is in the data. This observation suggests that factors such as the PW and the photoproduct must have an appreciable effect upon the shape of the ZPL MCD.

Another observation which may be made from both the simulated spectra (figure 4.23) and the data (displayed in figures 4.13 – 4.22) is that the contributions from E_1 and E_2 may be clearly seen in the hole MCD, but the identification of two (approximately Lorentzian) components in the hole absorption is particularly difficult.

In Ar matrices, ZnOep and ZnTbp are reported as having smaller CF splittings than ZnPc [8, 10, 60]. If this trend is followed in polymer matrices, then ZnOep and ZnTbp may be expected to have slightly larger Zeeman shifts than ZnPc (see equation 4.4). (ZnOep and ZnTbp have slightly narrower Q(0,0) bands in polymer films than ZnPc, suggesting that this trend may indeed be followed in polymer films. ZnPc has a Q(0,0) band 330 cm^{-1} wide, whilst ZnOep and ZnTbp have Q(0,0) bands 210 and 220 cm^{-1} wide respectively.) Any asymmetry in the hole MCD arising from Zeeman shifts is expected to increase in these chromophores on this basis. This explanation may rationalise the differences observed in the ZnOep and ZnTbp hole MCD spectra from the blue side of the band, as compared to the equivalent spectrum from ZnPc.

4.4 Magnetic circular dichroism measurements of sidehole spectra

The MCD of a sidehole spectrum was measured for the case of ZnPc/PMMA where the hole was burnt into a vibrational sideband (see section 3.2). The results are displayed in figure 4.24.

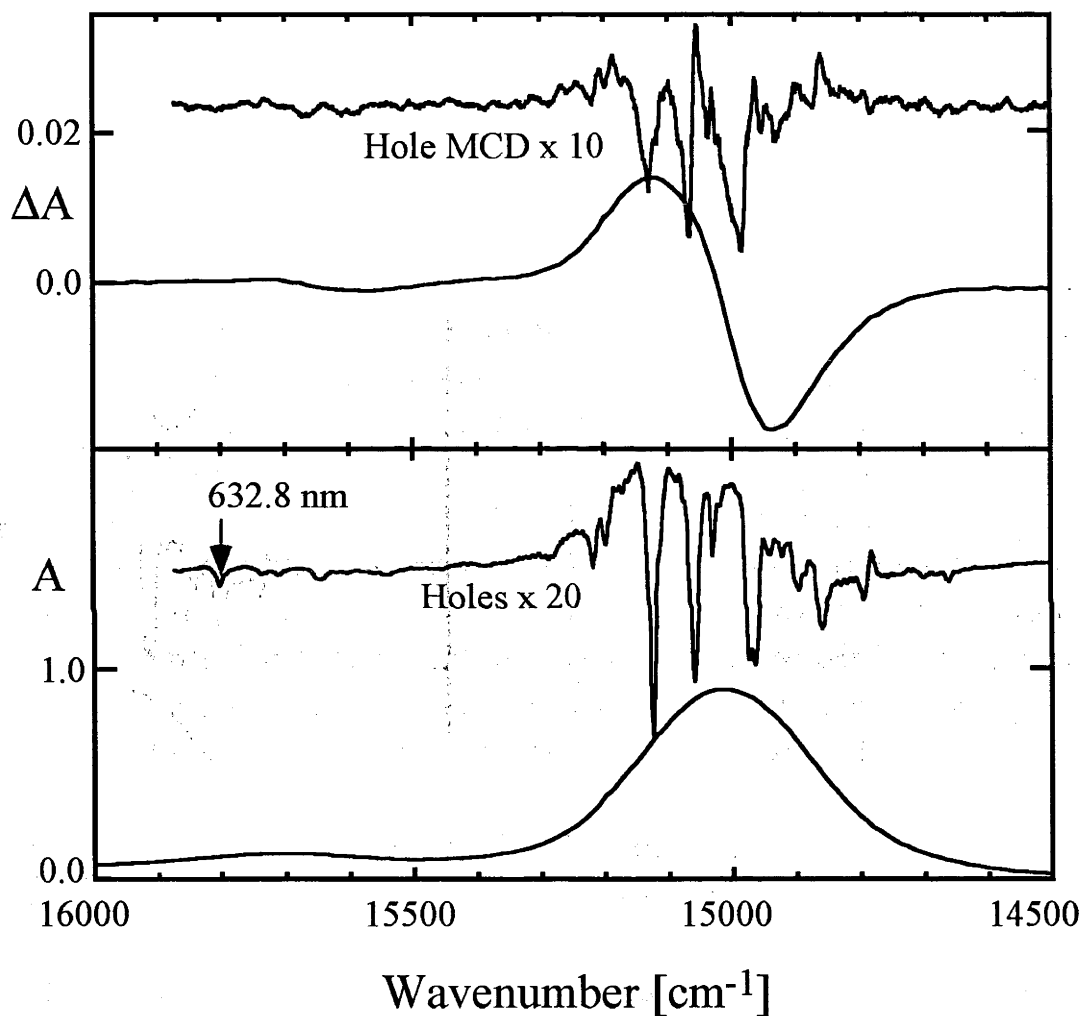


Figure 4.24: Absorption (lower) and MCD (upper) of a spectral hole and the accompanying sideholes as a result of burning at 632.8 nm. The broadband absorption and MCD are shown for comparison.

The hole at the burn energy shows no MCD signal. This may be because the broad vibrational sideband where the hole was burnt consists of many overlapping spectral features. At the energy of the laser, these vibrations can provide both positive and negative contributions to the MCD. Therefore, on average, the MCD signal will be reduced.

The overall nature of the sidehole MCD is accounted for by noting that the sideholes on the high-energy side of the Q band possess negative (\mathcal{B} -term) MCD signals, the sideholes on the low-energy side have positive (\mathcal{B} -term) signals, and central features are inverted MCD \mathcal{A} -terms. The MCD of the sidehole burn is thus a direct reflection of the distribution of upper and lower CF levels of the Q state.

The distribution of the photoproduct may be seen. The broad positive portions of the hole absorption may be assigned to the photoproduct. There appears to be slightly more photoproduct on the blue side of the sideholes.

This sidehole MCD experiment is, in some ways, very elegant. What such an experiment enables is the measurement of the wavelength dependence of the hole MCD across the band by burning only one hole. The sideholes are deep and broad, enabling the unambiguous identification of hole MCD shapes.

The MCD signal for each of the sideholes has a readily identifiable sign associated with it (either positive or negative or a combination of the two). These MCD signals do not show the different linewidths of the two CF components. If finer control of the hole shapes is desired, this experiment is not optimal. The sideholes acquire their widths ($\sim 10 \text{ cm}^{-1}$) as a result of rapid relaxation from vibrationally excited states (see section 3.2). If narrower holes are desired, so that the development with burn time of the contributions from E_1 and E_2 may be more closely monitored, and their linewidths compared, then holes must be burnt directly into the origin band.

5. Stark Spectroscopy and Spectral Hole-burning

The influence of an applied electric field on the absorption or emission spectrum of a sample (the Stark effect) has been used to yield information about the electronic structure of a variety of systems [64]. The application of spectral hole-burning techniques can be of benefit in the observation and interpretation of relatively small changes. Here, the Stark effect has been measured in ZnPc and in ZnTbp. The spectral holes were monitored holographically and in transmission.

5.1 Modelling of spectral hole shapes in an applied electric field

As previously mentioned (chapters 1 and 4), hole-burning with polarised light may be used to control the orientation of the selected chromophores. Chromophores with a small angle between their transition dipole, \mathbf{D} , and the electric field of the burning light, \mathbf{E}_{pol} , will be preferentially selected.

The shift in wavelength associated with a linear Stark effect is given by equation 1.21, restated here:

$$\Delta v_E = \frac{f}{h} \Delta \mu_{\text{eff}} \mathbf{E}_{\text{app}} \quad (5.1)$$

Chromophores where the angle, σ , that separates the change in dipole moment between the ground and excited state, $\Delta \mu_{\text{eff}}$, and the applied electric field, \mathbf{E}_{app} , is zero will have a maximal interaction with the electric field. Such chromophores must have $\Delta \mu_{\text{eff}}$ aligned either parallel or antiparallel with \mathbf{E}_{app} . The transitions associated with the parallel and antiparallel aligned chromophores will shift in opposite directions in an electric field. Consequently, in the regime of a linear Stark effect, a hole in an electric field will develop a broadening rather than a shift. If $\Delta \mu_{\text{eff}}$ is well defined, then this broadening will develop into a hole shape with a double maximum. If the photoselection is such that $\sigma = 90^\circ$, then a broadening appears as a result of a variation in σ (associated with the

slight variation in the photoselection). This broadening will not develop into a double maximum.

As outlined in chapter 1, $\Delta\mu_{\text{eff}}$ may be split into two components: $\Delta\mu_{\text{mol}}$ and $\Delta\mu_{\text{ind}}$. $\Delta\mu_{\text{mol}}$ is a dipole intrinsic to the chromophore. Generally, $\Delta\mu_{\text{mol}}$ has a well defined magnitude and is fixed at some angle, θ_{mol} , to \mathbf{D} . $\Delta\mu_{\text{ind}}$ is a dipole induced in the chromophore by host-guest interactions. $\Delta\mu_{\text{ind}}$ is more likely to have a distribution of magnitudes and angles.

Because of the distributed nature of $\Delta\mu_{\text{ind}}$, a linear Stark effect involving such a dipole leads to a broadening. A hole shape with a double maximum will not occur.

The different components of the dipole lead to characteristically different hole shapes in the presence of an electric field. Some of these different shapes are illustrated in figure 5.1.

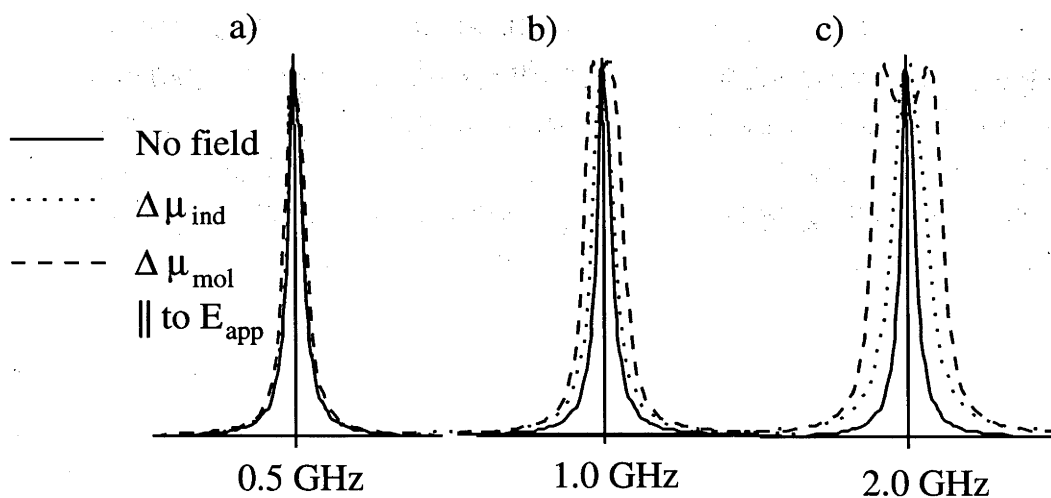


Figure 5.1: Characteristic changes in hole shape in an applied electric field for a random (induced) change in dipole ($\Delta\mu_{\text{ind}}$) and a fixed (molecular) dipole ($\Delta\mu_{\text{mol}}$) parallel to the electric field. A 1 GHz zero-field hole is modelled here with a) 0.5 GHz b) 1.0 GHz and c) 2.0 GHz changes in hole width shown for the two different dipoles.

For this calculation, rather than explicit dipoles and field strengths, the values of transition shifts were put directly into the calculation. Shifts of 0.5, 1.0 and 2.0 GHz were simulated.

If data with a good signal-to-noise ratio are obtained, with careful modelling and analysis, the magnitudes of the contributions from $\Delta\mu_{\text{mol}}$ and $\Delta\mu_{\text{ind}}$ may be extracted. The hole shape may be described by either a shape characteristic of a fixed dipole or a random dipole or a shape which is a sum of the two.

At this point it is worth mentioning that a model will describe data in terms of some fixed dipole ($\Delta\mu_{\text{fix}}$) and some random dipole ($\Delta\mu_{\text{ran}}$):

$$\Delta\mu_{\text{eff}} = \Delta\mu_{\text{fix}} + \Delta\mu_{\text{ran}} \quad (5.2)$$

As stated previously:

$$\Delta\mu_{\text{eff}} = \Delta\mu_{\text{mol}} + \Delta\mu_{\text{ind}} \quad (5.3)$$

but, $\Delta\mu_{\text{fix}}$ is not necessarily equal to $\Delta\mu_{\text{mol}}$ and $\Delta\mu_{\text{ran}}$ is not necessarily equal to $\Delta\mu_{\text{ind}}$ [65]. In the case where the matrix field which gives rise to $\Delta\mu_{\text{ind}}$ is isotropic, to assume that they are equal is acceptable, but in the case where the matrix field is anisotropic, this assumption is questionable. In the work here, $\Delta\mu_{\text{fix}}$ and $\Delta\mu_{\text{mol}}$ have been assumed to be equivalent, as have $\Delta\mu_{\text{ran}}$ and $\Delta\mu_{\text{ind}}$.

As mentioned previously, the characteristic shape associated with $\Delta\mu_{\text{mol}}$ will change with angle relative to \mathbf{E}_{app} . This means, by using the above-mentioned model, information about the angle of $\Delta\mu_{\text{mol}}$ may also be obtained. Ideally, to fully investigate the angle of $\Delta\mu_{\text{mol}}$, data should be collected at a number of experimental geometries (ie the angle of \mathbf{E}_{pol} relative to \mathbf{E}_{app} should be varied to change the angle of the selected chromophores, and therefore $\Delta\mu_{\text{mol}}$, relative to \mathbf{E}_{app}).

To be able to obtain detailed information by modelling data, data of a good signal quality are required. Holographic detection of spectral holes is well suited to this application, as it is a background-free detection technique. The data in the section which follows were measured by this means.

The information given above was mostly drawn from reference [24], but references [65, 66] are also good for this subject.

5.2 Holographic read-out of Stark broadened spectral holes in zinc phthalocyanine and zinc tetrabenzoporphyrin

Spectral holes were burnt at a number of wavelengths across the inhomogeneously broadened bands of ZnPc/PVB and ZnTbp/PVB to gain information about the wavelength dependence of the Stark broadenings. The positions of the holes are indicated by arrows in figures 5.2 and 5.3. The greater part of the discussion here is in reference to the holes burnt at 673.5 nm for ZnPc and 626.3 nm for ZnTbp.

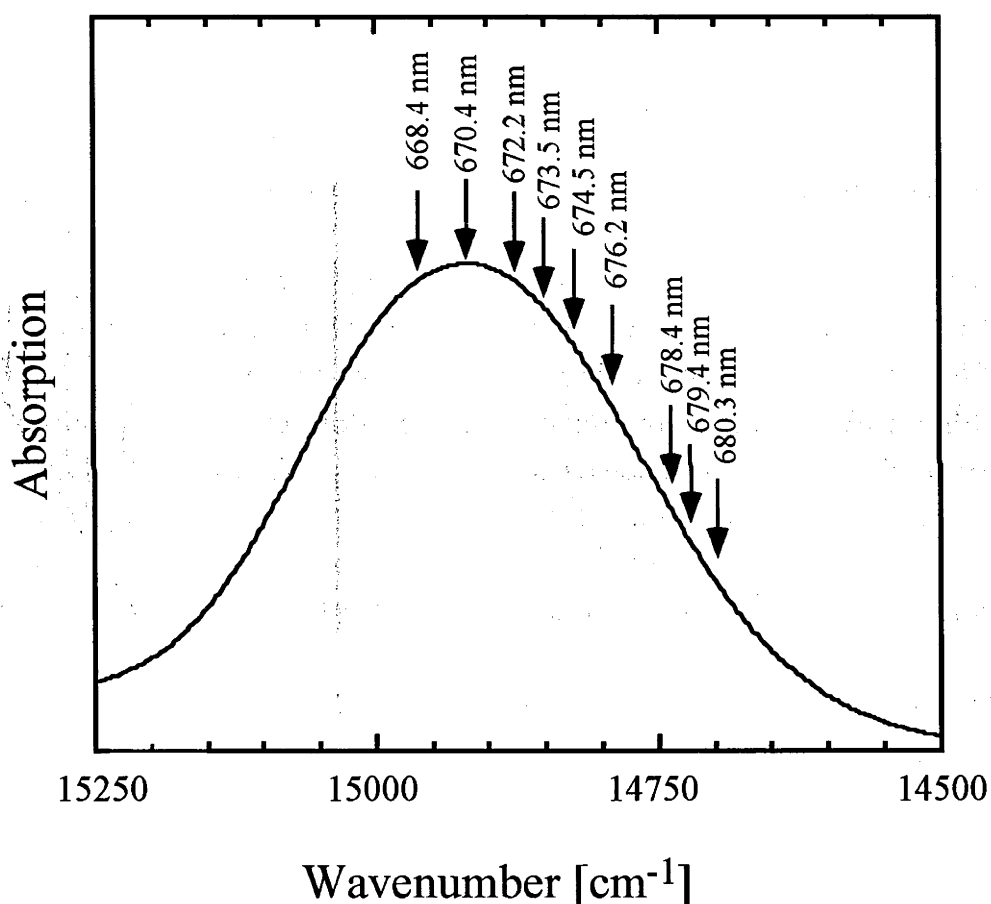


Figure 5.2: Absorption of the Q band of ZnPc/PVB showing the position of spectral holes burnt for the holographically detected Stark experiment.

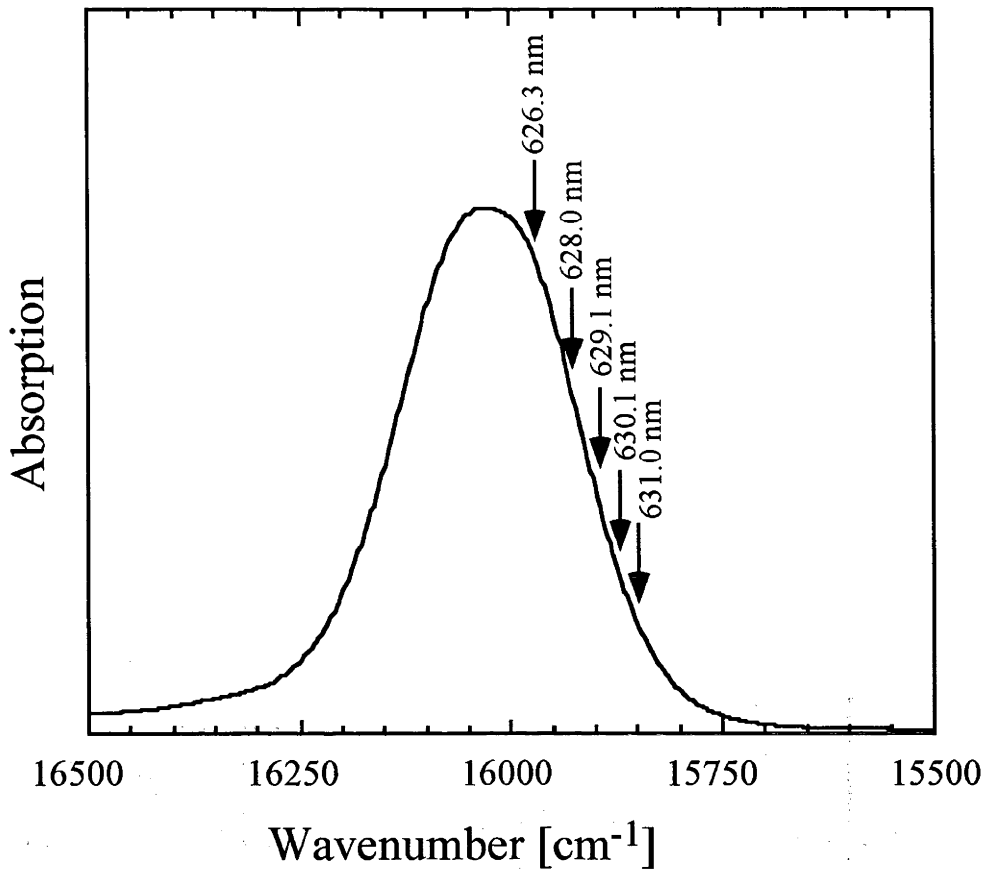


Figure 5.3: Absorption of the Q band of ZnTbp/PVB showing the position of spectral holes burnt for the holographically detected Stark experiment.

Holes, in the absence of an external field, were ~ 1 GHz wide, and a few per cent of the total absorption at that wavelength.

The changes in hole profile with electric field are displayed in figures 5.4 and 5.5. The corresponding plots of change in hole width with field strength are shown in figures 5.6 and 5.7. The holes broaden symmetrically about the centre of the hole in a linear fashion with the field, and no shift in the centre of the hole is observed. This behaviour is consistent with a linear Stark effect.

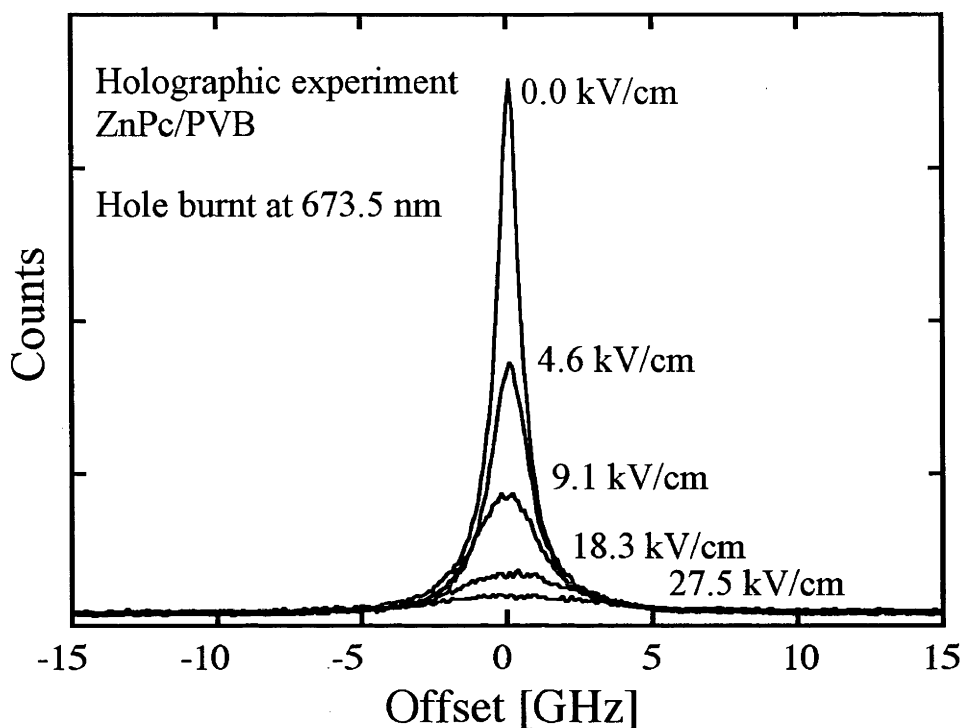


Figure 5.4: Changes in hole shape in ZnPc/PBV, monitored holographically, as a function of electric field.

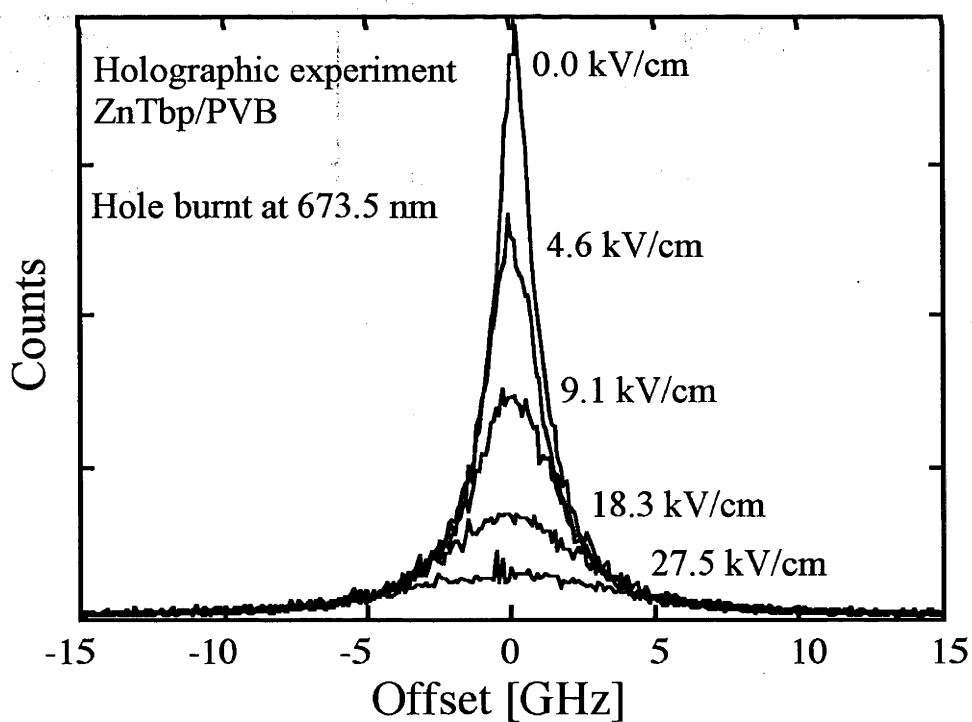


Figure 5.5: Changes in hole shape in ZnTbp/PVB, monitored holographically, as a function of electric field.

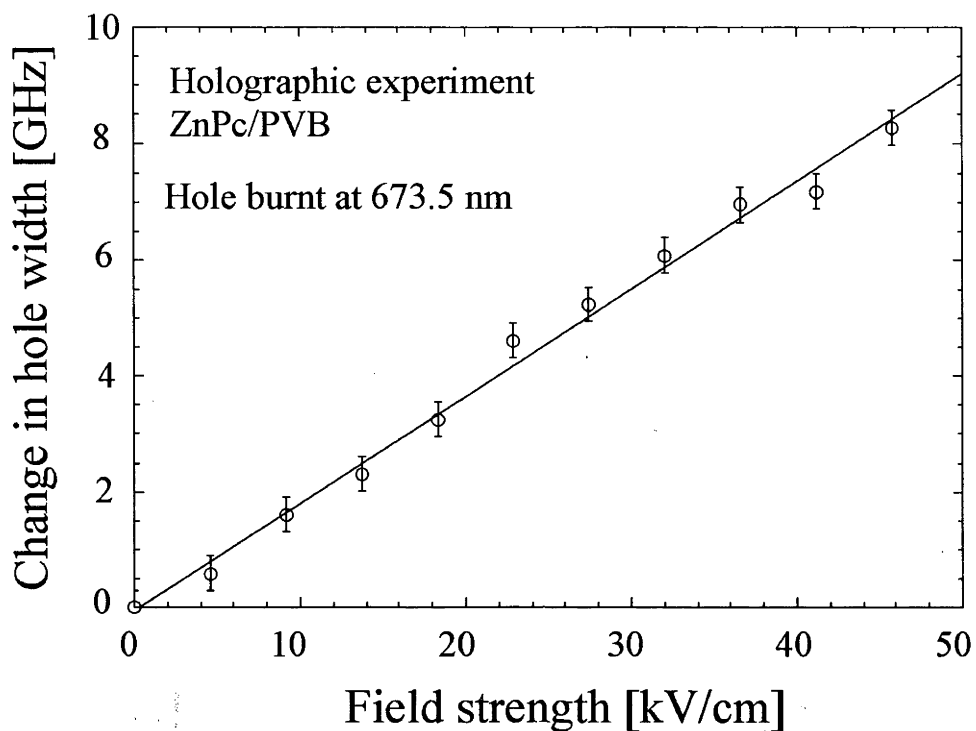


Figure 5.6: Change in hole width as a function of field strength for holes burnt in ZnPc/PVB.

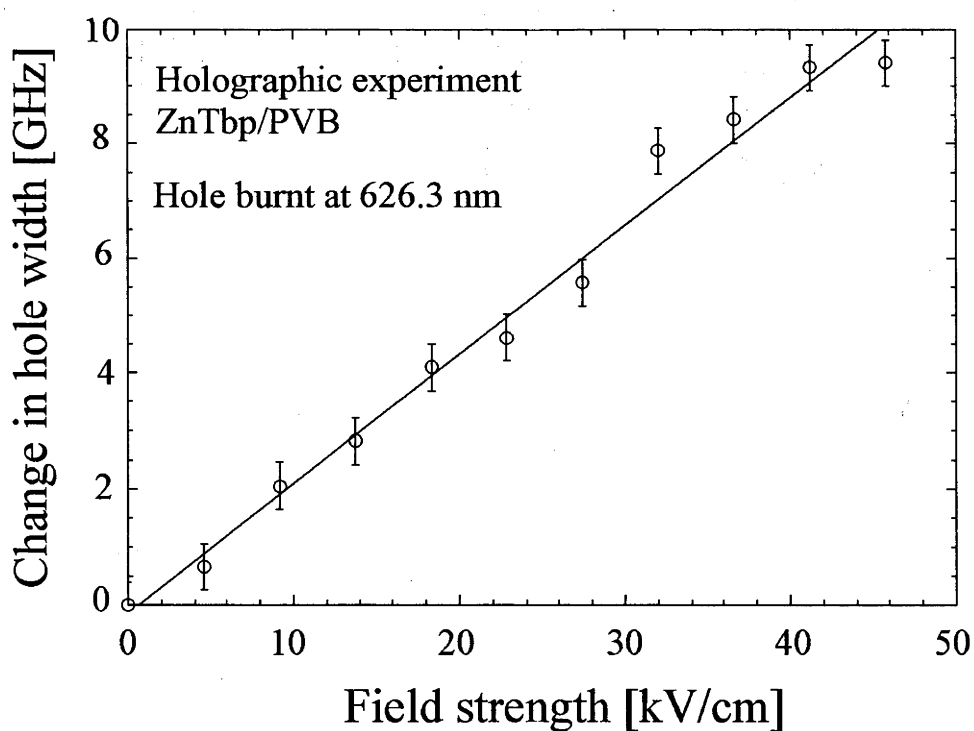


Figure 5.7: Change in hole width as a function of field strength for holes burnt in ZnTbp/PVB.

From the slope of the plots in figures 5.6 and 5.7 a change in dipole moment between the ground and excited state may be calculated using equation 5.1.

A value of $\epsilon = 2.55$ for PVB was used in the calculation of f [67].

By this means, a change in dipole moment of 0.243 ± 0.021 D may be calculated for ZnPc and 0.292 ± 0.03 D for ZnTbp. These results are given in table 5.1.

Sample	$\Delta\mu_{\text{eff}}$ [D]
ZnPc/PVB	0.243 ± 0.021
ZnTbp/PVB	0.292 ± 0.03

Table 5.1: $\Delta\mu_{\text{eff}}$ calculated from the change in hole width with electric field for ZnPc/PVB and ZnTbp/PVB for holographically read out spectral holes.

As stated in chapter 1, this class of chromophore nominally possesses D_{4h} symmetry [9, 60]. In this case, the excited state of the Q transition is doubly degenerate. A theoretical treatment of the influence of degeneracies on the interpretation of Stark data has been given for chromophores with D_3 symmetry [68]. An applied electric field in the xy plane of the chromophore leads to a removal of the degeneracy. If the application of an electric field has a similar effect on a chromophore with D_{4h} symmetry, then the interpretation of the data in the same way as for non-degenerate states is questionable.

In systems with D_{4h} symmetry no removal of electronic degeneracies occurs upon application of a uniform electric field. This result is readily determined from group theory.

According to group theory, for a Stark effect to occur, Γ^2 (where Γ is the irreducible representation of the state under consideration) must contain the irreducible representation of the dipole moment operator.

Assuming D_{4h} symmetry for the chromophore, the excited state of the Q transition transforms as E_u .

$$E_u \times E_u = A_{1g} + A_{2g} + B_{1g} + B_{2g}$$

In D_{4h} the electric dipole moment operator transforms as A_{2u} in the z direction and E_u in the x and y directions.

Γ^2 does not contain the irreducible representation of the dipole moment operator in any direction. Therefore no interaction occurs.

In general, any chromophore with a centre of symmetry will not interact with a uniform externally applied electric field. It is not until some loss of symmetry occurs (say, through interaction of the chromophore with its environment) that a Stark effect is observed.

The degeneracy of the excited state may also be expected to affect the shape of the zero-field hole. As discussed in chapter 4, in these relatively high resolution experiments, the effect of the degeneracy on the zero-field hole shapes may be neglected as only the contribution from the lower level is observed.

A number of authors [24, 66, 69, 70] have modelled changes in the shape of spectral holes upon the application of electric fields. As discussed previously, such models are useful for analysing contributions to a change in shape of a hole. The model used in this work closely follows that of Meixner et al. [24]. This model enables values for a change in permanent dipole moment, $\Delta\mu_{\text{mol}}$, and a root mean square value for a distribution of induced dipoles, $\Delta\mu'_{\text{ind}}$, to be obtained from the data according to the changes in hole shape with the applied field.

If one were to assume that ZnPc and ZnTbp are centro-symmetric, then the most appropriate model to use would be one where there were only contributions from matrix-induced dipoles. The best fit to the data was obtained, however, when there were both permanent and matrix-induced components. Having $\Delta\mu_{\text{ind}}$ in the plane of the phthalocyanine/porphyrin ring, and $\Delta\mu_{\text{mol}}$ perpendicular to the transition dipole yielded the best agreement for both samples. These fits yielded values of $\Delta\mu'_{\text{ind}} = 0.075 \pm 0.008$ D and $\Delta\mu_{\text{mol}} = 0.118 \pm 0.001$ D for ZnPc/PVB; and $\Delta\mu'_{\text{ind}} = 0.072 \pm 0.004$ D and $\Delta\mu_{\text{mol}} = 0.128 \pm 0.013$ D for ZnTbp/PVB. These results are summarised in table 5.2.

Sample	$\Delta\mu_{\text{ind}}$ [D]	$\Delta\mu_{\text{mol}}$ [D]
ZnPc/PVB	0.075 ± 0.008	0.118 ± 0.001
ZnTbp/PVB	0.072 ± 0.004	0.128 ± 0.013

Table 5.2: $\Delta\mu_{\text{ind}}$ and $\Delta\mu_{\text{mol}}$ calculated from modelling the change in hole shape with electric field for ZnPc/PVB and ZnTbp/PVB for holographically read out spectral holes.

Plots of changes in hole width versus applied field strength for the two components are shown in figures 5.8 and 5.9 for ZnPc and ZnTbp respectively.

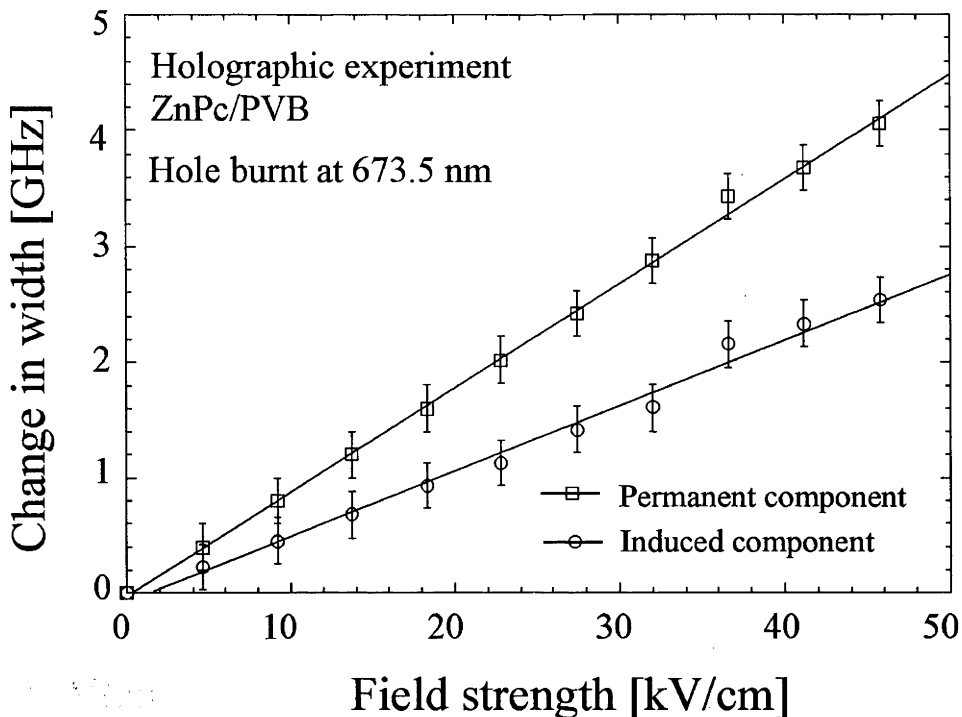


Figure 5.8: Change in width in ZnPc/PVB as a function of field strength for permanent and induced components as obtained from fitting to the model (see text).

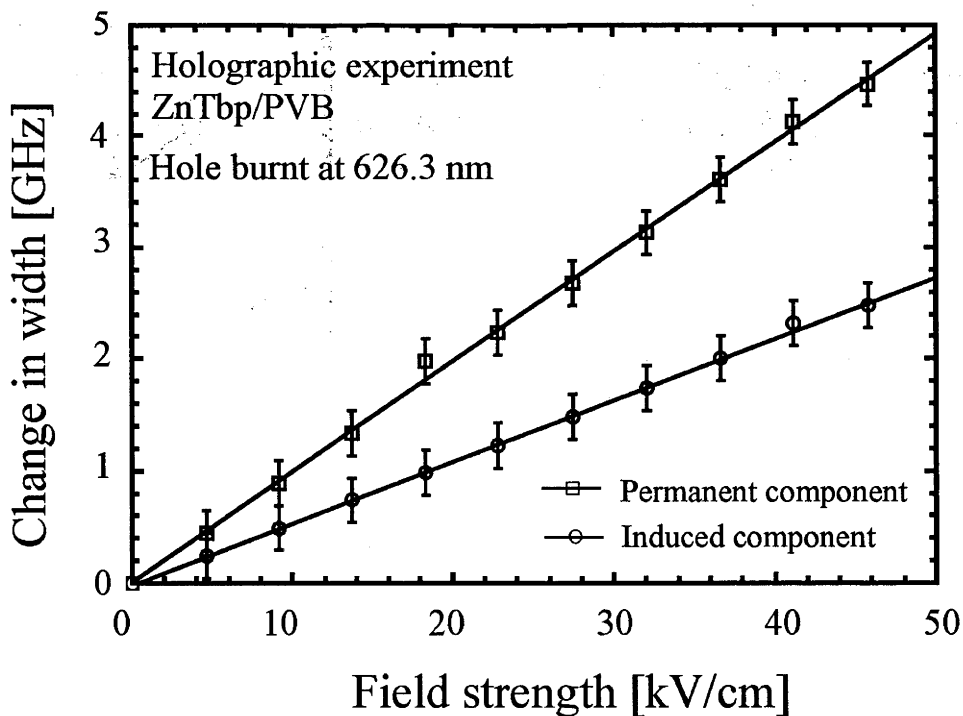


Figure 5.9: Change in width in ZnTbp/PVB as a function of field strength for permanent and induced components as obtained from fitting to the model (see text).

X-ray diffraction studies indicate that ZnPc is planar [71]. If there is an axial ligand on the metal in this class of chromophore, then a dipole perpendicular to the molecular plane is evident. Ligation in the axial position will cause the zinc atom to be displaced from the phthalocyanine plane [72] (see figure 5.10).

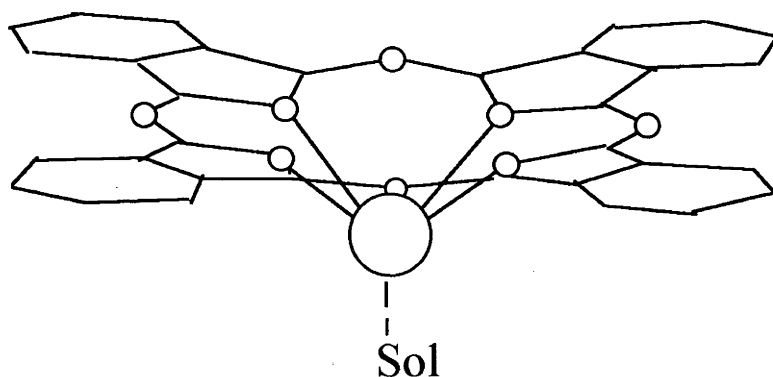


Figure 5.10: When ZnPc has an axial ligand, the Zn adopts an out-of-plane position. There is then a dipole perpendicular to the molecular plane. A solvent molecule (sol), for instance, may act as an axial ligand.

Altmann et al. [73], in their study of ZnOep/PVB, proposed the idea that the metal atom may be out of plane. This would lead to a dipole perpendicular to the transition moment. For this dipole moment to be detectable in these Stark experiments it would need to be different between the ground and excited states of the Q transition. The zinc atom is large compared to the cavity in the phthalocyanine/porphyrin ring [71]. It is perhaps plausible that, upon excitation of the phthalocyanine ring, the zinc atom 'pops out' of the phthalocyanine ring, thus causing a dipole change perpendicular to the phthalocyanine ring.

Axial ligation may come about through the method used to dissolve the chromophores. THF was used as the solvent in the preparation of the samples for these experiments. THF has a prominent oxygen atom. Oxygen possesses two lone pairs of electrons which may attach quite readily to the zinc atom in chromophores such as ZnPc and ZnTbp.

With the experimental geometry used in these experiments (the polarisation of the laser perpendicular to the direction of the applied field) a change in dipole moment with a fixed value ($\Delta\mu_{\text{mol}}$) perpendicular to the transition moment leads to a hole profile with a double maximum. In contrast, $\Delta\mu_{\text{ind}}$ leads to a broadening of the hole shape. In the data here there is no indication of a splitting to the hole shape arising from the contribution of $\Delta\mu_{\text{mol}}$.

Consider figure 5.11. Figure 5.11 is similar to figure 5.1 in that it shows the characteristic hole shapes for a fixed change in dipole moment parallel to an applied field and a random change in dipole moment. It is possible to envisage a situation at a certain field strength where the contribution from $\Delta\mu_{\text{ind}}$ is an appropriate magnitude to compensate for the 'dip' in the $\Delta\mu_{\text{mol}}$ hole shape. This results in a hole shape with a characteristic 'rectangular' appearance [74].

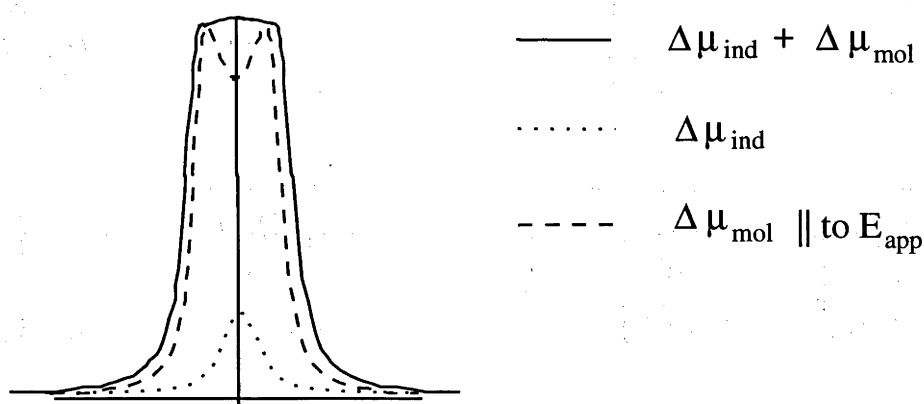


Figure 5.11: The sum of the contributions from $\Delta\mu_{\text{ind}}$ and $\Delta\mu_{\text{mol}}$ may be such that the resulting hole shape has a characteristic 'rectangular' appearance.

One of the high field (36.6 kV/cm) hole shapes is shown in figure 5.12 along with the accompanying fit. At higher fields still, this rectangular shape should develop a double maximum as the contribution from $\Delta\mu_{\text{mol}}$ becomes more evident. Taking the model used to fit the data to higher fields indicates that this would be the case.

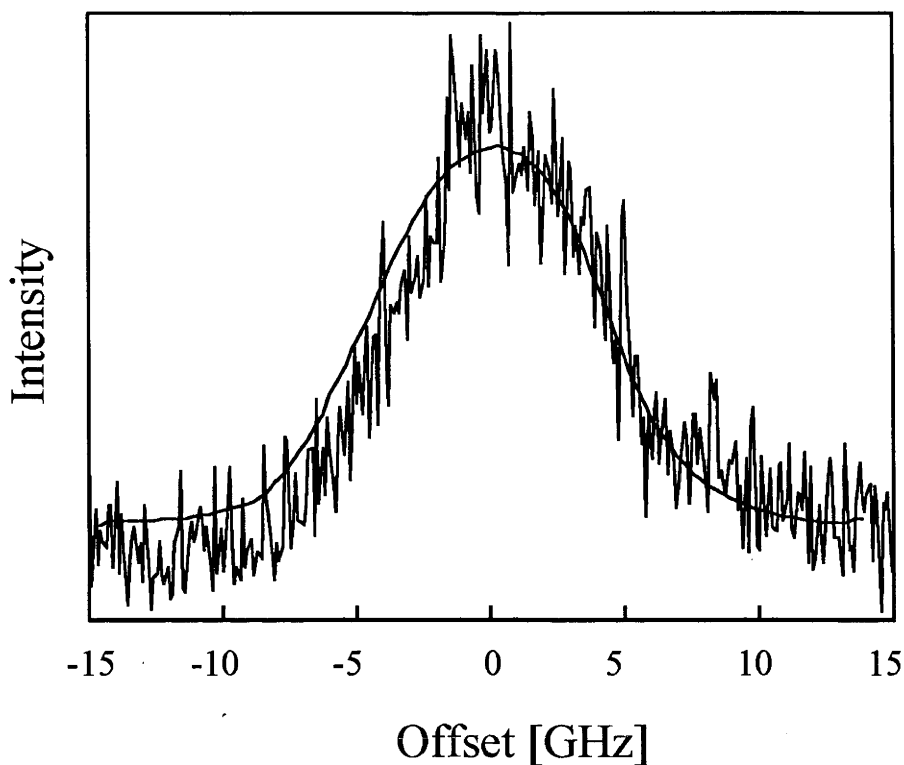


Figure 5.12: A holographically detected spectral hole burnt into ZnPc/PVB at 673.5 nm in an applied electric field of 36.6 kV/cm. It is accompanied by the model which accounts for both molecular and induced components.

The experimental geometry used in this work is most sensitive to a change in dipole moment perpendicular to the transition dipole. To probe the angular dependence of the change in dipole moments more fully, it is necessary to perform the experiment in two geometries: \mathbf{E}_{pol} parallel to \mathbf{E}_{app} , and \mathbf{E}_{pol} perpendicular to \mathbf{E}_{app} . Such an experiment was performed for the case of ZnPc, not holographically, but in transmission, and is described in the section which follows.

5.3 Polarisation dependence of Stark broadenings of spectral holes in zinc phthalocyanine

Once again, holes were burnt in a number of wavelengths across the inhomogeneously broadened band, but the greater part of the discussion here pertains to the holes at the band maximum.

Holes in the absence of an external field were ~ 2 GHz wide, and a few per cent of the total absorption at that wavelength.

The changes in hole profile for the perpendicular experimental geometry are shown in figure 5.13. Once again, a linear Stark effect is observed.

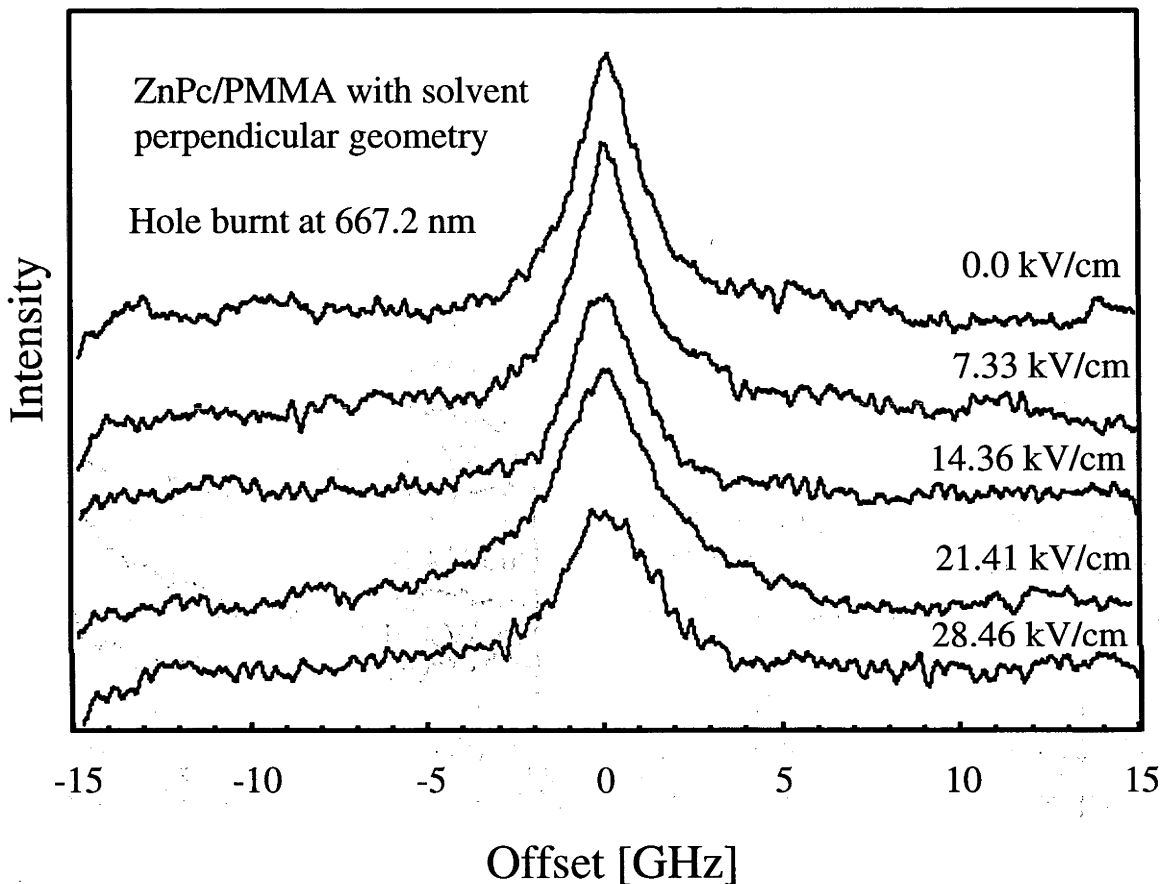


Figure 5.13: Changes in hole shape as a function of electric field for holes burnt into ZnPc/PMMA and read out in transmission.

The plot of the change in hole width with electric field strength is shown for both the parallel and perpendicular experimental geometries in figure 5.14. From this plot it can be seen that there is a characteristic difference between the two experimental geometries. From the slopes of these two data sets, changes in dipole moments of 0.042 ± 0.021 D for the perpendicular geometry and 0.012 ± 0.003 D for the parallel geometry can be calculated. These results are summarised in table 5.3.

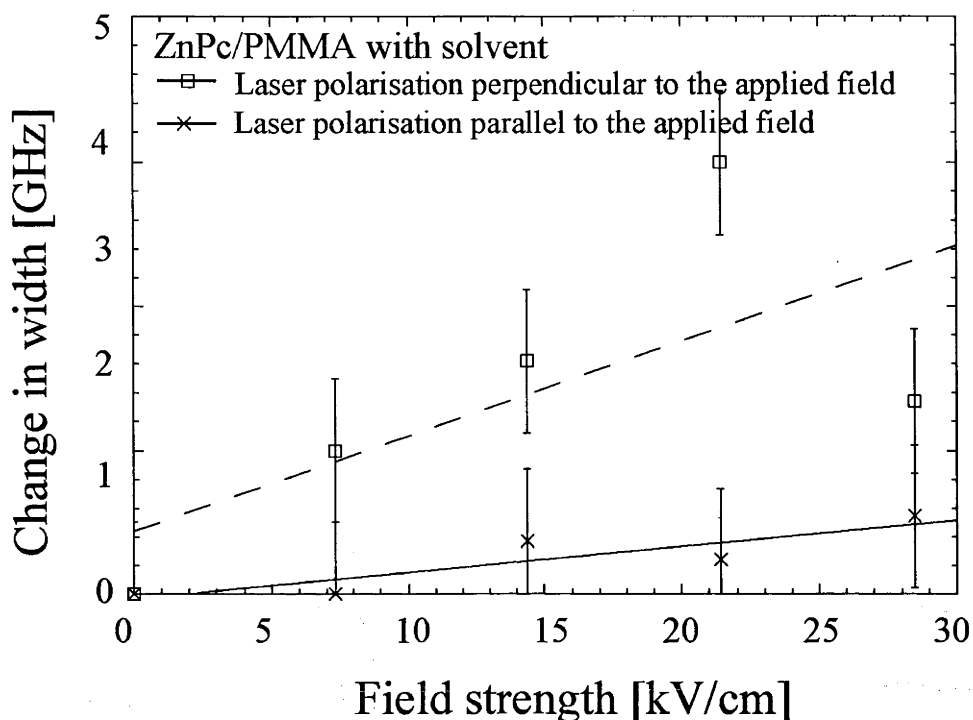


Figure 5.14: Changes in hole width as a function of electric field for ZnPc/PMMA showing the two different experimental geometries - perpendicular (boxes and dashed line) and parallel (crosses and solid line).

Experimental Geometry	$\Delta\mu_{\text{eff}}$ [D]
E_{pol} parallel to E_{app}	0.012 ± 0.003
E_{pol} perpendicular to E_{app}	0.042 ± 0.021

Table 5.3: $\Delta\mu_{\text{eff}}$ calculated from the change in hole width with electric field for ZnPc/PMMA for the two experimental geometries.

The dipole calculated from the perpendicular geometry is clearly larger than that calculated from the parallel geometry. This corroborates the data from the holographic experiment. Analysis of the transmission data in a manner similar to that done with the holographic data was attempted, but the small size (relative to the hole widths) of the Stark broadenings and the irregularities in the baseline meant that it was impossible to obtain unambiguous fits to the model.

To test the hypothesis that the dipole perpendicular to the molecular plane in ZnPc is caused by the solvent attaching to the zinc, a sample was made without any solvent using the procedure described in chapter 2. Stark experiments in the two experimental geometries were then repeated with this new sample.

Initially, no hole-burning was observed in this solvent-free sample. Such a result suggests that the solvent is vital to the hole-burning process. If no hole-burning occurs in this sample, then it may make an excellent sample for FLN experiments.

Accordingly, FLN experiments were done with this sample. Little emission was observed. Such behaviour aroused suspicion and an absorption spectrum was measured. No Q or B band absorption was observed. There was a very large band in the UV which is consistent with the absorption of the initiator. A possible explanation for the absence of hole-burning is that the initiator remaining from the polymerisation was converting ZnPc to ZnPc^{•+}. ZnPc^{•+} may not be stable and either oxidises further or decomposes.

A new sample was made without any initiator. Heating the MMA was found to be sufficient to cause it to polymerise. This new sample was found to undergo spectral hole-burning in a fashion appropriate for the experiment here.

The changes in hole profile for this new sample without solvent in the perpendicular experimental geometry are shown in figure 5.15. Holes, in the absence of an external field, were ~ 1 GHz in width.

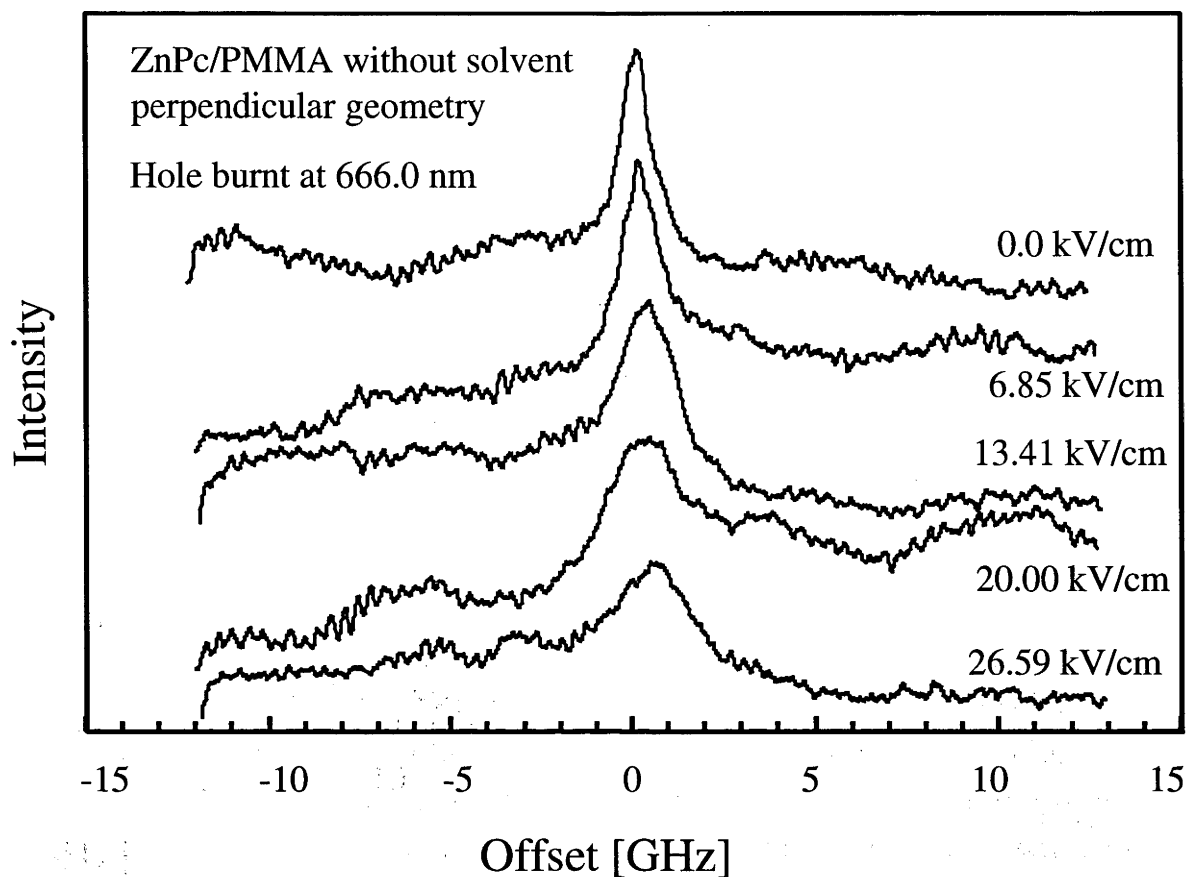


Figure 5.15: Changes in hole shape as a function of electric field for holes burnt into ZnPc/PMMA without solvent and read out in transmission.

Plots of the changes in hole width as a function of field strength for the two experimental geometries are displayed in figure 5.16. From the slopes of the lines of best fit, changes in dipole between the ground and excited state of 0.138 ± 0.014 D and 0.085 ± 0.009 D for the perpendicular and parallel geometries respectively were calculated. These results are summarised in table 5.4.

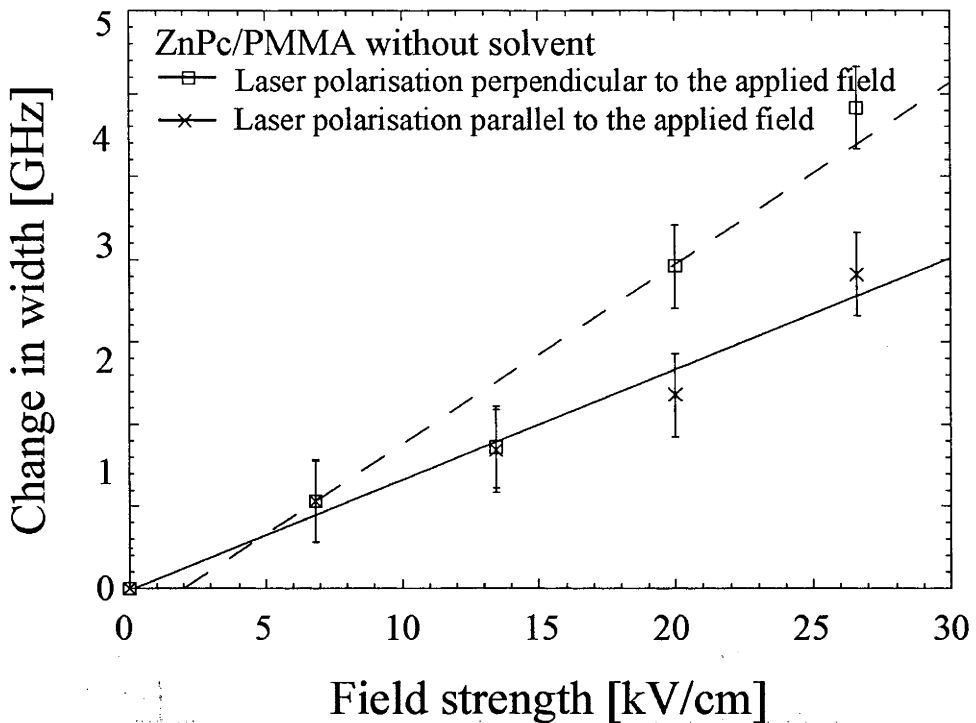


Figure 5.16: Changes in hole width as a function of electric field for ZnPc/PMMA without solvent showing the two different experimental geometries - perpendicular (boxes and dashed line) and parallel (crosses and solid line).

Experimental Geometry	$\Delta\mu_{\text{eff}}$ [D]
E_{pol} parallel to E_{app}	0.085 ± 0.009
E_{pol} perpendicular to E_{app}	0.138 ± 0.014

Table 5.4: $\Delta\mu_{\text{eff}}$ calculated from the change in hole width with electric field for ZnPc/PMMA without solvent for the two experimental geometries.

The three Stark experiments performed on ZnPc (the holographically read out experiment and the two transmission experiments - one performed on a sample containing solvent and the other without) yield strikingly different dipole moment differences. The holographic data (performed with a perpendicular geometry) give an overall dipole moment change of 0.22 D. The perpendicular geometry transmission data, on the other hand, results in dipole moment changes of 0.042 and

0.138 D for the sample with solvent and the sample without solvent respectively.

The purpose of performing the experiment with the solvent-free sample was to ascertain whether or not the solvent was involved in generating a dipole moment perpendicular to the molecular plane. If the result had been affirmative, then the solvent-free sample should have yielded a smaller dipole moment than the sample with solvent. Instead, the reverse happened: the dipoles calculated from the solvent-free sample are larger than those from the sample with solvent. The data from the sample with solvent and the sample without solvent both display a strong dependence upon polarisation. The polarisation dependence is consistent with an interaction of some description perpendicular to the molecular plane, but the magnitudes of the dipoles obtained from the two transmission experiments are not consistent with the solvent being entirely responsible for the interaction perpendicular to the molecular plane.

For the set-up used in the transmission experiments, fairly thick (~ 1 mm) samples are required. As a result of the method used to produce the sample with solvent, there is going to be a large quantity of solvent present in the resulting polymer block. This solvent is not going to be able to evaporate readily from such a thick piece of polymer. It may be the case that the solvent acts like a loose 'cage' around the chromophore. The interactions between the chromophore and the solvent may only be weak and thus the solvent acts like a shield between the chromophore and the polymer. When the shield is removed (by producing a sample without solvent) the strength of the interaction (and therefore the magnitude of the dipole) is increased. (See figure 5.17.)

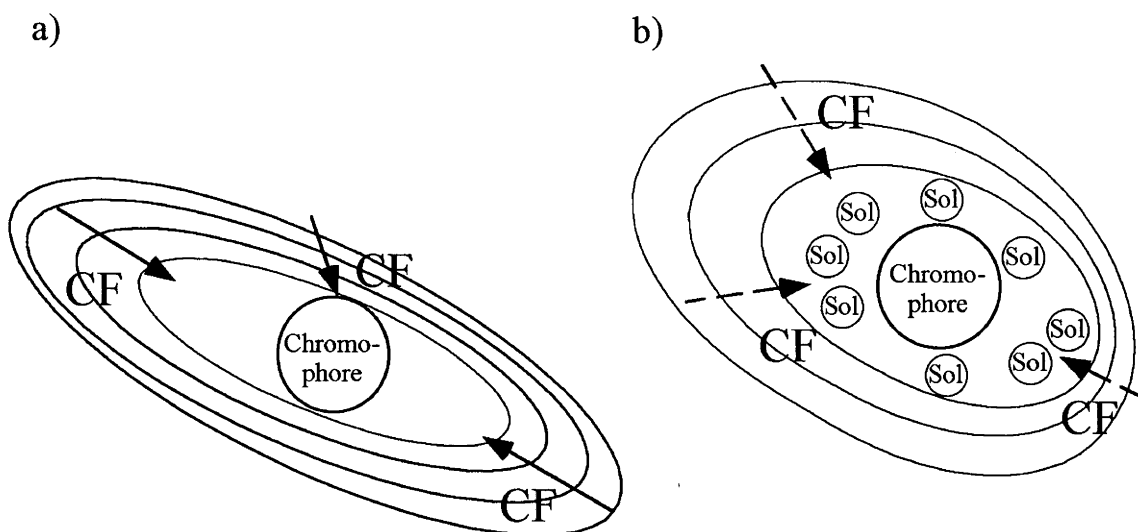


Figure 5.17: The presence of solvent may explain the reduction in the crystal field as the solvent forms a 'loose cage' around the chromophore. a) The chromophore experiences the CF fully. b) The solvent acts like a shield between the CF and the chromophore.

The above explanation accounts for the difference in magnitude of the Stark effect for the two different samples used in the transmission experiment, but does not explain the polarisation dependence. For both samples, the perpendicular experimental geometry gives a greater Stark broadening than the parallel experimental geometry. This suggests that, in both cases, there are significant interactions perpendicular to the molecular plane. A number of authors [75-77] have observed that magnesium porphyrin readily gains an axial ligand. In fact, if this chromophore is not provided with an appropriate ligand in its solvent, it then scavenges impurities from its environment to obtain axial coordination [76]. A similar process may be occurring with ZnPc. The degree of dissolution of ZnPc in MMA is only very slight. The dissolving of ZnPc may only happen to an extent where it can extract impurities to act as axial ligands. In fact, the provision of an axial ligand may be vital to the dissolution of ZnPc. ZnPc dissolves quite readily in solvents such as THF and pyridine, but dissolves poorly in many less readily coordinating solvents.

There are two main differences between the samples used for the transmission experiments and the samples used for the holographic

experiments. One difference is the polymer used. For the transmission experiments PMMA was used as the matrix. In the holographic experiments, PVB was used. The dielectric constants of the two polymers are quite similar (2.55 for PVB and 2.71 for PMMA, both at liquid He temperatures [67]). This similarity suggests that the bulk electrostatic properties of the two polymers are quite similar. On a microscopic scale they may interact differently with the chromophores doped into them.

The other difference is the manner in which the samples for the holographic experiment were prepared. These samples were made in a similar manner to that of the sample with solvent used in the transmission experiment. The chromophores were dissolved in THF before being added to the polymer solution. Therefore there will be some interaction between the THF and the chromophore. These samples were much thinner ($\sim 100 \mu\text{m}$) than the sample with solvent used in the transmission experiments. The samples used in the holographic experiments were carefully dried and pumped upon to remove excess solvent. It may be the case that any solvent which might form a 'cage' around the chromophore is removed by the drying procedure. The absence of extra solvent around the chromophore could explain the larger dipole, as would the presence of THF co-ordinating to the zinc. However, it is difficult to form any meaningful comparisons between the holographic data and the transmission data as the polymers were different.

The zero-field holes from the two sets of transmission data and the holographic data have different widths. The hole-burning efficiencies are also different in these data sets. In the case of the holographic experiments $\sim 100 \mu\text{W}/\text{cm}^2$ was applied to the sample for 60 s to produce zero-field holes of $\sim 1 \text{ GHz}$ in width. For the sample with solvent powers of $\sim 250 - 500 \text{ nW}/\text{cm}^2$ were applied for 10 s to produce holes $\sim 2 \text{ GHz}$ wide. And for the sample without solvent, powers of $250 - 500 \text{ nW}/\text{cm}^2$ and burn times of 2 - 3 minutes were used, resulting in zero-field holes of $\sim 1 \text{ GHz}$. This variation in burn times and powers indicates a variation in hole-burning quantum efficiency from system to system. It may be the case that the different preparation techniques produce three different chromophores with respect to the hole-burning mechanism. Different hole-burning mechanisms may also lead to different zero-field widths.

It has been proposed [50, 76] that the hole-burning mechanism in this style of chromophore is the movement of the metal ion in and out of the porphyrin/phthalocyanine plane. If this is the case, then the magnitude of the dipole perpendicular to the molecular plane observed in these hole-burning experiments may be associated with the hole-burning mechanism. The description given above allows the variation in dipole, the variation in hole-burning quantum efficiency, and the variation in zero-field hole width to be rationalised.

5.4 Wavelength dependence of Stark broadenings in spectral holes

There are a number of mechanisms which cause inhomogeneous broadening in condensed phases. These mechanisms may be classified as follows [78-80]:

$$\Delta\nu_s = \Delta\nu_{\text{disp}} + \Delta\nu_{\text{sc}} + \Delta\nu_{\text{cs}} + \Delta\nu_{\text{dd}} \quad (5.4)$$

where $\Delta\nu_s$ is the 'solvent shift'. The contributing factors to $\Delta\nu_s$ are:

- a) $\Delta\nu_{\text{disp}}$ which is a result of dispersion interactions;
- b) $\Delta\nu_{\text{sc}}$ is the polarisation of the environment by the dipole of the chromophore;
- c) $\Delta\nu_{\text{cs}}$ is the polarisation of the chromophore by dipoles in the environment;
- d) $\Delta\nu_{\text{dd}}$ is a dipole-dipole interactions between environment and chromophore.

Since ZnPc and ZnTbp are accepted as being nominally centro-symmetric here (and therefore have no dipole); contributions from $\Delta\nu_{\text{sc}}$ and $\Delta\nu_{\text{dd}}$ are neglected [80].

Dispersion interactions arise from instantaneous dipoles [81-84]. Instantaneous dipoles result from the instantaneous positions of the electrons in a molecule. An instantaneous dipole will polarise a

neighbouring molecule and the two dipoles interact to lower the energy (see figure 5.18). These interactions will differ from chromophore to chromophore and will also be different in the ground and excited state for a given chromophore. This leads to a distribution of transition energies.

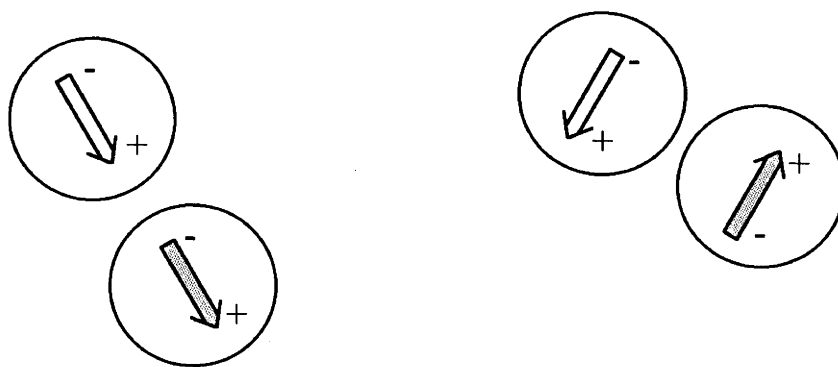


Figure 5.18: Dispersion interactions. An instantaneous dipole (shaded) on one molecule produces a dipole on another molecule. The two dipoles then interact to lower the energy. (After reference [84].)

The contribution to the solvent shift from Δv_{cs} is sometimes known as the 'solvent Stark effect'. The similarity to the Stark effect may be observed as follows:

The shift in transition energy associated with a linear Stark effect is given by equation 5.1. In the case of a chromophore in a given environment E_{app} is the 'matrix field' applied to the chromophore by the matrix, \mathbf{E}_{mat} . The dipole, $\Delta\boldsymbol{\mu}_{ind}$, is given by the dipole induced in the chromophore by the matrix field. This dipole may be expressed:

$$\Delta\boldsymbol{\mu}_{ind} = \mathbf{E}_{mat}\Delta\boldsymbol{\alpha} \quad (5.5)$$

where $\Delta\boldsymbol{\alpha}$ is the change in polarisability between the ground and excited states. The solvent shift from Δv_{cs} may therefore be written:

$$\Delta v_s = \mathbf{E}_{mat}\Delta\boldsymbol{\alpha}\mathbf{E}_{mat} \quad (5.6)$$

In an amorphous environment each host molecule is going to be in a slightly different micro-environment. With a variation in micro-

environment there is a variation in E_{mat} , and therefore a variation in transition energy (see figure 5.19).

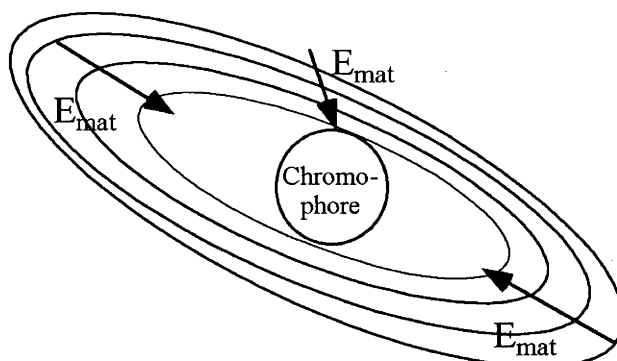


Figure 5.19: A chromophore in a matrix field. The chromophore is under the influence of an electric field, E_{mat} , as a result of the matrix. As the micro-environment which the chromophore resides in changes, so does the magnitude and angle of E_{mat} . Thus a shift in transition energy results.

The $\Delta\mu_{\text{ind}}$ of equation 5.5 is the same $\Delta\mu_{\text{ind}}$ probed in the Stark experiments. Therefore, as wavelength is varied (as a result of the variation in E_{mat}), so will the magnitude of $\Delta\mu_{\text{ind}}$ observed in the Stark experiments.

If $\Delta\nu_{\text{cs}}$ is the dominant mechanism involved in the homogeneous broadening, then the induced Stark effect should show a quadratic dependence upon wavelength. If the dispersion interactions are the dominant mechanism for the inhomogeneous broadening, then little wavelength dependence is expected for the Stark broadenings.

The wavelength dependence of Stark-broadened spectral holes has been investigated by a number of authors [65, 79, 80, 83, 85]. The wavelength dependence for the two holographic experiments and the four transmission experiments is shown in figures 5.20 - 5.25. From the amount of scatter in the data it is hard to tell whether $\Delta\mu_{\text{eff}}$ changes linearly or quadratically with wavelength. This matter aside, the linear data are plotted here, and it can be seen that the wavelength dependence in all cases is small.

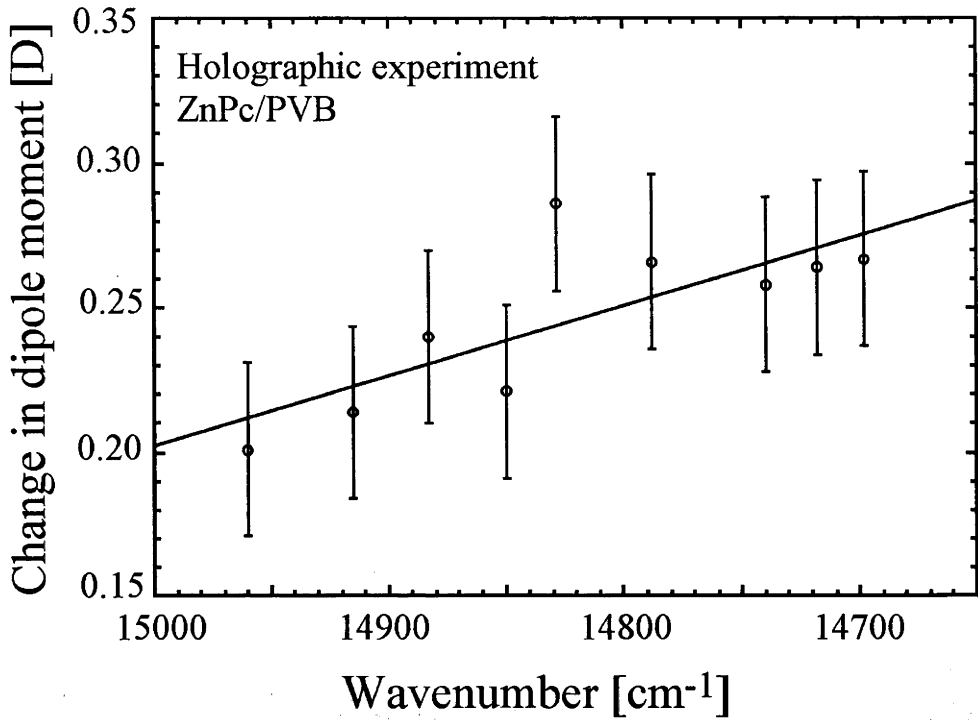


Figure 5.20: Wavelength dependence of the total dipole moment calculated for ZnPc/PVB from the holographically read out holes.

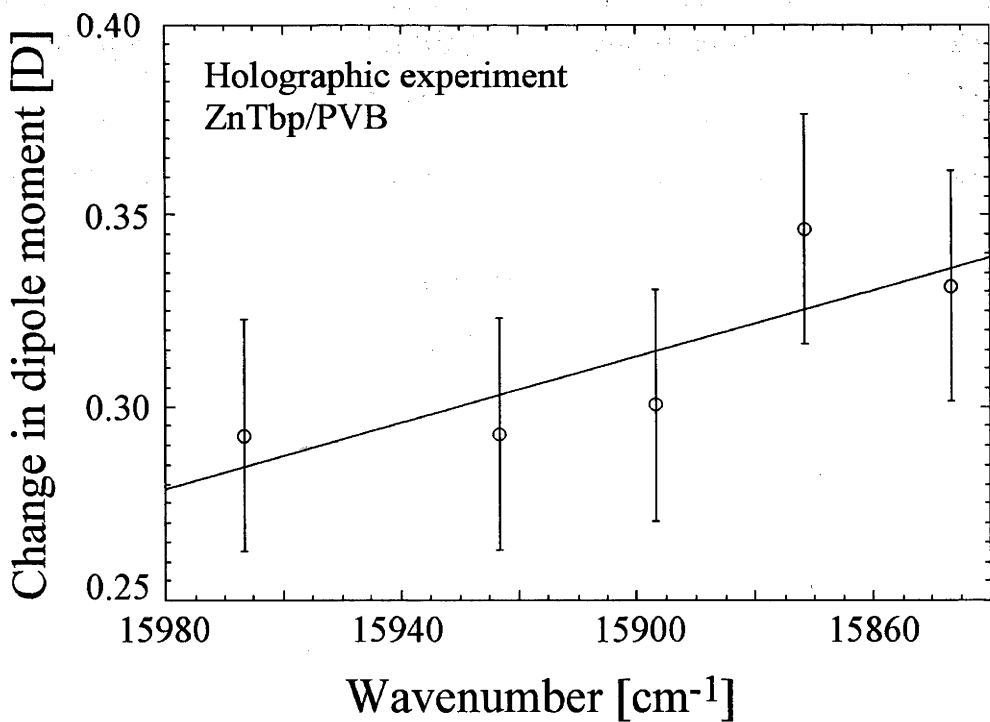


Figure 5.21: Wavelength dependence of the total dipole moment calculated for ZnTbp/PVB from the holographically read out holes.

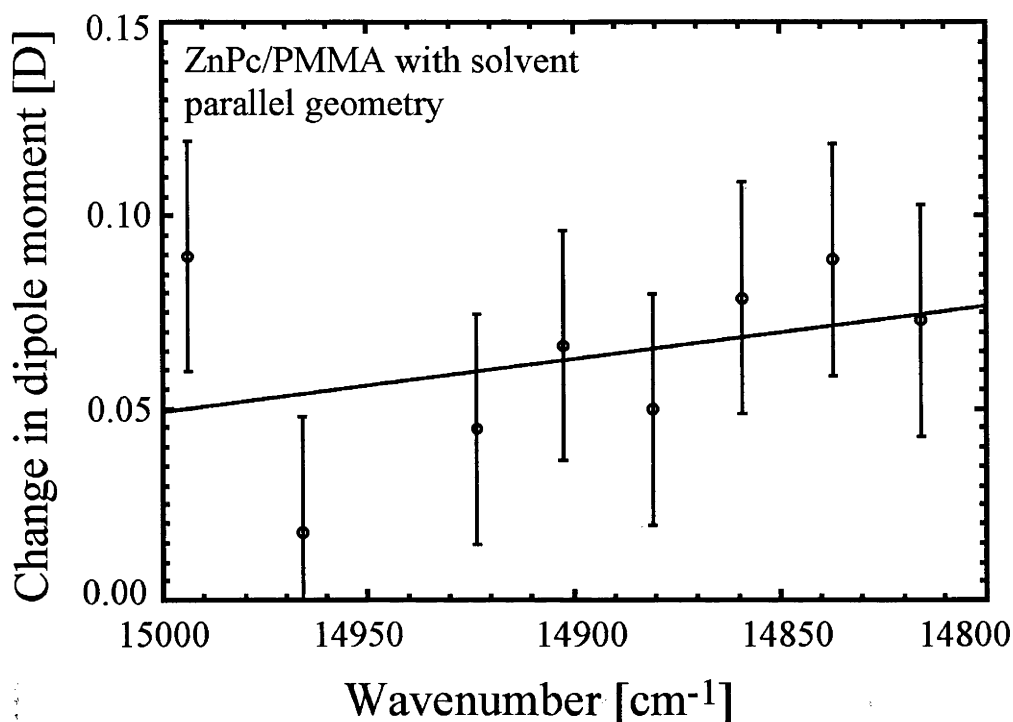


Figure 5.22: Wavelength dependence of the dipole moment calculated for the ZnPc/PMMA sample with solvent using the parallel experimental geometry.

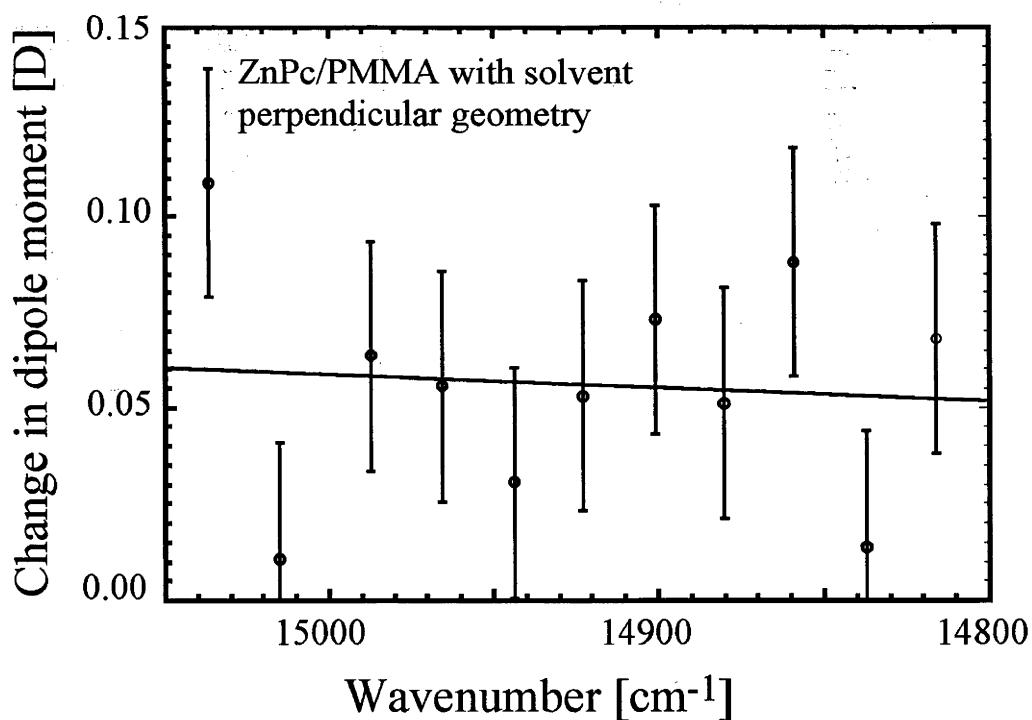


Figure 5.23: Wavelength dependence of the dipole moment calculated for the ZnPc/PMMA sample with solvent using the perpendicular experimental geometry.

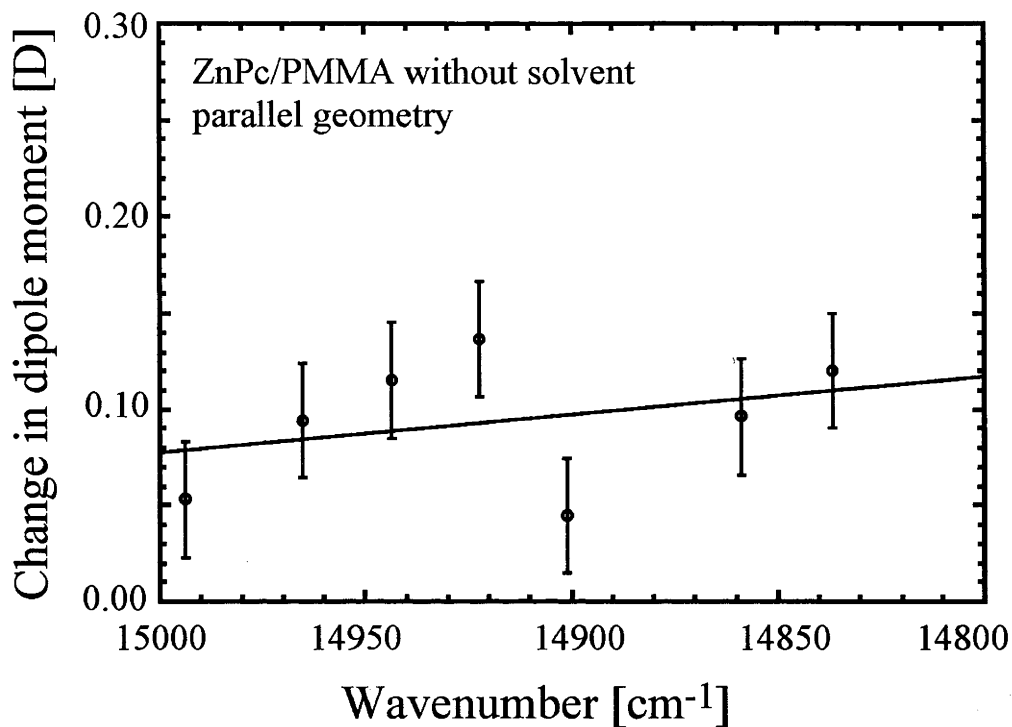


Figure 5.24: Wavelength dependence of the dipole moment calculated for the ZnPc/PMMA sample without solvent using the parallel experimental geometry.

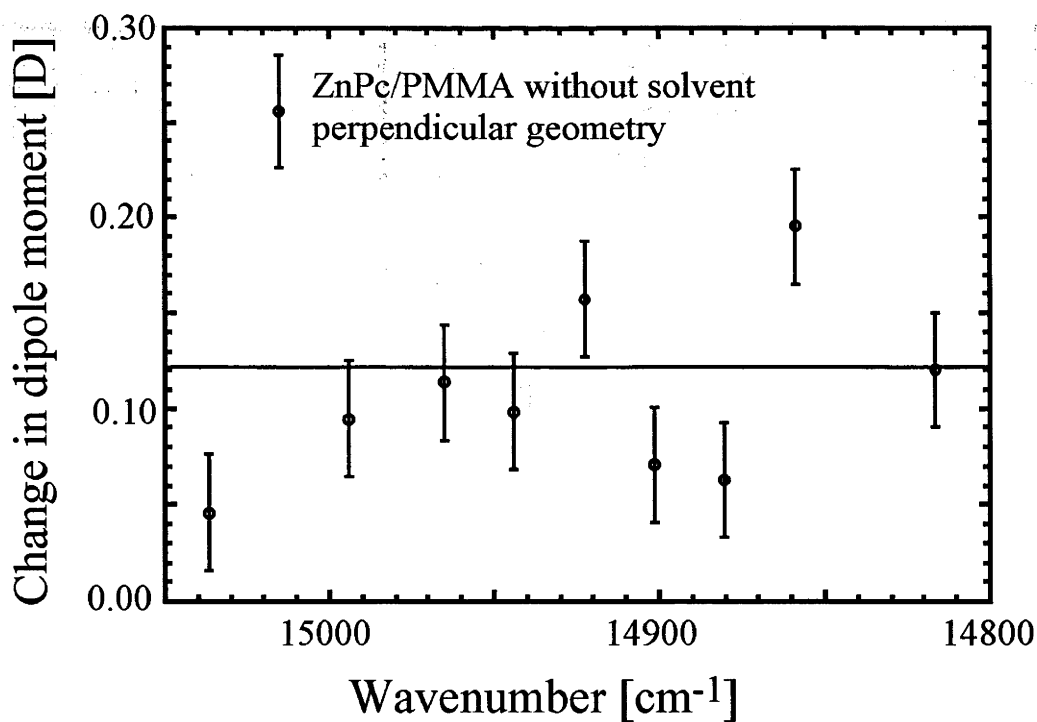


Figure 5.25: Wavelength dependence of the dipole moment calculated for the ZnPc/PMMA sample without solvent using the perpendicular experimental geometry.

In the case of the transmission experiments in particular, there is so much scatter on the data that it is hard to say anything meaningful about the wavelength dependence. However, whereas it can be seen that the dipole has a tendency to increase with transition energy in the case of the parallel experimental geometry, there is no such tendency in the data from the perpendicular geometry. This observation corroborates the assignment made in the fitting of the holographic data of a fixed 'molecular' dipole to the dipole perpendicular to the molecular plane and the distributed 'matrix-induced' dipole to the dipole in the molecular plane.

If the wavelength dependence is extrapolated to $\Delta\mu_{\text{eff}} = 0$, then a value for the 'free' molecule should be obtained. This value should be comparable with gas phase absorption maxima. Such an extrapolation was performed for the two parallel geometry experiments in transmission and the two sets of holographic data. The two transmission experiments yielded $15350 \pm 150 \text{ cm}^{-1}$ and $15390 \pm 150 \text{ cm}^{-1}$ for the sample with solvent and the sample without solvent respectively. The holographic data yielded $15830 \pm 150 \text{ cm}^{-1}$ for ZnPc and $16630 \pm 150 \text{ cm}^{-1}$ for ZnTbp. These results are summarised in table 5.5. Gas phase Q band absorption maxima are reported as 15150 cm^{-1} and 15128 cm^{-1} by references [86] and [87] respectively for ZnPc. A value of 16579 cm^{-1} is given for the Q band emission of ZnTbp in a supersonic expansion in reference [88].

Data set	Wavenumber at $\Delta\mu_{\text{eff}}=0$ [cm^{-1}]
ZnPc/PVB holo. expt	15830 ± 150
ZnTbp/PVB holo. expt	16630 ± 150
ZnPc/PMMA with solvent parallel geometry	15350 ± 150
ZnPc/PMMA with solvent perpendicular geometry	15390 ± 150

Table 5.5: The wavenumber resulting from a linear extrapolation of the wavelength dependent Stark data to $\Delta\mu_{\text{eff}} = 0$.

The values given by the extrapolation are of an appropriate magnitude, but they are not very reliable values. The error in the extrapolated values may be attributable to the amount of scatter in the Stark data. The greatest source of error in the holographic Stark measurements is the value for the thickness of the sample and therefore the magnitude of the applied field. In the transmission experiments, there is the added problem of intensity variations in the baseline. They are a substantial source of error, particularly in the data from the solvent free sample where the holes are shallower.

The lack of wavelength dependence in the Stark broadening indicates that the homogeneous broadening is predominantly caused by dispersion interactions. This result is similar to that in references [79, 83]. This result is also consistent with the lack of wavelength dependence in the Zeeman experiments. The in-plane dipole is related to the same interactions that give rise to the CF splittings which are probed in the Zeeman experiments.

6. Concluding Remarks

6.1 The aim of the project and the systems studied

The aim of this project was to obtain information about chromophores in condensed phases. This has been fulfilled particularly through the use of spectral hole-burning and the application of external fields.

The chromophores studied in this thesis are all porphyrin derivatives; namely ZnPc, ZnOep, ZnTbp, ZnObuPc and LuPc₂. The work has centred upon the lowest energy electronic transition - the Q band. With the exception of LuPc₂, these chromophores are nominally D_{4h}. Under this condition, the excited state of the Q transition is doubly degenerate. This degeneracy is lifted by CFs within the host. These systems are also known to be JT active. Despite a lack of structure in the optical spectra of their Q bands, the CF splittings and the JT activity may be probed in detail. Information about the interaction of the chromophores with their environment was also obtained.

6.2 The experiments

For this thesis a variety of experiments have been performed. Both high resolution and low resolution experiments have been done, as well as both Stark and Zeeman experiments.

The high resolution experiments are good for obtaining detailed information upon small changes in narrow spectral features. The holographic read-out, in particular, provides an excellent signal quality for measuring the small changes which may occur in a spectral hole upon the application of an external field. The holographic technique places restrictions upon the sample which may be studied.

The low resolution experiments, on the other hand, have the advantage of tunability. Although the resolution available with a single frequency scanning laser (~ 1 MHz) is not achievable with a lamp and a monochromator, much larger spectral ranges may be scanned. These

experiments enable broader features such as vibrational side holes, and the contributions from E_2 and PWs to be investigated. There is the potential for the resolution of these experiments to be increased (perhaps to a few GHz) and thus to become closer to matching the widths of the spectral features under investigation.

6.3 Summary of the results obtained

Excited state vibrational frequencies were obtained for ZnPc/PMMA, ZnPc/PVB, ZnTbp/PVB and LuPc₂/PMMA by burning into vibrational sidelines (see section 3.2). These agreed well with vibrational frequencies measured for this class of chromophore in Ar and Shpol'skii matrices.

Complementary to the experiments involving hole-burning in vibrational sidebands were FLN experiments. Such experiments were performed on ZnPc and ZnOep (see section 3.3). Little narrowing was observed in the FLN experiments. This was rationalised in terms of rapid hole-burning at the excitation wavelength.

An extrapolation to hole width at zero fluence was performed upon ZnPc/PVB (section 3.6). At 1.8 K and on a timescale of 30 s, an extrapolated value of 600 ± 50 MHz was calculated. This value is an order of magnitude larger than the lifetime limited value. Clearly, there are processes such as spectral diffusion adding to the hole width on this timescale and at this temperature. es

The contribution of the PW to the Q(0,0) band of ZnPc/PVB was measured (see section 3.7). A DWF of 0.63 was calculated.

Preliminary work was performed on ZnObuPc (section 3.8). A new absorption band to the red of the Q band appeared upon exposure to light. This was tentatively assigned to the ZnObuPc^{•+} radical. Both the Q band and this new absorption band showed efficient hole-burning.

Magneto-optical measurements were made upon ZnPc, ZnOep and ZnTbp. Zeeman experiments performed upon ZnPc/PMMA and ZnOep/PVB revealed anomalously small Zeeman shifts (see section 4.1.2). These small shifts were analysed in terms of the combined action

of local CFs and JT effects. High resolution Zeeman experiments were performed in the case of ZnPc/PMMA (section 4.1.3). These experiments enabled a more searching investigation of the CF splittings and JT activity in this system. From these experiments, through the use of modelling, a value of 110 cm^{-1} for the mean CF splitting and a Ham factor of 0.52 were calculated. The error between the data and the model was $\sim 10 - 20 \%$.

Hole MCD experiments were performed on ZnPc, ZnOep and ZnTbp (see section 4.2). Such experiments enable the distribution of E_1 and E_2 to be 'mapped' at discrete places across the inhomogeneously broadened band. Characteristic hole MCD shapes were measured and interpreted in terms of the position in the inhomogeneously broadened band in which the hole was burnt. Hole MCD proved to be a useful tool because E_1 and E_2 have two differently signed MCD signals associated with them, and therefore their respective contributions are readily identified.

Stark experiments were performed on spectral holes in ZnPc and ZnTbp. The first series of Stark experiments were read out holographically (section 5.2). The excellent signal quality obtainable from the use of this technique enabled the data to be modelled. The changes in hole shape in the electric field were attributed to in-plane distortions of the chromophore which remove its nominal four-fold symmetry (the same distortions which give rise to the CF splittings probed in the magneto-optical experiments) and a dipole perpendicular to the molecular plane which may arise as a result of axial ligation.

The assignment of the broadening to these two different sources was further investigated by performing Stark experiments (in transmission) on spectral holes with two different geometries: E_{pol} parallel to E_{app} and E_{pol} perpendicular to E_{app} (section 5.3). The data from these two experimental geometries were characteristically different. The dipole calculated from the perpendicular geometry was larger than that calculated from the parallel geometry.

To test the role of the solvent in axial ligation of the zinc atom, a sample without solvent was prepared (section 5.3). This sample showed the same characteristic behaviour for the two experimental geometries (the perpendicular experimental geometry yielded a larger change in dipole

than the parallel experimental geometry). For both experimental geometries, the dipoles were larger in the sample without solvent than in the sample with solvent. This observation was accounted for by the solvent forming a 'loose cage' around the chromophore. For both the sample with solvent and the sample without solvent the dipole perpendicular to the molecular plane indicated strong axial interactions. In the case of the solvent-free sample, this was attributed to the chromophore scavenging ligands from its environment.

The wavelength dependence of the Stark broadenings was measured (see section 5.4). Little wavelength dependence was observed. This result was attributed to the inhomogeneous broadening being dominated by dispersion interactions.

6.4 Further remarks about the results

The application of hole-burning techniques proved to be advantageous for two reasons: firstly, spectral holes are a relatively narrow feature compared to the inhomogeneously broadened band; the small changes (relative to the inhomogeneous bandwidth) which occur on the application of an applied field are easier to observe and interpret on the narrower feature. Secondly, spectral holes enable measurements to be made in a number of discrete places across the inhomogeneously broadened band. When a broadband measurement is made, an average is taken across the band. Spectral-hole burning enables changes which occur across the band to be investigated.

An observation which may be made as a result of the investigations here is that a chromophore may not be considered in isolation from its environment. The interaction of a chromophore with its environment has a profound effect upon its spectroscopy. Even small changes such as the sample preparation technique may alter the spectroscopic characteristics dramatically.

6.5 Possible future experiments

Hole-burning spectroscopy has been used to study energy transfer in biological systems. Extrapolated hole widths were used to obtain energy transfer times between chromophores [89-91]. Also, some Stark experiments have been performed to investigate the environments of systems of biological importance [92-94]. Experiments of the type described in this thesis lend themselves very well to studying these systems. Many biological systems are not readily removed from their environments and the broadband spectra are featureless. Broadband experiments may therefore be of limited usefulness. Furthermore, a biological system's activity is reliant upon its environment, particularly interactions with surrounding proteins. Thus, the experiments here may be extended to probe the mechanisms of the activity in these chromophores.

References

1. J. Friedrich and D. Haarer, *Angew. Chem. Int. Ed. Engl.*, **23**, 113-140 (1984).
2. W. Moerner (ed.) *Persistent Spectral Hole-Burning: Science and Applications, Topics in Current Physics*, vol. 44 (Springer-Verlag, Berlin, 1988).
3. H. Riesen and E. Krausz, *Comments Inorg. Chem.*, **14**, 323-347 (1993).
4. S. Völker, *Ann. Rev. Phys. Chem.*, **40**, 499 (1989).
5. T. Nyokong, Z. Gasyna and M. Stillman, *Inorg. Chem.*, **26**, 1087-1095 (1987).
6. T.-H. Huang, K.E. Rieckhoff and E.M. Voigt, *J. Chem. Phys.*, **77**, 3424-3441 (1982).
7. M. Gouterman in *The Porphyrins*, ed. D. Dolphin, pp. 1-165 (Academic Press, New York, 1978).
8. D.M. Metcalf, T.C. VanCott, S.W. Snyder, P.N. Schatz and B.E. Williamson, *J. Phys. Chem.*, **94**, 2828-2832 (1990).
9. T.C. VanCott, J.L. Rose, C.G. Misener, B.E. Williamson, A.E. Schrimpf, M.E. Boyle and P.N. Schatz, *J. Phys. Chem.*, **93**, 2999-3011 (1989).
10. Z. Gasyna, D.H. Metcalf, P.N. Schatz, C.L. McConnell and B.E. Williamson, *J. Phys. Chem.*, **99**, 5865-5872 (1995).
11. S.B. Piepho and P.N. Schatz, *Group Theory in Spectroscopy with Applications to Magnetic Circular Dichroism* (John Wiley, New York, 1983).
12. G. Herzberg, *Molecular Spectra and Molecular Structure III: Electronic Spectra and Electronic Structure of Polyatomic Molecules* (D. Van Nostrand, Princeton, New Jersey, 1966).
13. H. Maier, B.M. Kharlamov and D. Haarer, *Phys. Rev. Lett.*, **76**, 2085-2088 (1996).
14. W.E. Moerner, M. Gehrtz and A.L. Huston, *J. Phys. Chem.*, **88**, 6459-6460 (1984).
15. I. Renge, H. Wolleb, H. Spahni and U.P. Wild, *J. Phys. Chem. A*, **101**, 6202-6213 (1997).
16. A. Monnier, M. Schnieper, R. Jaaniso and H. Bill, *Radiat. Eff. Defects Solids*, **135**, 253-256 (1995).

17. R. Jaaniso and H. Bill, *J. Lumin.*, **64**, 173-179 (1995).
18. H. Bill, R. Jaaniso, H. Hagermann, D. Lovy, A. Monnier and M. Schnieper, *Opt. Eng.*, **34**, 2333-2338 (1995).
19. J. Friedrich, J.D. Swalen and D. Haarer, *J. Chem. Phys.*, **73**, 705-711 (1980).
20. W.M. Yen and P.M. Selzer (eds.) *Laser Spectroscopy of Solids, Topics in Applied Physics*, vol. 49 (Springer-Verlag, Berlin, 1981).
21. N.I. Ulitsky, B.M. Kharlamov and R.I. Personov, *Chem. Phys.*, **141**, 441-445 (1990).
22. W. Liptay in *Excited States*, ed. E.C. Lim, pp. 129-225 (Academic Press, New York, 1974).
23. C.J.F. Böttcher, *Theory of Electric Polarisation* (Elsevier, Amsterdam, 1973).
24. A.J. Meixner, A. Renn, S.E. Bucher and U.P. Wild, *J. Phys. Chem.*, **90**, 6777-6785 (1986).
25. B. Dick, *Chem. Phys.*, **136**, 429-442 (1989).
26. R. Stranger, L. Dubicki and E. Krausz, *Inorg. Chem.*, **35**, 4218-4226 (1996).
27. E. Krausz, C. Tomkins and H. Adler, *J. Phys. E: Sci. Instrum.*, **15**, 1167-1168 (1982).
28. E. Hecht, *Optics* (Addison-Wesley, Reading, Massachusetts, 1998).
29. A.J. Meixner, A. Renn and U.P. Wild, *J. Chem. Phys.*, **91**, 6728-6736 (1989).
30. S. Wolfram, *Mathematica A System for Doing Mathematics by Computer* (Addison-Wesley, Reading, Massachusetts, 1991).
31. E. Krausz, H. Riesen, P.N. Schatz, Z. Gasyna, C.L. Dunford and B.E. Williamson, *J. Lumin.*, **66&67**, 19-24 (1996).
32. C.L. Dunford, B.E. Williamson, P.N. Schatz, Z. Gasyna, E. Krausz and H. Riesen, *Chem. Phys. Lett.*, **260**, 522-528 (1996).
33. L. Bajema, M. Gouterman and C.B. Rose, *J. Mol. Spectrosc.*, **39**, 421-431 (1971).
34. M. Abkowitz and A.R. Monahan, *J. Chem. Phys.*, **58**, 2281-2287 (1973).
35. A.R. Monahan, J.A. Brado and A.F. DeLuca, *J. Phys. Chem.*, **76**, 446-449 (1972).
36. E.A. Lucia and F.D. Verderame, *J. Chem. Phys.*, **52**, 2307-2310 (1970).
37. F.T.H. den Hartog, C. van Papendrecht, R.J. Silbey and S. Völker, *J. Chem. Phys.*, **110**, 1010-1016 (1999).

38. D. Braun, A. Ceulemans, B. Dick and H. Konami, *Chem. Phys. Lett.*, **225**, 398-403 (1994).
39. B. Dick, *Chem. Phys.*, **136**, 413-428 (1989).
40. B.M. Kharlamov, L.A. Bykovskaya and R.I. Personov, *Chem. Phys. Lett.*, **50**, 407-411 (1977).
41. J. Friedrich and D. Haarer, *J. Chem. Phys.*, **79**, 1612-1615 (1983).
42. P.E. Fielding and A.W.-H. Mau, *Aust. J. Chem.*, **29**, 933-940 (1976).
43. E.I. Alshits, R.I. Personov, A.M. Pyndyk and V.I. Stogov, *Opt. Spectrosc.*, **39**, 156-159 (1975).
44. H.P.H. Thijssen and S. Völker, *Chem. Phys. Lett.*, **120**, 496-502 (1985).
45. A.T. Gradyushko and M.P. Tsvirko, *Opt. Spectrosc.*, **31**, 291-295 (1971).
46. S.P. McGlynn, T. Azumi and M. Kinoshita, *Molecular Spectroscopy of The Triplet State* (Prentice-Hall, Englewood Cliffs, New Jersey, 1969).
47. A. Starukhin, E. Zenkevich, A. Shulga and A. Chernook, *J. Lumin.*, **68**, 313-323 (1996).
48. K. Mairing, A. Suisalu, J. Kikas, E.I. Zenkevich, A.V. Chernook, A.M. Shulga and G.P. Gurinovich, *J. Lumin.*, **64**, 141-148 (1995).
49. R.J. Silbey, J.M.A. Koedijk and S. Volker, *J. Chem. Phys.*, **105**, 901-909 (1996).
50. J.M.A. Koedijk, R. Wannemacher, R.J. Silbey and S. Völker, *J. Phys. Chem.*, **100**, 19945-19953 (1996).
51. R. Wannemacher, J.M.A. Koedijk and S. Völker, *Chem. Phys. Lett.*, **206**, 1-8 (1993).
52. P.G. Seybold and M. Gouterman, *J. Mol. Spectrosc.*, **31**, 1-13 (1969).
53. B. Plagemann, I. Renge, A. Renn and U.P. Wild, *J. Phys. Chem.*, **102**, 1725-1732 (1998).
54. C. De Caro, A. Renn and U.P. Wild, *J. Lumin.*, **59**, 309-316 (1991).
55. G. Flatscher and J. Friedrich, *Chem. Phys. Lett.*, **50**, 32-35 (1977).
56. P.C. Minor, M. Gouterman and A.P.B. Lever, *Inorg. Chem.*, **24**, 1894-1900 (1985).
57. J. Mack and M.J. Stillman, *J. Am. Chem. Soc.*, **116**, 1292-1304 (1994).

58. J.F. Myers, G.W. Rayner Canham and A.B.P. Lever, *Inorg. Chem.*, **14**, 461-468 (1975).
59. P.S. Vincett, E.M. Voigt and K.E. Rieckhoff, *J. Chem. Phys.*, **55**, 4131-4140 (1971).
60. T.C. VanCott, M. Koralewski, D.H. Metcalf and P.N. Schatz, *J. Phys. Chem.*, **97**, 7417-7426 (1993).
61. B.E. Williamson, pers. comm., 1997.
62. N.I. Ulitsky, B.M. Kharlamov and R.I. Personov, *Chem. Phys.*, **122**, 1-8 (1988).
63. G. Jansen, M. Noort, G.W. Canters and J.H. Van der Waals, *Mol. Phys.*, **35**, 283-294 (1978).
64. G.U. Bublitz and S.G. Boxer, *Annu. Rev. Phys. Chem.*, **48**, 213-242 (1997).
65. E. Vauthey, K. Holliday, C. Wei, A. Renn and U.P. Wild, *Chem. Phys.*, **171**, 253-263 (1993).
66. P. Schätz and M. Maier, *J. Chem. Phys.*, **87**, 809-820 (1987).
67. R.B. Altmann, I. Renge, L. Kador and D. Haarer, *J. Chem. Phys.*, **97**, 5316-5322 (1992).
68. I.B. Talanina, M.A. Collins, L. Dubicki and E. Krausz, *Chem. Phys. Lett.*, **200**, 318-324 (1992).
69. M. Maier, *Appl. Phys. B*, **41**, 73-90 (1986).
70. V.D. Samoilenko, N.V. Razumova and R.I. Personov, *Opt. spectrosc.*, **52**, 346-348 (1982).
71. R.W. Scheidt and W. Dow, *J. Am. Chem. Soc.*, **99**, 1101-1104 (1977).
72. R. Timovich and A. Tulinsky, *J. Am. Chem. Soc.*, **91**, 4430-4432 (1969).
73. R.B. Altmann, D. Haarer, N.I. Ulitsky and R.I. Personov, *J. Lumin.*, **56**, 135-141 (1993).
74. L. Kador, D. Haarer and R. Personov, *J. Chem. Phys.*, **86**, 5300-5307 (1987).
75. G. Jansen and M. Noort, *Spectrochim. Acta*, **32A**, 747-753 (1976).
76. A.I.M. Dicker, L.W. Johnson, S. Völker and J.H. Van der Waals, *Chem. Phys. Lett.*, **100**, 8-14 (1983).
77. R.J. Platenkamp, *Mol. Phys.*, **45**, 113-127 (1982).
78. N. Mataga and T. Kubota, *Molecular Interactions and Electronic Spectra* (Marcel Dekker, Inc, New York, 1970).
79. L. Kador, S. Jahn, D. Haarer and R. Silbey, *Phys. Rev. B*, **41**, 12215-12226 (1990).

80. E. Vauthey, J. Voss, C. de Caro, A. Renn and U.P. Wild, *Chem. Phys.*, **184**, 347-356 (1994).
81. B.B. Laird and J.L. Skinner, *J. Chem. Phys.*, **90**, 3274-3281 (1989).
82. E.G. McRae, *J. Phys. Chem.*, **61**, 562-572 (1957).
83. T. Sesselmann, L. Kador, W. Richter and D. Haarer, *Europhys. Lett.*, **5**, 361 (1988).
84. P.W. Atkins, *Physical Chemistry* (Oxford University Press, Oxford, 1990).
85. N. Hartmannsgruber and M. Maier, *J. Chem. Phys.*, **96**, 7279-7286 (1992).
86. D. Eastwood, L. Edwards, M. Gouterman and J. Steinfeld, *J. Mol. spectrosc.*, **20**, 381-390 (1966).
87. L. Edwards and M. Gouterman, *J. Mol. Spectrosc.*, **33**, 292-310 (1970).
88. U. Even, J. Jortner and J. Friedman, *J. Phys. Chem.*, **86**, 2273-2276 (1982).
89. M.L. Groot, J.P. Dekker, R. van Grondelle, F.T.H. den Hartog and S. Völker, *J. Phys. Chem.*, **100**, 11488-11495 (1996).
90. C. De Caro, R.W. Visschers, R. van Grondelle and S. Völker, *J. Phys. Chem.*, **98**, 10584-10590 (1994).
91. H. van der Laan, C. De Caro, T. Schmidt, R.W. Visschers, R. van Grondelle, G.J.S. Fowler, C.N. Hunter and S. Volker, *Chem. Phys. Lett.*, **212**, 569-580 (1993).
92. P. Geissinger, B.E. Kohler and J.C. Woehl, *J. Phys. Chem.*, **99**, 16527-16529 (1995).
93. J. Gafert, J. Friedrich, J. Vanderkooi and J. Fidy, *J. Phys. Chem.*, **99**, 5223-5227 (1995).
94. J. Gafert, J. Friedrich and F. Parak, *Proc. Natl. Acad. Sci. USA*, **92**, 2116-2120 (1995).
95. C.L. Dunford, PhD Thesis, Universtiy of Canterbury, Chrsitchurch, New Zealand (1997).
96. T.C. VanCott, Z. Gasyna and P.N. Schatz, *J. Phys. Chem.*, **99**, 4820-4830 (1995).

Appendix: Publications and Presentations

The following publications and presentations have arisen from this work:

R. Purchase, E. Krausz, H. Riesen, B. Williamson, C. Dunford, P. Schatz, Z. Gasyna 'Chemical applications of FLN and spectral hole-burning: matrix isolated chromophores' in International Quantum Electronics Conference, 1996 OSA Technical Digest Series (Optical Society of America, Washington, D.C., 1996), pp. 192-193.

R. Purchase, E. Krausz, B.E. Williamson 'Magneto-optic measurements of spectral holes' presented at DPC '97 11th International Conference on Dynamical Processes in Excited States of Solids, Mittelberg Austria/Germany, 20-24 July 1997.

R. Purchase, E. Krausz, B.E. Williamson 'Magneto-optic measurements of spectral holes' in Journal of Luminescence **76&77**, 339-343 (1998).

R. Purchase, B. Plagemann, E. Krausz, U.P. Wild 'Electric-field-induced broadening of spectral holes in zinc phthalocyanine' presented at 2nd Australian Conference on Physical Chemistry, Brisbane Australia, 11-15 July 1998.

R. Purchase, M. Sellars, E. Krausz, N.B. Manson 'Electric-field-induced broadening of spectral holes in zinc phthalocyanine' presented at Australasian Conference on Optics, Lasers and Spectroscopy, Christchurch New Zealand, 14-17 December 1998.

R. Purchase, B. Plagemann, E. Krausz, U.P. Wild 'Electric-field-induced broadening of spectral holes in zinc phthalocyanine' submitted to Chemical Physics Letters.

A copy of the reprint from Journal of Luminescence, a miniature version of the poster presented at Australasian Conference on Optics, Lasers and Spectroscopy and the preprint sent to Chemical Physics Letters are included in the pages which follow. a



ELSEVIER

Journal of Luminescence 76&77 (1998) 339–343

JOURNAL OF
LUMINESCENCE

Magneto-optic measurements of spectral holes

Robin Purchase^{a,*}, Elmars Krausz^a, Bryce E. Williamson^b^aResearch School of Chemistry, Australian National University, Canberra, 0200, Australia^bChemistry Department, University of Canterbury, Christchurch, 8001 New Zealand

Abstract

The magneto-optic properties of spectral holes burnt in two porphyrin derivatives (zinc phthalocyanine and zinc octaethylporphyrin) in polymer films are reported. The Zeeman shifts and broadenings observed are anomalously small. This is interpreted as being due to the combined action of local crystal fields and Jahn–Teller effects. Hole magnetic circular dichroism (MCD) spectra are reported for features resulting from burning in both the Q band origin and vibrational sideline regions. The results provide information about the distribution of environmentally induced crystal-field splittings of the (nominally degenerate) excited state. Modelling of hole absorption and MCD provides new insights into the hole-burning processes in these systems. © 1998 Elsevier Science B.V. All rights reserved.

Keywords: Hole burning; Porphyrin; Magnetic circular dichroism

1. Introduction

Spectral hole-burning studies often concentrate on gaining information about homogeneous line widths, but the technique shows potential for a variety of other applications [1–4]. Hole-burning may enhance the ability to obtain detailed information about the electronic structure and potential-energy surfaces of chromophores in amorphous environments. The influence of an applied external magnetic field on a (relatively narrow) spectral hole may provide additional useful information. Shifts and broadenings of spectral holes, as well as magnetically induced polarisations, particularly magnetic circular dichroism (MCD) may provide informa-

tion regarding excited-state angular momenta and transition mechanisms. The ‘hole MCD’ is obtained by subtracting MCD spectra taken after burning from those taken before [5].

2. Experimental

The samples considered were two porphyrin derivatives – zinc phthalocyanine (ZnPc) and zinc octaethylporphyrin (ZnOep). The work has concentrated on the Q band, which is a ligand-centred π – π^* transition (${}^1A_{1g}$ – ${}^1E_{1u}$). The hosts used have been polymer films – usually polymethylmethacrylate (PMMA) or polyvinylbutyral (PVB). Absorption and MCD spectra for these systems are displayed in Fig. 1.

Experiments were performed at 1.6 K in an Oxford Instruments SM4 superconducting magnet cryostat. Holes in the origin bands were burnt with

*Corresponding author. Fax: +61 6 249 0750; e-mail: robin@rsc.anu.edu.au.

340

R. Purchase et al. / Journal of Luminescence 76 & 77 (1998) 339–343

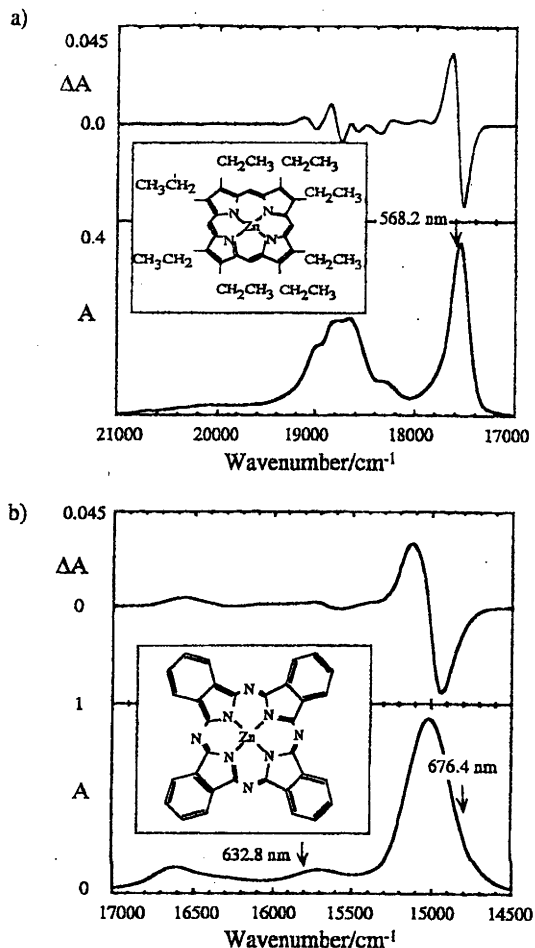


Fig. 1. Absorption and MCD at 5 T of (a) ZnOep and (b) ZnPc.

the 676.4 nm line of a Kr^+ laser for ZnPc, and with the 568.2 nm line for ZnOep. Holes burnt into the ZnPc sideband were burnt with a HeNe laser. Holes were approximately 10% of the absorption at that wavelength. The laser was defocused, and the entire area of the sample was evenly illuminated with a power density of $\sim 0.1 \text{ mW cm}^{-2}$. The holes were read in absorption using a 0.75 m Spex monochromator with a resolution of $\sim 1 \text{ cm}^{-1}$. MCD spectra were measured simultaneously with absorption [6].

3. Results and discussion

3.1. Magneto-optics of spectral holes

Zeeman experiments were performed on spectral holes in ZnPc and the results are displayed in Fig. 2a and Fig. 2b. When ZnPc and ZnOep have ideal D_{4h} symmetry, the excited state of the Q transition is doubly degenerate. However, the symmetry of the molecule is lowered by crystal fields in the environment of the polymer. Crystal-field splittings of $\sim 30 \text{ cm}^{-1}$ for ZnOep and $\sim 50 \text{ cm}^{-1}$ for ZnPc have been reported for the chromophores in Ar [7,8]. The absorption bands of ZnPc and ZnOep in polymer films are ~ 330 and $\sim 210 \text{ cm}^{-1}$ wide respectively, and crystal-field splittings of a similar (or slightly larger) magnitude

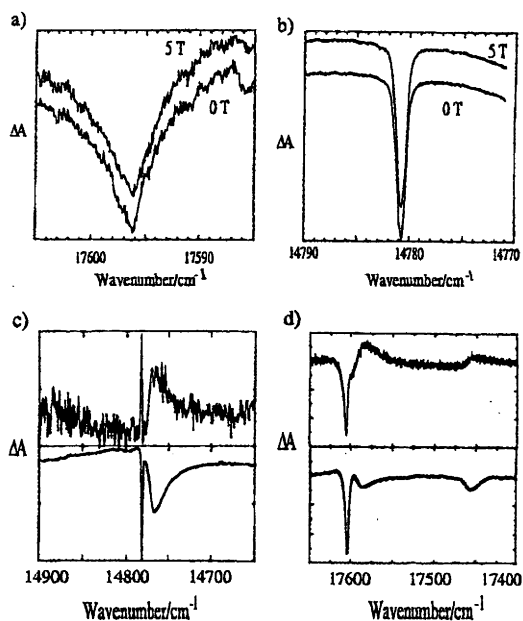


Fig. 2. (a) 5 and 0 T absorption spectra of the 568.2 nm hole in ZnOep/PVB. (b) 5 and 0 T absorption spectra of the 676.4 nm hole in ZnPc/PMMA. (c) 5 T hole MCD (upper) and absorption (lower) of the 676.4 nm hole in ZnPc/PMMA. (d) 5 T hole MCD (upper) and absorption (lower) of the 568.2 nm hole in ZnOep/PMMA. Hole absorption spectra are displayed by subtracting the pre-burn absorption spectrum from the post-burn spectrum. ΔA is thus the resulting change in absorption.

to those in Ar could easily be concealed within these bandwidths.

Upon the application of a magnetic field, the levels shift further apart. The extent of this Zeeman shift may be predicted by the use of a calculation based upon near-degenerate perturbation theory [9]:

$$\Delta v_B = \pm \frac{\Delta v_0}{2} \left\{ \left[1 + \left(\frac{2\mu \cdot B}{\Delta v_0} \right)^2 \right]^{1/2} - 1 \right\},$$

where Δv_0 is the crystal-field splitting, μ is the molecular static magnetic moment of the unsplit excited state and B is the magnetic field.

Using a value of $1.4 \text{ cm}^{-1} \text{ T}^{-1}$ for μ [9] and the above crystal-field splittings yields Zeeman shifts of 1.55 cm^{-1} for ZnOep and 0.96 cm^{-1} for ZnPc. This is far greater than the observed shifts. Since the molecules are randomly oriented in the host, the average Zeeman shifts will be reduced by a value close to $\frac{4}{15}$ [10]. With this reduction, the experimental shift ($< 0.2 \text{ cm}^{-1}$) remains lower than predicted. However, the Q excited states of both ZnPc and ZnOep are known to involve substantial Jahn–Teller interactions, which quench the magnetic moments. The extent of the quenching is determined by the Ham factor, which has been measured to be 0.67 for ZnOep and 0.63 for ZnPc [7,8]. These added contributions provide calculated Zeeman shifts of 0.19 cm^{-1} for ZnOep and 0.10 cm^{-1} for ZnPc which are compatible with the experimental observations. The crystal-field splittings in polymer films may be greater than in Ar, and this would reduce the Zeeman shifts further. We plan to improve the Zeeman experiments so that shifts become measurable.

The crystal-field components of the Q band are immediately distinguishable by the opposite signs of their MCD. Thus, MCD is a useful tool for determining which of the levels contribute to a given hole. Consider the hole in ZnPc/PMMA, which was burnt at 676.4 nm (Fig. 2c). This burn wavelength is approximately halfway down the red edge of the Q band. Therefore, the hole could be expected to be burnt predominantly in the lower of the crystal-field-split levels. The lower level gives a negative MCD and thus the hole MCD must be positive. This is indeed observed for both the zero-phonon line and the phonon side band.

In ZnOep, as shown in Fig. 2d, the 568.2 nm burn wavelength is close to the top of the absorption. Both the upper and the lower crystal-field levels may contribute. The hole MCD will thus have negative and positive MCD contributions. The excited state levels will shift relative to each other in an applied magnetic field, leaving the overall hole MCD with a sigmoid shape.

Other interesting features of the hole MCD of ZnOep are the side hole to the red of the burn energy and the sign of the phonon wing MCD. The side hole is indicative of hole-burning into a vibrational overtone of a (lower-energy) origin. The shift gives the energy of the Jahn–Teller-active vibration at $\sim 145 \text{ cm}^{-1}$. The side hole is broad ($\sim 25 \text{ cm}^{-1}$). This is likely to be due to interactions between the Jahn–Teller and crystal-field effects [10]. The area of the side hole is much smaller than the area of the hole at the burn energy. The hole at the burn energy is thus dominated by burning in the electronic origins.

The phonon wing shows an MCD signal of the opposite sign to that of the hole. The sign of the wing suggests that the phonons are associated purely with the lower crystal-field level. However, the corresponding zero-phonon line of the lower crystal-field component is not apparent from the hole MCD. Another means by which the sign of the phonon wing MCD may be reversed is if the phonons are Jahn–Teller active. This result contrasts the observations in ZnPc.

3.2. Simulations of spectral holes

Changes in shape of a spectral hole with increasing burn time may be simulated [11]. The calculation is readily generalised to a situation where there are two transitions with different line widths, in order to allow for the hole-burning processes in ZnPc and ZnOep. The simulations can be easily adapted to simulate hole MCDs in parallel, as well as to allow for the limited resolution of the read process.

Simulations show that a hole burnt into a transition with a narrow line width will deepen far more rapidly than a hole burnt into a transition with a broad line width. A hole which is burnt into a system with transitions with two different line widths is characterised by a broad shallow component, and a narrow deep component. When

342

R. Purchase et al. / Journal of Luminescence 76&77 (1998) 339–343

fully resolved, the narrow deep component dominates the spectrum. In absorption, it becomes difficult to discriminate between the broad component and the wings of the narrow component. Critical evidence of the presence of two components is provided by MCD spectra, as the signs of the two components are opposite. If the hole detection has limited resolution, the narrow component becomes less evident and the broad component dominates the spectrum. The results of such a calculation are shown in Fig. 3 for an advanced stage in burning as is the case for our experiments. Phonon wing contributions are not included in these calculations.

The application of an external magnetic field causes the two components of the hole to mix and shift relative to each other. Such effects are far more apparent in hole MCD spectra than simple hole spectra.

3.3. Side hole excitation

The broad vibrational side bands of the Q-band (Fig. 1) are well known to be composite, with many overlapping contributions.

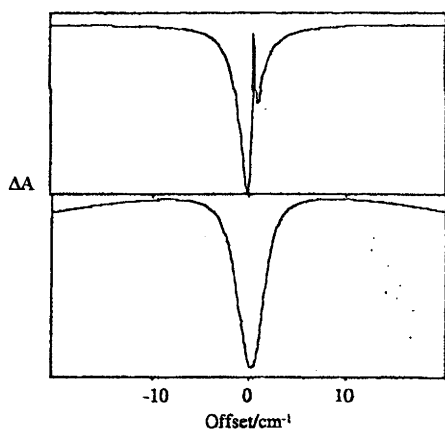


Fig. 3. Simulation of hole MCD (upper) and hole absorption (lower) in a band with two excited states. The two levels were assumed to have overlapping Gaussian distributions of 150 cm^{-1} FWHM and a separation of 120 cm^{-1} . A FWHM Lorentzian line width of 2 cm^{-1} was taken for the upper level and a laser limited value (0.1 cm^{-1}) for the lower level. The result was convoluted with a Gaussian of 1 cm^{-1} to allow for the resolution of the readout process.

Vibrational energies may be determined by burning in a vibrational side-band region, as strong side holes then appear in the origin Q band [5]. The spacing between the burn energy and the side holes corresponds to the energy of the vibration involved. An example of a side-hole burn in ZnPc/PMMA is shown in Fig. 4. The vibrational frequencies measured agree well with those obtained from a detailed fitting of both absorption and MCD line shapes [12] and from measurements in Shpol'skii matrices [13].

The hole and side hole features are broad (FWHM $\sim 10\text{ cm}^{-1}$) with Lorentzian profiles. Their broad shapes may be attributed to fast relaxation ($\sim 50\text{ fs}$) of the vibrationally excited states.

The complex MCD of a side hole burn is explicable by noting that the side holes on the high-energy side of the Q band possess a negative MCD signal, the side holes on the low-energy side have a positive signal, and central features are an inverted MCD A-term. The MCD of the side-hole

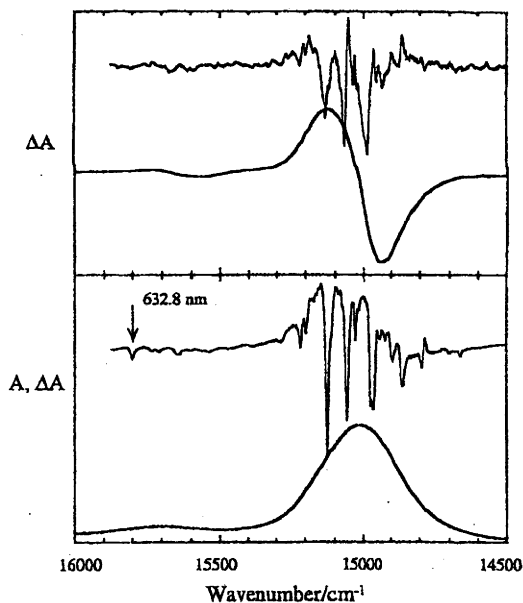


Fig. 4. 5 T MCD (upper) and absorption (lower) of a side hole burn in ZnPc/PMMA. The hole ΔA is $\times 20$ relative to the broad band A. The hole MCD ΔA is $\times 10$ relative to the broad band MCD.

burn is thus a direct reflection of the distribution of upper and lower crystal field levels of the Q state.

4. Conclusion

Measurements of the magneto-optical properties of spectral holes demonstrate an ability to provide information regarding the hole-burning processes into the upper and lower crystal-field components, the distribution of excited states, and Jahn–Teller processes. Zeeman shifts and MCD of spectral holes indicate that there is a considerable crystal-field splitting of the Q band and that there is a substantial Jahn–Teller interaction.

References

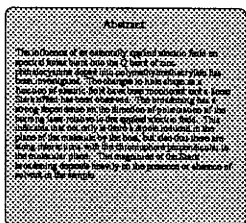
- [1] J. Friedrich, D. Haarer, *Angew. Chem. Int. Ed. Engl.* 23 (1984) 113.
- [2] D. Haarer, Photochemical hole-burning in electronic transitions, in: *Persistent Spectral Hole-Burning: Science and Applications*, Springer, Berlin, 1988, pp. 79–125.
- [3] S. Völker, *Annu. Rev. Phys. Chem.* 40 (1989) 499.
- [4] H. Riesen, E. Krausz, *Comments Inorg. Chem.* 14 (1993) 323.
- [5] E. Krausz, H. Riesen, P.N. Schatz, Z. Gasyna, C.L. Dunford, B.E. Williamson, *J. Lumin.* 66,67 (1996) 19.
- [6] R. Stranger, L. Dubicki, E. Krausz, *Inorg. Chem.* 35 (1996) 4218.
- [7] Z. Gasyna, D.H. Metcalf, P.N. Schatz, C.L. McConnell, B.E. Williamson, *J. Phys. Chem.* 99 (1995) 5865.
- [8] D.H. Metcalf, T.C. VanCott, S.W. Snyder, P.N. Schatz, B.E. Williamson, *J. Phys. Chem.* 94 (1990) 2828.
- [9] N.I. Ulitsky, B.M. Khariamov, R.I. Personov, *Chem. Phys.* 141 (1990) 441.
- [10] Bryce E. Williamson, unpublished results.
- [11] J. Friedrich, J.D. Swalen, D. Haarer, *J. Chem. Phys.* 73 (1980) 705.
- [12] T.C. VanCott, J.L. Rose, G.C. Misener, B.E. Williamson, A.E. Schrimpf, M.E. Boyle, P.N. Schatz, *J. Phys. Chem.* 93 (1989) 2999.
- [13] T.H. Huang, K.E. Rieckhoff, E.M. Voigt, *J. Chem. Phys.* 77 (1982) 3424.

Electric-field-induced Broadening of Spectral Holes in Zinc Phthalocyanine

R. Purchase,¹ M. Sellars,² E. Krausz,¹ N.B. Manson²

¹ Research School of Chemistry, The Australian National University, Canberra ACT 0200, Australia

² Research School of Physical Sciences and Engineering, The Australian National University, Canberra ACT 0200, Australia



The linewidth of a transition is given by:

$$\Gamma_{\text{hom}} = \frac{1}{\pi} \left(\frac{1}{T_1} + \frac{1}{T_2} \right)$$

Where:

- T_1 = Lifetime of the excited state
- T_2 = Pure dephasing time

T_2 is strongly temperature dependent, leading to a rapid increase of spectral linewidth with temperature.

In a multycrystal or an amorphous matrix each chromophore experiences a slightly different environment.

This leads to a distribution of transition energies.

Because of the strong temperature dependence of T_2 , hole burning experiments are performed at liquid helium temperatures. At these low temperatures, selectivity is maintained.

Spectral Hole Burning

Using a laser, which has a narrower bandwidth than the inhomogeneously broadened transition, chromophores at the energy of the laser may be selectively excited.

Photophysical hole burning may be understood as a "rearrangement" of the chromophore in its host. Photophysical hole burning is normally described in terms of a two level system (or TLS) model.

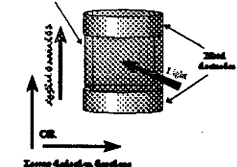
TLS Model

In an amorphous environment, there is a distribution of potential wells. Taking two adjacent wells for this model, a chromophore is excited from the ground state to the excited state. In the excited state, the barrier to tunnelling between wells is low. Thus, the resonant absorption is depleted, and may be absorbed in an adjacent well. This is only a small change which the molecule is undergoing. Because the energy difference between the hole and the photophysics is small, this small energy difference is characteristic of photophysical hole burning.

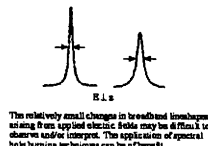
Why Spectral Hole Burning and Stark Spectroscopy?

What did we do?

Host of ZnPhthalocyanine (ZnPhthalocyanine)

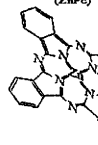


- Zinc Phthalocyanine (ZnPh) was doped into poly(methyl methacrylate) (PMMA). Samples were prepared both with and without solvent.
- The sample was placed in an Oxford Instruments helium bath cryostat. Experiments were performed at 1.8 K.
- Spectral holes were burnt into the sample using a Coherent 69 Single Frequency dye laser with DCM as the dye. An electric field was then put across the sample. The geometry of the experiment was as shown above.
- Holes were read out by scanning the laser used for burning about the frequency of the laser.
- The advantage of this experimental arrangement is that spectra can be obtained with the applied electric field either parallel or perpendicular to the polarization direction of the laser simply by rotating the laser.

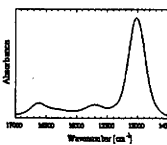


The Sample

Zinc Phthalocyanine (ZnPh)

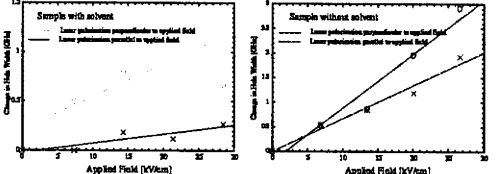
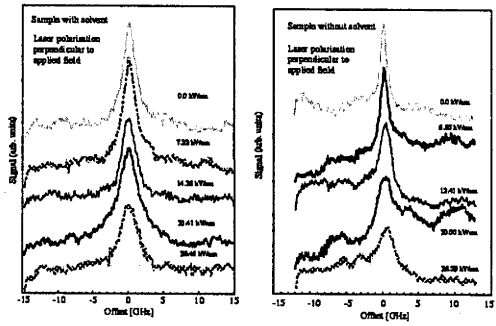


- Metallo-phthalocyanines (MPs) are of interest because of their strong colour for use as dyes.
- Their electronic properties have been widely studied. MPs are seen as having potential as charge carriers in devices such as solar cells.
- They are very similar to many biological systems.



The spectralscopy and electronic structure of MPs are fairly well understood. ZnPh possesses a central D_{4h} symmetry. The transition as seen in this work is a ligand-centred $n \rightarrow \pi^*$ transition (Fig. 1(b)). An absorption spectrum of ZnPh is shown adjacent.

What Happened?



- A linear Stark effect is observed (the hole broadens symmetrically about the centre of the hole in a linear fashion with the field, not just at the centre of the hole is observed).
- From the data, the following dipole moments may be calculated. 0.04 D and 0.01 D, respectively, for the parallel and perpendicular geometries for the sample with solvent. 0.03 D and 0.14 D for the parallel and perpendicular geometries for the sample without solvent.

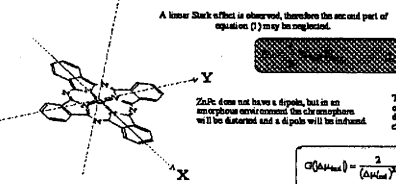
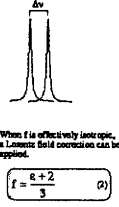
What Do The Results Tell Us?

Upon application of an external field, $\Delta\nu$ the transition under consideration will undergo a frequency shift $\Delta\nu$.

$$\Delta\nu = \frac{1}{h} \left(\mu_{\text{exc}}^2 E_{\text{app}}^2 + \mu_{\text{gnd}}^2 E_{\text{app}}^2 \right)$$

Where:

- μ_{exc} is the dipole moment in ground and excited state dipole moments.
- $\Delta\nu$ is the difference in polarizability tensor between the two states
- E is a vector which transforms the applied field into the local field experienced by the chromophore.



$$\langle \mu^2 \rangle = \frac{2}{3} \mu_{\text{exc}}^2 \langle \cos^2 \theta \rangle = \frac{2}{3} \mu_{\text{exc}}^2 \left(\frac{1}{3} \right)$$

When a spectral hole is burnt there is an angular selectivity associated with the polarization direction of the laser. By changing the angle of the applied electric field relative to the polarization of the laser, the angular dependence of the dipole may be investigated.

It may be observed in the data presented here that the broadening is far greater when the applied electric field is perpendicular to the laser polarization. It may be concluded then that there is some other dipole perpendicular to the plane of the molecule. A situation consistent with this is a solvent molecule (or some impurity in the case of the solvent free case) attaching to the zinc, giving an extra dipole as depicted above.

Another point worthy of note is that the magnitude of the Stark effect is the greater in the solvent than simply that in the sample with solvent. This suggests that the solvent has a very strong effect on the environment that the chromophore experiences. A clue to this observation is that the hole widths and burning efficiencies are different in the two samples, and if there were only two different solvents of chromophores being probed in the two experiments.

Conclusions

A linear Stark effect is observed in spectral holes in ZnPh doped into PMMA. This Stark effect shows a strong dependence on the polarization direction of the laser relative to the applied electric field. This indicates a dipole moment change not only induced in the plane of the molecule by the laser, but also strong dependence perpendicular to the molecule plane. The magnitudes of laser interactions depends heavily on the presence of solvent.

Electric-field-induced Broadening of Spectral Holes in Zinc Phthalocyanine

R. Purchase^a, B. Plagemann^b, E. Krausz^a, U.P. Wild^b

- a Research School of Chemistry, The Australian National University, Canberra, 0200, Australia
- b Physical Chemistry Laboratory, Universitätstr. 22, ETH Zentrum, CH-8092 Zürich, Switzerland

Abstract:

The influence of an externally applied electric field on spectral holes burnt into the Q band of zinc phthalocyanine doped into poly(vinyl-butyril) has been investigated. The changes in hole shape, as a function of electric field, have been monitored and a linear Stark effect has been observed. The broadening can be analysed as having contributions from in plane distortions of the chromophore that remove its nominal four-fold symmetry and thus the degeneracy of the Q band. Other contributions, perhaps associated with axial ligation of the chromophore, remove the plane of symmetry and contribute differently to the broadened profile. The Stark effect in conjunction with spectral hole burning shows promise as a technique to probe the interactions of a chromophore with its environment.

Introduction

The influence of an applied electric field on the absorption or emission spectrum of a sample has been used to yield information about the electronic structure of a variety of systems [1]. In the solid state, the changes in shape of spectral features are commonly attributed to two sources [2-5]: the change in dipole moment upon excitation associated with a permanent dipole moment intrinsic to the molecule (such is the case in non-centro-symmetric molecules) and the changes in dipole moment induced by the host matrix (this is often the dominating contributing factor in the case of centro-symmetric molecules). The relatively small changes in broadband lineshapes arising from applied electric fields may be difficult to observe and/or interpret. The application of spectral hole burning techniques can be of benefit.

The chromophore investigated in this paper is zinc phthalocyanine (ZnPc). The metalo-phthalocyanines are widely studied and their spectroscopy and electronic structure are fairly well understood [6]. ZnPc possesses nominal D_{4h} symmetry. The transition studied in this work is the Q band which is a ligand-centred $\pi - \pi^*$ transition (${}^1A_{1g} - {}^1E_{1u}$). An absorption spectrum of ZnPc is shown in figure 1.

The hole burning mechanism in ZnPc and related chromophores is photophysical [4,7,8]. This mechanism is in contrast to the proton tautomerism of the free-base porphyrins and phthalocyanines.

Hole Burning Stark Spectroscopy

The burning of a spectral hole selects a sub-set of chromophores from an inhomogeneously broadened distribution. Species with their transition dipoles parallel to the polarisation direction of the laser will tend to be selected in this process [9].

If the assumption is made that a guest species is described as a point dipole [10], then, upon application of an external electric field, E_{app} , the transition under consideration will undergo a frequency shift $\Delta\nu$:

$$\Delta\nu = \frac{1}{h} \left(\Delta\mu_{\text{eff}} \mathbf{f} \mathbf{E}_{\text{app}} + \frac{1}{2} \mathbf{f} \mathbf{E}_{\text{app}} \Delta\alpha \mathbf{f} \mathbf{E}_{\text{app}} \right) \quad (1)$$

Where: $\Delta\mu_{\text{eff}}$ is the difference in dipole moments between the ground and excited states; $\Delta\alpha$ is the difference in polarisability tensors between the two states; and \mathbf{f} is a tensor which transforms the applied field into the local field experienced by the host. When \mathbf{f} is effectively isotropic, a Lorentz field correction can be applied [11].

$$\mathbf{f} = \frac{\epsilon + 2}{3} \quad (2)$$

A value of $\epsilon = 2.55$ was used for the the dielectric constant of the host [12].

The Stark effect observed is linear in the electric field; therefore, the second portion of equation (1) may be neglected, leading to:

$$\Delta\nu = \frac{\mathbf{f}}{h} \Delta\mu_{\text{eff}} \mathbf{E}_{\text{app}} \quad (3)$$

$\Delta\mu_{\text{eff}}$ may be broken into two components. The first of these, $\Delta\mu_{\text{mol}}$, is associated with a dipole intrinsic to the species. $\Delta\mu_{\text{mol}}$ often has a well defined magnitude and is fixed at some angle, θ_{mol} , to the transition dipole, \mathbf{D} . The other component, $\Delta\mu_{\text{ind}}$, is a change in dipole moment induced by the environment experienced by the species. $\Delta\mu_{\text{ind}}$ more likely has a distribution of magnitudes and angles. The variation of the magnitude of $\Delta\mu_{\text{ind}}$ may be described by [3]:

$$G(|\Delta\mu_{\text{ind}}|) = \frac{2}{(\Delta\mu'_{\text{ind}})^2} |\Delta\mu_{\text{ind}}| \exp \left[- \left(\frac{|\Delta\mu_{\text{ind}}|}{\Delta\mu'_{\text{ind}}} \right)^2 \right] \quad (4)$$

$\Delta\mu'_{\text{ind}}$ is the root mean square value of the matrix-induced dipole moment. If \mathbf{E}_{app} is parallel to $\Delta\mu_{\text{ind}}$, then a hole burnt at zero field develops an apparent splitting upon the application of a strong field. If \mathbf{E}_{app} is perpendicular to $\Delta\mu_{\text{mol}}$, then the hole shape will broaden without splitting. For reasons associated with their distributed values, induced dipole moment changes are likely to lead to a broadening rather than an

apparent splitting. Hole burning allows the orientation of E_{app} to $\Delta\mu_{mol}$ to be influenced experimentally.

The different dipole moments, molecular and induced, and their various angular dependencies, result in distinctive hole shapes upon the application of an electric field. With careful modelling and analysis, these components may be separated. Hole burning Stark spectroscopy enables the detection of subtle changes in the symmetry of a chromophore and its environment.

Experimental

In this work, ZnPc was studied as a dopant in a thin film of poly(vinylbutyral) (PVB). A thin film of ZnPc doped into PVB was prepared by mixing a solution of ZnPc in tetrahydrofuran (THF) with a solution of PVB, also in THF. The resulting mixture was left to dry overnight. The films were further dried by being put in an oven at 80 °C at reduced pressure for approximately 20 hours. The concentration of the sample was chosen such that the maximum of the Q band had an optical density of ~ 1.5 . The thickness of the film was $\sim 110 \mu\text{m}$. The thickness was measured with a micrometer and electrically by measuring the capacitance of the sample.

Samples were prepared for Stark experiments by being sandwiched between two transparent electrodes. The electrodes consisted of a pair of glass plates coated with a conducting film of indium tin oxide (ITO) on their inner faces.

The hole burning was performed at 1.8 K in a helium bath cryostat. Holes were burnt using a Coherent CR899-29 single frequency dye laser operated with DCM as the dye. The sample was illuminated for 10 s with powers of $\sim 100 \mu\text{W}$ for burning, and then the power was reduced for reading. Electric fields of 0 kVcm^{-1} to 45 kVcm^{-1} were applied to the sample.

Holes were burnt in a number of places across the inhomogeneously broadened band to gain information about the wavelength dependence of the Stark broadenings. The positions of these holes are indicated by

arrows in figure 1. The greater part of the discussion in this paper is in reference to the hole burnt at the top of the band.

Holes, in the absence of an external field, were approximately 1 GHz wide, and a few per cent of the total absorption at that wavelength.

Holes were read out holographically. Details of holographic detection are given in reference 13. This procedure involved illuminating the sample with two overlapping beams during the burning process to burn a spatial grating into the sample. One beam was used for reading. Both the transmitted beam and the scattered beam were measured. The experimental set-up is shown in part (a) of figure 2. Holographic detection is an effective way of measuring small holes. It is a background-free detection technique. Even when the depth of a hole has been diminished through the application of an electric field, it remains readily detectable using this technique.

The geometry of the experiment was such that the polarisation of the laser was perpendicular to the direction of the applied electric field. This arrangement is depicted in part (b) of figure 2.

Results and Discussion

The changes in hole profile with electric field are displayed in figure 3. The corresponding plot of change in hole width with field strength is shown in inset (a) of figure 3. A linear Stark effect is observed (the holes broaden symmetrically about the centre of the hole in a linear fashion with the field, and no shift in the centre of the hole is observed).

From the data, a change in dipole moment between the ground and excited states of 0.243 ± 0.021 D may be calculated. This is larger than the results obtained for free-base porphyrin derivatives [3,4], but comparable with those from zinc tetrabenzporphyrin [5] and zinc octaethylporphyrin [4].

Nominally, ZnPc possesses D_{4h} symmetry. The excited state of the Q transition is then doubly degenerate. A theoretical treatment of the influence of degeneracies on the interpretation of Stark data has been

given [14] for chromophores with D_3 symmetry. An applied electric field in the xy plane of the chromophore leads to a removal of the degeneracy.

In systems with four-fold symmetry, no removal of a degenerate state occurs upon application of a uniform electric field. This result is readily determined from group theory. A shift may be observed in a transition when the inversion centre symmetry is lost. Furthermore, one may expect Stark effects to be fairly small compared to charge transfer excitations, as discussed in reference 14.

In an amorphous host, such as PVB, the nominally degenerate excited state is split by site inhomogeneity leading to a significant splitting having a distribution of values ($\sim 10 - 150 \text{ cm}^{-1}$) [15]. The split levels have very different lifetimes. The level at lower energy relaxes directly to the ground state with $\tau \approx \text{ns}$. The upper level relaxes to the lower level in $\tau \approx \text{ps}$ and thus their homogeneous linewidths are very different. At high resolution, spectral hole burning associated with an upper level is sufficiently broad ($\approx 100 \text{ GHz}$) so as to not influence measurements of hole shapes.

Altmann et al. [4] proposed the idea that the metal atom may be out of plane in their study of zinc octaethylporphyrin in PVB and this would lead to a dipole perpendicular to the transition moment. X-ray diffraction studies indicate that ZnPc is flat [16]. For the extra dipole moment to be detectable in these Stark experiments it would need to change upon excitation of the Q transition. The zinc atom is large compared to the cavity in the phthalocyanine ring. It is perhaps plausible that, upon excitation of the phthalocyanine ring, the zinc atom "pops out" of the phthalocyanine ring, thus causing a dipole change perpendicular to the phthalocyanine ring.

A dipole perpendicular to the phthalocyanine ring would be obtained upon ligation of the zinc atom in the axial position. Ligation in the axial position will cause the zinc atom to be displaced from the phthalocyanine plane [17]. THF was used as the solvent in the preparation of the sample for this experiment. THF has an oxygen with its lone pair on it which would attach quite readily to the zinc atom in ZnPc.

A number of authors [3,18,19,20] have modelled changes in the shape of spectral holes upon the application of electric fields. Such models are useful in analysing contributions to a change in shape of a hole. The model used in this work closely follows that of Meixner [3]. This model yields values for a change in permanent dipole moment, $\Delta\mu_{\text{mol}}$, and a root mean square value for a distribution of induced dipoles, $\Delta\mu'_{\text{ind}}$.

The best fit to the data was obtained when $\Delta\mu_{\text{ind}}$ was in the plane of the phthalocyanine ring, and $\Delta\mu_{\text{mol}}$ was perpendicular to the transition dipole. A possible regime is that the zinc metal is brought out of plane by the ligation of the THF. This fit yields values $\Delta\mu'_{\text{ind}} = 0.075 \pm 0.008$ D and $\Delta\mu_{\text{mol}} = 0.118 \pm 0.001$ D. $\Delta\mu'_{\text{ind}}$ is in good agreement with $\Delta\mu'_{\text{ind}}$ values obtained in free-base octaethylporphyrin [3,4]. A plot of hole width changes versus applied field strength for the two components is shown in inset (b) of figure 3.

The experimental geometry utilised in this work is most sensitive to $\Delta\mu_{\text{mol}}$ perpendicular to the transition dipole. This situation leads to a pseudo split hole profile. In contrast, $\Delta\mu_{\text{ind}}$ leads to a broadening of the hole shape. There is no indication of a double maximum in the data here. At higher fields, holes acquire a characteristic rectangular appearance. One of the high field (36.6 kV/cm) hole shapes is shown in figure 4 along with the accompanying fit. At higher fields still, the model used to fit the data indicates that this rectangular shape will develop a split appearance.

$\Delta\mu'_{\text{ind}}$ and $\Delta\mu_{\text{mol}}$ may be expected to have a dependence upon the position within the inhomogeneous profile at which the hole is burnt. This wavelength dependence has been investigated by a number of authors [21–24]. Inhomogeneous broadening arises because of the different matrix environments experienced by the guest molecules. The host–guest interaction may be categorised into four different forms: specific interactions such as hydrogen bonding and charge-transfer, dipole–dipole interactions, the interaction between the dipole of the solvent and a dipole induced in the guest, and dispersion interactions. The first of these interactions may be neglected here. The second two interactions will lead to a correlation between the position in the inhomogeneous band and the change in the dipole moment. This correlation occurs because those mechanisms which cause the distribution in transition energies are the

same mechanisms by which matrix-induced dipoles arise. Dispersion interactions do not lead to a wavelength dependence of Stark broadenings.

The wavelength dependence observed in these experiments is negligible. Thus, the matrix shift in ZnPc may be dominated by dispersion interactions.

Conclusions

The analysis indicates that ZnPc in PVB has degeneracy of the Q band removed by in-plane interactions with the host. There also appears to be out-of-plane interaction as evidenced by a significant $\Delta\mu_{\text{mol}}$ value. A dipole moment change in this direction may be interpreted owing to axial ligation of the Zn by solvent THF present in the sample.

Results obtained in this work encourage further experiments using a combination of Stark spectroscopy and spectral hole burning as a means of probing this class of chromophore. The experiment currently under consideration, with geometry as depicted in figure 2 (b), is more sensitive to changes in dipole moment perpendicular to the plane of the molecule. A logical step is to perform experiments with the polarisation direction of the laser parallel to that of the applied field. An advantage of the arrangement depicted in figure 2 (c) is that spectra can be obtained with the applied field either parallel or perpendicular to the polarisation direction of the laser, simply by rotating the latter.

Such experiments should yield further information regarding the interaction of the excited state with an amorphous environment. These types of experiments could also be usefully extended to biological systems and supplement work performed by other groups [9,25,26].

References

- [1] G.U. Bublitz, S.G. Boxer, *Annu. Rev. Phys. Chem.* 48 (1997) 213.
- [2] U. Bogner, P. Schätz, R. Steel, M. Maier, *Chem. Phys. Lett.* 102 (1983) 267.
- [3] A.J. Meixner, A. Renn, S.E. Bucher, U.P. Wild, *J. Phys. Chem.* 90 (1986) 6777.
- [4] R.B. Altmann, D. Haarer, N.I. Ulitsky, R.I. Personov, *J. Lumin.* 56 (1993) 135.
- [5] L. Kador, D. Haarer, R. Personov, *J. Chem. Phys.* 86 (1987) 5300.
- [6] Martin Gouterman, in: *The Porphyrins* vol. 3, ed. David Dolphin (Academic Press, New York, 1978) p. 1.
- [7] J. Friedrich, D. Haarer, *Angew. Chem. Int. Ed. Engl.* 23 (1984) 113.
- [8] S. Völker, *Annu. Rev. Phys. Chem.* 40 (1989) 499.
- [9] J. Gafert, J. Friedrich, F. Parak *Proc. Natl. Acad. Sci. USA* 92 (1995) 2116.
- [10] W. Liptay, in: *Excited States* vol. 1, ed. Edward C. Lim (Academic Press, New York, 1974) p. 129.
- [11] C.J.F. Böttcher, *Theory of Electric Polarisation* (Elsevier Scientific Publishing Company, Amsterdam, 1973).
- [12] R.B. Altmann, I. Renge, L. Kador, D. Haarer, *J. Chem. Phys.* 97 (1992) 5316.
- [13] A.J. Meixner, A. Renn, U.P. Wild, *J. Chem. Phys.* 91 (1989) 6728.
- [14] I.B. Talanina, M.A. Collins, L. Dubicki, E. Krausz, *Chem. Phys. Lett.* 200 (1992) 318.

- [15] R. Purchase, E. Krausz, B.E. Williamson, *J. Lumin.* 76&77 (1998) 339.
- [16] W.R. Scheidt, W. Dow, *J. Am. Chem. Soc.* 99 (1977) 1101.
- [17] R. Timkovich, A. Tulinsky, *J. Am. Chem. Soc.* 91 (1969) 4430.
- [18] P. Schätz, M. Maier, *J. Chem. Phys.* 87 (1987) 809.
- [19] V.D. Samoilenko, N.V. Razumova, R.I. Personov, *Opt. Spectrosc. (English Translation)* 52 (1982) 346.
- [20] M. Maier, *Appl. Phys.* B41 (1986) 73.
- [21] E. Vauthey, K. Holliday, C. Wei, A. Renn, U.P. Wild, *Chem. Phys.* 171 (1993) 253.
- [22] L. Kador, S. Jahn, D. Haarer, R. Silby, *Phys. Rev.* B41 (1990) 12215.
- [23] E. Vauthey, J. Voss, C. de Caro, A. Renn, U.P. Wild, *Chem. Phys.* 184 (1994) 347.
- [24] N. Hartmannsgruber, M. Maier, *J. Chem. Phys.* 96 (1992) 7279.
- [25] J. Gafert, J. Friedrich, J.M. Vanderkooi, J. Fidy, *J. Phys. Chem.* 99 (1995) 5223.
- [26] P. Geissinger, B.E. Kohler, J.C. Woehl, *J. Phys. Chem.* 99 (1995) 16527.

Figure Captions

Figure 1: Absorption spectrum of the Q band of ZnPc in PVB. The spectrum shows an origin band and vibrational side bands. The arrows indicate where hole burning has been performed. The structure of ZnPc is also displayed.

Figure 2: a) The experimental set-up for holographic detection of spectral holes. M=mirror; S=shutter. During burning, shutters 1 and 2 are open, while 3 and 4 are closed. During reading, shutters 1, 3, and 4 are open and 2 is closed. b) Current experimental geometry. c) Proposed experimental geometry. p =polarisation direction of laser; k =propagation direction of laser; E_{app} =direction of applied electric field.

Figure 3: Holographically detected spectral holes at fields of 0, 4.9, 9.1, 18.3, and 27.5 kV/cm. Inset a) Plot of change of hole width versus applied field strength. The change in hole width is linear with the field. Inset b) Change in hole width versus applied field strength for the two calculated components of the broadening of the spectral hole.

Figure 4: A Spectral hole at a field of 36.6 kV/cm with its accompanying fit.

Figure 1:

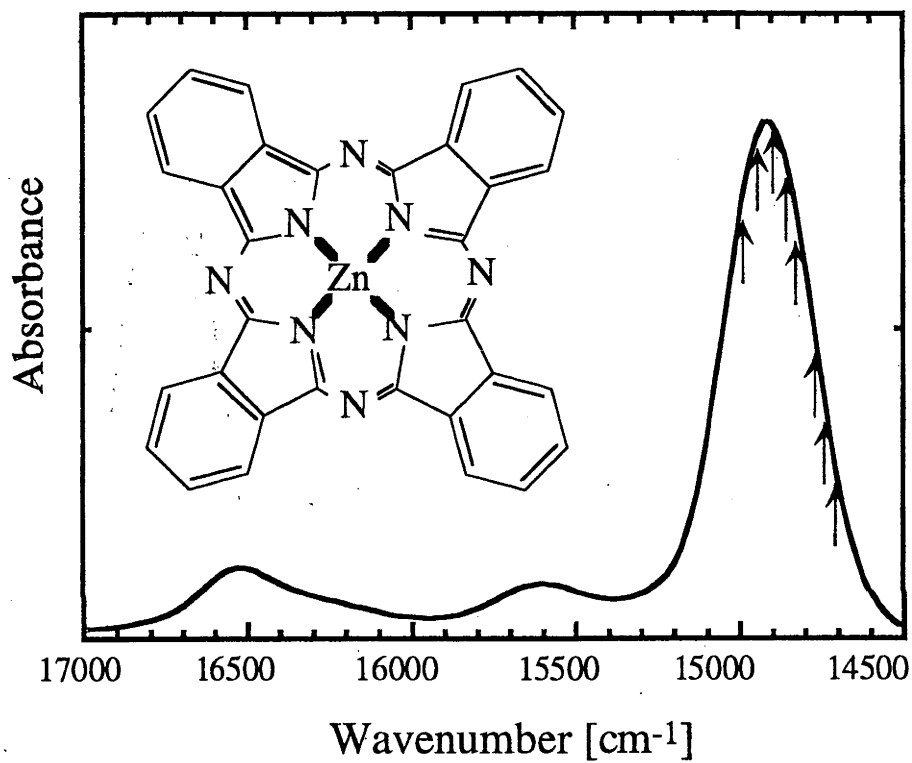
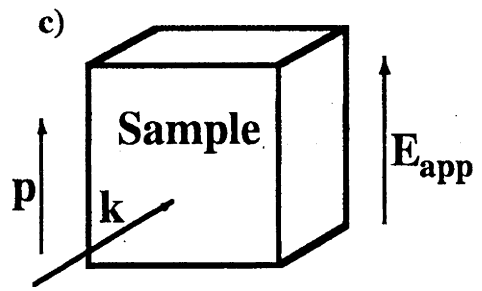
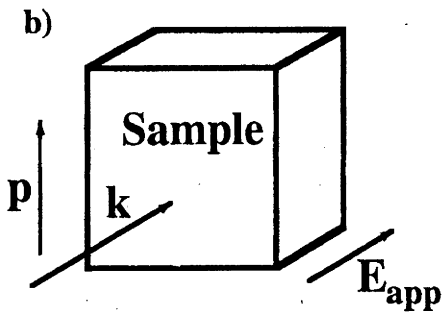
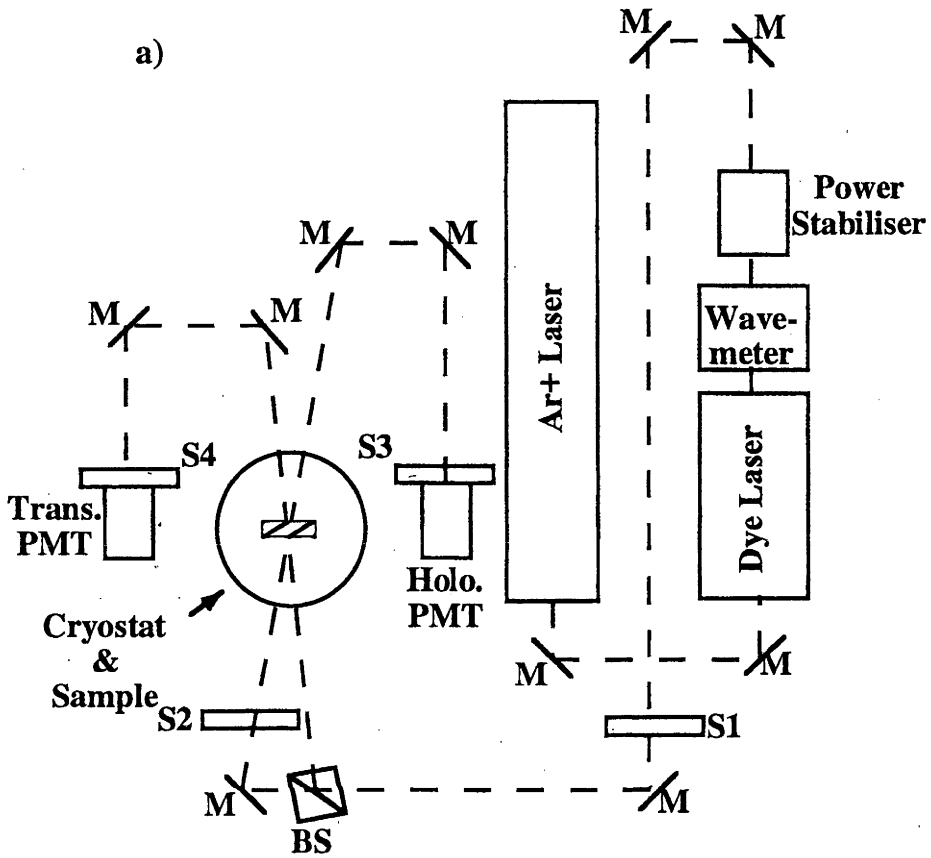


Figure 2:



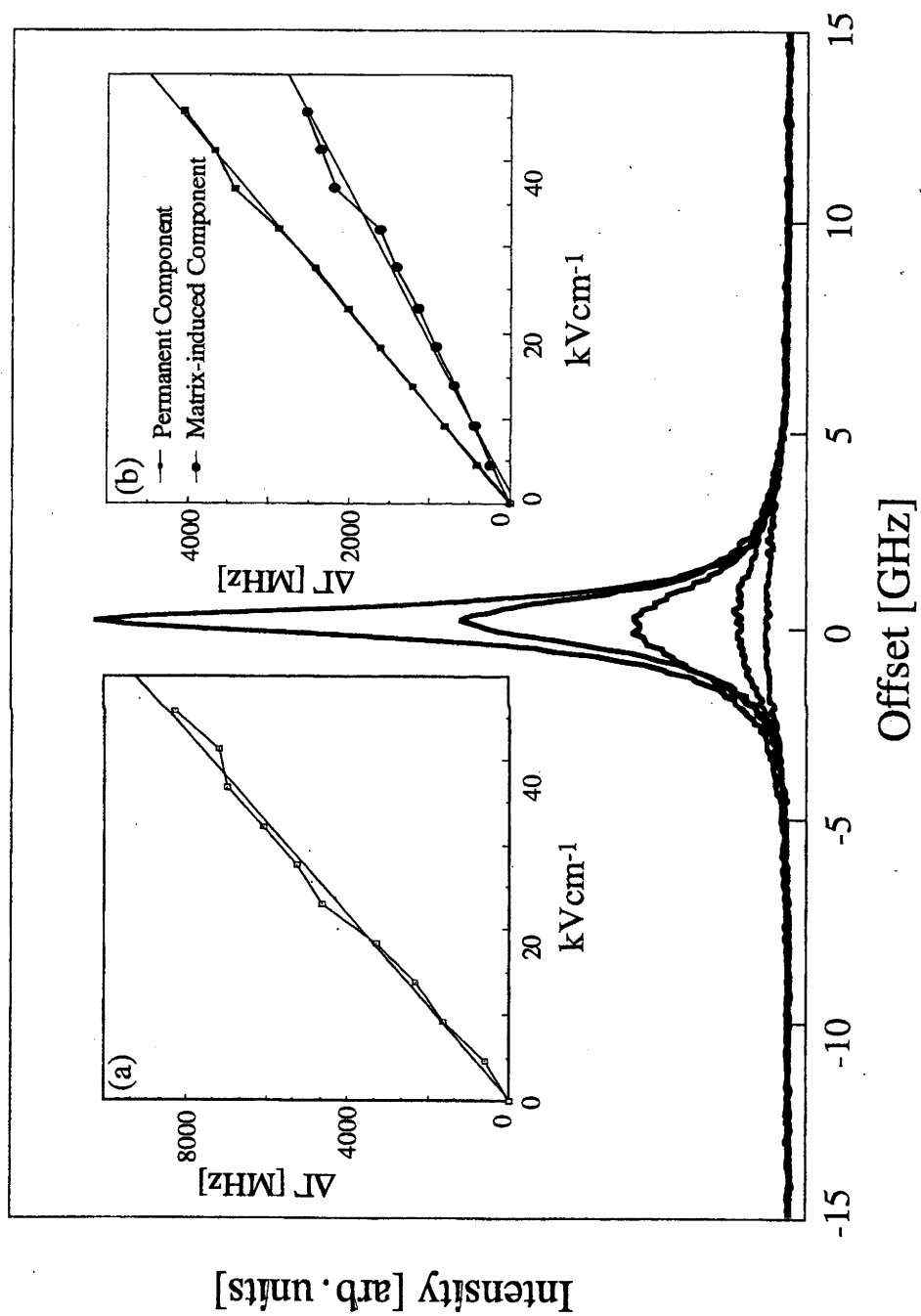


Figure 3:

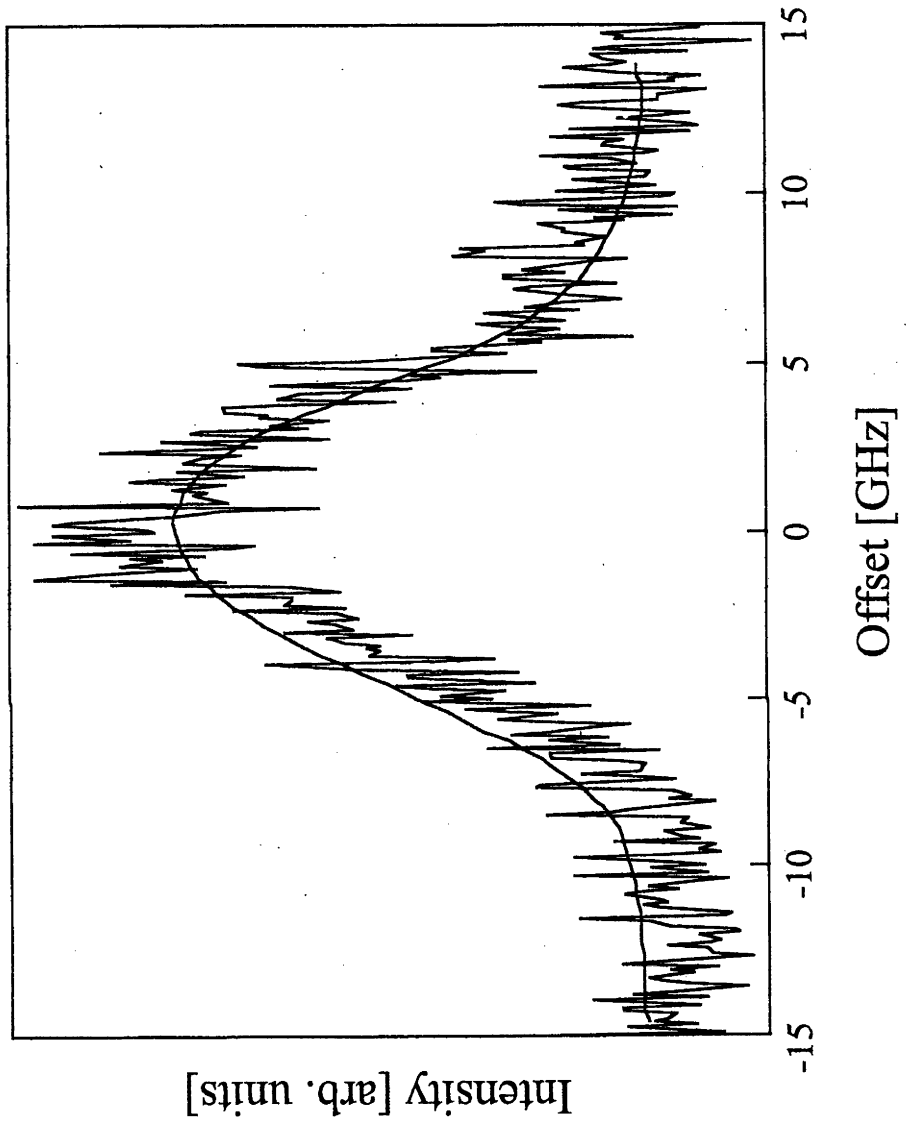


Figure 4: